PROCEEDINGS OF THE INTERNATIONAL NUCLEAR AND ATOMIC ACTIVATION ANALYSIS CONFERENCE AND 19th ANNUAL MEETING ON ANALYTICAL CHEMISTRY IN NUCLEAR TECHNOLOGY

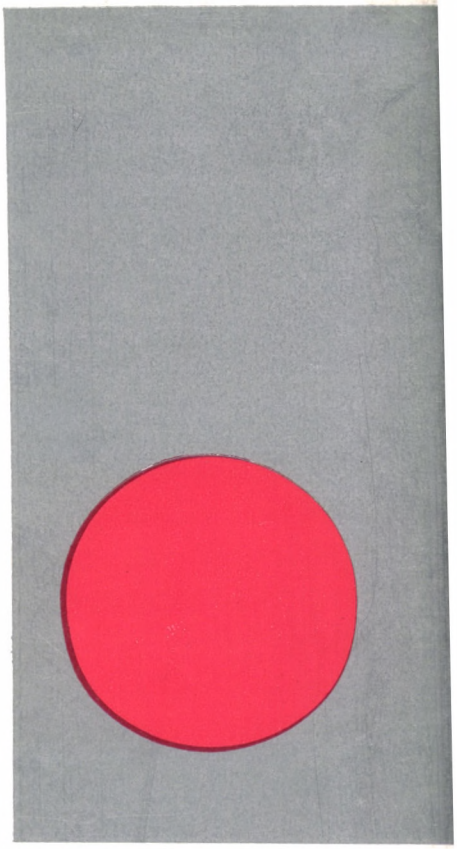

GATLINBURG, TENNESSEE, USA OCTOBER 14-16, 1975

EDITORS
W.S. Lyon, T. Braun and E. Bujdosó

AKADÉMIAI KIADÓ · BUDAPEST

PROCEEDINGS OF THE INTERNATIONAL

NUCLEAR AND ATOMIC ACTIVATION ANALYSIS

CONFERENCE AND 19th ANNUAL MEETING ON
ANALYTICAL CHEMISTRY IN NUCLEAR TECHNOLOGY

PROCEEDINGS OF THE INTERNATIONAL

NUCLEAR AND ATOMIC ACTIVATION ANALYSIS

CONFERENCE AND 19th ANNUAL MEETING ON
ANALYTICAL CHEMISTRY IN NUCLEAR TECHNOLOGY

GATLINBURG, TENNESSEE, USA
October 14–16, 1975

REPRINTED FROM THE
Journal of Radioanalytical Chemistry

EDITORS
W. S. LYON, T. BRAUN, E. BUJDOSÓ

AKADÉMIAI KIADÓ • BUDAPEST 1976

INTERNATIONAL NUCLEAR AND ATOMIC ACTIVATION ANALYSIS CONFERENCE AND NINETEENTH ANNUAL MEETING ON ANALYTICAL CHEMISTRY IN NUCLEAR TECHNOLOGY

Gatlinburg, Tennessee, USA
October 14–16, 1975

SPONSORED BY THE

Oak Ridge National Laboratory, Analytical Chemistry Division
American Nuclear Society, Isotopes and Radiation Division
Oak Ridge ANS Local Section

GENERAL CO-CHAIRMEN

WILLIAM S. LYON
LEO J. BRADY

TECHNICAL PROGRAM CHAIRMAN

ENZO RICCI

TECHNICAL PROGRAM REVIEW COMMITTEE

Chairman: ENZO RICCI (Oak Ridge National Laboratory)
Members: OSWALD U. ANDERS (Dow Chemical)
JOHN A. COOPER (ORTEC, Inc.)
MICHAEL D. D'AGOSTINO (Grumman Aerospace)

ISBN 963 05 1014 6

Printed in Hungary

CONTENTS

Introduction

The International Nuclear and Atomic Activation Analysis Conference brought together representatives from laboratories all over the world that are actively engaged in nuclear methods of analysis. The three days (and one evening) of presentations were well attended, with spirited discussion following every session often extending outside the conference hall. A highlight of the meeting was the presentation of the Hevesy Award to Dr. T. BRAUN and Dr. J. TÖLGYESSY.

A special word of thanks is due ENZO RICCI, Program Chairman, for his outstanding job in organizing the excellent program of papers. He carried the heaviest responsibility of anyone associated with the meeting.

This volume does not contain all of the papers given at the Conference. Some authors failed to submit their manuscript, while others felt the material they presented was not suitable for publication.

While these omissions are regretable, they certainly do not detract from the excellence and utility of this collection of papers itself. There is a wealth of information and data contained here, and this compilation should serve as a guide and reference for years to come. We who attended the Conference can look through this volume and remember with pleasure, for others it will be a new, and we hope, an enlightening experience.

W. S. LYON

Oak Ridge, Tennessee
December, 1975

Journal of Radioanalytical Chemistry, Vol. 32 (1976) 9–16

Neutron Activation Analysis in Biology

APPLICATION OF NEUTRON ACTIVATION ANALYSIS IN THE INVESTIGATION OF TRACE ELEMENT METABOLISM

D. BEHNE

Hahn-Meitner-Institut für Kernforschung, Berlin

The applications of neutron activation analysis in the investigation of trace element metabolism in animals and man are described and discussed. They include the determination of element distributions in the body, the study of correlations between trace element concentrations and physiological processes, the special methods of investigation of trace element metabolism in man and the identification of the chemical forms of the elements in the organism. Examples for each stage of application are given.

Introduction

A great deal of analytical work is devoted today to the determination and control of trace element levels in our environment and we are constantly inundated with data on the distribution of trace elements and the changes in their concentrations in a wide range of environmental materials. However, the significance of these changes for human health can so far only be assessed for a few elements. In many cases the data are still of little value as sufficient information is not yet at hand on the behaviour and the biological effects of the elements taken in by the body.

It is therefore necessary to carry out investigations on trace element metabolism on a large scale. These studies cannot be performed solely with tracer methods as little is known about the chemical forms of the elements on which their behaviour is largely dependent, and it cannot be guaranteed that all the compounds of an element in the body will be labelled when the tracer is administered in a certain chemical form.

Therefore, in addition, analytical methods such as neutron activation analysis must be applied to obtain information about the absorption, storage, mobilization and biological effects of the elements in question. The different stages of application, which are listed in Fig. 1, are shown by a few examples.

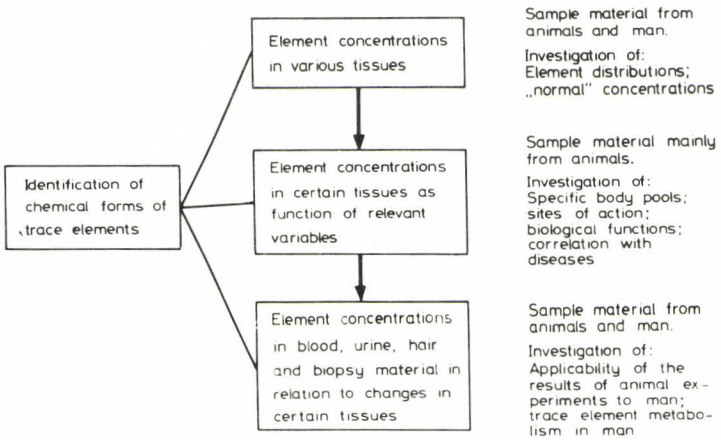

Fig. 1. Application of analytical methods in the investigation of trace element metabolism

Determination of element distributions in the body

The first step in the investigation of trace element metabolism by analytical methods is to measure the levels in the different tissues of animals and man in order to determine the element distributions in the body and to obtain information on "normal" concentrations. Although a relatively large amount of data has been collected, our knowledge in this field is still far from complete. For instance, only a few studies exist on the trace element content in the skeleton, which represents a considerably large proportion of the body.

We therefore determined the concentrations of as many elements as possible in human and animal bone. In Fig. 2 the contents of several elements which were measured in the compact tissue of a human tibia are shown as an example.[1] All elements reveal considerable variations in their concentrations along the bone. In general the element levels at the ends of the bone are higher than those in the shaft. The analysis of the distributions in other bones, which showed similar results, suggest that there might be a certain pattern in these variations.

In order to investigate the distribution of the trace elements within the bone, the mineral and the collagen of the cortex samples were separated from one another. It was found that scandium and zinc are contained mostly in the mineral, whereas the other elements are more or less evenly distrib-

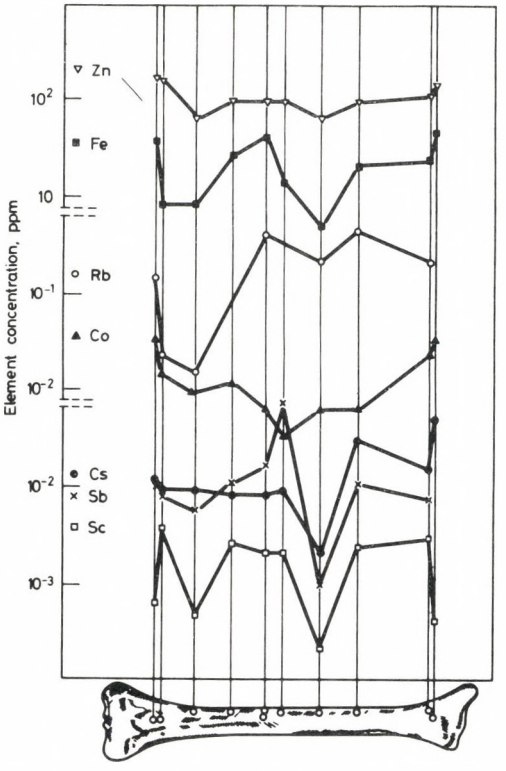

Fig. 2. Trace element distribution in the cortex of a human tibia

uted between the organic and the inorganic fractions. For antimony, caesium, chromium, cobalt, iron, rubidium, and zinc the concentrations in the solid parts of the bone marrow were higher than those in the bone mineral and collagen. If one compares the element concentrations in the bone with those in other tissues and considers the fact that the skeleton constitutes a fairly large proportion of the whole of the body, it becomes clear that a relatively high percentage of the total trace element content is contained in the bones.

Correlations between element concentrations and physiological processes

The finding of high element levels is, however, no evidence of the biological importance of the tissue in question, but it enables us to select areas of interest, which must then be further investigated. The next step is

to measure the local concentrations as a function of relevant variables such as substances with physiological functions, stress, pregnancy or diseases. By correlating the changes in the trace element concentrations with these factors, it is possible to obtain information about specific body pools from which the elements can be released when needed, about the available amounts of the accumulated elements, sites of action, biological functions and connections between trace elements and diseases.

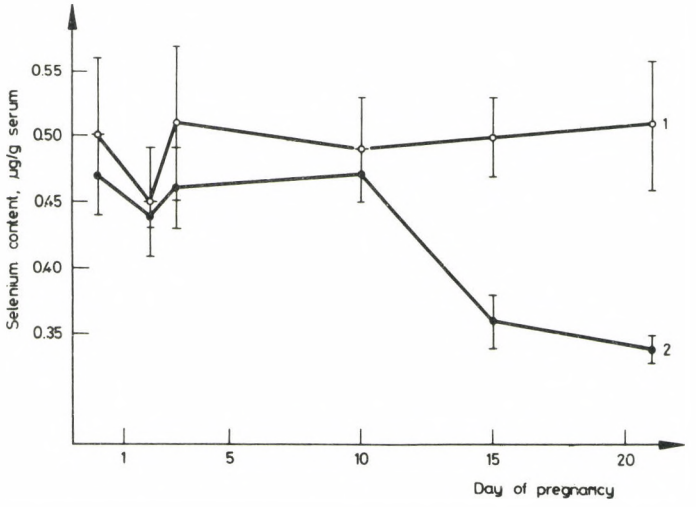

Fig. 3. Mean selenium concentration in the blood serum of female rats before and during pregnancy. Curve 1 – ovariectomized controls (5 animals), curve 2 – gravid rats (5 animals)

An example of this application of neutron activation analysis is the investigation of the behaviour of trace elements during pregnancy and lactation. It is very probable that during these periods great changes in the trace element metabolism of the mother take place, as the elements required by the fetus or infant have to be supplied to a large extent by the mother's element pools. This can lead to a deficiency of essential elements in the mother. On the other hand, toxic elements which have accumulated over a long period of time in a storage tissue of the mother, may be mobilized in large amounts and transferred from mother to child.

We are trying to investigate these effects of pregnancy and lactation on the trace element metabolism and to identify body pools which are of

importance during these periods. In a preliminary study the concentrations of bromine, caesium, cobalt, iron, rubidium, selenium, sodium, and zinc were measured in various tissues of female rats at the end of gestation.[2] Compared with the tissue levels in a control group, differences in the element distributions were found in the liver, the spleen and the suprarenal glands.

Some effects of pregnancy on trace element metabolism were also observed in blood serum where changes in the selenium concentration occurred.[3] As can be seen in Fig. 3, the element level in the gravid rats did not differ from that in the control group during the first ten days of gestation, however, it dropped significantly ($P < 0.001$) between the 10th and the 15th day. This decrease coincides with the transference of the luteotropic function of the pituitary to the placenta, and there is a possibility that the selenium metabolism is influenced by this change.

Investigation of trace element metabolism in man

The studies of trace element levels in particular tissues in relation to physiological processes are usually limited to animals. In man, especially where the element metabolism in health is being investigated, we are mostly restricted to materials which can easily be taken, such as blood, hair, urine or in some cases biopsy samples. In order to get a maximum of information from the analysis of these materials, the connections between their element levels and the concentrations in other tissues have to be known. These relations have to be studied in animal experiments. Then, if the applicability of the results to man can be established, the human trace element metabolism and the nutritional status can be investigated and controlled in a simple way.

In man, blood plasma is a most convenient indicator material, since the samples can be taken relatively easily without danger of contamination. But, as the element levels in blood may be strictly controlled by homeostatic mechanisms, they do not necessarily reflect the body stores, and it is not possible to obtain information on the amounts of elements in the tissues merely by determining the concentrations in the plasma. However, tests can be developed which cause the release of elements from physiologically important pools into the blood. By determining the concentration changes in the plasma it will then be possible to draw conclusions about the nutritional status and the availability of trace elements in man.

We are at present investigating the possibility of employing physical exercise as such a test. In an initial experiment we determined the trace elements mobilized from the body pools into the blood plasma of mice,

which had undergone considerable physical stress.[4] In Fig. 4 the element levels before and at several intervals after stress are shown as a percentage of the initial concentrations. Each point represents the mean of 20 animals. With the exception of selenium an increase in the concentrations was found immediately after stress for all the elements investigated. The increase was significant in the case of iron and zinc ($P < 0.001$) and rubidium and cobalt ($P < 0.05$). After 2 hrs the zinc value was still significantly higher than the

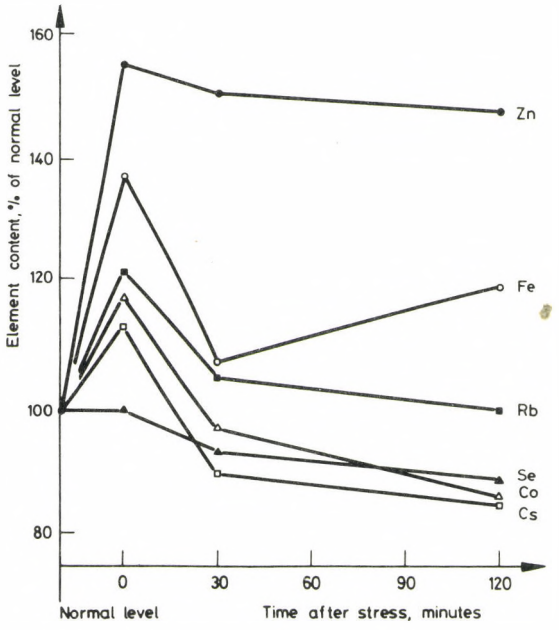

Fig. 4. Mean element concentrations in the blood serum of mice before and after physical stress

initial concentration. As it appears that in man some elements can similarly be mobilized into the blood, it may be possible to use physical exercise as an indicator test for the available body stores of trace elements.

Identification of the chemical forms of trace elements

The limitation of analytical methods such as neutron activation analysis in trace element research lies in the fact that only the total concentration of an element can be determined and no information is obtained about its

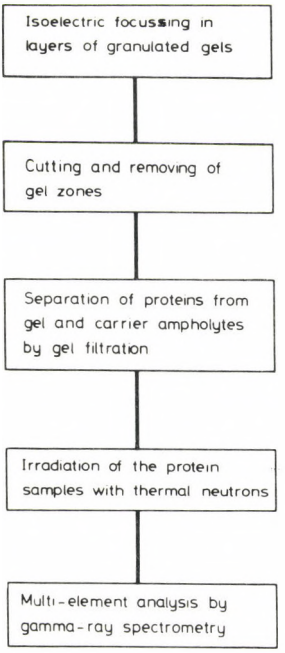

Fig. 5. Determination of protein-bound trace elements

chemical forms. However, the behaviour of an element in the body, its functions, its essentiality or toxicity, are to a large extent dependent on its chemical state. For example, the significance for the body of a certain content of cobalt in a tissue varies greatly according to whether the element is present as inorganic cobalt or in the form of vitamin B_{12}. But the analytical methods can only give us the total amount of the metal.

It is therefore exceedingly important to find ways of identifying and determining the chemical state of an element and its carrier molecules. As many of the trace elements in the body are coupled to proteins, we developed a method which enables us to determine the protein-bound trace elements. This is achieved by the separation and identification of the proteins in a sample and the subsequent analysis of the element content in the isolated fractions.[5] A survey of the experimental procedure is given in Fig. 5.

Isoelectric focussing in layers of granular gels is used as the separation method. Here the proteins are isolated with a very high resolution in a stable pH-gradient according to the differences in their isoelectric points.

The main source of error is the introduction of trace element impurities from the materials used for the separation, and these must therefore be thoroughly purified in advance. The gel zones, which contain the protein fractions, are isolated after the separation is completed. As the gel still contains considerable quantities of trace element impurities which are firmly bound and cannot be removed by the purification step, the proteins are separated from the gel by gel filtration before the element analysis. Then the trace element contents in the different protein fractions are determined by neutron activation analysis. The method is at present being used in the investigation of trace element - protein complexes in blood serum.

Conclusion

The applications of neutron activation analysis in the investigation of trace element metabolism, of which some examples are given here, are part of a relatively new area of research and, consequently, the results are still incomplete. It is to be hoped, however, that with the further development of this field of study neutron activation analysis will be of great service in establishing the role of trace elements in animals and man and in assessing the significance for human health of the changes in trace element concentrations in our environment.

References

1. D. BEHNE, P. BRÄTTER, C. KELLER, U. RÖSICK, 11th Intern. Symp. on Radioaktive Isotope in Klinik und Forschung, Bad Gastein, Austria, 1974. Strahlentherapie, Sonderband No. 74, p. 475.
2. D. BEHNE, P. BRÄTTER, W. VORLAENDER, to be published.
3. D. BEHNE, W. ELGER, W. SCHMELZER, M. WITTE, Bioinorg. Chem., (in the press).
4. D. BEHNE, G. HUBE, F. MAJOR, to be published.
5. W. SCHMELZER, D. BEHNE, in Progress in Isoelectric Focussing and Isotachophoresis, P. G. RIGHETTI (Ed.), North-Holland Publishing Company, Amsterdam, 1975, p. 257.

Journal of Radioanalytical Chemistry, Vol. 32 (1976) 17–23

MULTIELEMENT TRACE ANALYSIS BY ATOMIC ABSORPTION SPECTROMETRY AND NEUTRON ACTIVATION ANALYSIS IN BIOLOGICAL MATRICES

M. GALLORINI, M. DI CASA, R. STELLA, N. GENOVA, E. ORVINI

Centro di Radiochimica e Analisi per Attivazione del CNR, Istituto di Chimica Generale, Università di Pavia, 27100 Pavia (Italy)

The following elements: Cr, Zn, Co, Cd, Mn, V are determined in a sample of NBS (spinach) which has to be certified as a new standard. Both neutron activation analysis and atomic absorption spectrometry are used; a good agreement is found among the different techniques. Different procedures of samples chemical dissolution are compared.

Introduction

One of the most important problems in the field of trace element analysis is to have a standard matrix which fits the requirements of homogeneity, reproducibility, easy dissolution. The NBS Laboratory is making a great effort in preparing and delivering to laboratories involved in trace analysis studies the most suitable samples covering a wide spectrum of different matrices.

As a part of a program devoted to the evaluation of trace elements in food, we assayed for the same elements the NBS standards "spinach" and "orchard leaves". They reproduce, more closely than any other, such matrices as cereals and vegetables which were the objects of the above mentioned research.

Neutron activation analysis and atomic absorption spectroscopy were used to determine Cr, Cd, Cu, Mn, Zn, and Co; the first technique was the only applied to evaluate V content.

Experimental

Atomic absorption measurements

The following procedure was adopted to run atomic absorption measurements. Weighed fractions of the liophilized and finely powdered standard were dissolved by wet attack. $HNO_3/HClO_4$ mixture (3:1 volume ratio) was

chosen as the most effective dissolving medium. A white residue, probably $KClO_4$, is left at the end of the attack: the activation analysis showed that none of the investigated elements is absorbed by the residue, so we could discard it by spinning the solution at the end of dissolution. The procedure which employs H_2O_2 120 vol./HNO_3 mixtures gave lower results for Cr[1] and Co which reportedly show large variations depending upon the type of sample preparation procedures used.

Acid digestion in a Teflon lined Parr bomb led to a response which fairly agreed with the $HNO_3/HClO_4$ procedure data for all the investigated elements even for cadmium which is partly lost by volatilization (15%) in the $HNO_3/HClO_4$ attack of both "spinach" and "orchard leaves".

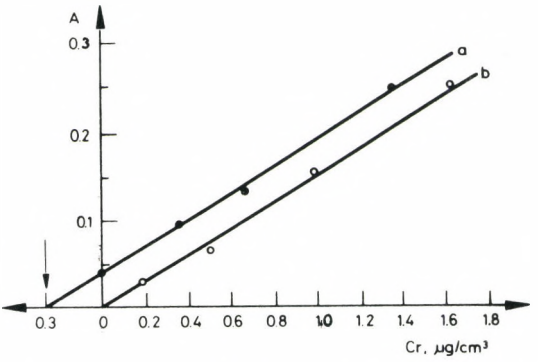

Fig. 1. Chromium by atomic absorption. Curve a – determined by the additions method; curve b – calibration curve

Care was taken in preparing standard dilute solutions just prior to use, in order to avoid surface adsorption effects which may lead to significant losses in concentration especially in the case of Cr.[2]

The linearity of the atomic absorption response to the element content was tested by adding varying measured amounts of the elements to a fixed amount of the "spinach" or "orchard leaves". The usual dissolution by $HNO_3/HClO_4$ mixture was accomplished on the doped samples. Linear responses were found for Co, Mn, Cu, Cr, Zn and Cd, as example curves are reported in Figs 1, 2 and 3 for the last three elements.

Care was taken in avoiding that the solutions could dry and reach a temperature higher than 150 °C at which cadmium volatilization becomes relevant.

Sample attack using a Teflon lined bomb is recommanded when Cd is to be determined, muffle ashing is for Cd the less reliable method of attack as it produces the higher, though constant, metal losses. Atomic absorption measurements were carried out by a Jarrel-Ash instrument using a water cooled burner with a 10 cm slot and an air acetylene flame.

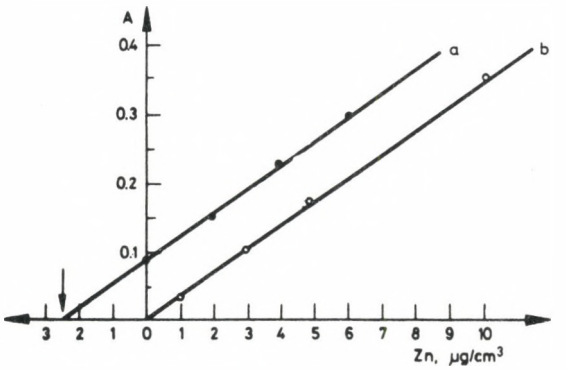

Fig. 2. Zinc by atomic absorption. Curve a – determined by the additions method; curve b – calibration curve

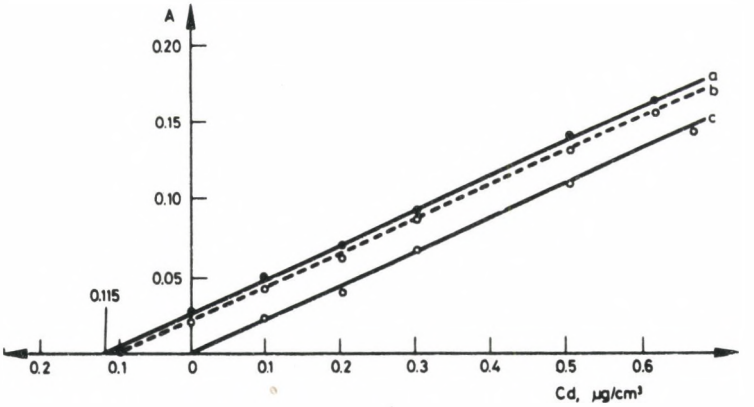

Fig. 3. Cadmium by atomic absorption. Curves: a – determined by the additions method after chemical attack in Parr bomb; b – determined by the additions method after chemical attack in open flask; c – calibration curve

Nuclear activation analysis

Nuclear activation analysis, coupled to destructive radiochemical methods, was used for Cr, Zn and Cd determinations, while V, Mn and Co were determined just instrumentally.

The radioisotopes used in the determinations are given in Table 1, along with necessary nuclear information.

Table 1

Nuclear data for elements determined in standards "spinach" and "orchard leaves"

Isotope	Abundance of parent, %	Cross-section, barn	Half-life	γ-Rays used, MeV
^{52}V	99.8	4.9	3.8 m	1.434
^{56}Mn	100	13.3	2.56 h	0.847, 1.811
$^{115}Cd - ^{115}In$	28.9	1.1	53 h	0.337, 0.528, 0.493
^{51}Cr	4.31	17	27.8 d	0.320
^{65}Zn	48.9	0.46	243.7 d	1.114, 0.510
^{60}Co	100	19	5.26 y	1.333, 1.173

Vanadium was instrumentally determined by irradiating 100 mg samples sealed in plastic vials for 2 minutes. Irradiations took place in the rabbit system of the LENA reactor of the University of Pavia at a neutron flux of $2.4 \cdot 10^{12}$ n $\cdot$ cm^{-2} $\cdot$ sec^{-1}. 2 min irradiation was found to be the most suitable irradiation time in order to reduce background noises without affecting the sensitivity. Same samples were 2 hrs later counted for Mn evaluation. Longer irradiations, up to 30 hrs, and samples sealed in high purity quartz vials were used for Co determination.

Radiochemical procedures

Several radiochemical methods based on solvent extraction[3, 4] ion exchange resins[5, 6] and CrO_2Cl_2 distillation were tested for chromium separation. Extraction with 5% tribenzylamine (TBA)[3] in chloroform was found to be the easiest and most selective method.

Samples, weighing 100-200 mg, were sealed in quartz vials and together with $K_2Cr_2O_7$, $ZnSO_4 \cdot 7H_2O$ and Al/Cd alloy 0.2% in Cd standards.

irradiated for 20 hrs in the TRIGA Mark II reactor at a neutron flux of $8 \cdot 10^{12}$ n $\cdot$ cm^{-2} $\cdot$ sec^{-1}.

After a cooling time of two days the vials were crushed in a Teflon lined Parr bomb, 10 mg of Cr(III), Zn and Cd were added and a mixture of HCl/HNO_3 (6:1) was used to dissolve completely the sample at 140 °C for 1 hr. The chemical attack into Parr bomb insures a complete leaching of quartz and therefore was adopted instead of the attack in open beaker. The solution is transferred to a Teflon beaker and divided into two equal fractions. Chromium is oxidized to Cr(VI) with hot concentrated perchloric acid into the first fraction. The solution is evaporated, then made 1N in HCl, shaken twice with an equal volume of 5% TBA in $CHCl_3$. The combined organic phases are equilibrated with 10 ml of 2N NaOH to back-extract Cr(VI) into the aqueous phase. To the hot solution acetic acid is added dropwise until pH 5.5 is reached; 3 ml of 5% barium acetate are then added and $BaCrO_4$ is precipitated to ensure a good decontamination from Zn.

Barium chromate is filtered, weighed for chemical yield determination, dissolved in hot 2N HCl and gamma-counted.

Zinc and cadmium were determined on the second fraction which was concentrated, brought to 9N HCl and passed through a column filled with

Table 2

Determination of elements by AAS, NAA, INAA in NBS standard orchard leaves

Element	Certified values, ppm	AAS, ppm	NAA, ppm	INAA, ppm
V	0.7			0.9 ± 0.02
Mn	91	96.2 ± 4.8		95.4 ± 2.1
Cu	12	10.3 ± 0.6		
Cd	0.11	0.15± 0.05	0.20 ± 0.08	
Cr	2.5	3.0 ± 0.2	3.2 ± 0.3	3.4 ± 0.5
Zn	25	22.5 ± 0.8	30.5 ± 1.2	
Co	0.11	0.12± 0.05		0.30 ± 0.04

AAS – Atomic absorption spectroscopy.
NAA – Neutron activation analysis.
INAA – Instrumental nuclear activation analysis.

Dowex 2X8. With 0.1N HCl Fe, Co and Cu were eluted. Water was used to elute zinc and finally 3N HNO_3 to elute cadmium.

Last two fractions were counted on the same Ge(Li) detector linked to a 4000 channel analyzer used for the other countings.

Results and discussion

As it may be seen from Tables 2 and 3 where the mean values of five determinations are reported, a satisfactory agreement is found among the different techniques.

It is confirmed that INAA technique, which combines the advantages of rapidity, non destructivity and sensibility must be preferred, if available, to other techniques when the amounts to be determined are in the range at least of the tenths $\mu g/g$. Low precision is obtained in the range of less than 1 $\mu g/g$ both for long and short lived isotopes, as it may be seen from V and Co results.

Table 3

Determination of elements by AAS, NAA, INAA in NBS standard spinach

Element	AAS, ppm	NAA, ppm	INAA, ppm
V			1.20 ± 0.06
Mn	102 ± 3		118 ± 3
Cu	9.1 ± 0.4		
Cd	2.0 ± 0.1	1.7 ± 0.1	
Cr	5.8 ± 0.2	4.5 ± 0.2	5.2 ± 0.5
Zn	72.8 ± 1.3	72.5 ± 1.6	
Co	3.2 ± 0.2		1.7 ± 0.1

AAS – Atomic absorption spectroscopy.
NAA – Neutron activation analysis.
INAA – Instrumental nuclear activation analysis.

*

We wish to thank Prof. M. A. ROLLIER for many useful comments and suggestion.

References

1. W. R. WOLF, F. E. GREENE, 7th Materials Research Symp. 1974, Atti, p. 32.
2. VIR D. ANAND, D. M. DUCHARME, 7th Materials Research Symp. 1974, Atti, p. 33.
3. R. A. NADKARNI, B. C. HALDAR, Radiochem. Radioanal. Letters, 8 (1971) 233.
4. R. K. BROOKSHIER, H. FREUND, Anal. Chem., 23 (1951) 1110.
5. A. L. BONI, Anal. Chem., 32 (1960) 599.
6. T. Z. BISHAY, Anal. Chem., 44 (1972) 1087.
7. H. J. M. BOWEN, Analyst, 89 (1964) 658.

Journal of Radioanalytical Chemistry, Vol. 32 (1976) 25–41

TRACE ELEMENT PATHWAYS FROM ENVIRONMENT TO MAN

G. F. CLEMENTE

Laboratorio Radiotossicologia C. S. N. Casaccia – CNEN
C. P. 2400 – Rome (Italy)

The ultimate purpose of all studies on environmental contamination is to protect human life; as a consequence the knowledge of the trace element pathways from environment to man is of paramount importance because it allows the assessment of a clear relationship between any environmental contamination and its effects on man. To this extent two different kinds of environmental studies will be described in this paper: (a) Studies of the geographic variations on the whole national territory of the natural levels of trace elements in water, food and some human tissues. (b) Studies of selected areas where a critical population group is exposed to abnormal levels of some trace elements. The main trace elements considered are: Co, Cr, Cs, Fe, Hg, Ni, Rb, Sb, Sc, Se and Zn; all the measurements were performed by means of non-destructive neutron activation analysis.

Introduction

A large number of stable elements occur in environment and in living tissues in such small amounts to present many difficulties for the determination of their precise concentrations with the analytical methods formerly available.

Such elements were therefore classified as "trace" elements and this term became widely accepted, although most of trace elements present in biological and environmental materials can now be measured accurately and reliably.

Furthermore no clear line of demarcation can be drawn between the trace elements and the element classified as "major" according to their concentration in biological materials; in practice those elements that occur in environmental samples and living tissues in concentrations expressed in μg/g or μg/l are generally considered as trace elements.

The classification of trace elements into different groups according to their toxicity is inaccurate and misleading; in fact all essential elements can be considered toxic at sufficiently high intake and the margin between levels that are beneficial and those that are harmful may be very small.

At the present time[1] there are 14 trace elements which are believed to be essential to human and animal life (Fe, I, Cu, Zn, Mn, Co, Mo, Se, Cr, Ni, Sn, Si, F, V); the other trace elements which can be normally found in biological materials can be classified, according to SCHWARZ,[2] into other two groups:

(a) likely to be essential or under special consideration;

(b) very unlikely to be essential.

Therefore it is quite probable that in the next future some other elements of the group (a) will be added to the essential elements.

The greatest problem regarding essential elements is to define the levels which are adequate to the well living of humans. Experimental data obtained on animals can be extrapolated to man with difficulties and consequently much remains to be learned about the metabolic functions of many essential trace elements and of their practical significance in the health and nutrition of man.

In order to increase our basic knowledge about the functions and the effects of these elements on human life it is extremely important to study

Table 1

Experimental approach for environmental studies on trace element effects on man

(1)	Preliminary choice of the specific area to be studied	
(2)	Determination of the geographic and hydrographic characteristics	
(3)	Study of the environmental levels	(a) in water (b) in air (c) in soil (d) in vegetables (e) in animals (f) in foods
(4)	Final choice of the interested area	
(5)	Determination of the critical environmental pathways and of the critical groups of population	
(6)	Study of the critical groups of population	(a) intake by ingestion (b) intake by inhalation (c) excretion (d) content of the principal tissues
(7)	Epidemiological studies on the critical groups of population	

their geographical world-wide distribution; the knowledge of such a distribution is in fact very helpful to distinguish between the natural levels of trace elements and those levels which are caused upon some local either source of pollution and deficiency.

Furthermore epidemiological studies on populations, living in areas with quite different contents in some trace elements, may led to recognize visible effects on human health which can be attributable to long-term exposure to abnormal trace element concentrations. An example of this kind of analysis is reported in those studies[3-10] on Cr, Zn and Se deficiency effects occurring in some areas with low content of those elements.

Nevertheless studies on the relationship between trace element environmental levels and the development of any particular disease in man present practical problems that are quite difficult to overcome at the present stage of scientific knowledge.

However, these local studies are greatly needed in order to identify all the critical pathways that are responsible of the transfer of the trace elements from the environment to man.

A summary of all steps included in an exhaustive environmental study on trace element effects on man is given in Table 1. The step 1 is clearly dependent on a previous basic knowledge of the geographical distribution at large of the trace elements considered.

As a practical application of all the problems discussed above such a paper will deal with:

(a) Studies on the geographical distribution in Italy of some trace elements in different items of particular interest (e. g. water, foods, human blood etc.).

(b) Studies of a selected area with population groups exposed to abnormal levels of Hg.

Experimental

All samples, enclosed in quartz vials, have been irradiated in the 1 MW Triga Reactor of the Casaccia Nuclear Centre for a time length, variable between 7 and 14 hrs according to the nature of the sample in a thermal flux of approximately $2.6 \cdot 10^{12}$ n $\cdot$ $cm^{-2} \cdot sec^{-1}$. Standard pure solutions of the elements considered were irradiated together with the samples. After irradiation the quartz vials were opened and the samples were transferred to polyethylene containers of various volumes, particularly designed for the gamma-measurements; during the operation the quartz vial

was carefully and repeatedly washed with 0.1N hydrochloric acid in order to remove any portion of the sample casually deposited on the internal surface of the vial.

The weight of the irradiated samples varied among fractions of a gram and various grams, according to the nature and the available amount of the samples. In the greater part of the cases very simple treatments have been given to the samples before irradiation.

A general scheme of the treatments given to all considered samples is reported in Table 2; more detailed information is given in previous papers.[11, 12]

During the collection of all samples particular care was taken to avoid any contamination; furthermore the simpleness of all treatments before irradiation avoids any loss or contamination during that phase of the method.

Table 2
Treatment given to the samples before irradiation and physical form of the irradiated samples

Nature of the sample	Treatment before irradiation	Physical form of the irradiated sample
Water	24 hr sedimentation	liquid
Vegetable	washed and dried in air	solid
Food-stuffs (meat, cheese, egg, etc.)	no treatment	solid
Fruit	washed or pealed	solid
Fish	washed and dissected	solid
Diet (complete meal)	homogenized and liophilized	powder
Sediments	dried in air	powder
Air filter	no treatment	solid
Blood	centrifugated and divided in two portions: (a) serum, (b) red and white cells	coagulated
Hair	washed	solid
Urine	sterilized*	liquid
Feces	sterilized*	solid
Autopsy tissues	sterilized*	solid

*In a gamma irradiation facility (40 Ci ^{137}Cs source); dose to the samples: $\simeq 5$ MRad

The gamma-spectrometer consisted of two Ge(Li) true coaxial detectors of about 10% efficiency and 2.5 keV resolution together with a 4096-channel analyzer (2048 channels for each detector) connected on-line to a DEC PDP 8/L computer. The energy region considered in the gamma-spectra was about 70–2000 keV ($\simeq$1 keV/channel).

The spectra were automatically processed by a program written for the DEC PDP 8/L computer; the output of such a program gives the following data for each peak of the spectrum:

(a) the energy of the peak, in keV;

(b) the net activity, in cpm;

(c) the standard deviation of the net activity, in cpm;

(d) the percentage standard deviation of the net activity, in %;

(e) the number of channels considered for the calculation of the area of the peak;

(f) the full width at half maximum for the single peak, in keV;

(g) an indication whether the peak is asymmetrical (peak due to two or more gamma-lines not resolved by the detector) or double (peak not completely resolved by the detector).

The program is well capable of evaluating the net activity and the errors of double peaks; the asymmetrical peaks were not considered for the elements determination.

The medium-lived (15 – 40 hrs) induced radionuclides were taken into consideration only in those cases where the knowledge of their distribution was recognized of particular importance.

Table 3 gives the values of the nuclear data together with the detection limits for different kinds of samples analyzed. The energies of the gamma lines used for the determination of the induced radionuclides are also given in Table 3; such energies were selected so as to minimize interferences with other peaks.

The only non (n, γ) reactions giving significant contributions are ^{54}Fe(n, p)^{54}Mn, particularly in blood samples, and ^{58}Ni(n, p)^{58}Co which is used to measure stable Ni.

Results and discussion

Natural distribution of trace elements in drinking waters

In Table 4 are reported for some trace elements the ranges and the mean values of the concentrations found in about fifty drinking waters in Italy.[13] The drinking waters analyzed are mainly classified as mineral waters and

Table 3
Nuclear data and minimum determinable amounts for

Element	Nuclide measured	γ-ray used, keV	Water ng/cc
Sc	83.9 d – ^{46}Sc	889	0.003
Cr	27.8 d – ^{51}Cr	320	2
Fe	45.6 d – ^{59}Fe	1095	80
Co	5.26 y – ^{60}Co	1332	0.2
Ni	71.3 d – ^{58}Co	810	20
Zn	245 d – ^{65}Zn	1115	7
Se	120.4 d – ^{75}Se	265	0.7
Rb	18.7 d – ^{86}Rb	1078	10
Sb	60 d – ^{124}Sb	1692	0.05
Cs	2.05 y – ^{134}Cs	796	0.15
Hg	47 d – ^{203}Hg	279	0.5

generally their source is from deep spring waters; these waters are extensively bottled and traded in a large part of the national territory. Surprisingly little data are available in the literature on the activation analysis determination of trace elements in surface, ground or drinking waters. In Table 4 are given the ranges and the mean values found in various drinking waters in the USA[14-16] and the average values for fresh waters reported by TUREKIAN[17] together with the concentration ranges found in the world's large rivers.[18] The data in Table 4 seem to be in quite good agreement, with the exclusion of the high Sb levels found in the USA drinking waters, probably due to some sort of contamination. In Table 5 are given the total average intakes due to drinking water for the trace elements considered, taking into account an amount of 2 liter of water consumed in Italy per day per person.

Natural distribution of trace elements in the Italian diet

A large program, based on the study of the geographical distribution of the trace element content in various items (diet, blood, urine, etc.), collected in different regions of Italy, was recently started by our Laboratory in cooperation with the National Institute of Nutrition. The main purpose

different kinds of samples analyzed

Minimum determinable amount			
Air filter, ng/m^3	Environmental samples, ng/g wet weight	Biological samples, ng/g wet weight	Diet, ng/g wet weight
0.005	0.07	0.03	0.01
4	35	20	10
200	1200	800	400
0.4	1.5	1	0.5
50	300	250	100
15	100	50	30
1.5	10	7	3
20	150	100	30
0.1	0.7	0.3	0.1
0.3	3	2	0.8
1.0	7	5	3

of this program is to correlate in the same population group the trace element dietary intakes with the corresponding concentrations found in some selected human tissues.

The data obtained seem to show a reasonable uniformity of the average trace element daily intakes through the diets collected in three different regions of Italy. In Table 5 the average daily intakes through air, water and diet are compared: these data can be considered as mean natural values in Italy. When environmental contaminations due to any sort of pollution are absent, the negligible influence to the human metabolic balance of the intakes through water and air appears evident. Moreover an important fraction of the inhaled trace elements going into the lungs is deposited in pulmonary tissues in insoluble form, thus accumulating with continuous exposure. Nevertheless, being the absorption and retention in man mainly due to the physico-chemical form of the trace elements ingested or inhaled, the contribution of the intake through water or air to the total metabolic balance in man of trace elements, should be in any case taken into account.

A comparison with the daily dietary intakes in USA [15-16, 19-21] shows very significant differences for Co only: no reasons have been found to explain it. As far as the low Se dietary content in Italy is concerned, it

Table 4
Trace elements in natural waters, ppb

Element	Drinking waters in Italy[13]		Drinking water in USA[14-16]		Fresh water[17]	Wordl's large rivers[18]
	Range	Mean value	Range	Mean value	Mean value	Range
Sc	<0.003 – 0.1	<0.01	–	–	0.004	–
Cr	≤2 – 30	<3	–	–	1	<5 – 80
Mn	<10 – 750	<10	0.4 – 40	3.7*	7	0 – 180
Fe	<80 – 1000	<100	–	–	670	<40 – 1670
Co	<0.2 – 5.4	0.8	<0.3 – 5.3	–	0.2	0 – 5
Ni	<20 – 400	<30	–	–	0.3	0 – 70
Zn	<7 – 504	60	<10 – 47	<38	20	–
			<0.3 – 2160	–		
As	<0.4 – 2	<0.5	0.02	<0.02	2	–
Se	<0.7 – 1	<0.7	–	–	0.2	–
Br	<2 – 390	60	50 – 320	156	20	–
Rb	<10 – 290	<40	<200	<200	1	0 – 10
Sb	<0.05 – 0.6	<0.05	16 – 57	34	1	–
Ag	<0.3 – 10	<0.3	–	–	0.3	0 – 5
Cs	<0.15 – 13	2.2	–	–	0.02	–
Hg	<0.5 – 1.5	<0.5	–	–	0.07	–

* A very high value (40 ppb) was discarded.

Table 5

Average daily intake in Italy of some trace elements through air, drinking water and diet, μg

Element	Intake through inhaled air	Intake through drinking water	Intake through cooked diet
Sc	0.04	<0.02	0.2
Cr	0.2	<6	50
Mn	–	<20	–
Fe	10	<20	10^4
Co	0.008	1.6	9
Ni	<1	<60	<600
Zn	5	120	$8 \cdot 10^3$
As	–	<1	–
Se	<0.02	<1.5	25
Br	–	120	–
Rb	0.5	<80	$2 \cdot 10^3$
Ag	–	<0.6	–
Sb	0.1	<0.1	2
Cs	0.004	4.5	20
Hg	0.05	<1	<20

has been suggested in other papers[8, 12] that in the Mediterranean area the environmental Se could be lower than in other parts of the world (e.g. USA).

In any case the Italian daily intakes of Cr, Fe, Co, Ni, and Zn seem to fulfil the requirements of the essential trace elements, according to the World Health Organization.[1]

Natural distribution of trace elements in the Italian population

In Table 6 are reported the preliminary data regarding the metabolic balance of some trace elements, referred to the Italian population. These data have been obtained by measuring trace element concentrations in biological samples, taken from the same population groups considered for the diet collection; as a consequence the dietary intakes and the data referred to blood, excretion and hair samples are related to the same groups of populations. The data given in Table 6 should be considered as preliminary, because they are referred to three groups only and these groups cannot be considered completely representative of the Italian population as a whole.

Table 6
Metabolic balance of some trace elements in the Italian population

Element	Daily intake, μg	Daily urinary excretion, μg	Total daily excretion.* μg	Blood concentration, ng/cc	Hair concentration, ng/g
Sc	0.2	<0.01	0.2	<0.03	<1
Cr	50	<5	50	<20	$2 \cdot 10^3$
Fe	10^4	<200	10^4	$4 \cdot 10^5$	$300 \cdot 10^3$
Co	9	2	2.5	2	300
Ni	<600	<50	<500	<250	$< 20 \cdot 10^3$
Zn	$8 \cdot 10^3$	500	$8 \cdot 10^3$	$5 \cdot 10^3$	$200 \cdot 10^3$
Se	25	20	25	60	300
Rb	$2 \cdot 10^3$	$1.5 \cdot 10^3$	$2 \cdot 10^3$	$2 \cdot 10^3$	$<4 \cdot 10^3$
Sb	2	<0.3	2	<1	<30
Cs	20	15	20	3	<100
Hg	<20	<2	<20	<5	$1.5 \cdot 10^3$

* These values are very approximate owing to the few samples of feces analyzed.

Nevertheless very significant differences have not been found in the three examined groups, dislocated in quite different parts of Italy, as the trace element contents are taken into consideration. A comparison with the data reported in literature for blood[22] and hair[23] samples, taken from subjects living permanently in USA, shows a good agreement for almost all elements. The Se blood content only can be considered significantly lower in the Italian population than in populations living in other countries (Canada,[24] Sweden,[25] England,[26] USA[27]). Scarce data[28] are available on urinary and fecal excretion of trace elements: in any case the Co urinary excretion, given in Table 6, is an order of magnitude lower than that reported by SCHROEDER et al.,[16] thus confirming the low dietary Co intake in Italy. On the other hand the Co blood concentration reported in Table 6 is not significantly lower than the values recently given in literature,[29,30] as a consequence it can be argued that a Co daily dietary intake of few micrograms is sufficient to give normal values of Co blood concentration in man. Furthermore such low Co dietary intake in a normal healthy population can justify the hypothesis that Co is not essential in human nutrition, other than as an integral part of the vitamin B_{12} molecule (0.04 μg of Co for 1 μg of vitamin B_{12}).

Studies on Hg and Se distribution in a defined environment and in its population (Amiata Mt. Area)

These studies take part of a general survey on Hg and Se pathways from the environment to man, in a particular area of Italy that is well known for its large mineralization due particularly to Hg.

The main aim of these studies is to collect information on the distribution of Se and Hg in the environment and in man and on their reciprocal interaction.

The Se and Hg concentrations have been measured in many environmental samples, diets and in some biological samples such as blood, urine, feces, hair and autopsy tissues. These samples were obtained from selected groups of inhabitants in the area studied, exposed to different degrees and chemical form of Hg contamination. A detailed description of this work is given in previous papers[12,31] and the main results only will be summarized here. In Table 7 is reported the metabolic balance of Co, Se, and Hg in the three population groups studied. A careful examination of these data and a comparison with the results reported in literature suggest the following considerations:

(a) The Hg levels in blood, excretions and hair for non exposed people are in very good agreement with the normal natural value,[32] thus showing

Table 7

Metabolic balance of Co, Se and Hg in the

Group	Element	Daily intake, μg	Daily urinary excretion, μg
Non-exposed subjects	Se	17 **	6
	Co	12 **	0.8
	Hg	26**	4
Workers in a Hg mine	Se	17 **	7
	Co	12 **	0.7
	Hg	–	6
Workers near to the furnaces*	Se	17**	8
	Co	12 **	0.5
	Hg	1000***	265

* The furnaces are used to extract the metallic mercury from the ore.

** Through the diet; the inhaled quantity is negligible.

*** Based on a Hg air concentration of 0.1 mg/m^3 and 10 m^3 of air inhaled during 8 hours working day.

that daily dietary intake of 26 μg of Hg can be considered as acceptable.

(b) The two exposed groups present a Hg internal contamination much higher than the non exposed group; such contamination is particularly evident for the subjects working near to the furnaces where the metallic mercury is extracted. Those subjects are exposed to an inorganic Hg vapour with an air concentration of about 0.1 mg Hg/m^3.

(c) The miners group is not very critically exposed, probably owing to the particular metabolism of the ore dust ingested or inhaled by the miners during working time; in fact the ore dust is heavily retained in lung, if inhaled, or easily excreted, if ingested. Furthermore the exposure to inorganic Hg vapour is, for such group, negligible.

(d) The Se content in blood is more pronounced in subjects with the highest Hg levels. Such a finding can be explained by a more evident retention of Se in the body in presence of elevated Hg intake, probably due to the binding of both Se and Hg to proteins together with sulphur. A close relationship between Hg and Se in various animals and man has been also reported by other authors.[33-36]

Amiata Mt. Area population

Total daily excretion, μg	Blood content, ng/ml	Hair content, μg/g
12	77	0.35
–	1.7	0.11
25	<5	1.8
13	113	0.43
–	1.4	0.08
73	<5-36	4
14	133	0.45
–	0.5	0.08
560	59	25

(e) The Co content in blood is less pronounced in subjects with the highest Hg levels. This result is probably due to a lower retention of vitamin B_{12} and consequently of Co, in presence of high Hg intake. Further studies on this argument are needed for a clear explanation of this effect.

The data on Se and Hg concentrations in various food-stuffs and environmental samples collected in the Amiata Mt. Area have been reported in detail in previous papers.[12, 31, 37, 38] The study of the environmental Se and Hg exposure for the population living in the Amiata Mt. Area and not working in the Hg mining industry, showed no critical pathways and consequently critical groups of subjects have not been detected.

In Table 8 are reported some data on the Hg and Se content in autopsy samples taken from miners of the Amiata Mt. Area.

The Hg content seems to be strictly dependent upon the exposure time, the critical organs being mainly the kidneys and the lungs. The high Hg content found in thyroid is in good agreement with the results reported by KOSTA et al.;[35] unfortunately, when the autopsy samples on subject 1 were taken, it was impossible to separate from the brain tissues the pituitary

Table 8
Mercury and selenium levels in autopsy samples from miners of the Amiata Mt. Area

Subject	Organ	Hg content, μg/g wet weight	Se content, μg/g wet weight	Hg/Se
1	Kidneys	4.6	1.6	2.9
Aged: 61 y	Suprarenal glands	3.3	1.1	3.0
Exposed: >20 y	Thyroid	2.1	0.76	2.8
	Lungs	4.7	0.07	67
	Liver	0.2	0.19	1
	Testes	1.3	0.55	2.4
	Spleen	0.04	0.07	0.6
	Brain	0.16	0.09	1.8
2	Kidneys	0.24	0.27	0.9
Aged: 55 y	Liver	0.05	0.14	0.4
Exposed: 17 y	Brain	0.08	0.06	1.3
	Bone	0.02	0.05	0.4
3	Kidneys	2.8	0.52	5.3
Aged: 58 y	Liver	1.0	0.13	8.0
Exposed: 30 y	Brain	0.2	0.08	2.5
	Bone	0.02	0.04	–
4	Kidneys	3.0	0.68	4.4
Aged: 68 y	Liver	0.2	0.13	1.5
Exposed: 38 y	Brain	0.03	0.04	0.6
	Bone	0.02	0.04	–

glands, which are suspected to be a very critical organ for Hg, as reported in literature.[35] Only the organs reported in Table 8 were available for subjects 2 - 4.

The autopsy data seem to confirm the hypothesis previously suggested of a stronger retention of Se in man when high Hg intakes are present.

Furthermore the lung data given in Table 8 show that the exposure to Se is negligible in miners; as a consequence the high Se content in some organs as kidneys, thyroids, testes is strictly linked to the Hg accumulation.

It was reported in literature[33, 39, 40] that the Se compounds have a protective effect against the toxic action of mercury compounds. Conse-

quently the high Se levels found in some organs of subjects exposed to a particularly high exposure to Hg may be due to such protective effect.

Such hypothesis has been also supported by KOEMAN et al.[36] to explain the 1:1 Hg/Se molecular ratio found in marine mammals.

Conclusions

The present paper shows that much remains to be learned about trace element pathways from environment to man. Furthermore it appears evident that the knowledge of trace element content of foods and of their influence on the human life is at present unsatisfactory. The following conclusions based on the data reported in the paper can be drawn:

(a) When environmental pollution is absent the diet is the main trace element pathway from environment to man: as a consequence an effort has to be made to obtain reliable information on trace element content of foods. Furthermore the establishment of effective systems for monitoring the trace element content of food-stuffs in relation to agricultural and industrial development of any country should be encouraged.

(b) Further studies should be done on the interactions on man among the various trace elements. The influence of high Hg intakes on Se and Co retention in humans has been shown in this paper. In order to obtain more information in that field the human metabolic balance and the concentration in some human tissues, as blood, should be very well known for the trace elements which are considered essential or representing a real or potential hazards to human health (e. g. Cd, Pb and Hg).

(c) Critical groups of subjects exposed to a particularly high intake of some trace elements should be studied in great detail. They offer the unique possibility to study directly on humans the effects of abnormal trace element intake and consequently any effort should be made to select these groups.

Furthermore these studies can be of great help to understand the influence of the physico-chemical form on the human metabolism of the trace element.

*

The kind of study described in this paper requires the cooperation of many individuals and I should like to acknowledge with particular gratitude the contributions of the following: Dr. L. CIGNA-ROSSI and Dr. G. G. MASTINU of the Laboratory of Continental Contamination (CNEN), G. P. SANTARONI of the National Institute of Nutrition, Dr. R. ROSSARO physician of the Hg mine of Abbadia S. Salvatore (Siena, Italy) and Dr. PINCELLI Health Officer of Abbadia S. Salvatore.

References

1. Trace Elements in Human Nutrition, WHO Tech. Report 532, 1973.
2. K. SCHWARZ, Proc. of the Conf. on Nuclear Techniques in the Life Sciences, IAEA, Vienna, 1972, p. 3.
3. W. MERTZ, Physiol. Rev., 49 (1969) 163.
4. C. T. GURSON, G. SANER, Amer. J. Clin. Nutr., 24 (1971) 1313.
5. K. SCHWARZ, Lancet, i (1965) 1335.
6. R. F. BURK, W. N. PEARSON, R. P. WOOD, F. VITERI, Am. J. Clin. Nutr., 20 (1967) 723.
7. D. H. DAYTON, L. J. FILER, C. CANOSA, Fed. Proc., 28 (1969) 488.
8. V. MAXIA, S. MELONI, M. A. ROLLIER, A. BRANDONE, V. N. PATWARDHAN, C. I. WASLIEN, S. EL SHAMI, Proc. of the Conf. on Nuclear Techniques in the Life Sciences, IAEA, Vienna, 1972, p. 527.
9. A. S. PRASAD, A. MIALE Jr., Z. FARID, H. H. SANSTEAD, A. R. SCHULERT, J. Lab. Clin. Med., 61 (1963) 537.
10. V. CAGGIANO, R. SCHNITZLER, W. STRAUSS, R. BAKER, A. CARTER, A. JOSEPHSON, S. WALLACH, Amer. J. Med. Sci., 257 (1969) 305.
11. G. F. CLEMENTE, G. G. MASTINU, J. Radioanal. Chem., 20 (1974) 707.
12. L. CIGNA-ROSSI, G. F. CLEMENTE, G. P. SANTARONI, J. of Environ. Health (in the press).
13. Le acque minerali italiane: gli elementi stabili, Quaderno FAST, GSA/GLR/2, FAST, Milano, 1975.
14. R. L. BLANCHARD, G. W. LEDDICOTTE, D. W. MOELLER, J. Am. Water Works Assoc., 51 (1959) 967.
15. H. A. SCHROEDER, A. P. NASON, I. H. TIPTON, J. J. BALASSA, J. Chron. Dis., 20 (1967) 179.
16. H. A. SCHROEDER, A. P. NASON, I. H. TIPTON, J. Chron. Dis., 20 (1967) 869.
17. K. K. TUREKIAN, Yearbook of Science and Technology, McGraw Hill, New York, 1969, p. 161.
18. W. H. DURUM, J. HAFFTY, Geochim. Cosmochim. Acta, 27 (1963) 1.
19. H. A. SCHROEDER, D. V. FROST, J. J. BALASSA, J. Chron. Dis., 23 (1970) 227.
20. H. A. SCHROEDER, Circulation, XXXV (1967) 570.
21. H. A. SCHROEDER, Arch. Envir. Health, 21 (1970) 798.
22. G. W. LEDDICOTTE, Methods of Biochemical Analysis, 19 (1971) 345.
23. H. A. SCHROEDER, A. P. NASON, J. Invest. Derm., 53 (1969) 71.
24. R. C. DICKSON, R. H. TOMLINSON, Clin. Chim. Acta, 16 (1967) 311.
25. D. BRUNE, K. SAMSAHL, P. O. WESTER, Clin. Chim. Acta, 13 (1966) 285.
26. H. J. M. BOWEN, P. A. CAWSE, Analyst, 88 (1963) 721.
27. W. H. ALLAWAY, J. KUBOTA, F. LOSEE, M. ROTH, Arch. Envir. Health, 16 (1968) 342.
28. I. H. TIPTON, P. L. STEWART, P. G. MARTIN, Health Phys., 12 (1966) 1683.
29. W. H. HALLER, R. FILBY, L. A. RANCITELLI, J. A. COOPER, Proc. of Intern. Conf. on Modern Trends in Activation Analysis, Natl. Bureau of Standards, 1968, p. 971.
30. W. H. HALLER, R. TILBY, L. A. RANCITELLI, Nucl. Appl., 6 (1969) 365.
31. P. CAGNETTI, L. CIGNA-ROSSI, G. F. CLEMENTE, G. P. SANTARONI, Proc. of the Conf. on Recent Advances in the Assessment of the Health Effects of Environmental Pollution, Paris 24 28 June 1974 (in the press).
32. S. SKERFYING, in L. FRIBERG, J. VOSTAL (Eds), Mercury in the Environment, CRC Press, 1972, p. 109.
33. H. E. GANTHER, C. GONDIE, M. L. SUNDE, M. J. KOPECKY, P. WAGNER, OH SANG-HWAN, W. G. HOCKST, Science, 175 (1972) 1122.

34. J. H. KOEMAN, W. H. M. PEETERS, C. H. M. KOUDSTAL-HOL, P. S. TJIOE, J. J. M. DE GOEJI, Nature, 245 (1973) 385.
35. L. KOSTA, A. R. BYRNE, V. ZELENKO, Mercury-Selenium Association in Person Exposed to Inorganic Mercury, in Proc. of the Conf. on Recent Advances in the Assessment of the Health Effects of Environmental Pollution, Paris 24–28 June 1974 (in the press).
36. J. H. KOEMAN, W. S. M. VAN DE VEN, J. J. M. DE GOEJI, P. S. TJIOE, J. L. VAN HAAFTEN, The Science of the Total Environm., 3 (1975) 279.
37. M. A. BOMBACE, L. CIGNA-ROSSI, G. F. CLEMENTE, G. ZUCCARO-LABELLARTE, M. ALLEGRINI, E. LANZOLA, L. GATTI, Igiene e Sanità Pubblica, XXIX (1973) 191.
38 M. A. BOMBACE, L. CIGNA-ROSSI, G. F. CLEMENTE, Proc. of the Conf. on Comparative Studies of Food and Environmental Contamination, Vienna, 1974, p. 341.
39. J. PARIZEK, I. OSTADALOVA, Experientia, 23 (1967) 142.
40. J. PARIZEK, I. OSTADALOVA, J. KALONSKOVA, A. BABICKY, J. BENES, in W. MERTZ, W. E. CORNATZER (Eds), Newer Trace Elements in Nutrition, Marcel Dekker, New York, 1971, Ch. 6.

Journal of Radioanalytical Chemistry, Vol. 32 (1976) 43–50

Charged-Particle and Photon Activation Analysis

CHARGED-PARTICLE ACTIVATION ANALYSIS

STUDIES ON CARBON, NITROGEN AND OXYGEN MAINLY IN SEMICONDUCTOR SILICON

T. NOZAKI,* Y. YATSURUGI,** Y. ENDO**

**Institute of Physical and Chemical Research, Wako-shi, Saitama (Japan)*
***Komatsu Electronic Metals Co., Shinomiya, Hiratsuka (Japan)*

High utility value of charged-particle activation analysis is exemplified by the study on carbon, nitrogen and oxygen in semiconductor silicon. A summary of the present authors' works is shown, and the equilibrium of carbon and oxygen in a silicon melt with ambient carbon monoxide is discussed. Also, a note is given about the chemical separation of ^{18}F for the ^{3}He activation analysis of various matrices.

Introduction

The highest utility value of charged-particle activation analysis is found in the determination of light element impurities in high-purity substances. We have made use of this method for the study of carbon, nitrogen and oxygen in semiconductor silicon. Our aim was not only to establish reliable and sensitive analytical procedures for the three elements but also to measure some physical constants concerning them, to find out their effects on electronic properties of semiconductor silicon, to know their behaviour in its industrial production, etc. Radiotracer techniques and IR spectrophotometry were also used together with the activation analysis.

We have obtained various meaningful results, and have already reported most of them. Carbon and oxygen concentrations in a silicon single crystal have thus been shown to have some correlation with carbon monoxide concentration in ambient atmosphere of the crystal formation. We now study in detail this correlation by determining the equilibrium constant among them

and by then considering kinematical factors in the practical crystal formation of semiconductor silicon.

The methods and techniques used in our study of silicon can be regarded as applicable, with slight modifications, to many other high-purity matrices. We now try to make a manual for the analysis of oxygen in many matrices by ^{3}He activation. We intend to obtain phase diagrams for very low concentrations of oxygen in various high-purity substances by the use of this manual after its completion.

This paper consists of the following three parts: (1) summary of our already-reported works, (2) study of equilibrium between carbon and oxygen in silicon with ambient carbon monoxide in the crystal formation, and (3) note on the chemical separation of ^{18}F for the ^{3}He activation analysis of oxygen in various matrices.

Summary of our already-reported works

Various commercial semiconductor silicons with known histories were collected as the sample. Also, high-purity silicon crystals were grown under various selected conditions for the measurement of the physical constants. The cyclotron of the Institute of Physical and Chemical Research (160 cm, variable energy, ordinary type) was used for activation. About 600 silicon wafers in total have ever been analyzed.

We have so far obtained the following results. (1) Down to a few ppb of carbon and oxygen and 1 ppb of nitrogen have proved to be determined reliably by activation with the reactions of $^{12}C(^{3}He, \alpha)^{11}C$, $^{16}O(^{3}He, p)^{18}F$ and $^{14}N(p, \alpha)^{11}C$, respectively, followed by chemical processes devised for the separation of the product nuclides.[1] (2) Carbon and oxygen contents of semiconductor silicon have been shown to vary significantly depending mainly on conditions of single crystal formation.[2] As for nitrogen, less than always a few ppb was found in unionized state.[3] (3) The phase diagrams of C – Si, N – Si and O – Si systems in extremely low C, N and O concentration ranges have been made clear from the measured solubilities and equilibrium distribution coefficients.[2,3] Coexistence of substitutionally dissolved carbon and SiC particulates is thus shown to be possible. (4) Reliability and accuracy in IR spectrophotometry of carbon and oxygen in silicon have been noticeably improved.[3,4] (5) Combined use of charged particle activation analysis and IR spectrophotometry has enabled us to make the individual determination of the two forms of carbon.[4,5] (Only the substitutional carbon is sensitive to the absorptiometry, but both kinds of carbon are equally activated.) (6) Information about the coagulation state of the SiC particulates has also been given by treatment of the activated sample by

such chemical procedures as to attack the particulates to different degrees according to their coagulation states.[5, 6] (7) Formation of the SiC particulates caused by heat treatment of semiconductor silicon has been found to lower its breakdown voltage with softening of V – I characteristics.[7] (8) Impurities such as N, F, Na, P and Be have been found to evaporate readily from molten silicon, but carbon has been shown to leave it only in the presence of oxygen, forming CO.[8] Based on these studies, we can now infer about the behaviour of impurities in the industrial production of semiconductor silicon.

Equilibrium between C and O in Si with ambient CO

It has been generally accepted that higher carbon and oxygen concentrations in Czochralski silicon crystals than in float zone crystals are due to the higher ambient CO concentration in the crystal formation. Also, evolution of CO has been observed to begin soon after a silicon melt, even when its carbon content is very low, is brought into contact with an oxygen-supplying surface.[8] It is of great importance for semiconductor silicon producers to control carbon and oxygen contents of their products as low as possible. An equilibrium among C and O in a silicon melt and ambient CO is thought to exist, though kinetical factors would usually affect noticeably the C and O contents of the silidified silicon.

Equilibrium constant

As is obvious from the phase diagrams, SiC is the chemical form of carbon coexistible with carbon-saturated silicon and SiO is that of oxygen with oxygen-saturated silicon at its melting point.[2, 3] Hence, the pressure of CO in the reaction of

$$SiC + SiO \rightleftharpoons CO + 2Si \qquad (1)$$

is the same as the pressure of ambient CO in equilibrium with silicon saturated with both C and O. Although no direct measurement of this CO pressure has ever been reported, it can be calculated by the well known thermochemical relation

$$K_p = [CO] = \exp[-\Delta G/RT] \qquad (2)$$

where K_p – equilibrium constant for Reaction (1),
$[CO]$ – pressure of CO,
ΔG – free energy of this reaction,
R – gas constant,
T – temperature.

From the values in thermochemical tables,[9] ΔG is calculated to be 28.6 kcal at the melting point of silicon (1683 °K) and thus K_p is obtained as $2.0 \cdot 10^{-4}$ atm. Uncertainty in ΔG is not clear but can be guessed to be about 5 kcal, which corresponds to an uncertainty as large as a factor of 4.5 in K_p owing to the high temperature.

It is then clear, from the mass action law, that the following relation holds:

$$K_p = \frac{[CO]}{([C]/[C]_{sat})\,([O]/[O]_{sat})} = 2.0 \cdot 10^{-4} \text{ atm}, \qquad (3)$$

where [C] and [O] are concentrations of C and O in silicon, and $[C]_{sat}$ and $[O]_{sat}$ are their saturation concentrations or solubilities. The solubilities at the melting point of silicon are shown in Table 1, together with the equilibrium distribution coefficients.[3] From Table 1 and Eq. (3), the equilibrium constant in question is obtained to be, at the melting point of silicon, as

$$\frac{[CO]}{[C]\,[O]} = \begin{cases} 2.2 \cdot 10^{-7} & \text{for liquid Si} \\ 2.1 \cdot 10^{-6} & \text{for solid Si,} \end{cases} \qquad (4)$$

with uncertainty of a factor of 5, where [C] and [O] are expressed in wt ppm and [CO] is in atm. Table 2 shows C and O contents of solid silicon in equilibrium with ambient CO, as calculated thermochemically, with neglect of their uncertainties.

Table 1
Solubility at the melting point of silicon and equilibrium distribution coefficient

Element	Solubility, ppm		Equilibrium distribution coefficient
	in solid Si	in liquid Si	
C	2.8 ± 0.3	39 ± 4	0.07 ± 0.01
O	32 ± 2	25 ± 2	1.25 ± 0.17
N	0.045 ± 0.010	ca. 60	$7 \cdot 10^{-4}$

Table 2
Equilibrium concentrations for C and O in molten Si and ambient CO at the melting point of Si (calculated)

Element	C, ppm	O, ppm	CO, atm	[SiO] / [CO]
C: Saturation O: Saturation	39	25	$2.4 \cdot 10^{-4}$	8
C: Saturation O: Below saturation	39	[O]	$1 \cdot 10^{-5}$ [O]	8
C: Below saturation O: Saturation	[C]	25	$1 \cdot 10^{-6}$ [C]	0.2 [C]
C: Below saturation O: Below saturation	[C]	[O]	$2 \cdot 10^{-7}$ [C][O]	300/[C]

Experimental check of the equilibrium constant

With care to maintain the system in close equilibrium, silicon crystals of small diameters (20 mm) were slowly grown (0.5 mm/min) by Czochralski's method in argon streams containing CO of given concentrations, which were monitored by gas chromatography. Only a small fraction of the melt was pulled into crystal (about 100 g from 1700 g melt).

The crystals were cut into wafers, and their C and O contents were measured by charged particle activation. The two elements showed fairly homogeneous distributions in the crystals. Some of the experimental data are given in Table 3. The discrepancy between the measured and calculated

Table 3
Equilibrium between C and O in Si with ambient CO

Sample. No.	C, ppm	O, ppm	CO, atm	[CO] / [C][O]
1.	1.7	9.0	$2.0 \cdot 10^{-4}$	$1.3 \cdot 10^{-5}$
2.	1.6	10.0	$2.8 \cdot 10^{-4}$	$1.7 \cdot 10^{-5}$
3.	1.0	8.5	$1.4 \cdot 10^{-4}$	$1.6 \cdot 10^{-5}$
Calculated				$2.1 \cdot 10^{-6}$

equilibrium constants is regarded as not very serious, when the uncertainty in the latter and some inevitable deviation from equilibrium in the crystal formation experiment are taken into account.

Discussion

The volatility of SiO makes the equilibrium difficult to be maintained in the practical production of silicon single crystals. Charged-particle activation analysis indicated that in the course of practical crystal formation,

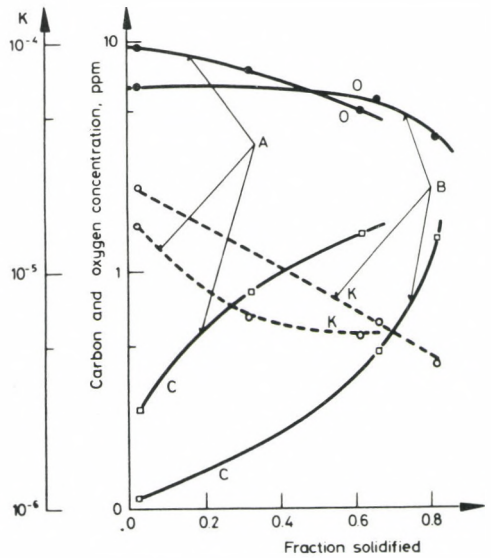

Fig. 1. Distribution of carbon and oxygen in Czochralski silicon crystals. □ – Carbon concentration, × – oxygen concentration, ○ – K = [CO] / ([C] [O]) in atm/(wt ppm)^2. Ambient CO: Crystal A, $5 \cdot 10^{-5}$ atm, Crystal B, $2 \cdot 10^{-5}$ atm (both in Ar). Crystal diameter: 30 mm, pulling rate: 0.7 mm/min; total silicon melted: 2 kg

carbon is often continuously incorporated into molten silicon from ambient CO, with no remarkable change of its oxygen content. This phenomenon is more pronounced in float zone melting, especially in the absence of inert gas as the ambient atmosphere, than in Czochralski's process. In such cases, the experimentally obtained equilibrium constant is still larger than that in Table 3. In zone melting in low pressure CO, deposition of SiO on the wall near the silicon melt is observed.

It is also clear that carbon and oxygen contents of silicon crystals are influenced noticeably by the considerable variation of their effective distribution coefficients with conditions in the crystal formation.[2,3] Carbon and oxygen distributions in Czochralski crystals made in CO-doped argon are shown in Fig. 1.

A note on the chemical separation of ^{18}F

Although charged-particle activation analysis is of the highest sensivity for impurity oxygen, only a quite limited number of matrices have ever been analyzed for its sub-ppm levels. This is regarded as due to the difficulty and tediousness in the inevitable chemical separation of the radio-nuclides. The two reactions, $^{16}O(^3He, p)^{18}F$ and $^{16}O(p, \alpha)^{13}N$, can be used for the oxygen analysis, but the latter is less useful because of the short life of ^{13}N (T = 10 min). In order to make a manual for the ^3He analysis of oxygen in various matrices (Al, Ti, Fe, Cu, Ge, Zn, Ag, Pb, U, stainless steel, etc.), we should find out proper methods of surface etching, sample dissolution and chemical separation.

Most matrices have proved to be decomposed satisfactorily by alkali dissolution, acid dissolution within a closed system, or electrochemical dissolution. In acid dissolution, the sample is decomposed in a stoppered bottle of flexible polyethylene after air is squeezed out from it. By electrochemical displacement (e.g., $Zn + Cu^{2+} \longrightarrow Zn^{2+} + Cu$) or by electrolysis without gas evolution on the pole of the sample (e.g., $|Ti(+)|HCl|C(-)|$), the sample can be decomposed without any loss of the ^{18}F.

Separation of the ^{18}F in the resultant solution has been achieved for most matrices by selected combination of the following steps, though strict care should sometimes be taken for complete removal of radio-nuclides formed from the matrix itself (e.g., ^{73}Se from Ge matrix): (1) removal of the matrix from the solution by precipitation, (2) collection of the fluorine as PbFCl or with $CaCO_3$ precipitate, (3) distillation of the fluorine as H_2SiF_6, and (4) adsorption of the SiF_6^{2-} on anion-exchange resin or precipitation of the fluorine as LiF.

In the adsorption of the SiF_6^{2-}, over its 90% is adsorbed on 1 g resin (strongly basic, 100 to 200 mesh, Cl-type) from 100 ml distillate instantaneously, together with a limited number of other elements. Since SiF_6^{2-} is inert to oxidation and reduction, the adsorption selectivity is often increased by addition of an oxidizing or reducing agent to the distillate. Carrier recovery is measured precisely by the La^{3+} titration with the aid of a fluoride-sensitive electrode. Before the titration the resin is stirred in a hot NaOH solution (2N), which is then neutralized with CH_3COOH. In the

determination of ppb levels of oxygen, further purification of the ^{18}F is often necessary. Adsorption of interference activities by a Ag_2CO_3 column from the distillate after its neutralization has proved effective for this purpose.

References

1. T. NOZAKI, Y. YATSURUGI, N. AKIYAMA, J. Radioanal. Chem., 4 (1970) 87.
2. T. NOZAKI, Y. YATSURUGI, N. AKIYAMA, J. Electrochem. Soc., 117 (1970) 1566.
3. Y. YATSURUGI, N. AKIYAMA, Y. ENDO, T. NOZAKI, J. Electrochem. Soc., 120 (1973) 975.
4. Y. ENDO, Y. YATSURUGI, N. AKIYAMA, T. NOZAKI, Anal. Chem., 44 (1972) 2228.
5. T. NOZAKI, Y. MAKIDE, Y. YATSURUGI, Y. ENDO, N. AKIYAMA, Bull. Chem. Soc. Japan, 45 (1972) 2776.
6. T. NOZAKI, Y. YATSURUGI, N. AKIYAMA, Y. ENDO, Y. MAKIDE, J. Radioanal. Chem., 19 (1974) 109.
7. N. AKIYAMA, Y. YATSURUGI, Y. ENDO, Z. IMAYOSHI, T. NOZAKI, Appl. Phys. Letters, 22 (1973) 630.
8. T. NOZAKI, Y. MAKIDE, Y. YATSURUGI, N. AKIYAMA, Y. ENDO, Int. J. Appl. Radiat. Isotopes, 22 (1971) 607.
9. E.g., O. KUBASCHEWSKI, E. Ll. EVANS, C. B. ALCOCK, Metallurgical Thermochemistry, Pergamon, Oxford, 1967, p. 226; JANAF Thermochemical Tables, compiled by D. R. STULL et al., distributed from Clearinghouse, USA 1965–1967.

Journal of Radioanalytical Chemistry, Vol. 32 (1976) 51–70

THE YIELDS OF PHOTONUCLEAR REACTIONS FOR MULTIELEMENT PHOTON-ACTIVATION ANALYSIS

T. KATO,* K. MASUMOTO,* N. SATO,** N. SUZUKI*

**Department of Chemistry, Faculty of Science, Tohoku University, Sendai (Japan)*
***College of General Education, Iwate University, Morioka (Japan)*

A comprehensive study on the yields of photonuclear reactions of various types has been performed, and sensitivities and the effects of interferences in multielement photon-activation analysis have been evaluated by bremsstrahlung activation of many elements with maximum energies ranging from 30 to 60 MeV. The applicability and reliability of the method were demonstrated by analyzing standard round-robin samples and then by presenting the elemental abundances in several geological, biological and environmental materials. The method was almost insensitive to matrix effects and was assessed to be promising for nondestructive multielement determination of the materials of wide variety, giving good reproducible results for 20 or more elements.

Introduction

In view of the increasing concern regarding trace element material balances in environment, much effort has so far been paid to develop improved techniques for the measurement of concentrations of many elements in a complex multielement material. Because of its high sensitivity and the multielement capability, instrumental neutron activation analysis has successfully been applied for this purpose, but this method is plagued with very high induced activities from abundant elements or trace species with high neutron capture cross-sections, and is not capable of analyzing all of the elements of interest. Similar advantages are offered also by the photon and particle excited X-ray fluorescence techniques, which are of particular significance in analysis of environmental materials.[1, 2] This method is, however, subject often to suffer from potential matrix effects for which careful correction or standardization will be necessary.

An alternate nuclear method which can meet various requirements of the problem is photon-activation analysis. A substantial feature offered by this method has been summarized by several reviews,[3-6] and the reports con-

cerning the application of instrumental photon-activation technique to the analysis of geological,[7-10] biological[11-14] and environmental materials[15, 16] have also been published previously. Most of these works involved the use of electron energies below 45 MeV. The success of the method appeared strongly to depend on the energy-dependent photonuclear cross-section for the reaction, the photon flux and the duration of exposure. In multielement analysis of a complex material by nondestructive means, however, the inter-element interference problems should also be taken into account. Thus, studies on the reaction yields given at an electron energy and their dependences on excitation energies should provide useful information in designing multielement photon-activation procedure with high-energy bremsstrahlung. A considerable amount of work of this sort with 30 MeV bremsstrahlung has previously been presented along with the sensitivity data derived from irradiations of each pure element from carbon to bismuth.[17] The photon-activation method has also been applied to the multielement determinations in several silicate rocks[9, 10] and biological materials.[14]

This paper deals with further study on the yields of photonuclear reactions, mainly with 60 MeV bremsstrahlung, using a linear electron accelerator of Tohoku University. The relative probability of forming a nuclide from various target elements was discussed from a standpoint of sensitivity and interference in multielement photon-activation analysis. Finally, the procedure with 30 MeV bremsstrahlung was applied to the multielement determination in various specimens involving geological, biological and environmental materials. From the data thus obtained, applicability, reliability and versatility of the method were discussed.

Experimental

Sample materials

For the determination of individual reaction yields, samples were prepared from either pure elements or simple compounds from beryllium to bismuth. The metallic samples were small discs 6 mm in diameter with a thickness of about 0.1 mm. The powdered samples were individually wrapped in small pieces of aluminum foil and made into small discs 6 mm in diameter with thickness less than 2 mm. In order to monitor the bremsstrahlung flux, accurately weighed discs of copper, 0.1 mm thick, were placed on the front and back of each sample and irradiated together with the sample. The ^{64}Cu activities produced by the $^{65}Cu(\gamma, n)^{64}Cu$ processes were used for comparisons. A mean specific activity was used to determine the dose rate of bremsstrahlung to which the sample was exposed. The samples and copper monitors were encapsulated into a silica tube and this unit was placed in a

water-cooled sample holder on the bremsstrahlung beam axis directly behind the photon-producing converter for irradiation.

Several of the intercomparison standard materials were used to check the accuracy and precision of the method. They were the USGS G-1 granite, GSJ JB-1 basalt, NBS SRM-1571 Orchard Leaves and NBS SRM-1633 Fly Ash. The JB-1 and Orchard Leaves were also used as the multielement comparative standards in the later real analyses. Comparative standards used for round-robin materials were the synthetic multielement discs or pellets which were prepared by adding known amounts of trace elements (up to 33) to the matrices of similar compositions and were made into discs or pellets with the same size as the sample to be analyzed. The detail involving elemental composition and preparation of the standards for geological materials was essentially the same as described in our previous reports.[9, 10] Cellulose powder and boric acid were used as matrix materials for Orchard Leaves and Fly Ash, respectively, and, after mixing with the elements of interest, each 1 g portion of these mixtures were compressed into cylindrical pellets with a diameter of 13 mm.

Samples subjected to real analysis in this work were Bruderheim meteorite, Indochinite tektite, several brands of cigarette tobacco and the atmospheric particulate matter collected from ambient air. The meteorite and tektite were finely powdered in an agate mortar, each wrapped in a small pieces of aluminum foil and then made into discs with a diameter of 9 mm and about 4 mm high. The cigarette samples were taken from commercial cigarette packets available on the open markets. The wrapping paper and filters were rejected, and the tobaccos were individually powdered in an agate mortar. They were dried at 90 ^{o}C for 24 h as recommended by NBS for Orchard Leaves.[18] Portions each weighing 1 g were pelletized for irradiation. Atmospheric materials were collected on a 20 x 25 cm format of a Millipore AA membrane filter (0.8 μm pore diameter) by pumping 1000 m^3 air through this filter at 0.62 m^3/min with a high-volume electric vacuum pump. Collections were carried out on the roof of the four-story Miyagi Prefectural Office Building in Sendai, Japan. The air-filter sample was divided into two halves and each half was holded and pelletized as described above. In all cases, the sample and the comparative standards were stacked in a silica tube so that the standards were placed on the front and back of the sample for simultaneous irradiation.

Irradiation

A linear electron accelerator of Tohoku University was the bremsstrahlung source. All irradiations were performed with the high-current accelerating section of the machine, which provided a high-intensity electron current,

the peak current being at least 100 mA, with energies up to 75 MeV. The pulse repetition rate was mostly 200 pps with a pulse width of 3 μsec. The electrons were made to impinge on a 3 mm thick platinum target located 3 cm from the beam exit window. The average beam current was measured at the converter using a current monitor, and found, for typical operating conditions, to be 70 – 100 and 150 – 200 μA at 30 and 60 MeV, respectively. The tube containing the samples was aligned along the beam axis with the front face of the tube. Further detail involving the operation characteristics and the target-sample configuration used for activation was reported earlier.[17] In order to prevent chemical decomposition of organic materials during irradiation, these samples were positioned far from the converter. Under the typical irradiation conditions with a 70 μA beam (on the average) of 30 MeV electrons, no significant damage was observed for a period of up to 2 h at 10 cm, or up to 6 h at 15 cm, downstream from the converter. Irradiations lasted 1 – 6 h.

Radioactivity measurement

The counting equipment consisted of a lithium-drifted germanium detector with a sensitive volume of 33 cm^3, ORTEC Model 8101-0525, and its associated electronics coupled to a 4096-channel pulse-height analyzer made by Toshiba Electric Co. Ltd., Japan. The counting system had a resolution of 2.4 keV for the 1332 keV gamma-line of ^{60}Co. Additionally, a 68 cm^3 Ge(Li) detector, Camberra Model 7200-7600-1423, coupled to a 4096-channel pulse-height analyzer was also used. In the case of a sample in an aluminum wrapper, the wrapping foil was rejected and the content was again wrapped in aluminum foil for gamma-counting. Counting has been made consecutively for increasing intervals over a period of one month or longer. To absorb positrons from a number of positron emitting nuclides, if needed, lucite plates with proper thickness were placed on the front and back of the sample to be measured. Characterization of gamma-rays was obtained from a knowledge of the gamma-ray spectra gained by irradiating pure elements and nuclear data listed in the Table of Isotopes.[19] In obtaining full-energy peak areas, total peak counts were computed and background contributions were subtracted, assuming linear variation of background over the peak of interest. Decay curve analyses were made to check for interferences. To the initial decay rates of the various products, normalizations were applied for dose rate and sample weight.

Yield determination

A yield was defined as the rate of production of a nuclide due to a certain photonuclear reaction in dps at the end of irradiation of one mole of a parent nucleus. This was converted to the corresponding saturation rate. With 30 MeV bremsstrahlung, the dose rate was determined in the same manner as reported earlier,[17] and the yield was expressed in the form of dps/mole · R. In obtaining the yield values at much higher excitation energies, those values for both the $^{65}Cu(\gamma, n)^{64}Cu$ and the $^{12}C(\gamma, n)^{11}C$ reactions were calculated as functions of bremsstrahlung maximum energy by using the tables of the bremsstrahlung spectrum for a thin platinum radiator,[20] energy flux required to produce unit roentgen vs. the photon energy,[21] and excitation functions for the above reactions.[22, 23] For instance, the yield values used as reference at 60 MeV were 2.99×10^6/mole · R for the $^{65}Cu(\gamma, n)^{64}Cu$ reaction and 1.00×10^5/mole · R for the $^{12}C(\gamma, n)^{11}C$ reaction. In a typical operating condition at 60 MeV, a dose rate of $1.37 \cdot 10^7$ R · min^{-1} was obtained at the sample position. This dose rate corresponds to about three times higher than that obtained at 30 MeV. In some cases, proper wet-chemical steps were introduced to separate much lower activities of interest from an irradiated sample.

Abundance determination

The concentrations of each element in 12 samples subjected to analyses were calculated by means of the comparative method. A mean specific activity in terms of the peak areas for any specified gamma-rays from the comparative standards on both sides was used for calculating the abundance of an element in question. In order to provide information on the reproducibility of the method, analyses were performed in duplicate for each of the sample materials.

Results and discussion

Reaction yield

Yields of various photonuclear reactions determined with 60 MeV bremsstrahlung were plotted against the atomic number of the elements as shown in Fig. 1. Fig. 1 covers the yields of the reactions of the types (γ, n), $(\gamma, 2n)$, $(\gamma, 3n)$, $(\gamma, 4n)$, (γ, p), $(\gamma, 2p)$, (γ, pn), (γ, α) and $(\gamma, \alpha n)$. In many cases, a radioactive end-product can be formed through several different reaction paths in an irradiated element. The main reaction

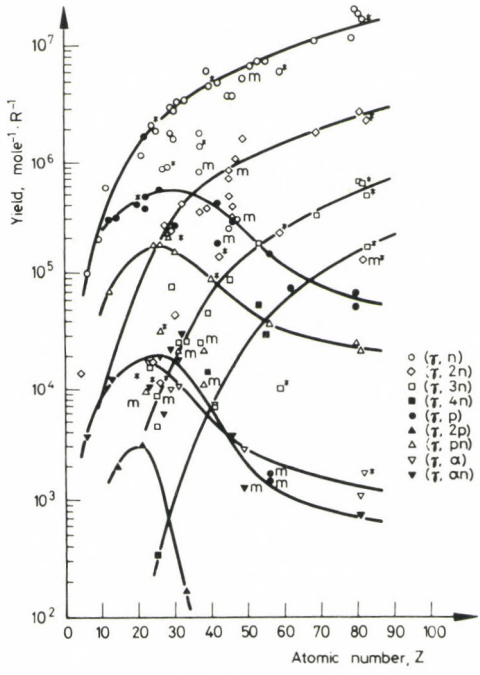

Fig. 1. The reaction yields as a function of atomic number with 60 MeV bremsstrahlung. m – yields of metastable isomers, * – yields for the reactions on target nuclides of neutron or proton magic

path was assumed by considering natural isotopic abundances, mass-thresholds, potential barrier heights and other nuclear effects. In comparing the yield curves obtained here with those obtained previously with 30 MeV bremsstrahlung,[17] the shapes and the magnitude of the yield values for the (γ, n) and (γ, p) reactions are almost similar to each other. As have been observed and discussed earlier with 30 MeV bremsstrahlung, anomalously small yield values were obtained for the reactions on parent nuclides with magic neutron or proton numbers. The yields of metastable state isomers having the large spin differences from the target nuclei are also low in general. The yield of a reaction with the emission of more than one neutron or one proton appears to be strongly energy-dependent. As seen in Fig. 1, the yields for the (γ, xn) reactions appear likely to show almost an order of magnitude decrease with each unit increasing in x. The (γ, 5n) reactions could occur even with 60 MeV bremsstrahlung in certain heavier elements e. g. bismuth. The marked enhancements of the yield values were also recognized for the

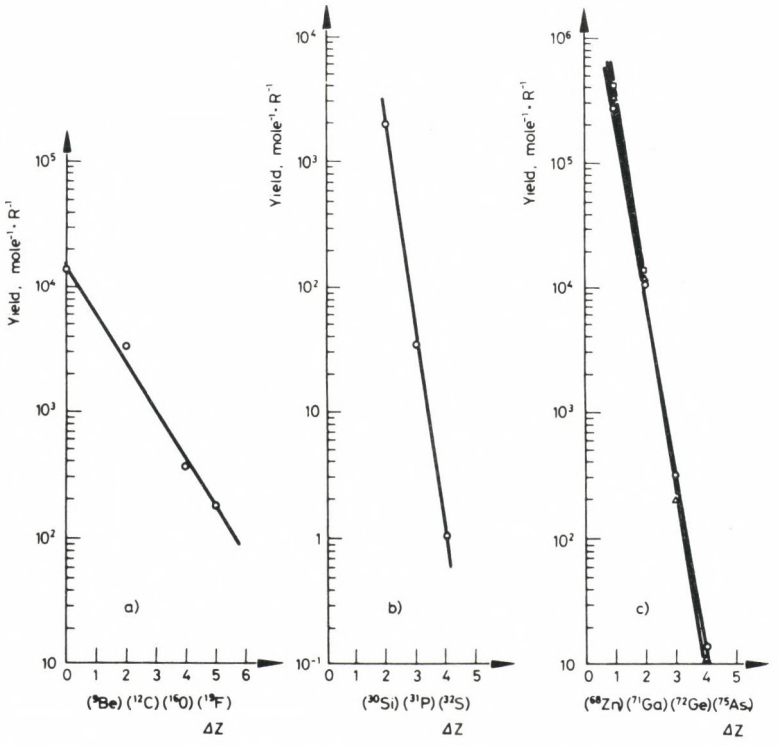

Fig. 2. The reaction yields leading to (a) ^{7}Be, (b) ^{28}Mg, and (c) ^{67}Cu as functions of differences in atomic number between target and product nuclides (ΔZ). □– $E_{\gamma,\ max}$ = 30 MeV, △ – $E_{\gamma,\ max}$ = 45 MeV, ○ – $E_{\gamma,\ max}$ = 60 MeV

(γ, pn) and (γ, αn) reactions which would involve the direct emissions of more energetic photoprotons or photoalpha particles. For several lighter elements, the (γ, 2p) reaction products were measured. Besides the reactions discussed above, several of the other complex reactions with the emission of more particles, up to 9, were observed. The yields for the reactions of such types are, however, very small, and usually found to be less than 10^{3}/mole · R. These reactions are generally of little practical use, but may cause severe interference problems in multielement photon-activation analysis.

Relative probability of forming a nuclide to be used for determination from adjacent elements in the periodic table was then considered. The yields of forming such "fixed" product are shown in Fig. 2 in which the yields of the reactions leading to ^{7}Be, ^{28}Mg and ^{67}Cu were plotted against differences

Table 1
Pertinent nuclear data and

Element	Process	Product nuclide	Half-life	γ-ray used for determination, keV	Other γ-rays observed**
As	(γ, n)	^{74}As	17.9 d	596	634, 1204
Ba	(γ, n) + (γ, γ')	^{135m}Ba	28.7 h	268	
Br	(γ, 2n)	^{77}Br	57 h	521	239, 297, 579
Ca	(γ, p)	^{43}K	22.4 h	374	219, 394, 593,
Ca	(γ, p)	^{43}K	22.4 h	617	990, 1021, 1524 (^{42}K)
Ca	(γ, n)	^{47}Ca	4.53 d	1298	160(^{47}Sc), 488, 808
Ce	(γ, n)	^{139}Ce	140 d	166	
Cl	(γ, n)	^{34m}Cl	32.0 m	2130	2280(DE), 2793(SE), 3320
Co	(γ, n)	^{58}Co	71.3 d	811	
Cr	(γ, n)	^{51}Cr	27.8 d	319	
Fe	(γ, p)	^{56}Mn	2.576 h	847	1811, 2110
I	(γ, n)	^{126}I	13 d	667	386
K	(γ, n)	^{38}K	7.71 m	2170	
Mg	(γ, p)	^{24}Na	15.0 h	1368	1732(DE), 2243(SE), 2754
Mn	(γ, n)	^{54}Mn	303 d	835	
Na	(γ, n)	^{22}Na	2.60 y	1275	1786(sum)
Nb	(γ, n)	^{92m}Nb	10.16 d	934	
Ni	(γ, n)	^{57}Ni	36.0 h	1378	1757, 1918
Pb	(γ, n)	^{203}Pb	52 h	279	401
Rb	(γ, n)	^{84}Rb	33.0 d	881	1076, 1897
Sb	(γ, n)	^{122}Sb	2.80 d	564	1171(^{120m}Sb)
Sr	(γ, n)	^{87m}Sr	2.83 h	388	
Ti	(γ, p)	^{47}Sc	3.43 d	160	
Ti	(γ, p)	^{48}Sc	1.83 d	1314	983, 1040
Y	(γ, n)	^{88}Y	108 d	1836	898
Zn	(γ, p)	^{67}Cu	59 h	185	93.3, 1115(^{65}Zn)
Zr	(γ, n)	^{89}Zr	78.4 h	910	

* See the text for definition.
** SE and DE designate single and double escape peaks, respectively.

detectability of the products

Suitable decay time for measurement	Practical detection limit*		
	JB-1, μg	Orchard Leaves, μg	Air-filter sample, ng/m^3
10 – 15 d	–	0.3	0.4
1 – 2 d	37	–	–
2 – 3 d	–	36	120
1 – 2 d	123	140	85
1 – 2 d	200	190	110
10 – 15 d	470	130	140
30 – 40 d	1.0	–	0.5
30 – 60 m	–	200	90
30 – 40 d	2.1	–	0.6
10 – 15 d	13	–	3.6
2 – 5 h	400	170	85
10 – 15 d	–	0.7	0.5
10 – 30 m	130	2400	280
1 – 2 d	37	41	13
>10 d	5.2	2.5	2.5
>10 d	82	6.9	31
10 – 15 d	0.5	–	–
1 – 2 d	19	1.1	2.9
1 – 2 d	–	7.5	12
10 – 15 d	2.6	0.9	0.6
1 – 2 d	–	0.4	1.1
2 – 5 h	3.9	0.5	0.04
2 – 5 h	3.8	–	5.6
1 – 2 d	130	–	72
>10 d	1.0	–	0.3
2 – 3 d	–	18	20
10 – 15 d	1.1	0.1	1.4

in atomic number between target and product nuclides. For a given product and an excitation energy, the exponential decrease in the yield versus the difference in atomic number is shown. The gradient of the logarithm of the yield against the difference in atomic number increases as the excitation energy decreases. Despite the empirical relationship, these results may prove useful in a general consideration of the selection of an electron energy, as well as of sensitivity and interference in multielement photon-activation analysis.

Sensitivity and interference

Since a yield of photonuclear reaction is strongly energy-dependent, much higher sensitivity can be expected with much higher electron energy. With our accelerator, it can be improved by a factor of 3 for many elements. In nondestructive multielement analysis, however, severe interference problems have often be accompanied with higher electron energies. In our previous work,[9,10,14] therefore, an electron energy of 30 MeV was selected. In Table 1, the elements determinable by multielement photon-activation analysis are given together with the pertinent nuclear data, suitable decay times for measurements and practical detection limits. It is difficult to define the detection limits uniquely, since they strongly depend on the experimental conditions and the matrix nature. In this work, three different standard matrices were selected and the estimation of the detection limits was based on the spectral data of these samples. They were measured at the time intervals shown in Table 1 and were calculated under the criterion in order to validate the peaks. They were the amounts of the elements to give a full-energy peak area which corresponded to three-sigmas of the area under the peak of interest, assuming 30 MeV bremsstrahlung activation for periods of 5 h for JB-1, 2 h for Orchard Leaves and 6 h for air-filter sample, 500 mg of JB-1, 1 g of Orchard Leaves and 500 m^3 of urban air, and detection with a 33 cm^3 Ge(Li) detector. In selecting gamma-rays to be used for determinations, those intense and free from spectral interferences were given prior consideration. The other peaks from same element, where available, were used for confirmations. For several elements, such as calcium and titanium, it was possible to select more than one gamma-ray to obtain precise abundance data. The spectral overlapping problems, where occurring, could normally be resolved by decay analyses. In certain instances, its contribution was calculated and subtracted from the photopeak under consideration. Some comments on these problems will be given later.

When the simultaneous determination of the elements in Table 1 are undertaken, a number of competing reactions can also take place, and, even in the energy region of 30 MeV bremsstrahlung, some of these contri-

Table 2
Interferences in multielement photon-activation analysis with 30 MeV bremsstrahlung

Element to be determined	Nuclide measured	Major competing reaction	-Q, MeV	Effect of interference *
As	^{74}As	$^{76}Se(\gamma, pn)^{74}As$	19.72	$Se/As = 5.5 \cdot 10^3$
		$^{77}Se(\gamma, p2n)^{74}As$	27.14	
Ba	^{135m}Ba	$^{139}La(\gamma, d2n)^{135m}Ba$	29.08	ND**
		$^{140}Ce(\gamma, \alpha n)^{135m}Ba$	11.06	ND**
Br	^{77}Br	$^{78}Kr(\gamma, p)^{77}Br$	8.25	–
Ca	^{43}K	$^{45}Sc(\gamma, 2p)^{43}K$	19.06	$Sc/Ca = 7.2 \cdot 10^1$
		$^{46}Ti(\gamma, 3p)^{43}K$	29.41	ND**
Ca	^{47}Ca	$^{49}Ti(\gamma, 2p)^{47}Ca$	20.77	ND**
Ce	^{139}Ce	$^{141}Pr(\gamma, pn)^{139}Ce$	14.34	ND**
Cl	^{34m}Cl	$^{39}K(\gamma, \alpha n)^{34m}Cl$	20.00	$K/Cl = 3.9 \cdot 10^1$
Co	^{58}Co	$^{60}Ni(\gamma, pn)^{58}Co$	20.02	$Ni/Co = 7.2 \cdot 10^1$
Cr	^{51}Cr	$^{56}Fe(\gamma, \alpha n)^{51}Cr$	19.74	$Fe/Cr = 1.6 \cdot 10^4$
Fe	^{56}Mn	$^{59}Co(\gamma, 2pn)^{56}Mn$	28.12	ND**
		$^{55}Mn(n, \gamma)^{56}Mn$	–	$Mn/Fe = 2.8$
I	^{126}I	$^{128}Xe(\gamma, pn)^{126}I$	17.32	–
		$^{129}Xe(\gamma, p2n)^{126}I$	24.22	–
K	^{38}K	$^{40}Ca(\gamma, pn)^{38}K$	21.42	$Ca/K = 4.9$
Mg	^{24}Na	$^{27}Al(\gamma, {}^3He)^{24}Na$	23.72	$Al/Mg = 2.1 \cdot 10^2$
		$^{27}Al(n, \alpha)^{24}Na$	–	
Mn	^{54}Mn	$^{56}Fe(\gamma, pn)^{54}Mn$	20.48	$Fe/Mn = 1.2 \cdot 10^2$
Na	^{22}Na	$^{24}Mg(\gamma, pn)^{22}Na$	24.11	$Mg/Na = 7.7 \cdot 10^1$
		$^{27}Al(\gamma, \alpha n)^{22}Na$	22.51	$Al/Na = 1.3 \cdot 10^3$
Nb	^{92m}Nb	$^{94}Mo(\gamma, pn)^{92m}Nb$	17.46	$Mo/Nb = 1.7 \cdot 10^3$
		$^{95}Mo(\gamma, p2n)^{92m}Nb$	24.60	
Ni	^{57}Ni	None		
Pb	^{203}Pb	None		
Rb	^{84}Rb	$^{86}Sr(\gamma, pn)^{84}Rb$	20.06	$Sr/Rb = 1.1 \cdot 10^4$
Sb	^{122}Sb	$^{123}Te(\gamma, p)^{122}Sb$	8.14	$Te/Sb = 2.4 \cdot 10^3$
		$^{124}Te(\gamma, pn)^{122}Sb$	17.56	
Sr	^{87m}Sr	$^{89}Y(\gamma, pn)^{87m}Sr$	19.01	$Y/Sr = 5.9 \cdot 10^2$
		$^{92}Zr(\gamma, \alpha n)^{87m}Sr$	14.89	ND**
		$^{90}Zr(\gamma, 2pn)^{87m}Sr$	27.32	

Table 2 (cont.)

Element to be determined	Nuclide measured	Major competing reaction	−Q, MeV	Effect of interference*
Ti	^{47}Sc	$^{51}V(\gamma, \alpha)^{47}Sc$	10.26	V/Ti = $2.4 \cdot 10^1$
		$^{48}Ca(\gamma, n; \beta^-)^{47}Sc$	8.11	Ca/Ti = $6.8 \cdot 10^1$ (after 136 h)
Ti	^{48}Sc	$^{51}V(\gamma, {}^3He)^{48}Sc$	22.62	V/Ti = $1.7 \cdot 10^3$
		$^{51}V(\gamma, pd)^{48}Sc$	28.10	
Y	^{88}Y	$^{90}Zr(\gamma, pn)^{88}Y$	20.20	Zr/Y = $4.3 \cdot 10^2$
		$^{93}Nb(\gamma, \alpha n)^{88}Y$	13.76	ND**
Zn	^{67}Cu	$^{71}Ga(\gamma, \alpha)^{67}Cu$	5.14	Ga/Zn = $1.5 \cdot 10^1$
Zn	^{65}Zn	None		
Zr	^{89}Zr	$^{94}Mo(\gamma, \alpha n)^{89}Zr$	14.04	Mo/Zr = $2.3 \cdot 10^4$
		$^{92}Mo(\gamma, 2pn)^{89}Zr$	24.70	

*See the text for definition.

** Not detected.

butions are seriously dependent on the matrix nature of the sample. These problems are demonstrated in Table 2 in which major competing reactions yielding the nuclides identical to those used for abundance determinations are given. Degrees of their contributions were also determined experimentally by irradiating each pure element with 30 MeV bremsstrahlung. These effects of interferences are given in the last column in Table 2. They were expressed as a ratio of the weights of the elements to produce same amounts of the nuclide under consideration. In some cases, neutron-induced reactions other than the photonuclear processes are the major source of interferences. These interferences will be considered in detail in the later real analyses.

For nickel and lead, competing reactions can not occur energetically with 30 MeV bremsstrahlung activation. The ^{65}Zn activity is also free from competing reactions, but the 1115 keV peak of ^{65}Zn overlaps with nearby 1121 keV peak of ^{46}Sc from titanium. Hence, the interference-free zinc analysis using ^{65}Zn can be performed only for a sample of low titanium content like biological materials.

Multielement determination

Geological materials. In this work, the applicability and reliability of the method in this application with 30 MeV bremsstrahlung

were demonstrated by analyzing 4 kinds of geological materials of different rock types, USGS G-1 granite, GSJ JB-1 basalt, Bruderheim meteorite and Indochinite tektite. The results obtained are shown in Table 3. The analyses were made in duplicate and the results for the standard rocks are the averages with deviations from these values. The average relative deviation for all of the elements determined here based on duplicate samples was ±4%. In comparing our results for G-1 and JB-1 rocks with those reported by FLEISCHER[24] for the G-1 rock and by ANDO et al.[25] for the JB-1 rock, the average of the ranges between them was 8%. Reproducible results were also obtained for 16 elements in Bruderheim and tektite. The elemental abundances in Bruderheim determined by this method are found to be quite similar to those for olivine-hypersthene meteorites reported by GREENLAND and LOVERING.[26] The results for the tektite are also compatible with the general composition of similar materials.[27] Trace amounts of niobium in geological materials can successfully be determined by measuring the 934 keV peak of ^{92m}Nb, but the spectral overlapping with the 934 keV peak of ^{52}Mn produced by the reaction ^{54}Fe(γ, pn)^{52}Mn required the correction for this contribution. This contribution could be estimated and subtracted from combined photopeak by using the 1432 keV peak of ^{52}Mn. It turned out to be 50% for Bruderheim meteorite with very high iron content.

Calcium results in Table 3 are the average values obtained for each of the 374, 617 and 1298 keV peaks. The values obtained from these three different peaks fell within the range from the mean of ±2% for all of the samples studied. For titanum, both the 160 keV peak of ^{47}Sc and the 1314 keV peak of ^{48}Sc were used for quantitations, and the results were given as the average of the values from these two peaks. For most of the geological materials, major interference problems due to competing reactions are the ^{56}Fe(γ, pn)^{54}Mn contribution to the total ^{54}Mn activity in the manganese determination and the ^{27}Al(n, α)^{24}Na contribution to the total ^{24}Na activity in the magnesium determination. The ^{54}Mn activity due to the ^{55}Mn(γ, n)^{54}Mn reaction for a given sample was calculated as reported earlier.[9] A correction of 45% was required for the Bruderheim meteorite, which had the highest iron-to-manganese ratio among the rocks studied. The effects of interferences due to the ^{27}Al(n, α)^{24}Na reaction were corrected by using the value in Table 2 and the literature values for aluminum. A correction of 14.7% was required for G-1 rock which had the highest aluminum-to-magnesium ratio. Interferences from the sources other than the above were also considered and found to be negligible in all of the materials.

Table 3
Elemental abundances

Major constituent, %	USGS G-1 rock	
	This work*1	Recommended value*2
CaO	1.24 ± 0.07	1.39
Fe_2O_3 (Total Fe as)	1.83 ± 0.05	1.94
MgO	0.41 ± 0.02	0.38
MnO	0.034 ± 0.002	0.03
Na_2O	3.35 ± 0.02	3.32
TiO_2	0.26 ± 0.01	0.26
Trace element, ppm		
Ba	1050 ± 5	1200
Ce	207 ± 6	170
Cr	ND	22
Co	2.5 ± 0.1	2.4
Ni	ND	1 - 2
Nb	18 ± 1	20
Rb	203 ± 7	220
Sr	271 ± 6	250
Y	15 ± 1	13
Zr	209 ± 2	210

*1 Average of duplicate analyses. Range is the deviation from the mean.
*2 M. FLEISCHER (1969).
*3 A. ANDO et al. (1974). Consensus averages.
*4 Results of duplicate analyses.

Biological materials. The NBS SRM-1571 Orchard Leaves sample was used to check the accuracy and precision of the method. This standard material was also used as the comparative standard for analysis of tobaccos. The results of elemental abundances in all of the materials studied are given in Table 4. Calcium results are the average values obtained for each of the 374, 617 and 1298 keV peaks. As seen in Table 4,

of geological materials

GSJ JB-1 rock		Bruderheim meteorite[*4]	Indochinite tektite[*4]
This work[*1]	Literature[*3]		
9.35 ± 0.27	9.24	1.77, 1.90	1.98, 2.07
8.74 ± 0.04	8.96	33.7, 33.6	5.19, 5.32
7.96 ± 0.08	7.74	15.7, 16.2	2.06, 2.14
0.14 ± 0.01	0.15	0.314, 0.295	0.093, 0.094
2.73 ± 0.01	2.80	1.09, 1.09	1.32, 1.36
1.21 ± 0.01	1.34	0.11, 0.12	0.82, 0.83
534 ± 50	490	345, 319	413, 440
70 ± 2	67.3	1.2, 3.8	88, 89
424 ± 10	405	3050, 3545	84, 72
42 ± 1	39.1	748, 731	12, 16
129 ± 11	135	14800, 14400	30, 33
15 ± 1	21	1.5, 1.1	11, 11
46 ± 2	41.2	1.7, 1.7	124, 123
448 ± 1	435.2	9.2, 7.1	132, 130
27 ± 1	25.5	3.5, 3.6	3.5, 3.6
144 ± 3	153	6.9, 6.3	333, 336

reproducibility of the method was again satisfactorily good. Our values in Orchard Leaves are also quite compatible with the NBS certified values.[28] When the values from duplicate analyses were averaged and compared with those certified by NBS, the relative deviations from the means based on 9 elements were within 11%. When considering the low aluminum-to-magnesium ratios in ordinary plant materials, the $^{27}Al(n, \alpha)^{24}Na$ interference

Table 4
Elemental abundances of biological materials

Element, ppm unless indicated	NBS SRM-1571, Orchard Leaves		Cigarette tobacco*4			
	This work*1	NBS*2	Imported		Japanese	
			Brand A	Brand B	Brand C	Brand D
As	11 ± 1	11 ± 2	0.9, 1.0	0.8, 0.9	0.4, 0.4	0.6, 0.6
Ca, %	1.97 ± 0.05	2.09 ± 0.03	2.41, 2.41	3.60, 3.52	2.23, 2.15	2.71, 2.59
Cl, %	0.072 ± 0.014	(0.07)	0.57, 0.58	0.47, 0.44	1.05, 1.13	1.45, 1.43
Fe	332 ± 84	300 ± 20	466, 446	851, 806	330, 350	540, 500
K, %	1.45 ± 0.08	1.47 ± 0.03	4.86, 4.92	2.89, 2.87	3.25, 3.33	4.04, 3.97
Mg, %	0.615 ± 0.007	0.62 ± 0.02	0.483, 0.482	0.546, 0.553	0.458, 0.444	0.545, 0.539
Mn	95 ± 4	91 ± 4	176, 178	134, 150	166, 163	227, 216
Na	87 ± 11	82 ± 6	295, 283	119, 202	212, 207	251, 257
Rb	13 ± 1	12 ± 1	14, 14	15, 18	20, 19	30, 30
Sb	3.3 ± 0.2	3.0*3	<0.4	<0.4	<0.4	0.6, 0.5
Sr	37 ± 1	(37)	55, 52	81, 81	84, 80	106, 102
Zn	27 ± 3	25 ± 3	32, 34	26, 30	96, 130	16, 21

*1 Average of duplicate analyses. Error limits are standard deviations based on counting statistics of sample and standards.
*2 Certified values. Values in parentheses are NBS noncertified values.
*3 G. H. MORRISON, N. M. POTTER, Anal. Chem., 44 (1972) 839.
*4 Results of duplicate analyses.

does not cause a serious problem, normally less than 0.1%. As to the $^{56}Fe(\gamma, pn)^{54}Mn$ interference in the manganese analysis, a correction of 3.4% was required for Orchard Leaves.

The elements determined here include essential minor elements such as Ca, Cl, K, Na and Mg, essential trace elements such as Fe, Mn and Zn, and possibly toxic elements such as As and Sb. This method appears likely to provide accurate and precise results for Rb and Sr in biological materials. As seen in the analytical results for cigarette tobaccos, there are considerable variations of the concentrations of the elements from one brand to another. Since minor elements are usually in a highly mobile form, their levels would depend on differences in growing conditions and on different sources including the soil, fertilizers and agricultural sprays. The levels could also have varied by handling processes in the cigarette manufacture.

Environmental materials. Table 5 gives the analytical results for the NBS SRM-1633 Fly Ash and atmospheric particulate materials. Seventeen elements in fly ash and 21 elements in air-filter samples were measured quantitatively. Fly ash from coal-fired, heat-generation source is a matrix characterized by its very high contents of Al, Mg, Ca and Fe.[29] Such composition made it unable for us to determine Cl, I, Pb and Zn that are of considerable environmental concern. These elements could, however, be measured in air-filter samples. Abundance determination of As, Ni and Pb are quite important because of their known toxicities. When our results for fly ash were compared with those reported either by NBS[28] or by ONDOV et al.,[29] the average of the ranges between them was 10%. For fly ash, the $^{27}Al(n, \alpha)^{24}Na$ to the total ^{24}Na activity could be estimated to be 3.7%, and the $^{56}Fe(\gamma, pn)^{54}Mn$ contribution to the total ^{54}Mn activity was 56%. The only element for which the filter-blank value was a problem in this study was Cl. Further results and discussion in this application will be published elsewhere.[30]

Conclusion

Because of the multielement capability and reasonable sensitivity and reliability, photon-activation analysis can be applied to the multielement determination in materials of a broader range as a useful complement to other analytical method. The amount of activation, or sensitivity, is very dependent on electron energy, but the interference problems become serious under such conditions. The yield data for various photonuclear reactions presented in this work should, therefore, be valuable in estimating the relative probability of forming a nuclide of interest from adjacent elements

Table 5
Elemental abundances of environmental materials

Element	NBS SRM-1633 fly ash, ppm unless % indicated		Atmospheric concentration in Sendai, Japan, ng/m^3	
	This work[a]	Literature[b]	Sample 1[c]	Sample 2[d]
As	65 ± 1	61 ± 3	12	1.5
Ca	(5.10 ± 0.03) %	(4.7 ± 0.6) %[e]	15400	2350
Ce	153 ± 1	146 ± 15[e]	8.6	1.6
Cl	–	42 ± 10[e]	570	475
Co	42 ± 3	41.5 ± 1.2[e]	2.7	1.5
Cr	142 ± 9	125 ± 10	20	25
Fe	(4.24 ± 0.19) %	(6.2 ± 0.3) %[e]	8760	1180
I	–	2.9 ± 1.2[e]	10	5.7
K	(1.59 ± 0.05) %	(1.61 ± 0.15) %[e]	1510	1215
Mg	(1.50 ± 0.01) %	(1.8 ± 0.4) %[e]	2730	475
Mn	491 ± 10	495 ± 30	437	77
Na	(0.386 ± 0.013) %	(0.320 ± 0.040) %[e]	5270	1805
Ni	96 ± 3	98 ± 3	13	4.8
Pb	–	70 ± 2	220	166
Rb	95 ± 1	125 ± 10[e]	9.5	0.6
Sb	7.1 ± 0.7	6.9 ± 0.6[e]	3.4	1.8
Sr	1244 ± 6	1700 ± 300	52	5.3
Ti	(0.766 ± 0.007) %	(0.740 ± 0.030) %[e]	1040	163
Y	67 ± 1	62 ± 10[e]	6.2	0.5
Zn	–	210 ± 20	280	215
Zr	298 ± 6	301 ± 20[e]	25	2.6

[a] Average of duplicate analyses. Error limits are standard deviations based on counting statistics of sample and standards.
[b] NBS probable certified values.
[c] Sample collection: 18 – 19 February 1974, 27 h, clear weather.
[d] Average of duplicate analyses. Sample collection: 2 – 3 September 1974, 25 h, cloudy weather.
[e] Ref. 29

in the periodic table. Of the elements determinable by this method, Pb, Y and Zr are the elements to which the instrumental thermal-neutron activation analysis can hardly be applied. Because of a number of elements to be determined, the use of a multielement material with the similar nature of the matrix and the elemental abundances is desired as the comparative standard. The JB-1 basalt and Orchard Leaves can be used better as the comparative standards than the synthetic materials in multielement photon-activation analysis of geological and biological materials, respectively.

*

The authors would like to express their appreciation to members of linac machine and radioisotope groups at the Institute of Nuclear Science, Tohoku University, for their kind cooperation with the irradiations.

References

1. J. A. COOPER, Nucl. Instr. Methods, 106 (1973) 525.
2. J. V. GILFRICH, P. G. BURKHALTER, L. S. BIRKS, Anal. Chem., 45 (1973) 2002.
3. C. ENGELMANN, in J. M. A. LENIHAN, S. J. THOMSON, V. P. GUINN (Eds), Advance in Activation Analysis, Vol. II, Academic Press, London, 1972, Chap. 1.
4. J. HOSTE, J. OP DE BEECK, R. GIJBELS, F. ADAMS, P. VAN DEN WINKEL, D. DE SOETE, Instrumental and Radiochemical Activation Analysis, Butterworths, London, 1971, p. 87.
5. G. J. LUTZ, Anal. Chem., 41 (1969) 424.
6. L. KOSTA, M. DERMELJ, J. SLUNEČKO, Pure Appl. Chem., 37 (1974) 251.
7. R. A. SCHMITT, T. A. LINN, Jr., H. WAKITA, Radiochim. Acta, 13 (1970) 200.
8. J. S. HISLOP, D. R. WILLIAMS, Rept. U. K. Atom. Energy Auth., AERE–R 6910, 1971.
9. T. KATO, I. MORITA, N. SATO, J. Radioanal. Chem., 18 (1973) 97.
10. N. SATO, T. KATO, N. SUZUKI, Radiochim. Acta, 21 (1974) 63.
11. G. H. ANDERSON, F. M. GRABER, V. P. GUINN, H. R. LUKENS, D. M. SETTLE, Nuclear Activation Techniques in the Life Sciences, Amsterdam, IAEA, Vienna, 1967, p. 99.
12. J. S. HISLOP, D. R. WILLIAMS, J. Radioanal. Chem., 16 (1973) 329.
13. R. D. COOPER, D. M. KINEKIN, G. L. BROWNELL, Nuclear Activation Techniques in the Life Sciences, Amsterdam, Vienna, 1967, p. 65.
14. T. KATO, N. SATO, N. SUZUKI, Anal. Chim. Acta, 81 (1976) 337.
15. N. K. ARAS, W. H. ZOLLER, G. E. GORDON, G. J. LUTZ, Anal. Chem., 45 (1973) 1481.
16. A. CHATTOPADHYAY, R. E. JERVIS, Anal. Chem., 46 (1974) 1630.
17. T. KATO, J. Radioanal. Chem., 16 (1973) 307.
18. Provisional certificate of analysis, SRM–1571, Orchard Leaves, National Bureau of Standards, Washington, D. C., January, 1971.
19. C. M. LEDERER, J. M. HOLLANDER, I. PERLMAN, Table of Isotopes, 6th ed., Wiley, New York, 1967.

20. A. S. PENFOLD, J. E. LEISS, Analysis of Photo Cross-Sections, Rept. Physics Res. Lab., Univ. Illinois, 1958.
21. H. E. JOHNS, L. KATZ, R. A. DOUGLAS, R. N. H. HASLAM, Phys. Rev., 80 (1950) 1062.
22. L. KATZ, A. G. W. CAMERON, Canad. J. Phys., 29 (1955) 73.
23. W. C. BARBER, W. D. GEORGE, D. D. REAGAN, Phys. Rev., 98 (1955) 73.
24. M. FLEISCHER, Geochim. Cosmochim. Acta, 33 (1969) 65.
25. A. ANDO, H. KURASAWA, T. OHMORI, E. TAKEDA, Geochem. J., 8 (1974) 175.
26. L. GREENLAND, J. F. LOVERING, Geochim. Cosmochim. Acta, 29 (1965) 821.
27. C. C. SCHNETZLER, W. H. PINSON, Jr., in J. A. O'KEEFE (Ed.), Tektite, Univ. Chicago Publ., 1963, p. 95.
28. P. D. LaFLEUR, J. Radioanal. Chem., 19 (1974) 227.
29. J. M. ONDOV, W. H. ZOLLER, I. OLMEZ, N. K. ARAS, G. E. GORDON, L. A. RANCITELLI, K. H. ABEL, R. H. FILBY, K. R. SHAH, R. C. RAGAINI, Anal. Chem., 47 (1975) 1102.
30. T. KATO, N. SATO, N. SUZUKI, Talanta, (to be published).

Journal of Radioanalytical Chemistry, Vol. 32 (1976) 71–83

THE DETERMINATION OF NITROGEN IN STEELS BY DEUTERON BOMBARDMENT

C. OLIVIER,* M. PEISACH, T. B. PIERCE**

Southern Universities Nuclear Institute, P. O. Box 17, Faure (South Africa)

The measurement of prompt particles from reactions induced by 1.2 MeV deuterons on nitrogen can serve as a rapid method for determining nitrogen in steels in ppm range. With suitable absorbers the energy of the prompt alpha-particles can be reduced to that of the prompt protons and counts from both be integrated over a single energy region. Analyses require between 2 and 100 min. Interference from boron and silicon is discussed.

Introduction

Because of the effects that small concentrations of light elements can have on many materials, there is currently intense interest in analytical methods not only for determining these elements at concentrations in the parts per million range, but also for establishing the sites where these elements occur in the specimen. Nitrogen is one such element where analytical techniques for its determination are tedious and time-consuming. However, recently a nuclear method was described[1] which permitted a position-sensitive technique to be used, capable of providing analytical information on nitrogen in steels. In the described technique successive adjacent sites had to be analysed, with the result that the duration of an entire measurement mitigated against the use of the technique for routine analysis. Attempts to reduce the duration of a scan were made by using a beam of 1.9 MeV deuterons in order to provide the highest yield possible with the available equipment, while still retaining the relatively small extent of interference from matrix components of higher atomic number.

*Permanent address: Department of Chemistry, University of Stellenbosch 7600, Republic of South Africa.

**Permanent address: Applied Chemistry Division, A. E. R. E. Harwell, Oxfordshire, OX 11 ORA, England.

Nevertheless, the concentration range of applicability was not much below about one percent.

In an attempt to satisfy the need for determining nitrogen in the $\mu g/g$ range, a different approach was followed in the present investigation. Instead of using higher bombarding energies to increase the yield of prompt nuclear reaction products, the same effect was achieved by measuring at forward angeles, a method impossible to apply in the scanning arrangement previously used.[1] In this way, bombarding deuteron beams of 1.2 MeV could be used, thereby further reducing the possibility of interference from heavy metal components in the sample.

Kinematic considerations

The prompt charged particles from deuteron-induced reactions on ^{14}N are produced by the nuclear reactions[2]

$$^{14}N(d, p)^{15}N \qquad Q_0 = 8.609 \text{ MeV}$$

$$^{14}N(d, \alpha)^{12}C \qquad Q_0 = 13.575 \text{ MeV}$$

It is clear that there will be an energy difference between p_0 and α_0 particles of a few MeV for deuteron beams of any energy attainable with a 6 MV Van de Graaff accelerator. If these prompt particles are to be used for analytical purposes, their count rates will have to be corrected for the corresponding backgrounds. It is then possible that the improved precision expected through the use of the sum of the counts obtained from the p_0 and α_0 prompt products, will be made poorer by the need to subtract two different backgrounds. If, however, the energies of these prompt products can be made effectively equal, the total count rate will be accumulated over a single energy interval requiring only a single background correction.

With deuterons of 1.2 MeV the maximum energies attainable by the prompt light products from these two reactions (at 0^o) are 9647 keV for the protons (p_0) and 12289 keV for the alpha-particles (α_0). However at these energies the respective rates of energy loss in gold[3] are about 18.4 and 145.4 keV cm^2/mg, so that by an appropriate choice of absorber thickness the energies of the two particles can effectively be made equal. The energy of the p_0 and α_0 prompt particles is shown in Fig. 1 as a function of absorber thickness for a measuring angle of 45^o. Under these circumstances an absorber thickness of about 17 mg/cm^2 gold foil would be sufficient for this purpose. On the other hand the rate of change of energy with measuring direction is greater for the α_0 particles, as is shown in Fig. 2,

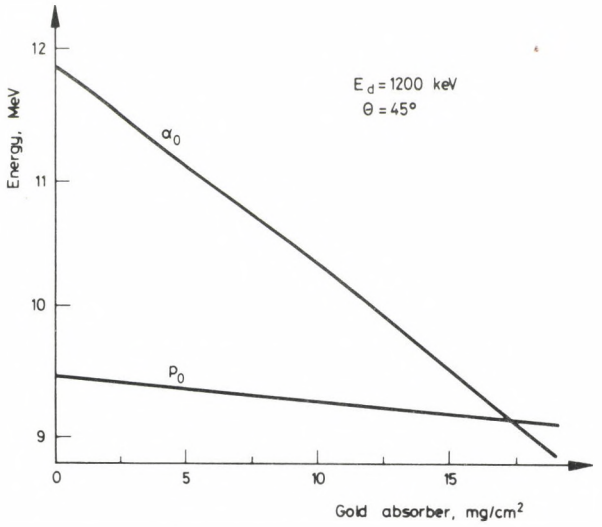

Fig. 1. Energy at the detector of p_0 and α_0 prompt product groups from the deuteron bombardment of ^{14}N, as a function of absorber thickness

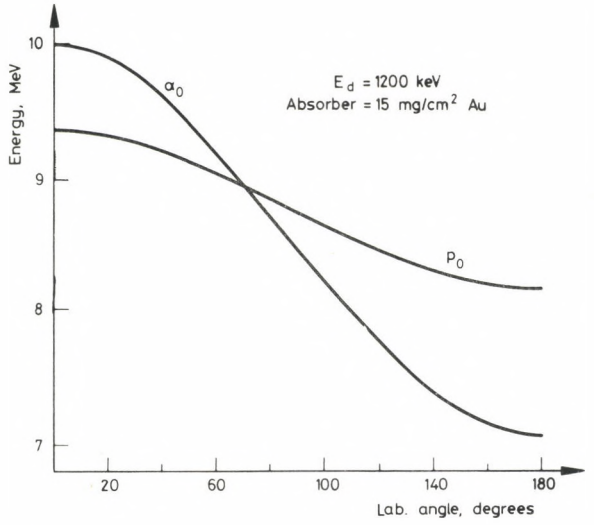

Fig. 2. Energy at the detector of p_0 and α_0 prompt product groups from the deuteron bombardment of ^{14}N, as a function of measuring angle

where the values were calculated for a gold absorber of 15 mg/cm^2. Here, a measuring direction of about 66° would achieve equality in the energies of the p_0 and α_0 products. From the above two examples it is thus evident that with the use of an absorber of about this thickness, equal energies can be attained by suitably adjusting the direction of measurement.

Experimental

Preparation of standards and samples

Steel and metal samples of up to about 25 mm diameter were polished to a mirror-like finish using abrasive powders. They were then thoroughly washed with water containing detergents, under excitation with ultrasonic sound waves, to loosen and eliminate remaining traces of abrasives. Final washings to eliminate organic materials were carried out with hot alcohol and acetone. Standards obtained from the U. S. Bureau of Standards, Washington, and analysed materials obtained from AERE Harwell, were similarly treated. Specimens containing more than 1000 μg/g are considered to be in the high-nitrogen range.

The standard reference materials SRM 1090, 1091 and 1092 of the U. S. Bureau of Standards are issued as rods 6.4 mm in diameter and the analysed specimens R50 and B19 from Harwell, measure 7 mm in diameter. The small physical size of these samples resulted in difficulties at the irradiation stage, where great care had to be exercised to limit the bombarding beam to the sample surface.

Powdered materials, used mainly for qualitative identification were prepared for irradiation by compressing them to pills of 13 mm diameter, under vacuum, to prevent the trapping of air.

Irradiation

Samples for irradiation were mounted on aluminium holders which fitted into an electrically insulated scattering chamber. To allow for measuring the prompt products in a forward direction, the targets were positioned at an angle of 35° to the direction of incidence of the beam. The beam used for this investigation was collimated down to a diameter of 1.7 mm. This resulted in a beam spot on the sample surface, oval in shape with a major axis of about 3 mm. There was thus less than 2 mm on either side of the beam spot for positioning. By focussing with a quadrupole magnet placed immediately in front of the scattering chamber, it was possible to compress the beam spot to nearly circular in shape. The adjustments to the beam shape and positioning of the targets were carried out using a quartz disc mounted on the same target holder, and viewed by television camera.

A liquid nitrogen cold finger of aluminium was positioned immediately in front of the target to condense traces of organic vapours.

To reduce possible contamination from atmospheric nitrogen, purified argon was let into the vacuum chamber during target changes.

Irradiations were carried out using 1.2 MeV deuteron beams of between 80 and 180 nA. Depending on the nitrogen content and the precision required, analyses could be carried out between 2 and 100 minutes.

Measurement

The absolute accuracy of the analyses will depend on the accuracy of measuring the bombarding current. For this reason the scattering chamber was insulated to act as its own Faraday cup, and the target assembly was electrically connected to it. Secondary electron loss could occur only through the beam entrance aperture which subtended a negligibly small solid angle at the target. Secondary electrons from the collimators were prevented from entering the scattering chamber by the antiscatter device.

Prompt particle spectra were recorded by a separately earthed silicon surface barrier detector, mounted behind a gold absorber, but insulated from it with a thin annulus of perspex. The detector was about 20 mm from the bombarded spot on the target and the acceptance solid angle was limited by a collimator of 7 mm in diameter.

A gold foil of nominally 15 mg/cm^2 was used as the absorber, and the measuring angle was adjusted to about 45° where the p_0 and α_0 prompt product groups satisfactorily coincided.

Results and discussion

Prompt particle spectroscopy

The shape of the spectrum from nitrogen was obtained by bombarding barium nitrate, and is shown in the upper portion of Fig. 3. At the bombarding energy used here, the Coulomb barrier effects suppress any noticeable yields from barium, and the only isotope of oxygen likely to yield prompt products in the region of interest is ^{17}O which has a natural abundance of only 0.039 atom% and a Q_0-value for the (d, α) reaction almost 4 MeV lower than that of ^{14}N. Accordingly, the only active component in barium nitrate was nitrogen.

At the high energy end of the spectrum appears a shoulder due to the relatively low yields of the α_0 group from surface layers of the target. Superimposed on it is the sharply rising peak of the p_0 group. The shape of the spectrum is then determined by the excitation functions of these

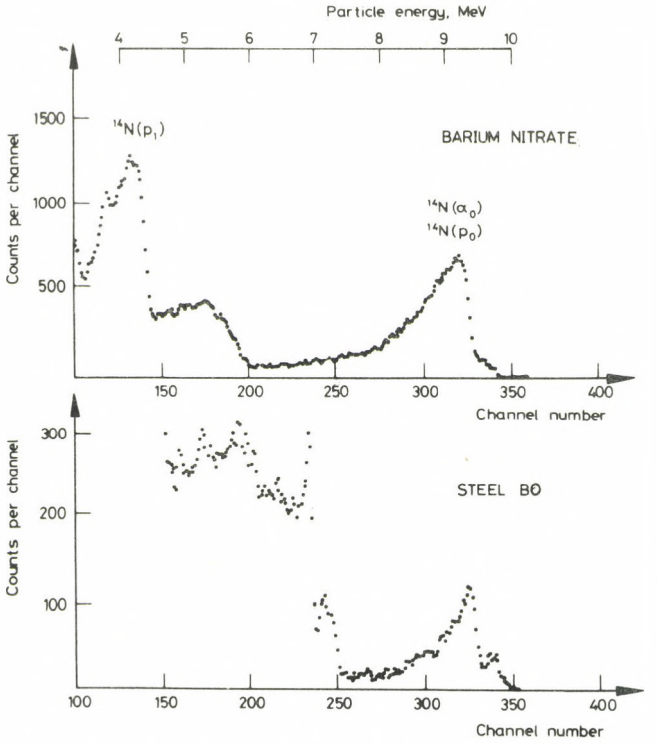

Fig. 3. Prompt particle spectra obtained from barium nitrate (upper curve) and a steel specimen containing nitrogen. The high-energy portion of the spectrum from barium nitrate is entirely due to the nitrogen in the material. E_d = 1.2 MeV, $\theta = 45^o$

two groups. At measured energies between 5 and 6 MeV another broad shoulder appears due to the α_1 group, unlabelled in Fig. 3, followed at lower energies by another sharply rising peak due mainly to p_1 and p_2 groups.

In the lower part of Fig. 3, a spectrum is given of a typical steel specimen containing nitrogen. The difference between the two spectrum shapes below about 7.5 MeV is due to the metal constituents in the steel.

It should be noted that the broadening of spectral peaks due to the absorber is of little consequence with thick targets where the energy losses of the bombarding particles in the target material far exceed losses in the absorber. Accordingly the relatively small loss of resolution due to the absorber does not materially alter the thick target spectrum shape.

Possible sources of interference

The high Q_0-values for both the (d, p) and (d, α) reactions on ^{14}N imply that few other nuclides could yield prompt charged particles in the same energy region. However, the region for integrating counts from nitrogen ranged upwards from about 8 MeV, so that any reaction producing prompt protons or alpha-particles, for which the Q_0-value is within about 1.5 MeV from that of the corresponding reaction on nitrogen-14, could possibly interfere.

The (d, p) reactions with the highest Q_0-values are listed in Table 1 together with the maximum energies of the prompt protons emitted at 45°, and the table extends to reactions with Q_0-values within 2.36 MeV from that of ^{14}N. Only reactions on nuclides that are likely to be found in steels, are included in the table. The elements that are most likely to cause interference are B, Si, S, Ti, V, Cr, Fe and Ni. Spectra of the pure

Table 1

(d, p) reactions most likely to interfere with nitrogen determinations

Target nuclide	Natural abundance, %	Q-value, MeV	Proton energy for E_d = 1.2 MeV and 45°, MeV
^{47}Ti	7.5	9.403	10.482
^{33}S	0.75	9.190	10.224
^{10}B	19.8	9.231	9.937
$^{50}V^*$	0.25	8.828	9.922
^{49}Ti	5.5	8.723	9.816
^{61}Ni	1.1	8.372	9.489
^{14}N	99.64	8.609	9.467
^{29}Si	4.7	8.385	9.415
^{57}Fe	2.14	7.818	8.935
^{53}Cr	9.50	7.496	8.611
^{54}Fe	5.8	7.074	8.195
^{50}Cr	4.35	7.037	8.156
^{58}Ni	68.3	6.775	7.905
^{46}Ti	8.0	6.651	7.764
^{32}S	95.0	6.419	7.451
^{28}Si	92.2	6.249	7.318

*Radioactive.

elements and of their pure compounds were measured for each of these, and some of these spectra are shown as examples, the silicon spectrum is given in Fig. 4, spectra from Ni, Ti and S are given in Fig. 5 and that of boron is shown in Fig. 6 together with a spectrum from a boron-containing steel specimen.

The spectrum from silicon shows that counts obtained in the nitrogen region of interest could possibly be due to nitrogen impurity on the specimen. However, even if all these counts were due to silicon-29, the equivalent

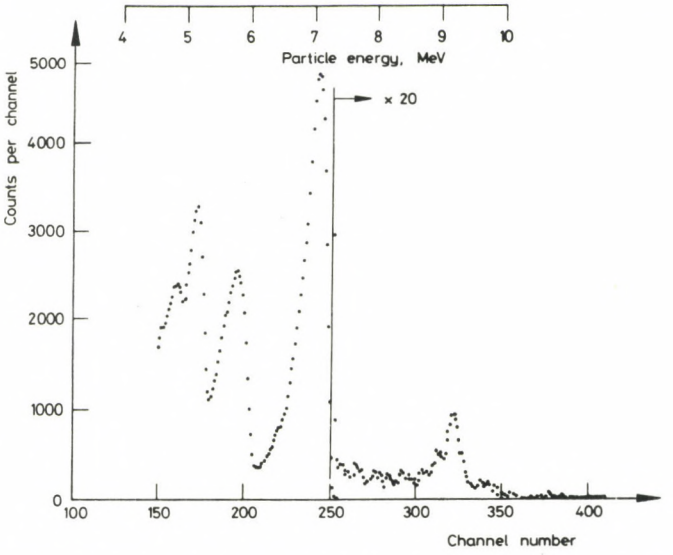

Fig. 4. Energy spectrum of prompt particles obtained from elemental silicon

interference in nitrogen analysis would be only 1.4 μg/g for every 1% silicon content in the metal. However, if the silicon content becomes appreciably greater than this level, curve stripping can be used to eliminate the interference, by reference to the very sharp peak at about 7 MeV.

The spectral shapes of the curves in Fig. 5 are very similar to that obtained for nitrogen at energies above about 8 MeV. There is thus a strong indication that the high energy portions of these spectra were due to nitrogen impurities, especially when the natural abundances of the target isotopes are taken into account (see Table 1). Similar effects were observed for V, Cr and Fe. A further indication that nitrogen was present is observed in the spectrum of sulphur, where prompt protons should have been detected with energies greater than that from nitrogen, but no such evidence was found.

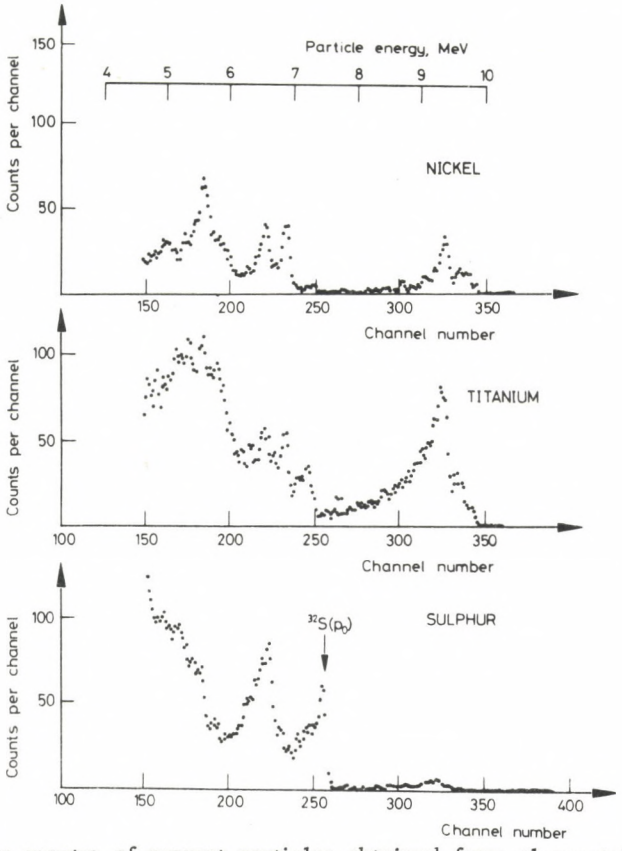

Fig. 5. Energy spectra of prompt particles obtained from elemental nickel and titanium and for sulphur using a lead sulphide target

It is therefore concluded that all specimens analysed contained traces of nitrogen and interference from the bulk specimens was negligible. The exception is the case for boron.

Interference from boron

From Table 1 it is evident that ground state protons induced in boron-10 can produce serious interference when boron is present in steel samples. Furthermore, the only other (d, α) reaction which would yield prompt alpha-particles, with energies approximating to those from ^{14}N, is

$$^{10}B(d, \alpha)^{8}Be \qquad Q_0 = 17.822 \text{ MeV}.$$

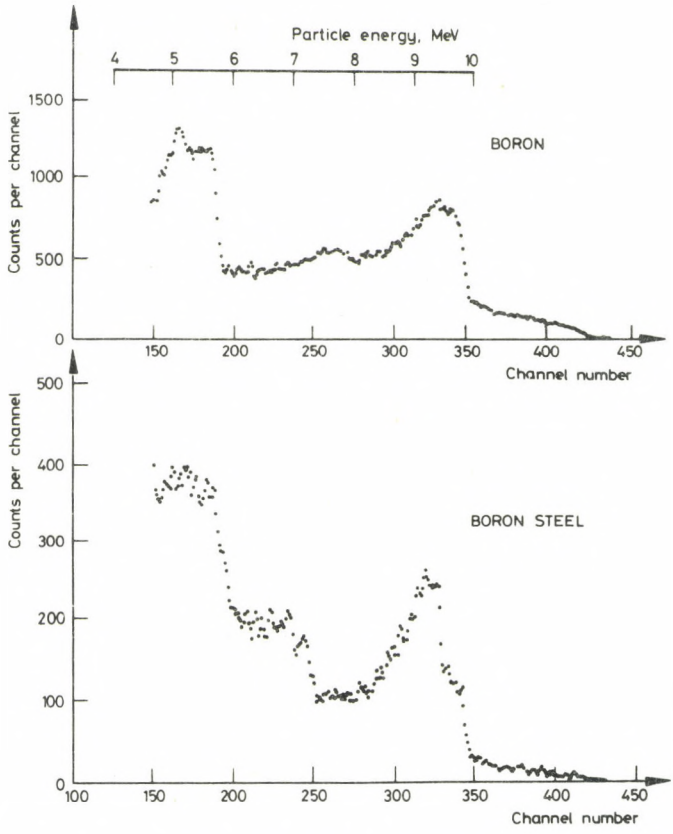

Fig. 6. Energy spectrum from elemental boron (upper spectrum) and that from a boron steel containing nitrogen as well

The energy spectrum of prompt particles from elemental boron is shown in the upper portion of Fig. 6. A comparison between this spectrum and that of nitrogen in Fig. 3 shows that while the main peaks between 9 and 10 MeV interfere mutually, there exists an elongated slope in the boron spectrum due to prompt ground state alpha-particles. It is thus possible, from Fig. 6 to obtain a correlation between the unique high energy yield from boron[4] and the corresponding contribution in the region of integration for nitrogen. This correcting factor can then be applied to steels in which both nitrogen and boron are present. The spectrum for such a case is shown in the lower portion of Fig. 6.

Calibration of the results

The difficulty of obtaining suitable standards in the low-nitrogen range with the required homogeneity was overcome by using analysed steels with much higher nitrogen concentrations. Two such steels containing respectively 0.49 and 0.60% nitrogen by weight were analysed by this method. Thereafter the standard steel specimen, containing about 860 μg N/g, which had the highest nitrogen content in the low-nitrogen range, was analysed and the results were compared with those from high-nitrogen specimens (see Table 2). The calibration values given in the last column of the table refer to integrated counts per mC bombarding beam per unit nitrogen content of 1 μg/g. These values are entirely dependent on the geometrical configuration of the counting assembly and should be separately determined.

Table 2
Calibration of the method

Sample, No.	Results by other methods		Calibration value, counts/mC/ppm
	Nitrogen content	Method used*	
B 19	0.60%	Vacuum fusion	55.1
R 50	0.49%	Vacuum fusion	55.4
SRM 1091	837 μg/g	Micro-Kjeldahl	55.4
	865 μg/g	U. S. B. S. certified	53.6
	871 μg/g	Inert gas value	53.2
	877 μg/g	Vacuum fusion	52.8

*Performed at AERE Harwell, except where otherwise stated.

There is good agreement between the calibration values obtained from the two high-nitrogen steels. This implies that a linear calibration line would pass very near the origin. Confidence in the validity of this calibration is added by the fact that the calibration value for SRM 1091 steel is also in agreement with the other values, depending on the value that is accepted as the nitrogen content of this material. Attempts to obtain data from nitrogen-free blanks were unsuccessful, because in each case the presence of nitrogen was clearly indicated by the shape of the spectrum in the region of interest.

Analyses of standard steels

Standard steels obtained from the U. S. Bureau of Standards and from AERE Harwell were analysed by this method using the calibration obtained above. The results, listed in Table 3, are in fair agreement with those from other techniques within the precision of the method. There is little value in reporting the results obtained from numerous repeat analyses, because the bombarded site either coincided with or largely overlapped previously bombarded sites, and the results thus cannot be accepted as replicates. Measurements with the microbeam technique[1] using 1900 keV deuteron confirmed that these standard samples were not homogeneous, but this, nor the relatively large root mean square error of ±12 μg/g, explain the very high value found for SRM 1090. An alternative analysis on this sample with the microbeam assembly[1] gave a mean value of 58 μg/g.

Table 3
Analysis of standard steels

Sample, No.	Known nitrogen content, μg/g		Found μg/g
	Micro-Kjeldahl	U. S. B. S. value	
SRM 1091	837	865	837[a]
SRM 1090	49	60	126
SRM 1092	–	10	26
BO	37 45[b]	–	39
AP	30	–	45
		Root mean square error:	12

[a]Calibration value.
[b]Vacuum fusion method.

Conclusions

The technique extends the applicability of the method of prompt proton spectrometry to very low nitrogen concentrations in steels. The method is very sensitive for the detection of nitrogen in surface layers of the materials.

*

Financial assistance from the South African C. S. I. R. and Atomic Energy Board is gratefully acknowledged. We would like to thank the staff of the Southern Universities Nuclear Institute for technical help during the experiments. The steel specimens were polished at the Department of Gemology of the University of Stellenbosch.

References

1. C. OLIVIER, J. W. McMILLAN, T. B. PIERCE, Nucl. Instr. Methods, 124 (1975) 289.
2. N. B. GOVE, A. H. WAPSTRA, Nucl. Data Tables, 11 (1972) 127.
3. C. F. WILLIAMSON, J.-P. BOUJOT, J. PICARD, C. E. A. Report 3042, 1966.
4. C. OLIVIER, M. PEISACH, J. Radioanal. Chem., 11 (1972) 105.

Journal of Radioanalytical Chemistry, Vol. 32 (1976) 85–97

Atomic and Nuclear Excitation Methods

AN ION MICROPROBE STUDY OF THE TENSILE FAILURE OF A Pt–Rh–W ALLOY

W. H. CHRISTIE, D. H. SMITH, H. INOUYE

Analytical Chemistry Division and Metals and Ceramics Division,
*Oak Ridge National Laboratory,**
Oak Ridge, Tennessee 37830 (USA)

An ion microprobe has been used to identify silicon as the embrittling agent responsible for the tensile failure of a Pt–30Rh–8W alloy. Silicon was found to be segregated on the grain boundaries of the alloy, and to have a concentration gradient along them from the outer surfaces toward the interior of the sample.

Introduction

One stage in the development of alloys for high temperature applications includes a determination of the thermal stability of the alloy at the anticipated service temperature. Consequently, tensile specimens of an experimental Pt-30Rh-8W (wt %) alloy were aged in an ion-pumped vacuum furnace for 1074 hrs at an average pressure of 10^{-8} torr. The specimens were mounted in an openended Al_2O_3 tube which was maintained at 1100 °C by resistance-heated tungsten wire. The temperature of the specimens was monitored with an Al_2O_3 insulated Pt/Pt-10% Rh thermocouple.

The data in Table 1 show that this particular heat was completely brittle at 1316 °C after the aging treatment, the normal melting point of the alloy is near 2000 °C.

Scanning electron micrographs of the failure region showed complete intergranular failure and a eutectic-like structure on some of the grains. It was obvious that one or more impurities had segregated to the grain

*Operated by Union Carbide Corporation for the Energy Research and Development Administration.

Table 1
Ductility of Pt-30Rh-8W (wt %) aged for 1074 hrs at 10^{-8} torr pressure[a]

Test temperature, °C	Elongation, %	
	Control	Aged
25	44.4	11.2
1316	39.8	0.0

[a] 0.020" thick sheet tested at a strain rate of 0.2 min^{-1}.

boundaries, embrittled the alloy, and depressed the local melting point by about 700 °C.

This report describes the instrument and technique used to identify silicon as the embrittling impurity and the probable source of this contaminant.

Instrumental

The phenomenon of segregation of impurities or solute species to grain boundaries is well known, and several instrumental techniques have been used in investigating it. Field ion microscopy,[1,2] Auger spectroscopy,[3-5] electron microprobe analysis,[6] and ion microprobe analysis[7,8] have all been used to elucidate problems in this area. Survey articles by JOSHI and STEIN[9] and by AUST and CHALMERS[10] discuss the problem in more general terms, the subject to 1964 is well covered by WESTBROOK.[11]

The ORNL ion microprobe (IMMA), manufactured by Applied Research Laboratories,[12] is based on the design of LIEBL.[13] The capabilities of the instrument have been described by ANDERSEN and HINTHORNE[14] and by MCHUGH.[15] The instrument is basically two mass spectrometers. A magnetic analyzer focuses a mass-analyzed primary beam onto the sample surface. The minimum diameter of this primary beam is about 2 μm, current densities of 5 mA/cm^2 are readily attained. Ions formed by various mechanisms in the sputtering process are collected by an extraction electrode and accelerated by an electrostatic lens into a secondary mass spectrometer, where mass analysis of the sputtered ions occurs. To enhance sensitivity, ion detection is achieved in pulse counting mode with a DALY detector,[16] which allows counting of individual ions.

Experimental

IMMA requires a sample with a smooth surface. A rough surface would cause distortion in the electrostatic field of the extraction electrode and unpredictable anomalies in ion extraction efficiencies. The samples for IMMA were mounted in vacuum-worthy epoxy, polished with diamond paste, fixed in the IMMA mounts, and coated with a thin layer of carbon to provide a conducting film to prevent charge buildup on the insulating regions of the sample surface. An O_2^+ primary beam was used in this work because bombardment with an electronegative species enhances ion formation of electropositive elements.[17]

Data were taken in one of three primary beam modes: point mode held the beam fixed on a single spot, X line profile allowed the beam to traverse repetitively a line in the horizontal direction up to ~ 400 μm long, raster mode scanned the beam repetitively over a rectangular area up to $\sim$400 μm x 320 μm in a manner similar to a scanning electron microscope. Sputtering rates ranged from <1 Å per second to several hundred Å per second. The background counting rate during these studies was 1 – 2 counts/sec.

Results and discussion

Fig. 1 is a photomicrograph showing a portion of the fracture surface. The dark circular burn is the result of the spark from a spark-source mass spectrometric analysis, various grain boundaries are clearly visible. The fracture surface was too rough to study directly, so a region on the surface of the alloy some 200 – 300 μm from the fracture region was investigated using a 20 keV O_2^+ analyzing beam. Fig. 2 is a photomicrograph of this region, a grain boundary junction is indicated by the arrow for orientation purposes. Fig. 3 is an ion micrograph of this region taken with the secondary mass spectrometer adjusted to detect the $^{28}Si^+$ beam. Light areas are regions of enhanced $^{28}Si^+$ emission and clearly show the same grain boundary structure observable in Fig. 2, the arrows indicate the same point in each figure. The area of Fig. 3 is 280 μm by 250 μm. Dendritic deposits containing Si are also evident, indicating a high concentration of silicon on the surface of the alloy.

The question now to be answered was that of the source of the silicon on the grain boundaries. Spark-source mass spectrometric analysis of the sample showed that the alloy contained a bulk concentration of 100 ppm Si,[18] making internal migration of silicon to the grain boundaries a

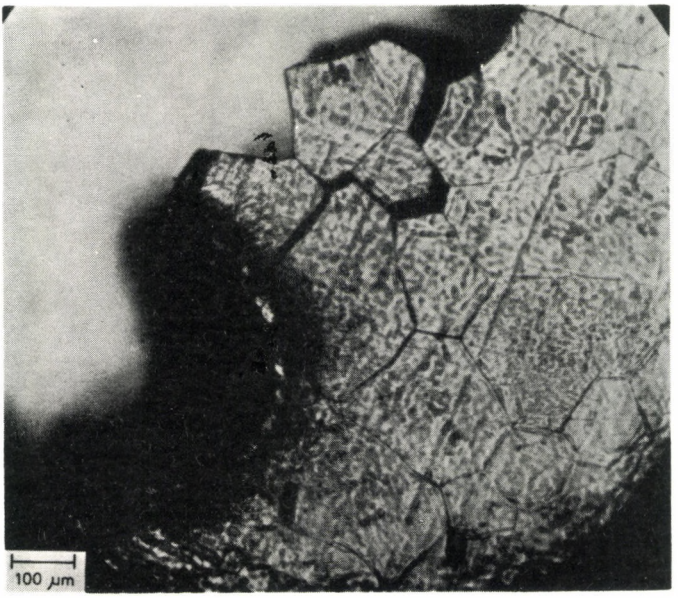

Fig. 1. Optical micrograph showing the fracture surface

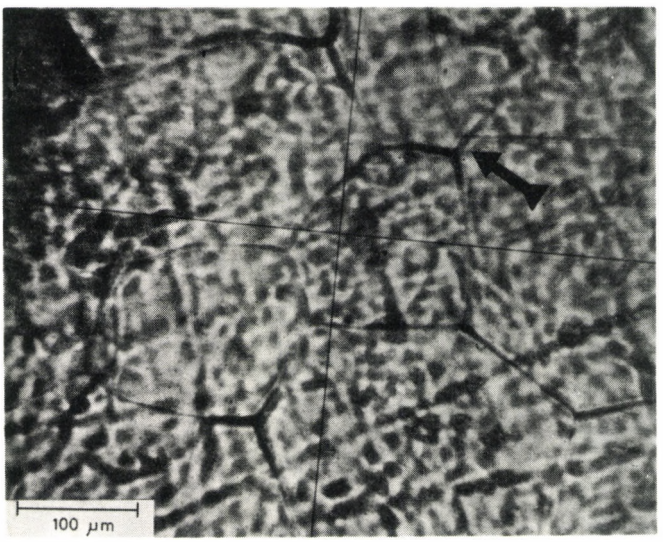

Fig. 2. Optical micrograph of the region analyzed by IMMA, ~250 μm away from the area shown in Fig. 1. The arrow points to a feature also shown in Fig. 3

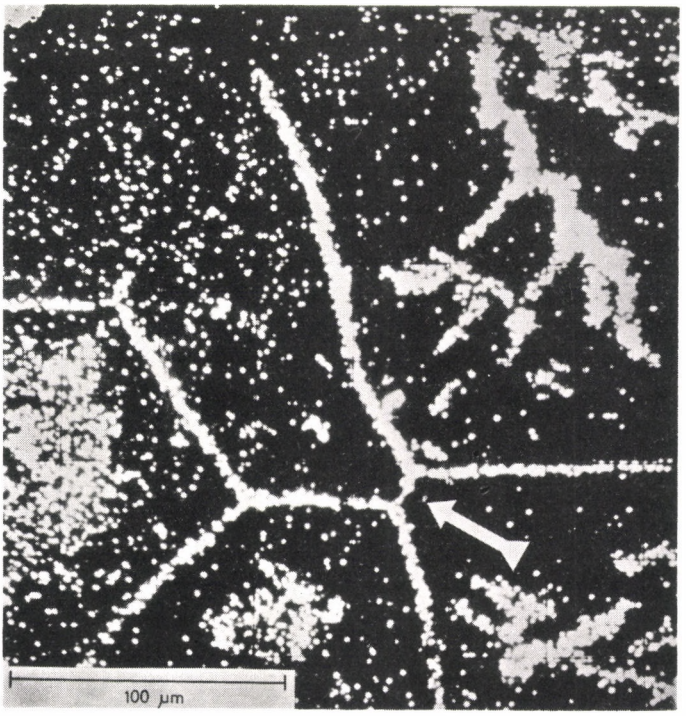

Fig. 3. $^{28}Si^{+}$ ion micrograph of part of the region shown in Fig. 2. The arrow indicates a grain boundary junction also visible in Fig. 2

possible explanation of its segregation there. A second possible origin of silicon was a source external to the alloy. At the temperatures involved (1100 ^{o}C), it was conceivable that Si from the surroundings, e.g., the alumina mount, had migrated into the alloy along the grain boundaries. To resolve this question, a new piece of the same sample was mounted that had been cut at 90^{o} to the original. In this way, the distribution of silicon in the alloy matrix could be observed.

No structure was visible on the surface of the alloy when the conducting carbon film was first sputtered away, but grain boundaries gradually developed under continued bombardment with O_2^+. Fig. 4 is an optical micrograph of a typical region, 280 μm x 250 μm. The photograph reveals a network of grain boundaries and crystallites of varying reflectivity.

Fig. 5 is a $^{28}Si^{+}$ ion micrograph of this region. Concentration gradients of Si^{+} along the grain boundaries from the outer surface into the interior

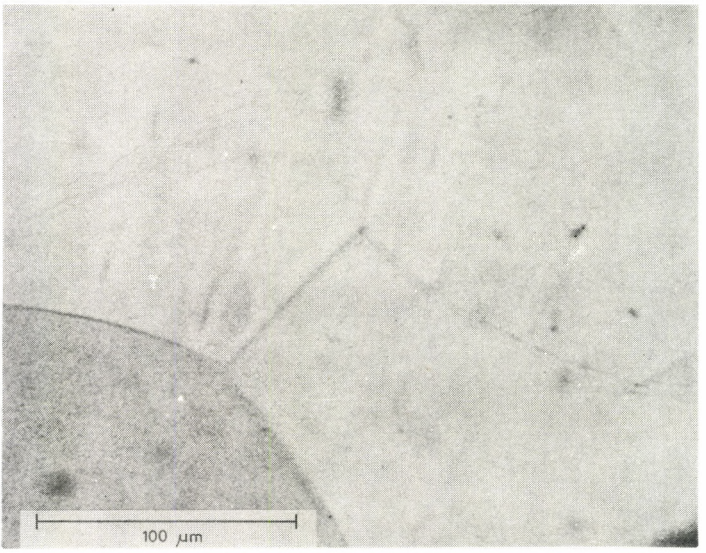

Fig. 4. Optical micrograph of an area on the surface cut at 90° to that shown in Figs 2 and 3. Note the network of grain boundaries

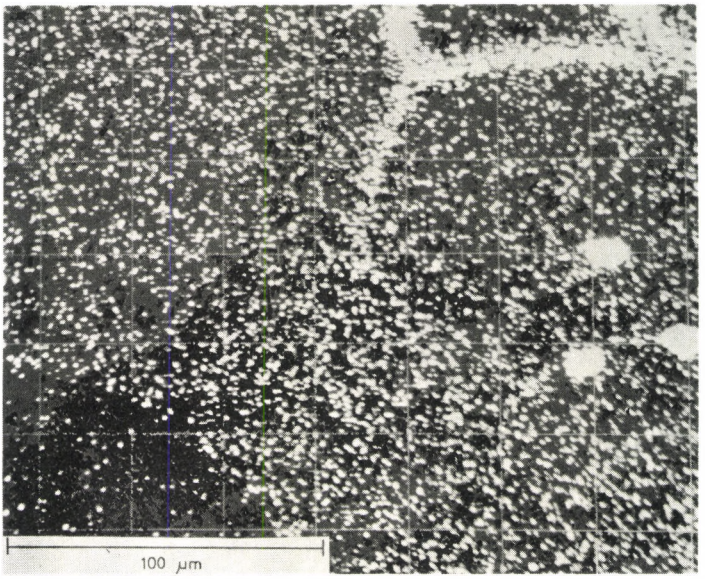

Fig. 5. $^{28}Si^{+}$ ion micrograph of the area shown in Fig. 4. Note the concentration gradients

of the sample are readily apparent. The three bright dots in the right center of the micrograph were correlated optically with specks of surface contamination. Further IMMA investigation revealed them to be magnesium aluminum silicates. Note, in the lower left corner, a crystallite exhibiting markedly poorer ion emission than the rest of the surface. This will be discussed in more detail later.

An attempt was made to arrive at a more quantitative representation of the data than those presented in Fig. 5. A series of concentration profiles was made across grain boundaries at 46 different locations. These data were taken in point mode while mechanically scanning the precision sample stage, which is controllable and reproducible in the X and Y directions to ± 1 μm. Count rates were continuously monitored, and the profiles were taken as nearly normal to the grain boundaries as convenient. These data are presented schematically in Fig. 6. The numbers near some of the points represent the number of counts per second of $^{28}Si^+$ detected at the grain boundary. Each number has been corrected for the bulk $^{28}Si^+$ count rate on either side of the boundary. Most of the count rates have been omitted to avoid unnecessary clutter in the drawing, but in every case $^{28}Si^+$ showed a monotonically decreasing count rate as the beam progressed from the outer surface toward the center of the alloy. Grain boundaries roughly parallel to the outer surface had roughly constant Si concentrations along them, particularly if

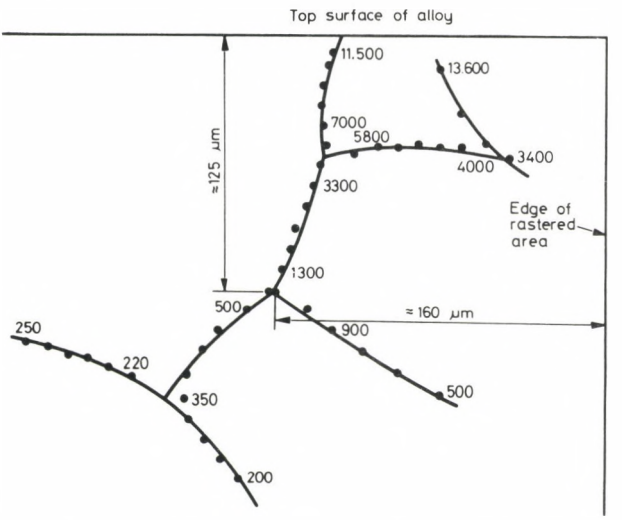

Fig. 6. Schematic drawing of the area shown in Fig. 5. Each dot represents a data point, the numbers at some points show the $^{28}Si^+$ counts above background found on the grain boundary

each end of the boundary connected to others approximately equidistant from the surface. In the center of the alloy (not shown in Fig. 6), count rates along grain boundaries were barely above the bulk rate. At the other outside edge of the sample, however, the same marked concentration gradients were observed.

From these data, it seems clear that the source of the Si was external to the alloy, and that diffusion from the outer surfaces along grain boundaries was the principal mechanism by which silicon was introduced into the matrix.

All other species giving a count rate greater than a few counts per second were investigated, but only aluminum, in extremely low concentration, showed a tendency to segregate on a few grain boundaries, it was not present on all of them. It is probable that some aluminum from the mounting apparatus had migrated into the alloy along with Si.

Since O_2^+ was being used for the analyzing beam, it was not possible to determine the chemical form in which silicon migrated, since any SiO_2^+ or SiO^+ observed could have been formed in the sputtering process. To obtain more data on this question, the O_2^+ primary beam was replaced by Ar^+. A new region, which had never been bombarded with O_2^+, was investigated. An SiO^+ signal larger than that of the Si^+ was observed segregated along the grain boundaries. This suggested that silicon was present as an oxide, but should not be interpreted as definite proof. Not enough is known of the chemistry of the sputtering process to allow a definite statement.

The localization of silicon along grain boundaries points to a very high ratio of the diffusion coefficient along grain boundaries to that through the bulk.[19] Following the presentation of MCLEAN[19] after treatments developed by FISHER[20] and WHIPPLE,[21] the natural logarithm of the concentration (represented by the count rates given in Fig. 6) was plotted against distance along the grain boundary from the surface. The boundary chosen is the leftmost one reaching the surface of the sample (see Figs 5 and 6). The plot is presented in Fig. 7, with the location of a grain boundary junction indicated. The presence of this junction complicates matters by providing alternate paths both for diffusion and enrichment at that point. The FISHER treatment assumes a constant surface concentration of the diffusion material, possibly not valid here. The more rigorous treatment of WHIPPLE also gives essentially a straight line when ln concentration is plotted versus distance. Unfortunately, the value of the lattice diffusion coefficient for Si in the alloy is unknown, making it impossible to calculate a value for the grain boundary diffusion coefficient.

Fig. 8 is a typical silicon concentration profile obtained when the ion beam was linearly scanned across the alloy surface. Two grain boundaries

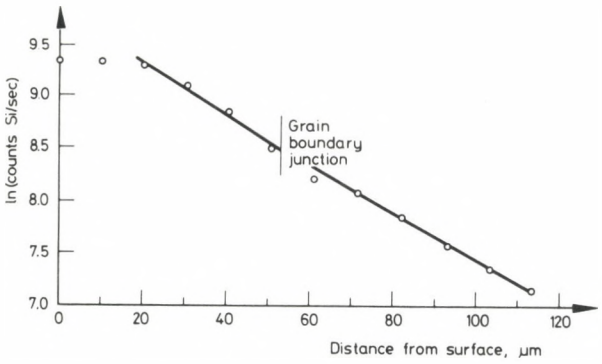

Fig. 7. Plot of the natural logarithm of the concentration vs distance from the surface for one grain boundary

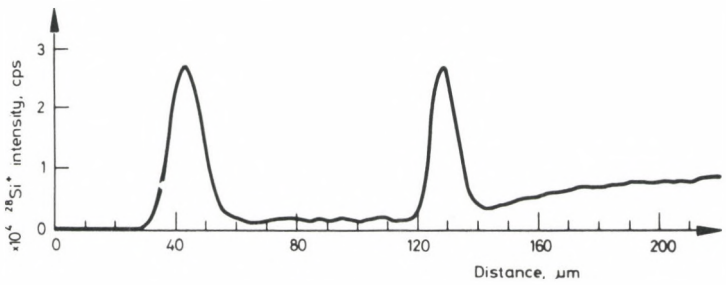

Fig. 8. Concentration profile across two grain boundaries

were intercepted during the scan. The scan length was 210 μm, and the resolving power of the primary beam was 5 μm. The extreme localization of Si on the grain boundaries is apparent. The width of the peak is due to the diameter of the primary beam, the only statement concerning width of the grain boundaries that can be made from these data is that they are less than 5 μm wide. This observation is consistent with field ion microscope[2] and electron microprobe studies,[6, 22] where the width of grain boundaries has been found to be on the order of a few atomic diameters.

Fig. 9 is a $^{56}Fe^{+}$ ion micrograph of the same region depicted in Figs 4 and 5. The various crystallites are clearly defined by their differing ion emission efficiencies. The crystallite in the lower left shows the poorest emission for Fe^{+}, just as it did for Si^{+} (Fig. 5). The direct correlation of the various grains in all three figures is obvious. Ion micrographs of other

species (RhO^+, Pt^+, etc.) show similar variations, with the same regions showing enhanced or decreased emission in each case. These observations clearly indicate that a variation in ion emission as a function of crystal face, rather than as a function of concentration, is being observed. This phenomenon has been previously documented[22-27] with maxima and minima in sputtering being correlated with the density of lattice points.[22, 23, 27] Channeling of the incident beam in the crystal lattice is believed to play

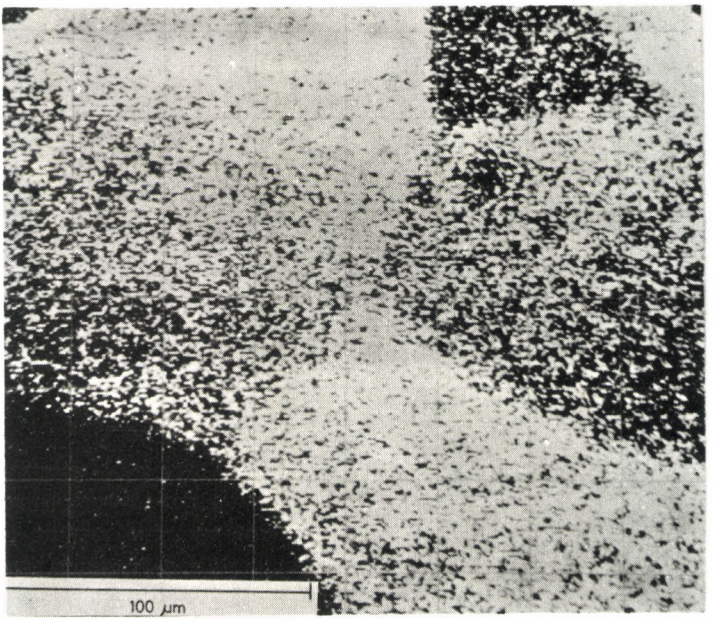

Fig. 9. $^{56}Fe^+$ ion micrograph of the region shown in Fig. 5. Note the variation in ion emission efficiency

the dominant role in the process,[27, 28] with the variation of work function with crystal face also making a contribution.[29] KAMINSKY has reviewed the matter in detail.[28] Inspection of the sample through an optical microscope revealed that the poorest emitting surface (lower left corner in Figs 4, 5, and 9) had the least material sputtered away from it in the course of several hours of rastering. The crystal face perpendicular to the sample surface was clearly visible in reflected light of grazing incidence set at the proper angle, and allowed identification of the grain from which the least material had been sputtered.

Fig. 10. Scanning electron micrograph of a grain boundary. Magnification is 10,000X

Fig. 10 is an electron micrograph of a typical grain boundary after sputtering for ~1-1/2 hours, taken with a Jeolco USM U3 scanning electron microscope. Magnification is 10,000X. The grain boundary shows as a wall, with a dimension in the plane perpendicular to the paper, indicating that it separates "plateaus" of two grains of different heights, confirming that the various grains sputter at different rates. The difference in elevation of these two grains was estimated to be on the order of 0.5 μm.

Since the alloy under investigation is not too dissimilar from the Pt/Pt-10Rh thermocouple used to monitor the temperatures during thermal stability testing, one might expect to observe degradation of the thermocouple over the course of the test. Table 2 presents data showing that no degradation was observed.

DARLING et al.[30] have discussed the behavior of Pt/Pt-Rh thermocouples in the presence of various refractory materials and in various atmospheres and found that silicon and aluminum were involved in the failure of a Pt/Pt-13Rh thermocouple.

Table 2
Comparison of standard and experimental thermocouples

Standard thermocouple temperature, °C	Experimental thermocouple* temperature, °C
471	472
604	604
696	696
831	832
922	923

*After 1074 hrs at 1100 °C at a pressure of 10^{-8} torr.

Conclusions

The source of the silicon contaminant was found to be the alumina mounting apparatus. This is consistent with the statement of DARLING et al. that contamination of Pt/Pt-Rh thermocouples is representative of the impurities in refractory mounting shields rather than of the refractory itself.[30]

The ion microprobe was thus able to establish unequivocally the cause of the tensile failure of the Pt-30Rh-8W alloy. It is a powerful analytical tool with great potential in solving similar problems, and is unaffected by the parameters which limit the use of the electron microprobe, notably the sensitivity limitations imposed by low Z number and the X-ray continuum. In this particular case, since the silicon Kα and tungsten Mα X-ray lines fall at essentially the same energy, the electron microprobe would have had great difficulty in detecting the embrittling agent.

*

We wish to thank R. S. CROUSE and T. HENSON for making the scanning electron micrographs.

References

1. M. A. FORTES, B. RALPH, Acta Met., 15 (1967) 707.
2. D. G. BRANDON, B. RALPH, S. RANGANATHAN, M. S. WALD, Acta Met., 12 (1964) 813.
3. W. C. JOHNSON, D. F. STEIN, Metall. Trans., 5 (1974) 549.
4. G. J. DOOLEY, J. Vac. Sci. & Technology, 9 (1971) 145.
5. D. F. STEIN, A. JOSHI, Met. Sci. J., 6 (1972) 67.
6. C. R. SHASTRY, G. JUDD, Metall. Trans., 3 (1972) 337.
7. H. G. SELL, D. F. STEIN, R. STICKLER, A. JOSHI, E. BERKEY, J. Inst. Met., 100 (1972) 275.
8. J. M. WALSH, B. H. KEAR, Metall. Trans., 6A (1975) 226.
9. A. JOSHI, D. F. STEIN, J. Test. & Eval., 1 (1973) 202.
10. K. T. AUST, B. CHALMERS, Metall. Trans., 1 (1970) 1095.
11. J. H. WESTBROOK, Metall. Reviews, 9 (1964) 415.
12. Applied Research Laboratories, Sunland, Calif.
13. H. LIEBL, J. Appl. Phys., 38 (1967) 5277.
14. C. A. ANDERSEN, J. R. HINTHORNE, Science, 175 (1972) 853.
15. J. R. McHUGH, in Methods and Phenomena, Methods of Surface Analysis, S. P. WOLSKY and A. W. CZANDERA, (Eds), Elsevier Oublishing Co., Amsterdam (in press).
16. N. R. DALY, Rev. Sci. Instr., 31 (1960) 264.
17. C. A. ANDERSEN, Int. J. Mass Spec. and Ion Phys., 3 (1970) 413.
18. J. C. FRANKLIN, unpublished results.
19. D. McLEAN, Grain Boundaries in Metals, Clarendon Press, Oxford, 1957, Chapter 8.
20. J. C. FISHER, J. Appl. Phys., 22 (1951) 74.
21. R. T. P. WHIPPLE, Phil Mag., 45 (1954) 1225.
22. P. K. ROL, F. P. VIEBÖCK, M. DE JONG, Proc. 4th Intern. Conf. on Ionization Phenomena in Gases, North Holland Publishing Co., Amsterdam, 1960.
23. O. E. ALMEN, G. BRUCE, Nucl. Instr. Meth., 11 (1961) 257.
24. D. ONDERLINDEN, F. W. SARIS, P. K. ROL, Nucl. Instr. Meth., 38 (1965) 269.
25. D. ONDERLINDEN, Appl. Phys., 8 (1966) 8.
26. D. ONDERLINDEN, Can J. Phys., 46 (1968) 739.
27. M. BERNHEIM, G. SLODZIAN, Int. J. Mass Spec. and Ion Phys., 12 (1973) 93.
28. M. KAMINSKY, Atomic and Ionic Impact Phenomena on Metal Surfaces, Academic Press, New York, 1965, Chapter 10.
29. Z. JURELA, Int. J. Mass Spec. and Ion Phys., 12 (1973) 33.
30. A. S. DARLING, G. L. SELMAN, R. RUSHFORTH, Pt. Metals Rev., 15 (1971) 13.

Journal of Radioanalytical Chemistry, Vol. 32 (1976) 99–104

DETERMINATION OF GOLD, SILVER AND COBALT IN ALUMINUM BY FLAMELESS ATOMIC ABSORPTION SPECTROSCOPY

R. J. MCELHANEY

Oak Ridge Y–12 Plant, Oak Ridge, Tennessee (USA)*

Flameless atomic absorption spectroscopy has been successfully applied to the analysis of trace levels of gold, silver and cobalt in milligram quantities of aluminum. The two-line method of background correction was used with good, but not total, success. The reproducibility of the measurements was excellent, and the results compared very well with the expected values.

Introduction

Aluminum metal rod that is traced with either 0.06% gold, 0.15% silver, 0.66% or 0.17% cobalt is used as a monitor alloy in neutron flux measurements of nuclear reactors. The Y-12 Plant Laboratory was requested to provide the necessary analytical services to verify the tracer content of these rods. The samples were received as short sections of rod weighing approximately 1.0 mg. Flameless atomic absorption spectroscopy possesses the necessary accuracy and sensitivity to analyze such small samples. A limited number of papers dealing with the analysis of metals and alloys by flameless atomic absorption had been written at the time the analysis was carried out,[1,2] so the applicability of this technique was of great interest.

Experimental

Apparatus

Atomic absorption measurements were made using a commercial dual-double beam (two channel) atomic absorption spectrophotometer. With this instrument the silver, cobalt or gold atomic absorption can be monitored on

*Prepared for the U.S. Atomic Energy Commission under U.S. Government Contract W-7405 eng 26.

channel A while a nearby non-absorbing line can be used on channel B to correct for background. A dual channel recorder allows monitoring the corrected atomic absorption signal (A-B) on one channel while the background signal (B) is monitored on the other channel.

A commercial carbon rod furnace, with a workhead modified to accept 0.25 in. ID x 2.5 in. long graphite tubes,[3] was used for atomization of the sample. A mixture of 1.7 /min argon and 56 ml/min P-10 gas (10% methane — 90% argon) was used as the furnace purge gas. The methane produces a thin pyrolytic graphite coating over the hot center portion of the cell and significantly prolongs the useful lifetime of a graphite tube.[4]

Reagents

All standards were prepared from 1000 μg/ml stock solutions which were made by dissolving 1.000 g of the pure metal in the appropriate acid and diluting to 1000 ml with deionized water. Standards were matched to the samples with respect to aluminum and acid concentration.

Procedure

The samples containing gold or cobalt were dissolved with 0.5 ml aqua regia and diluted to 25 ml with deionized water. The samples containing silver were dissolved with 0.5 ml H_2SO_4 and diluted to 25 ml with deionized water.

Results

Cobalt

Channel A was set to the 240.7 nm absorbing cobalt line and channel B was set to the 238.9 nm non-absorbing cobalt line. Slits of 0.2 nm were used in both channels. Fig. 1 shows the background corrected absorption signals for standards and samples. Duplicate 10 μl injections were made at ~0.7/10X scale expansion. Atomization was carried out at ~2700 °C for 8 sec. The blank value is negligible and reproducibility is excellent.

Silver

Channel A was set to the 338.3 nm absorbing silver line and channel B was set to the 337.6 nm non-absorbing neon line. Slits of 0.2 nm were used in both channels. Fig. 2 shows the background-corrected absorption signals for standards and samples. Duplicate 10 μl injections were made at ~0.5/10X scale expansion. Atomization was carried out at ~2300 °C for 7 sec. Again,

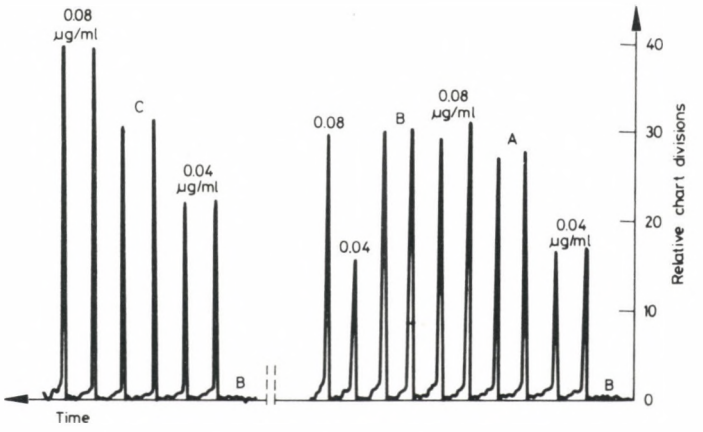

Fig. 1. Recorder readout of Co absorption peaks

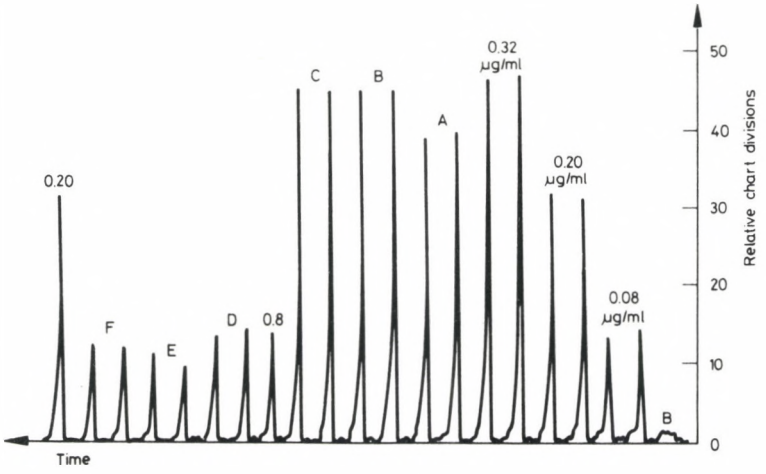

Fig. 2. Recorder readout of Ag absorption peaks

the blank is negligible and reproducibility is very good. The discontinuity results from a time delay in the analysis of the last sample with a resultant shift in sensitivity.

G o l d

Channel A was set to the 242.8 nm absorbing gold line and channel B was set to the 238.8 nm non-absorbing gold line. Slits of 0.2 nm were used in both channels. Fig. 3 shows the background corrected absorption signal for standards and samples. Duplicate 25 μl injections were made at ~0.8/10X scale expansion. Atomization was carried out at ~2500 ^{o}C for 7 sec. Reproducibility is very good, however, we now have a blank that cannot be dismissed. The aluminum stock solution used for matrix matching of the standards was found to be the source of the blank, but emission spectrographic analysis of the aluminum stock solution showed no gold contamination. A check of the blank at the absorbing gold wavelength with a hydrogen hollow cathode lamp showed the blank signal to be background scatter from atomized aluminum. The two-line method of background correction did not work in this instance because the background was not the same at the absorbing wavelength as at the non-absorbing wavelength. One possible explanation for this fact concerns the separation of the absorbing and non-absorbing wavelengths. For gold, where two-line background correction did not work, the separation between the absorbing and non-absorbing wavelengths was 4.0 nm. For cobalt, where two-line background correction

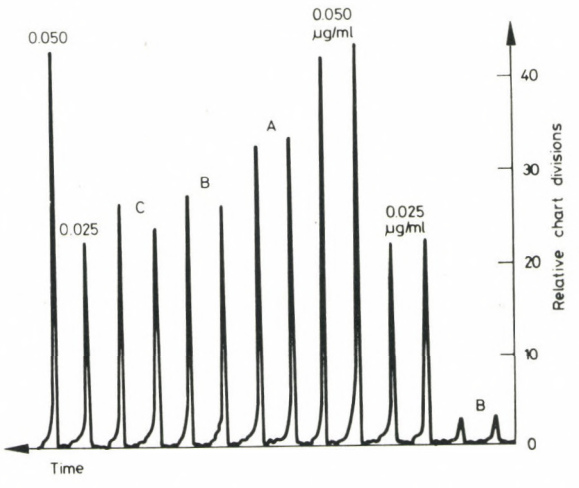

Fig. 3. Recorder readout of Au absorption peaks

Table 1
Results of analysis

Sample	Weight, mg	Au, %	
		Expected	Found
Au-A	1.45	0.06	0.065
Au-B	1.22	0.06	0.062
Au-C	1.15	0.06	0.061

Sample	Weight, mg	Ag, %	
		Expected	Found
Ag-A	1.22	0.15	0.146
Ag-B	1.41	0.15	0.139
Ag-C	1.16	0.15	0.131

Sample	Weight, mg	Co, %	
		Expected	Found
Co-A	1.17	0.66	0.56
Co-B	1.42	0.66	0.53
Co-C	1.37	0.66	0.55
Co-D	1.18	0.17	0.18
Co-E	0.94	0.17	0.16
Co-F	1.03	0.17	0.18

did work in the same wavelength region (240.0 nm), the separation between absorbing and non-absorbing wavelengths was 1.8 nm. At any rate, the gold "blank" was treated as a component of the standard and sample signals for final calculations.

The results of the entire analysis are shown in Table 1. The results agree very well with the nominal values supplied by the manufacturer, except in the case of the 0.66% cobalt traced material. The results indicate an average cobalt content of ~0.55%. There is no reason to doubt the accuracy of the results, although the small sample size made a methods comparison impossible.

In summary, flameless atomic absorption spectroscopy has been shown to be a valuable tool in the analysis of very small samples of aluminum alloys and should be applicable to the analysis of other alloys as well.

References

1. J. B. HEADRIDGE, D. R. SMITH, Talanta, 19 (1972) 833.
2. M. YANAGISAWA, T. TAKEUCHI, M. SUZUKI, Anal. Chim. Acta, 64 (1973) 381.
3. R. W. MORROW, R. J. McELHANEY, Appl. Spectrosc., 27 (1973) 386.
4. R. W. MORROW, R. J. McELHANEY, Atom. Absorp. Newl., 13 (1974) 45.

Journal of Radioanalytical Chemistry, Vol. 32 (1976) 105–116

DETERMINATION OF FLUORINE BY THE SPECTROMETRY OF PROMPT GAMMA-RAYS

I. S. GILES, M. PEISACH

Southern Universities Nuclear Institute, P. O. Box 17, Faure, 7131 (South Africa)

The use, for analysis, of prompt gamma-rays excited by 5 MeV alpha-particles from the reactions $^{19}F(\alpha,\alpha'\gamma)^{19}F$, $^{19}F(\alpha, n\gamma)^{22}Na$ and $^{19}F(\alpha, p\gamma)^{22}Ne$, was studied. The precision of the analyses depended on the gamma-ray energy used for the measurement. Relative standard deviations were ±1.8, ±0.9 and ±1.3% using the 110-, 197- or 1275 keV gamma-rays. The method was tested with N. I. M. standard materials of calcium fluoride and fluorspar, and was used as a rapid method for the determination of fluorine in cements.

Introduction

Nuclear methods for the determination of fluorine frequently make use of resonances in the reaction

$$^{19}F(p, \alpha\gamma)^{16}O$$

and the one most often used[1] occurs for a proton energy of 1375 keV: a smaller resonance is also observed at 1348 keV. The gamma-rays emitted are from excited levels of ^{16}O and those used for analytical purposes have energies of 6.058 MeV, 6.138 MeV and 7.122 MeV. The use of these gamma-rays enables very sensitive depth determination to be made because the cross-section of the reaction is very high over the short proton energy range of the resonance. On either side of the resonances the cross-section falls to a very low value.[2] The yield is thus highly sensitive to fluorine concentration changes in the proximity of that part of the particle range where the energy passes through the resonance.

By contrast the gamma-rays produced as a result of inelastic scattering are much less subject to drastic yield changes. The use of such gamma-ray yields for analyses is much more suitable for the determination of average fluorine concentrations. The excitation functions for two of the different

gamma-rays resulting from inelastic scattering of alpha-particles on a calcium fluoride target are shown in Fig. 1.

The inelastic scattering reaction

$$^{19}F(\alpha, \alpha')^{19}F$$

causes excitation of the fluorine nucleus which on prompt decay emits gamma-rays characteristic of the excited levels of ^{19}F. This Coulomb excitation occurs by purely electromagnetic interaction between passing charged particles and nuclear protons.[3] As long as the energy of the bombarding particle is below the Coulomb barrier, other types of reaction

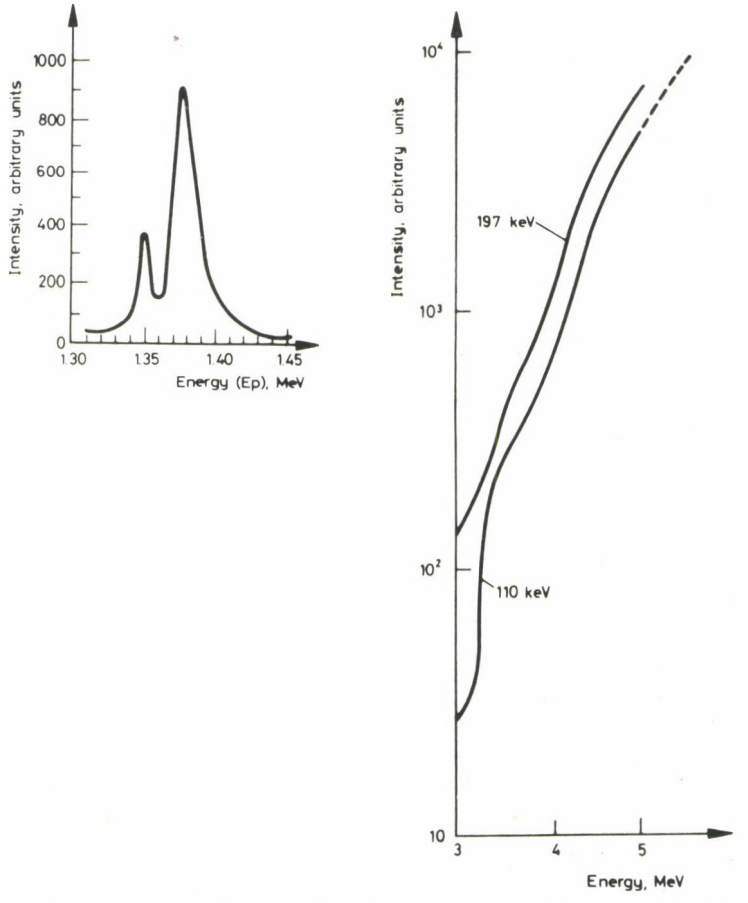

Fig. 1. Excitation function for the gamma-rays of 110 and 197 keV generated by bombardment with $^4He^+$ ions from 3 to 5 MeV. The inset shows the yield from the proton-induced resonance[2]

occur with much reduced probability. The Coulomb barrier for alpha-particles is much higher than for protons or deuterons, hence at energies of a few MeV alpha-particles cause reactions with far fewer nuclei. In practice the cross-section for 5 MeV alpha-particles falls to a negligible level if the atomic number of the target nucleus exceeds 16. When, therefore, inelastic scattering is used for the analytical determination of fluorine, interference from heavier nuclides is much reduced by the utilisation of alpha-particles as the means of excitation.

Experimental

Preparation of standards and samples

Samples for bombardment, whether standard or unknown, were crushed and pressed into pills with a diameter of 13 mm, using a 10-ton press. In a few cases where the material itself did not form a suitable pill, a known weight of binder, usually KBr or borax, was added to a weighed amount of the material and the analytical results were then corrected for the dilution effect.

Chemically pure fluorides of many different metals were bombarded in order to establish the identity of the large number of gamma-ray peaks recorded in the spectrum. The yields of fluorine gamma-rays from these pure fluorides served to establish the linear relationship between yield and concentration, and were used to construct a coarse calibration.

Standards of known fluoride content were prepared by mixing known weights of calcium fluoride and calcium hydroxide in the solid state in a mill. Since it is known that such mixing may result in a product that is not always homogeneous an attempt was made to improve homogeneity, by combining suspensions of known amounts of each of these materials in hexane under agitation with ultrasonic sound waves, and subsequently removing the hexane by distillation. Analyses of the different mixtures later showed that there was no discernible difference in homogeneity of the products.

For the final calibration homogeneous powdered samples of the standard[4] fluorspar materials, 9/69, 42/70, 63/70, 27/72 and 36/72 were obtained from the National Institute for Metallurgy, Johannesburg, South Africa.

The electronic measuring system

A block diagram of the electronic system is shown in Fig. 2. Essentially there are three separate measuring systems counting gamma-rays, charged particles and neutrons. The gamma-ray spectra are required for the analysis, while the charged particle data are used to obtain information on the major

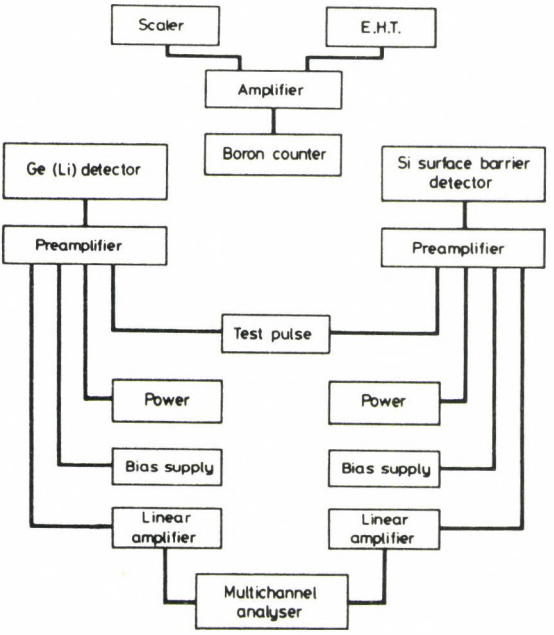

Fig. 2. Block diagram of the electronic apparatus

elements in the sample matrix. Data from the multichannel analyser were stored on magnetic tape and processed by computer.

It was necessary to monitor the neutron yield from the sample under bombardment. Some Ge(Li) detectors contain fluorine in their assembly and these are known[5] to show characteristic fluorine gamma-ray peaks in spectra collected under neutron bombardment. When such a detector was used, background effects were corrected for through the use of the monitored neutron count. At a later stage it was possible to select a Ge(Li) detector which showed a drastically reduced fluorine content. Spectra generated by fast neutrons in each of these detectors are shown in Fig. 3.

The scattering chamber

The irradiations were carried out in a scattering chamber specially designed for analytical purposes. Although constructed for simultaneous use with five detectors (Fig. 4) in this investigation only two of these were used, the surface barrier and the Ge(Li) detectors. The remaining three positions that were available were ports for a Si(Li) X-ray detector, a thin planar intrinsic germanium detector for low energy gamma-rays and an

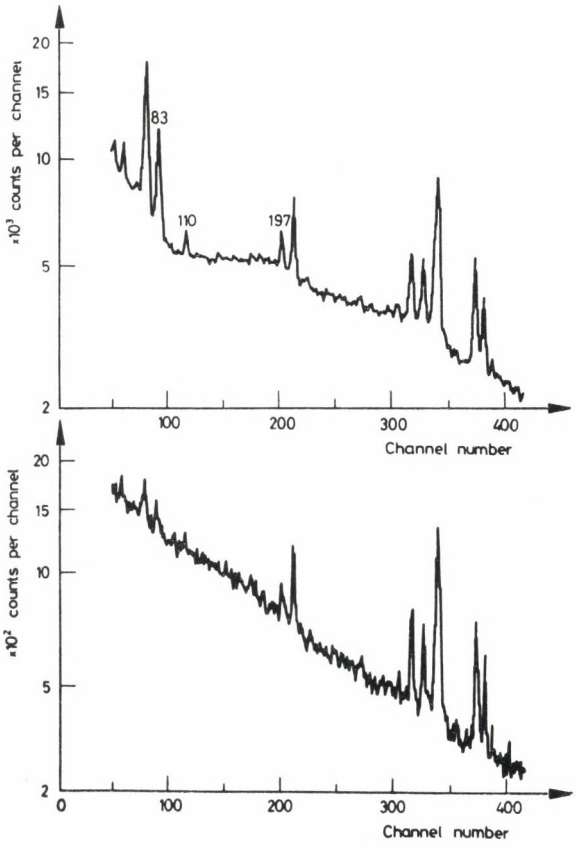

Fig. 3. Comparison of spectra generated by fast neutrons in two different Ge(Li) detectors. The presence of fluorine peaks in the upper curve is clearly evident

annular surface barrier detector for charged particle measurements near 180° scatter. The wall of the scattering chamber in front of the Ge(Li) detector was thinned to reduce absorbtion of gamma-rays.

Because it is essential that the total bombarding current be accurately integrated, the chamber was constructed as a self-contained Faraday cup, electrically insulated from the beam tube and from all the detectors. Collimation of the bombarding beam was achieved in the beam tube outside the chamber. The beam entered the chamber through an aperture about 5 mm in diameter in front of which was placed an anti-scatter copper collimator electrically charged to -300 V to prevent secondary electrons from entering

the chamber. Secondary electron loss from the target could take place at two points, through the beam entrance aperture and through the collimator in front of the surface barrier detector, but their combined solid angle subtended at the target was negligibly small.

Irradiation and measurement

The sample pills were mounted in a target holder placed normal to the direction of incidence of the bombarding beam. The axis of the Ge(Li) detector was at an angle of 45° and the surface barrier 135° to the incidence direction. Both detectors could be shifted away from the target to cope with excessive count rates but could be positioned to cover a large solid angle when warranted by the low count rate.

Beams of 5 MeV $^4He^+$ ions collimated to 3.5 mm in diameter were used to generate the prompt gamma-rays. Beam currents were adjusted so that the deadtime in the multichannel analyser did not exceed 10%. With this restriction the beam currents ranged from 10 to 100 nA. When qualitative data were accumulated, irradiations lasted about 30 minutes each, but during routine analysis on materials with fluoride content 0.1% or more sufficient counts were accumulated within a much shorter time.

Results and discussion

Energy spectrum of prompt gamma-rays

A typical gamma-ray spectrum obtained from the irradiation of calcium fluoride is shown in Fig. 5. Under the conditions of the experiment gamma-rays from calcium were not observed in the spectrum. In the figure the energies corresponding to the peak positions are given in keV.

Prompt gamma-rays are emitted from the product nucleus of a reaction but the analyst is really concerned with that component of the sample on which the nuclear reaction was carried out. Accordingly, for analytical purposes, it is more meaningful to label spectral peaks with the target nucleus. In defining the conditions of the analysis the nature of the bombarding beam is known and need not be stressed, thus the reaction is uniquely identified if the light product particle is given. Accordingly the following convention is used for peak assignment.[6]

In the nuclear reaction

$$A(a, b\gamma)B$$

peak assignment is written A b(r, s) where b is the prompt light particle of the reaction and the gamma-ray quantum is emitted by the de-excitation of

the heavy product nucleus from level r to level s. If the target nucleus can be inferred unambiguously it may be omitted. All prompt gamma-ray peaks in spectra reported in this paper are labelled according to this convention.

Fig. 5 shows the intense peaks from gamma-rays of 110, 197 and 1275 keV each of which can be used for analytical purposes. The gamma-rays of 583 keV appear to be intense but the signal to background ratio in this region of the spectrum is detrimental to attaining good precision. Strong peaks were

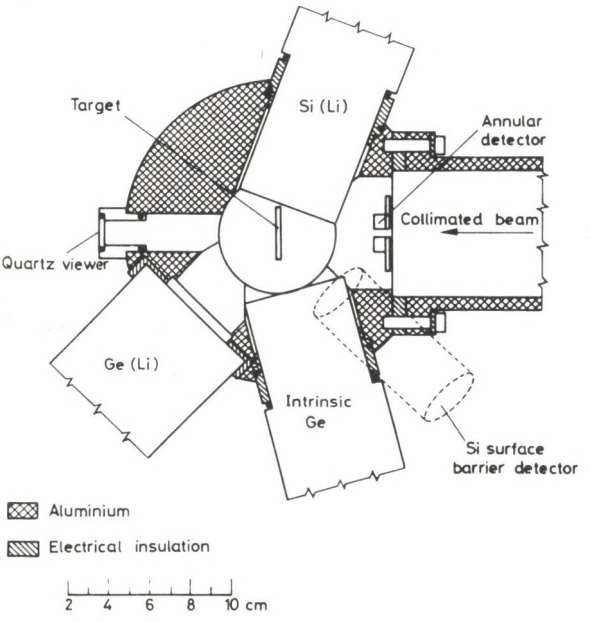

Fig. 4. The construction of the scattering chamber for analysis

observed corresponding to gamma-rays of 87, 110, 197, 1236, 1355 and 1459 keV that could be assigned to the decay of excited levels of ^{19}F produced by $(\alpha, \alpha'\gamma)$ inelastic scattering. In addition gamma-rays from the reaction $^{19}F(\alpha, n\gamma)^{22}Na$ were observed with energies of 73, 583, 637, 891, 1281, 1369 and 1528 keV as well as the 511 keV annihilation gamma-ray. The strong 1275 gamma-ray already mentioned and the gamma-rays of 687, 2081, 2165 and 3182 keV were observed from the reaction $^{19}F(\alpha, p\gamma)^{22}Ne$. The origin of these prompt gamma-rays is shown diagrammatically in Fig. 6.

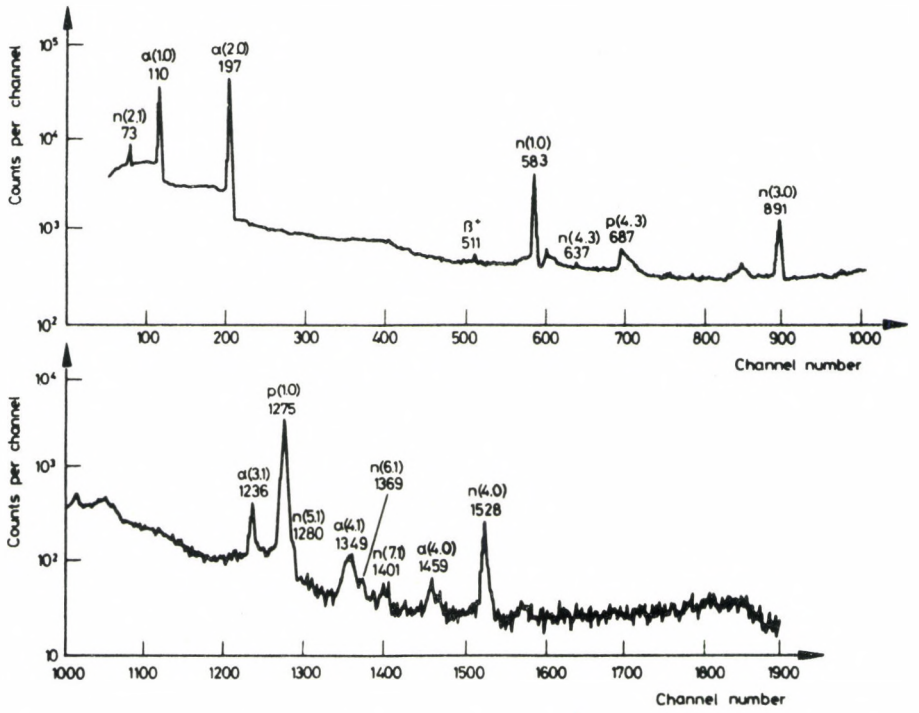

Fig. 5. Prompt gamma-ray spectrum of calcium fluoride bombarded with 5 MeV $^4He^+$ ions. Peak energies are given in keV and the peak assignment is written in the convention described in the text. Gamma-rays from calcium were not observed

Precision of the method

Using the mixtures of calcium hydroxide and calcium fluoride described above, repeat and replicate analyses were carried out using the intensity of the 197 keV γ-rays as a measure of the fluorine content. Samples covered the fluorine range from 0.8 to 32.8% by weight and the relative standard deviation of the results was $\pm$6%. Since the statistical precision based on the count rate was far better than this value it was deduced that this relative standard deviation referred largely to the degree of inhomogeneity of the mixture.

A more detailed test of the precision was carried out using accurately analysed fluorspar standards from the National Institute for Metallurgy. The

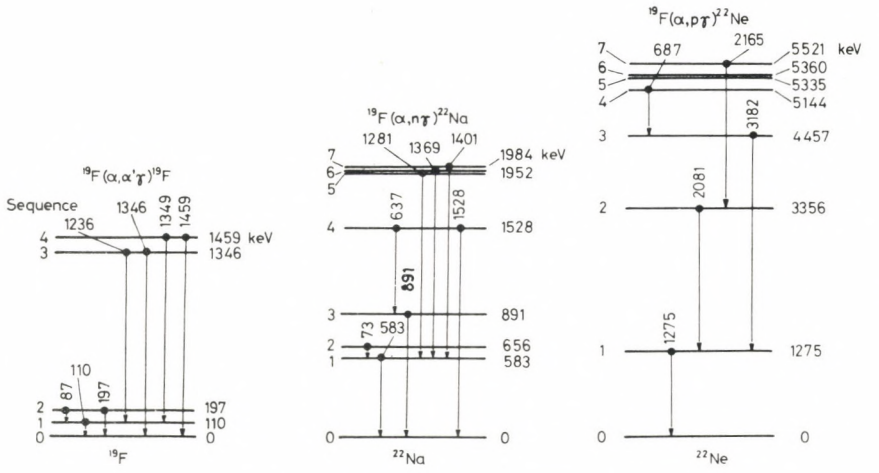

Fig. 6. Decay transitions resulting in observed gamma-rays for the reactions $^{19}F(\alpha, \alpha'\gamma)^{19}F$, $^{19}F(\alpha, n\gamma)^{22}Na$ and $^{19}F(\alpha, p\gamma)^{22}Ne$

results for these are given in Table 1, using each of the gamma-rays 110, 197, 1275 keV as a measure of the fluorine content. The observed relative standard deviations were 1.84, 0.89 and 1.24%, respectively. The improved precision using the 197 keV as compared to that using the 110 keV gamma-rays reflects the decreased efficiency of measuring the lower energy radiation. The good precision using the 1275 keV gamma-rays is ascribed to the comparatively lower background in the vicinity of this energy.

Sensitivity of the method

Attempts to deduce the practical sensitivity limit of the method were made using targets consisting of small known amounts of aqueous solutions of NaF evaporated on backings of carbon. Backings of tantalum could not be used because of the large number of low energy gamma-rays this element generated. Although the precision of the results decreased with decreasing fluorine content, it was found that fluorine contents of the order of 100 ng could still be measured and concentrations of 10 ppm could be detected.

Application to cement analyses

Cement samples from local producers were analysed by the method of prompt gamma-ray spectrometry. A typical spectrum is shown in Fig. 7.

Table 1
Precision of the method

Material	Known fluorine content, %wt	Counts per μC per 1% F		
		110 keV	197 keV	1275 keV
CaF_2	46.86	546.6	761.9	103.1
		549.2	768.9	102.2
		551.4	769.1	103.2
		548.2	768.3	103.9
		539.5	767.2	102.1
		537.9	766.9	103.6
		540.7	766.9	102.1
		575.9	786.4	105.0
		562.5	779.2	103.4
		574.1	783.4	102.8
Fluorspar 63/70	46.89	555.9	771.3	102.9
		556.7	778.1	104.6
		562.2	782.5	104.8
		560.7	778.2	103.1
		544.3	767.9	103.4
		538.3	764.5	103.5
Fluorspar 9/69	40.19	551.7	765.1	100.1
		560.4	774.6	100.3
		553.9	770.7	102.7
		547.9	760.9	100.9
		554.4	772.8	102.7
		557.0	772.4	102.2
		555.8	771.1	101.9
	Mean	553.27	771.68	102.80
	Rel. stand. dev.	±1.84%	±0.89%	±1.24%

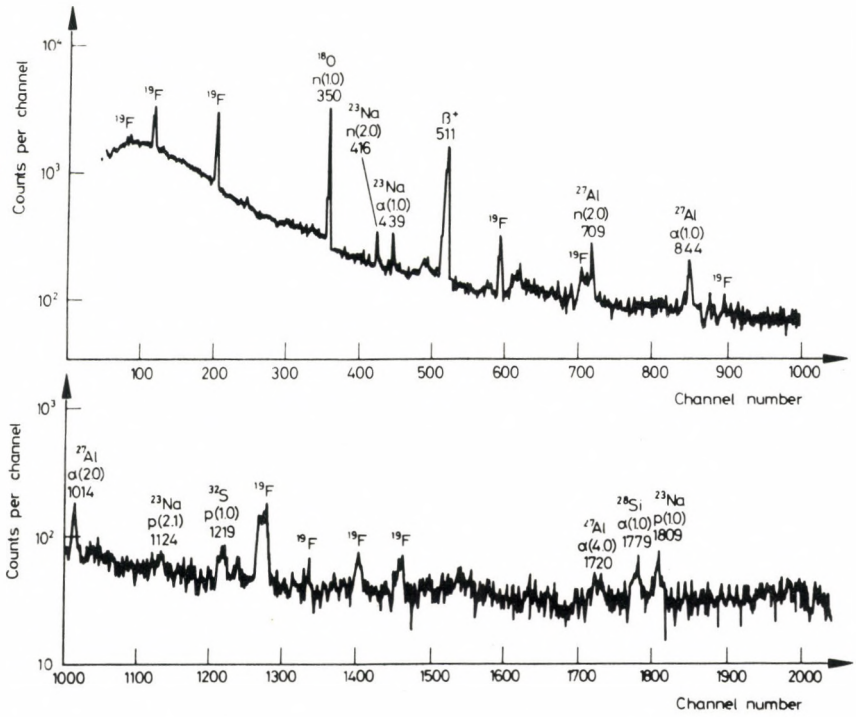

Fig. 7. Typical prompt gamma-ray spectrum obtained from cement bombarded with 5 MeV $^4He^+$ ions. Gamma-ray peaks from fluorine are marked but their energies are omitted. (For gamma-ray energies from fluorine, see Fig. 5)

Some of the results are given in Table 2. The observed standard deviation is of the same order as the measured precision, except for one sample, where the difference is ascribed to inhomogeneity.

The total volume of material analysed is determined by the diameter of the beam used and the effective range of the alpha-particles in the matrix which at these energies is very small. It can be calculated that the total mass sampled is of the order of 0.5 mg. The accuracy of the analysis will then depend on the extent to which this small sampled mass represents the bulk of the material. For control purposes the cited results were considered to be sufficiently accurate.

It may be pointed out that the results of the N. I. M. standards reported in the previous section show a remarkable degree of homogeneity.

Table 2
Some analyses of cements using the 197 keV gamma-rays

	Fluorine content, %wt			
	Cement 1	Cement 2	Cement 3	Cement 4
	0.269	0.280	0.259	0.256
	0.265	0.284	0.257	0.258
	0.269	0.282	0.258	0.256
	0.272	0.293	0.260	0.264
	0.273	0.273	0.255	0.268
	0.258	0.249	0.264	0.256
Mean	0.267	0.277	0.259	0.260
Rel. stand. dev.	±2 05%	±5.37%	±1.22%	±1.96%

*

Financial assistance from the South African Council for Scientific and Industrial Research and the Atomic Energy Board is gratefully acknowledged. The University of Stellenbosch is thanked for the use of their hydraulic press in the early stages of this investigation and our gratitude is expressed to the National Institute for Metallurgy for supplying samples of their standards free of charge.

References

1. E. MOLLER, N. STARFELT, Nucl. Instr. Methods, 50 (1967) 225.
2. S. GANGADHARAN, S. YEGNASUBRAMANIAN, Bhabha Atomic Research Centre, Report B.A.R.C. 654 (1972).
3. N. P. HEYDENBURG, G. M. TEMMER, Ann. Rev. Nucl. Sci., 6 (1956) 77.
4. H. STOCH, National Institute for Metallurgy Report 1649, 1974.
5. C. CHASMAN, K. W. JONES, R. A. RISTEN, Nucl. Instr. Methods, 37 (1965) 1.
6. M. PEISACH, J. Radioanal. Chem., 12 (1974) 251.

Journal of Radioanalytical Chemistry, Vol. 32 (1976) 117–124

Neutron Activation Analysis in Environmental Science

APPLICABILITY OF PROTON ACTIVATION ANALYSIS TO DESCRIBE THE OCCURRENCE OF LEAD ALONG A FREEWAY IN A RURAL AREA

G. DESAEDELEER, C. RONNEAU

Laboratoire de Chimie Inorganique et Nucléaire, Université de Louvain, 2, chemin du Cyclotron, 1348 – Louvain-la-Neuve (Belgium)

The applicability of proton activation analysis to the determination of trace amounts of lead in atmospheric particulate matter and the problem of evaluating background levels for measuring the characteristic sources of emissions is discussed.

Introduction

Since 1970, the University of Louvain has been implanting a new campus (Louvain-la-Neuve) in a rural area 30 kilometers southeast of Brussels. The population of the campus is expected to be 30000 by 1980. The implantation offered a unique opportunity to study the changes in microclimate and air quality due to the building of a city in a rural area. Therefore as early as 1969, five pollution stations and four meteorological stations were set up around the future campus site.[1] Routine determinations of SO_2 and total suspended particulates are performed by the "Institut d' Hygiène et d' Epidémiologie" in Brussels,[2] and meteorological conditions are compiled by the "Institut Royal Météorologique" in Brussels[3] and the "Institut d' Astronomie et de Géophysique Georges Lemaître" of Louvain-la-Neuve.[4] Due to the particular features of the campus, e. g. central heating through natural gas combustion, and the contribution of close and farther sources of emission, these indicators of an alteration in air quality may not be as suitable as trace elemental characterization. For instance, for the steady increase in automotive traffic around the developping campus, airborne lead

will be more indicative. The present paper deals with (a) the applicability of proton activation analysis to the determination of trace amounts of lead in atmospheric particulate matter and (b) the problem of evaluating background levels which afterwards will allow one to price the contribution of characteristic sources of emissions, e.g. a freeway or the edification of a city.

Experimental

Sample characterization

Five stations located around Louvain-la-Neuve (Fig. 1) collect routinely samples on a 24 hrs basis by filtration of low air volumes (1.5 m^3) through 20 cm^2 filter papers. Samples collected from April 1972 to December 1973 at stations 1, 2, 3 and 4 were analyzed for lead. In June 1973, a new freeway (E 40) was opened to the traffic, so that the contribution of the freeway to earlier lead concentrations could be evaluated.

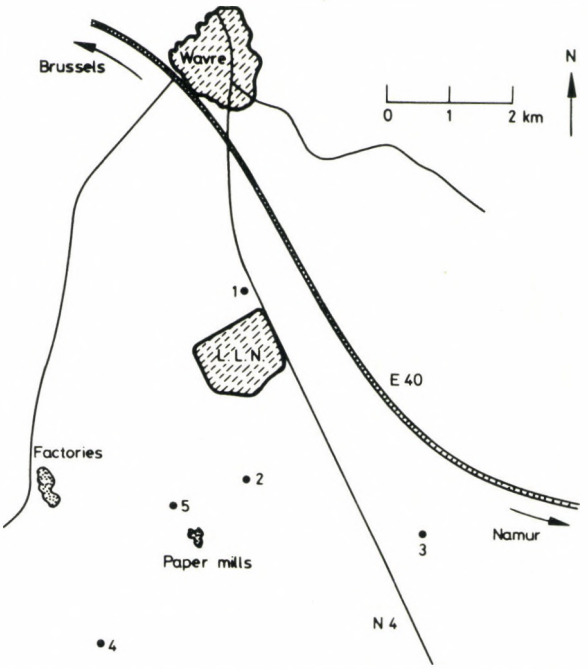

Fig. 1. Location of the five monitoring stations (numbered from 1 to 5) around Louvain-la-Neuve (L. L. N.) as compared to the local emission sources

Lead analysis by proton activation

Because of the low lead contents of the filters, flameless atomic absorption was a poor technique for accurate analysis. It was decided to study the feasibility of nuclear activation analysis by means of proton bombardment.[5] The new isochronous cyclotron of Louvain-la-Neuve can deliver proton beam intensities up to 16 μA at 90 MeV or 40 μA at 40 MeV. Since cyclotron time requests are extensive, a major criterion for routine analysis is shortening of irradiation time. The choice of the most suitable radioisotope for lead analysis and the design of a multitarget thin sample holder were directed towards this necessity. ^{204}Bi with a half-life of T = 11.2 hrs presents interesting characteristics: (a) it is produced by activation via ^{206}Pb(p, 3n), ^{207}Pb(p, 4n), ^{208}Pb(p, 5n) reactions, (b) it is a multigamma-ray emitter, (c) its half-life is short enough so that short irradiation times (30 min) are sufficient for the determination of nanograms levels and

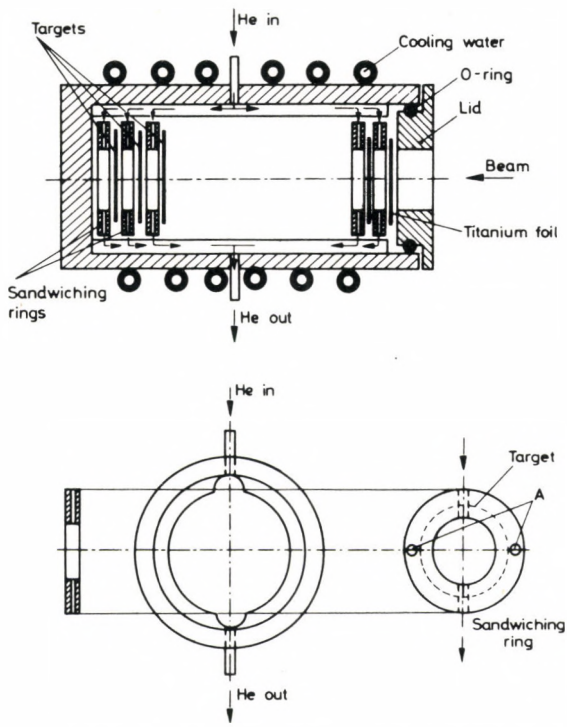

Fig. 2. Scheme of the target holder used for the irradiation of paper filters by means of a cyclotron beam

(d) its half-life is long enough that a large number of samples - up to 40 - can be irradiated simultaneously, and subsequent counting may be achieved.

The filter paper discs are wrapped into high purity thin aluminium foils (1 mg/cm^2) and sandwiched between aluminium rings. In these rings holes are drilled, providing helium circulation to cool the targets. They are maintained and aligned by means of two brass rods which are driven through the holes A (Fig. 2), allowing easy dismounting.

1 cm^2 filter paper areas are submitted to a 50 MeV proton beam of 1 μA for 30 min. Several standards interleaved with sets of 3 samples are irradiated simultaneously.

Radionuclides are identified by gamma-spectroscopy by means of a Ge(Li) detector coupled with conventional multi-channel analyser. The samples are counted without chemical separations, after at least 6 hrs cooling time in order to reduce the activity induced in the paper. The 374.7 keV gamma-ray of ^{204}Bi is usually used for lead identification, the 899.3 keV gamma-ray may also be used. Standards and samples are counted as extracted from the target holder, counting times lapse from 5 to 50 min according to the loading. Quantitative analysis is achieved by comparison of the activities induced in the samples and in the set of interleaved standards.

The analyses for trace determination of atmospheric lead are essentially interference-free. Sensitivities of less than 1.0 ng/cm^2 are routinely obtained and the precision of the analysis is better than 15%.

Results

Until now, about 500 lead analysis have been carried out on samples collected at stations 1, 2, 3 and 4 (Fig. 1), between April 1972 and December 1973. For days where wind was blowing steadily from one direction, the mean values and standard deviations were calculated. These values categorized as "before" and "after" the opening of the freeway in June 1973 are reported in Table 1. Figs 3-5 represent the mean values as a function of the wind direction, for stations 1, 3 and 4.

Before the opening of the freeway

At station 1 and 4 higher lead concentrations are associated with N-SE winds while at station 3 they are with SW-N winds, implying the transport of automotive lead from the road N 4. The mean lead concentrations are higher with NE winds than SW winds because eastern winds are generally associated with lower wind velocity and more stable meteorological

Table 1
Mean lead concentrations at three locations near Louvain-la-Neuve, Belgium, and variations with wind direction

Wind direction	Concentration of lead, ng/m^3					
	Station 1		Station 4		Station 3	
	Before*	After*	Before*	After*	Before*	After*
N – NE	216± 48	1470±315	272±174	428	67± 25	616±164
NE – E	536±380	1181±577	430±486	592	150± 93	312±133
E – SE	628±348	1389±809	236±115	327±147	367	283±146
SE – S	291±226	434±208	115± 24	237	117±133	53± 25
S – SW	217±180	193±186	191±173	176±110	134±110	58± 30
SW – W	125±104	368±307	144± 62	147±143	383±140	84± 42
W – NW	260±111	602±258	145± 18	273±209	369± 83	325±100
NW – N	185±112		105± 59	187	345±142	

*Before and after the opening of freeway E40.

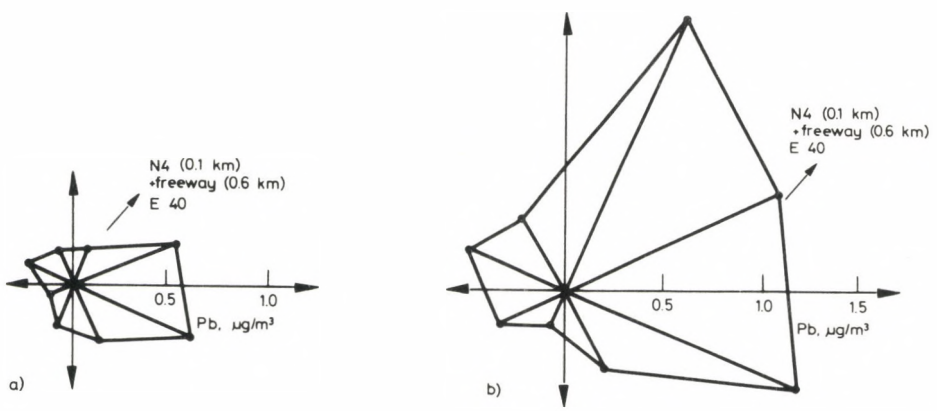

Fig. 3. Mean lead concentration at station 1 as a function of wind directions, before (a) and after (b) the opening of the freeway

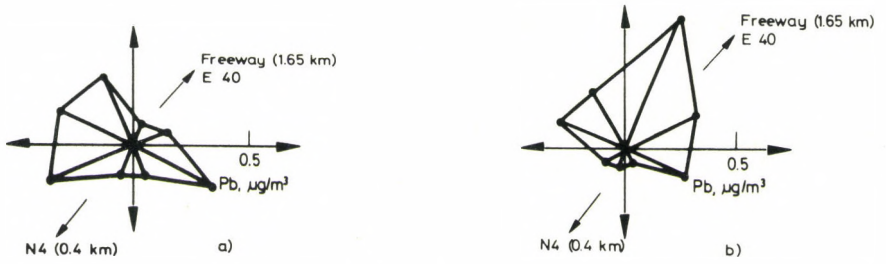

Fig. 4. Mean lead concentration at station 3 as a function of wind directions, before (a) and after (b) the opening of the freeway

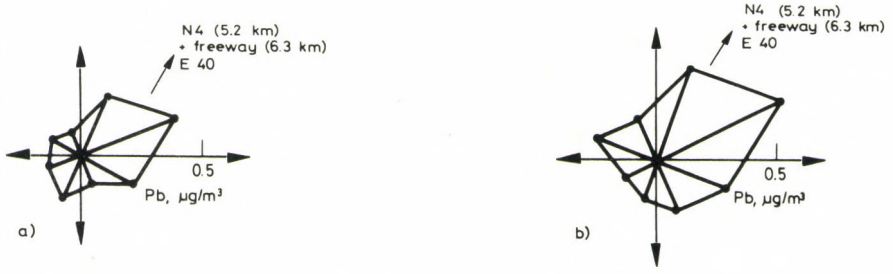

Fig. 5. Mean lead concentration at station 4 as a function of wind directions, before (a) and after (b) the opening of the freeway

conditions. The rather large standard deviation is due to the variability in meteorological conditions encountered within a specific wind direction. Under stability conditions associated with eastern winds, lead concentrations at station 4, 5 kilometers downwind, are closely the same as at station 1, showing that in these circumstances the diffusion is limited in altitude. Therefore, not only wind direction, but more general meteorological conditions as stability, precipitation, frequency of precipitation, humidity, etc. play a predominant factor when assessing the transport of pollutants.

A f t e r t h e o p e n i n g o f t h e f r e e w a y

Lead concentrations are now higher, for all wind directions excepted S-SW, at stations 1 and 4 than they were before the opening of the freeway to automobile traffic. At station 3, NE winds prevail now in the transport

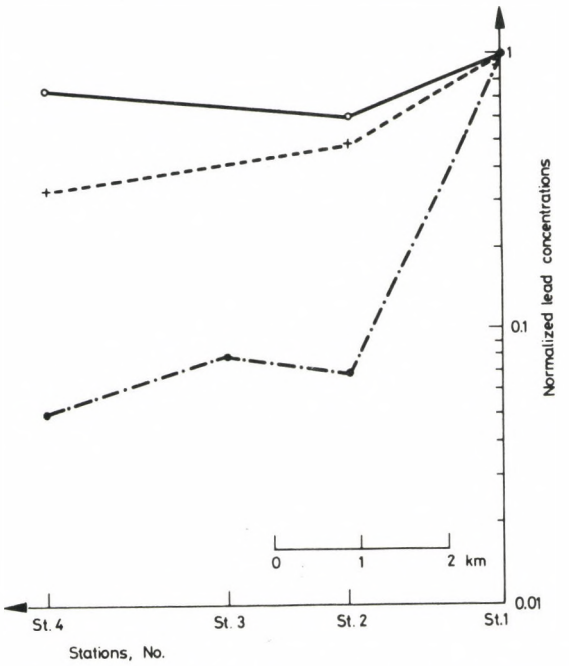

Fig. 6. Some cases of transport of lead as a function of distance from the freeway, under different meteorological conditions (○ very stable, ● very unstable, + lightly unstable), associated to NE-E winds. The lead concentrations are normalized to station 1

of lead from the freeway E 40 and SW winds bring much less pollution since the traffic on the road N 4 is less dense. Again the variability in meteorological conditions assess the variations in lead concentrations. Fig. 6 shows some cases of transport of airborne lead as a function of the distance from the freeway under different meteorological conditions associated to NE-E winds. The values are normalized to station 1. At station 4, 5 kilometers downwind of station 1, normalized lead concentrations vary from 0.75 to 0.05 for stable to unstable meteorological conditions, respectively.

Discussion and conclusion

In order to price the contribution of new emission sources to the pollution of a site, an evaluation of background levels prior to the implantation is requested. The determination of background levels are, however, extremely

difficult because of the large variations in concentrations, associated to changes in meteorological conditions. Not only wind direction, but meteorological parameters as variation of temperature with altitude, precipitation and humidity, are preponderant in assessing the diffusion and transport of pollutants to rather remote areas. A direct comparison of mean values with wind directions and source locations to price the contribution of emission sources has to be considered with great care because of this variability and may obscure the available information. A statistically significant number of samples treated by multicomponent statistical analysis[6] including the different meteorological variables together with pollution indicators present an interesting alternative to describe complex pollution cases and to assess responsability of some specific emission sources.

*

The authors are particularly grateful to Prof. D. APERS and Prof. J. W. WINCHESTER for their helpful discussion and interest. J. CARA, N. JACOB, J. LIGOT, G. MICHOTTE and P. NEMEGEER are acknowledged for their technical assistance. We are indebted to the cyclotron staff and Prof. P. MACQ for providing irradiation facilities. The study was conducted with financial assistance from the "Centre National d'Etude de la Pollution Atmosphérique par la Combustion", Brussels.

References

1. G. DESAEDELEER, C. RONNEAU, D. APERS, C.N.E.P.A.C., Progress Report 5, Brussels, Belgium, 1975.
2. Bulletins Mensuels de l'Institut d'Hygiène et d'Epidémiologie et de l'Institut Royal Météorologique, "Pollution atmosphérique: Fumées et SO_2", Brussels, Belgium.
3. Bulletins quotidiens du temps, Institut Royal Météorologique de Belgique, Brussels, Belgium.
4. Bulletins climatologiques mensuels, Institut d'Astronomie et de Géophysique Georges Lemaître, Université de Louvain, Louvain-la-Neuve, Belgium.
5. G. DESAEDELEER, C. RONNEAU, D. APERS, Anal. Chem., 48 (1976) 572.
6. G. DESAEDELEER, E. SCHIFFLERS, Atmosph. Envir., (submitted).

Journal of Radioanalytical Chemistry, Vol. 32 (1976) 125–135

ELEMENTAL ANALYSIS OF WATER AND AIR SOLIDS BY NEUTRON ACTIVATION ANALYSIS

L. C. BATE,* S. E. LINDBERG,** A. W. ANDREN***

**Analytical Chemistry Division*
Oak Ridge National Laboratory, Oak Ridge, TN (USA)
***Environmental Sciences Division,*
Oak Ridge National Laboratory, Oak Ridge, TN (USA)
****Water Chemistry Laboratory, University of Wisconsin, Madison, Wisconsin (USA)*

Instrumental neutron activation analysis was used to determine the elemental concentrations in water and air solid samples collected on Nuclepore and Whatman filters from the Walker Branch Watershed. The results from this study show that the trace element concentrations removed by water from the watershed vary seasonally, as well as geographically. The data point up the usefulness and versatility of absolute neutron activation analysis. The NBS Standard Orchard Leaves was assayed in a similar manner, and good agreement was obtained between results here and standard values.

Introduction

This study is to measure the elemental output via the solids in the stream run off from the Walker Branch Watershed and the elemental input from the aerosols. The Walker Branch Watershed (WBW) has been described in detail elsewhere.[1] The study site (Fig. 1) is 97.5 hectare catchment, located on the Oak Ridge Reservation in Oak Ridge, Tennessee. It consists of two gaged subcatchments: the east and the west branches, which contain 59.1 and 38.4 hectare, respectively. Both catchments are drained by small, perennial springfed streams. Discharge is maximum during the winter months and lowest in late summer.

Stream water samples, collected at each of the spring and weir (basin) sites indicated in Fig. 1, were filtered through 0.4-micron Nuclepore filters immediately upon collection, and suspended sediments were then analyzed. Aerosol samples were collected at the weir sites (see Fig. 1) using both Whatman 41 filter papers and Nuclepore filters.

Blank filters for the water samples were washed with a liter of distilled water to remove any soluble trace elements they contained. Blanks for the air filter were used as they came from the box.

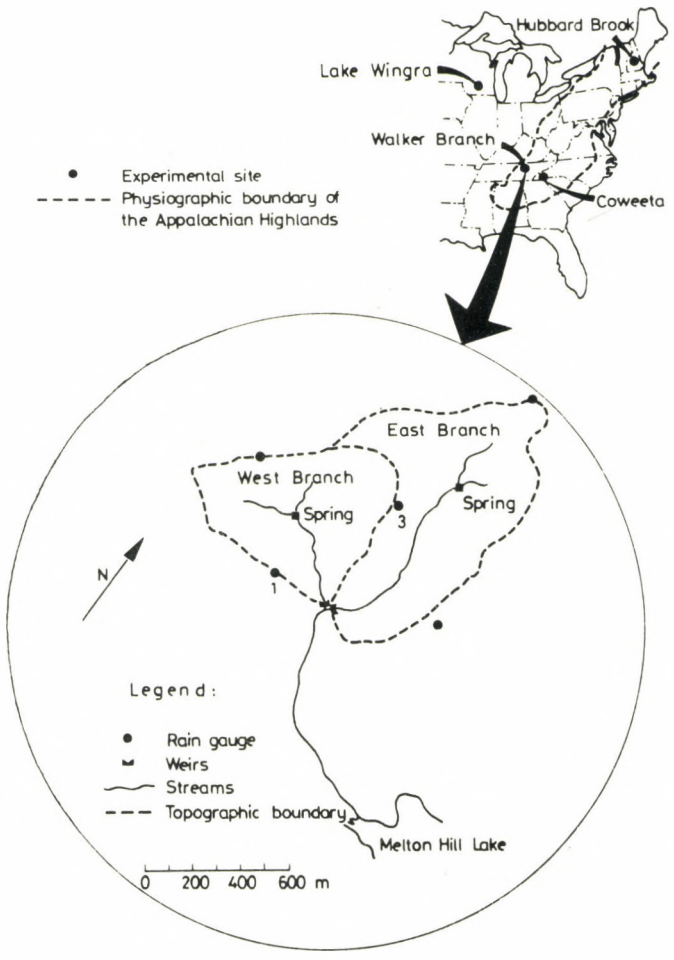

Fig. 1. Walker Branch Watershed. Location of sampling stations

The sample filters were sealed in polyethylene inserts after they were reweighed to determine the weight of solids collected.

To detect and determine quantitatively the maximum number of trace elements in each sample of filtered water or air, the samples were irradiated in the ORNL High Flux Isotope Reactor (HFIR) pneumatic system, which has a thermal flux of $5.5 \cdot 10^{14}$ n $\cdot$ cm^{-2} sec^{-1}. The γ-rays from the induced radioactive nuclides were counted on a Ge(Li) detector coupled to a computer-based multichannel analyzer. The study reported here uses the

optimum irradiation and decay times to achieve the maximum useful data from the minimum number of gamma-measurements and irradiations. The procedure was evaluated using NBS Standard Orchard Leaves. The data were processed by MONSTR computer program written by J. F. EMERY.[2]

Experimental

NBS Orchard Leaves samples

The NBS Orchard Leaves samples of 100 to 150 milligrams were weighed and sealed in polyethylene inserts for irradiation. The samples were irradiated for 11 seconds in the HFIR, the induced radioactivity measured on Ge(Li) detectors, and the resulting spectral data processed by program MONSTR[2] for the trace element concentration. Several measurements were made to select the decay time to detect and measure the most short-lived radionuclides. After a week's delay to allow the induced radioactivity to decay, the samples were re-irradiated for 600 seconds. The induced radioactivities in the samples were measured after one day's decay and for several days thereafter until only long-lived radionuclides remained.

The results of the analysis of NBS Orchard Leaves with NBS values are in Table 1. These values by absolute neutron activation analysis agree closely with the NBS values. The methods used by NBS to obtain their data on the

Table 1
Trace element concentration in NBS Orchard Leaves by absolute neutron activation analysis

Element	Concentration, $\mu g/g$	
	This work	NBS*
Al	333	340
Cl	739	700
Ca	2.13%	2.09%
V	0.58	0.58
Mg	0.70%	0.62%
K	1.50%	1.47%
Mn	89.9	91.4
Na	84.4	82

*See text for methods used for standardization.

Orchard Leaves include: (1) atomic absorption spectroscopy, (2) flame emission spectrometry, (3) neutron activation, and (4) optical emission spectroscopy.

The decay time chosen to follow the short irradiation is usually several minutes so as to allow the ^{28}Al to decay until it is not the predominant radioactivity. This decay time depends upon the composition of the sample but usually ^{28}Al is the major radioactivity. By allowing the ^{28}Al to decay a few minutes, the precision and standard deviation of the minor peaks are improved as the ratio of the radioactivity in the respective γ-ray peak can be more accurately analyzed. After the long irradiation, a decay time of about two days (three if the sodium is very high) allows for the detection and measurement of the medium half-lived trace elements in the presence of the ^{24}Na radioactivity. If the measurement is made too soon, the only gamma photo peaks observed are those of ^{24}Na. The long-lived radionuclides are measured after two weeks of decay, or when the ^{24}Na has decayed out and the samples can then be counted near the detector. This measurement usually requires overnight counting to obtain good counting statistics and/or limits of detection for the long-lived radionuclides.

Filter blanks

The choice of filters in air and water particulate sampling depends on flow characteristics and elemental impurities of the filters. Recent studies[3] have shown that Whatman #41 has a low level of trace element impurities. This filter was used for part of the air particulate studies.

The Nuclepore filter has a similar level of trace element impurities per gram and was used in most of the sampling for water and air solids. Several blank filters were irradiated, their radioactivity measured after appropriate decay times, and the trace element concentration determined.

The trace element values from these data were used after air filtration. Another set of four filters was used to filter one liter of distilled water to determine any leaching effects on the trace elements in the filters. These were then irradiated and the radioactivity assayed as above. The comparative data on washed and unwashed filters are reported in Table 2. The data for the washed filter are very similar to the unwashed except for zinc and cobalt, which were removed by the washing. The iron concentration varied widely from filter to filter, but the averages obtained for washed and unwashed were nearly equal.

Another set of filters was washed in another lab, but apparently the same precautions were not used (Table 3). The potassium and bromine in these filters were considerably higher than the unwashed or other washed filters.

Later, a new batch of larger Nuclepore filters was received and used for sampling. Then the used and new filters were irradiated for the trace elements

Table 2

Trace elements in washed and unwashed 47-mm Nuclepore filters

Element	Concentration,* μg/filter			
	Unwashed	Standard deviation	Washed	Standard deviation
Al	0.81	0.027	0.72	0.12
Cl	1.96	0.45	1.60	0.15
Mn	0.014	0.006	0.015	0.009
V	0.006	0.001	0.001	0.000
Na	1.15	0.05	0.57	0.19
Br	0.012	0.001	0.027	0.004
Co	0.061	0.028	<0.001	0.001
Zn	0.61	0.02	<0.02**	-
Cr	0.34	0.04	0.35	0.00
Fe	1.58	1.40	1.57	1.49

* Average of 4 filters each.
** < = limit of detection for condition used in analysis.

Table 3

Selected trace elements in Nuclepore filter blanks before and after washing

Treatment	Concentration,* μg/filter				
	Zn	Na	K	As	Br
Unwashed	0.61	1.15	<0.20	<6.0E-4	0.012
Washed[a]	<0.03**	0.57	0.31	2.5E-3	0.12
Washed[b]	<0.03**	0.57	<0.2**	<8.7E-5	0.027

* Average of 4 determinations.
** < = limit of detection for conditions used in analysis.
[a] Laboratory 1.
[b] Laboratory 2.

It was immediately evident that the new batch of filters contained uranium. The uranium content ranged from 16 micrograms per filter to less than 2 micrograms per filter as compared to none for original filters. Hence, they were not used as the induced radioactivity from the uranium was much greater than the induced radioactivity from the collected sample. Thus all new batches of filters should be analyzed prior to use to ensure that their trace element content is satisfactory.

Element grouping

The radionuclides to be determined were grouped according to their half-lives; where two or more radioisotopes of the same elements were produced, the sensitivity and interferences dictated the choice. Due to the presence of ^{56}Mn, ^{38}Cl, ^{24}Na, ^{82}Br, and ^{140}La in varying concentrations in all irradiated samples, the detection and measurements were made on the longer lived isotope (with asterisk) in the following elements: ^{65}Zn*, ^{69m}Zn; ^{87m}Sr, ^{85}Sr*; ^{139}Ba, ^{131}Ba*; ^{122}Sb, ^{124}Sb*; ^{60m}Co, ^{60}Co*, ^{66}Cu, ^{64}Cu* and ^{108}Ag, ^{110m}Ag*.

The elements – Mg, Al, Cl, Ti, Mn, V, and I – were determined after the 11-second irradiation and 10-minute decay. Following the 600-second irradiation and 48 hours decay, the elements – Na, K, Cu, As, Br, Mo, La, W, Au – were measured. Then, after a decay of at least 14 days, the long-lived radionuclides ($T > 3.0$ d) were counted overnight to accurately determine the concentration or a lower limit of detection.

Results

The particulate solids were filtered from a liter of water each month immediately after sampling through 0.4 microns Nuclepore filter paper. The trace elements in the solids were determined by the established neutron activation procedures developed with standard samples and blank filters. The spectral data were processed with program MONSTR for the trace element concentrations. The major trace elements measured in West Spring water solids over a period of one year are presented in Table 4. The other sampling stations (see Fig. 1) had a similar variation in the trace element concentration during the year. The trace element data from the Walker Branch Watershed for the 2 February 1975 sampling are presented in Table 5. This table shows all the trace elements determined each month in the suspended solids, and this month's data are typical for the other months.

The aerosol samples were collected at the weir sites using 5 $l \cdot min^{-1}$ vacuum pumps with Nuclepore filters as collection surface. Also, Hi-Vol air

Table 4
Trace element variation in West Spring water solids during 1974

Element	Concentration, μg/liter				
	February	April	June	August	December
Al	236	182	118	70.8	107
Br	0.43	0.10	0.11	0.17	0.048
Ce	0.17	0.22	0.22	0.17	0.12
Cr	0.80	0.14	0.22	0.25	0.42
Cs	0.028	0.013	8.0E-3	6.1E-3	5.5E-3
Fe	68.2	57.5	47.8	28.8	40.6
Hg	0.10	6.0E-3	0.021	0.059	1.E-4
K	29.3	23.4	18.6	14.3	13.5
La	0.080	0.11	0.12	0.083	0.057
Mn	0.61	2.18	7.05	5.97	0.66
Na	0.38	0.67	0.74	0.36	0.78
Ti	8.50	7.74	8.40	9.81	3.60
Th	0.031	0.026	7.0E-3	0.013	0.014
V	0.27	0.22	0.16	0.091	0.13
Zn	4.91	1.40	2.29	0.75	1.13
Total solids, mg/liter	2.9	2.4	3.3	2.9	1.1

Table 5
Walker Branch Watershed suspended sediment of February 2, 1975

Element	Trace element concentration, μg/liter			
	West Basin	West Spring	East Basin	East Spring
Mg	22.3	9.40	28.5	33.2
Al	174	107	268	292
Cl	0.97	1.06	1.20	1.30
Ca	<5.0	3.12	<7.8	4.79
Ti	7.24	3.60	7.73	8.38
V	0.22	0.13	0.32	0.33
Mn	3.93	0.66	3.77	1.75

Table 5 (cont.)

Element	Trace element concentration, μg/liter			
	West Basin	West Spring	East Basin	East Spring
Cu	<0.25	≤0.16	≤0.48	≤0.20
Sr	≤2.04	<0.8	<1.5	≤0.86
I	0.047	0.035	≤0.069	0.035
Ba	1.08	0.52	1.00	0.84
Na	0.99	0.78	1.39	1.01
K	24.4	13.5	35.2	45.4
As	0.037	0.018	0.047	0.046
Br	0.15	0.048	0.056	0.045
Mo	<0.04	<0.05	<0.05	<0.04
Cd	<0.1	<0.07	<0.1	<0.10
La	0.14	0.057	0.15	0.18
W	1.8E-3	8.0E-4	≤1.6E-3	≤2.3E-3
Au	5.0E-3	7.1E-4	2.9E-3	5.6E-3
U	<0.01	<7.0E-3	0.015	0.013
Sc	0.041	0.022	0.058	0.068
Cr	0.67	0.42	0.29	0.66
Fe	65.2	40.6	102	126
Ni	<3.1	<1.4	<2.5	<2.6
Co	0.050	0.020	0.059	0.041
Zn	2.66	1.13	2.02	<0.2
Se	≤0.02	<8.2E-3	<0.01	≤0.014
Rb	0.14	0.065	0.21	0.27
Zr	<1.3	<0.6	<1.0	<1.1
Sb	0.043	0.14	0.16	0.16
Cs	0.012	5.5E-3	0.017	0.020
Ce	0.27	0.12	0.35	0.31
Nd	<0.1	<0.06	0.14	0.25
Eu	4.2E-3	1.9E-3	4.0E-3	5.0E-3
Tb	3.5E-3	1.5E-3	2.8E-3	4.9E-3
Yb	0.010	5.3E-3	0.012	0.013
Lu	4.2E-3	1.9E-3	4.3E-3	5.1E-3
Hf	0.019	5.1E-3	0.011	9.0E-3
Ta	≤1.8E-3	≤1.5E-3	≤2.1E-3	≤1.9E-3
Hg	0.010	1.E-4	3.3E-3	1.9E-3
Ag	<0.01	<6.2E-3	<0.01	<0.01
Th	0.024	0.014	0.035	0.039

Table 6
Trace elements in aerosols

Element	Concentration, ng/m^3	
	A 224 cu meter	B 202 cu meter
Mg	<92	<105
Al	714	713
Cl	11	6.4
Ca	<93	<110
Ti	36	<29
V	2.41	2.30
Mn	14	11.8
Cu	<9	<9
Sr	<7	<7
I	0.49	0.34
Na	125	122
K	208	205
As	1.52	1.89
Br	8.35	8.61
Mo	4.33	3.71
Cd	4.29	4.21
La	0.49	0.54
W	<0.1	<0.1
Au	<0.003	<0.003
U	<0.62	<0.49
Sc	0.13	0.12
Cr	2.1	2.2
Fe	274	246
Ni	<9.4	<10
Co	0.14	0.13
Zn	14.6	15.5
Se	0.98	0.94
Rb	0.80	1.44
Zr	28.7	23.6
Ag	<0.04	<0.04
Sb	0.31	0.30
Cs	0.058	0.059

Table 6 (cont.)

Element	Concentration, ng/m^3	
	A 224 cu meter	B 202 cu meter
Ba	29.8	27.1
Ce	1.56	1.49
Nd	0.85	1.14
Eu	0.012	0.011
Tb	<0.009	<0.007
Yb	0.004	0.004
Lu	0.012	0.011
Hf	0.041	0.044
Ta	0.012	0.010
Hg	0.067	0.074
Th	0.12	0.11

samplers were used with Whatman 41 filter paper. The aerosol samples had a total volume of 224 and 202 m^3, respectively. The results of the aerosol samples are given in Table 6. The Hi-Vol aerosol sampler was used to collect aerosols for one set of experiments, and our data show the copper contamination in these samples to average 200 ng/m^3 with a range from 180 – 300 ng/m^3 compared to values collected with low flow vacuum pumps of about 9 ng/m^3. This copper contamination of aerosol samples when using Hi-Vol samplers has also been reported by HOFFMAN and DUCE.[4]

Conclusions

The absolute neutron activation analysis method of determining the trace elements in samples has been evaluated with NBS Standard Orchard Leaves, and acceptable data were obtained. The sensitivity and accuracy for this number of elements in a single sample using the HFIR as a neutron source and absolute neutron activation analysis methods cannot be duplicated by other analytical methods. By using absolute neutron activation analysis, considerable time is saved with the elimination of standards for all elements found in the samples. Thus, the cost per analysis is comparable or lower than other analytical methods for the same number of elements per sample.

This study confirms that instrumental absolute neutron activation analysis using Ge(Li) detector greatly enhances the simultaneous determination of a large number of trace elements in small quantities of water solids and aerosols.

*

Research sponsored by the National Science Foundation-RANN Environmental Aspects of Trace Contaminants Program, NSF interagency agreement Ag 389, under Union Carbide Corporation's contract with the United States Energy Research and Development Administration.

ORNL, Oak Ridge, Tennessee 37830, operated by Union Carbide Corporation for the U. S. Energy Research and Development Administration.

References

1. A. W. ANDREN, S. E. LINDBERG, L. C. BATE, Atmospheric Input and Geochemical Cycling of Selected Trace Elements in Walker Branch Watershed. ORNL–NSF–EATC–13. June, 1975.
2. J. F. EMERY, F. F. DYER, Multielement Determination in Environmental NAA Using MONSTR. Proc. Second Intern. Conf. on Nuclear Method in Environmental Research, Columbia, Missouri (in press).
3. R. DAVIS, K. A. RAHN, J. W. WINCHESTER, Env. Sci. Technol., 6 (1972) 441.
4. G. L. HOFFMAN, R. A. DUCE, Env. Sci. Technol., 5 (1971) 1134.

Journal of Radioanalytical Chemistry, Vol. 32 (1976) 137–150

MULTIELEMENT TRACE ANALYSIS OF COALS, ASHES AND RELATED MATERIALS FROM COAL–TREATMENT FACILITIES BY INSTRUMENTAL NEUTRON ACTIVATION ANALYSIS*

E. T. KUCERA, R. R. HEINRICH

Chemical Engineering Division, Argonne National Laboratory, 9700 South Cass Avenue, Argonne, Illinois 60439 (USA)

Concentration of trace elements found in coal, ash, and materials used in a fluidized-bed combustion process have been determined by thermal neutron activation and absolute Ge(Li) gamma-ray spectrometry. Described are the calibration of detectors and corrections associated with the method along with estimated uncertainties. A brief description of the computer code used in the processing of the Ge(Li) spectra is presented. Comparisons of instrumental neutron activation analysis results with NBS standards and those obtained by the atomic absorption technique are tabulated. A total of 21 trace elements have been determined or identified in the fluidized-bed products and these results are used in identifying trace element depositions in various stages of the fluidized-bed combustion process.

Introduction

The modifications and innovations in coal treatment facilities have provided the analytical chemist with a myriad of samples for trace element determination. In an effort to reduce emission of trace elements from coal combustion, the deposition and enrichment of trace elements in coal combustion products have been characterized using a variety of analytical procedures. In an extensive investigation, RUCH and co-workers[1] at the Illinois State Geological Survey laboratories have analyzed over a hundred coals and ash for major, minor, and trace elements by various analytical methods. SHEIBLEY[2] has reported on the analysis of a large number of coals and ash for minor and trace elements, which he analyzed solely by instrumental neutron activation analysis (INAA). Mass balances for trace elements in

* Work performed under the auspices of the U. S. Energy Research and Development Administration.

conventional coal-fired combustion systems have relied mainly on isotopic dilution mass spectrometry,[3] atomic absorption,[4,5] X-ray fluorescence;[5] BOLTAN et al.[6] used INAA with complementary support from spark-source mass spectrometry and atomic absorption methods to obtain mass balances. Trace element studies for a coal gasification process have been reported by ATTARI.[7]

One of the many endeavours of Argonne National Laboratory has been the operation of an experimental bench-scale fluidized-bed combustor[8] for reducing

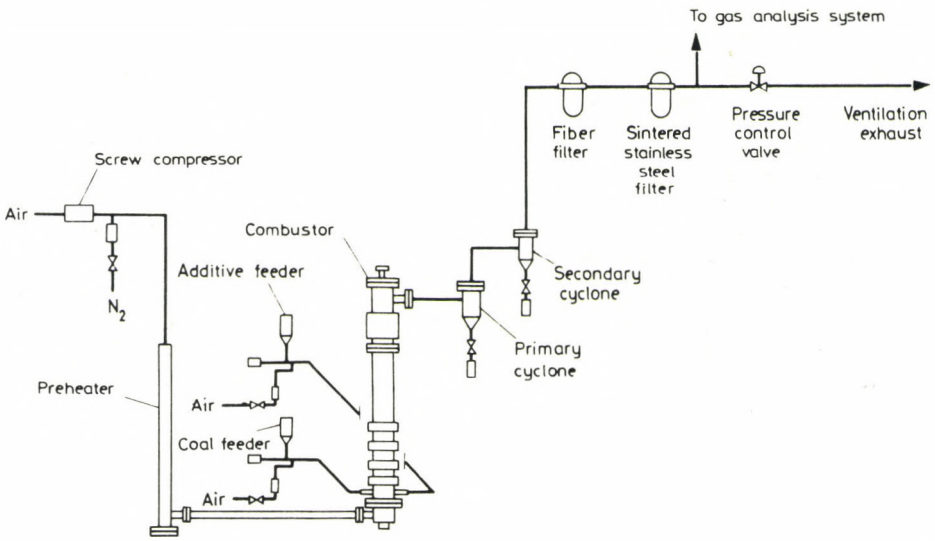

Fig. 1. Simplified equipment flowsheet of bench-scale fluidized-bed combustor and associated equipment

emission of SO_2 and NO_x. This experimental unit (Fig. 1) is a six-inch pressurized combustor in which additives of lime or dolomite are used to effect SO_2 removal. Because the operating temperature of a fluidized-bed combustor is well below that of a conventional coal-fired power plant, experiments were designed to evaluate this system for trace element emissions.[9]

The samples for the analytical work were generated in four fluidized-bed coal combustion experiments in which either alumina or dolomite additive was used, and the operating temperature and pressure were varied. The results of these experiments are compared with results obtained by an independent laboratory for trace element analysis of coal and ash samples generated in a

Lurgi gasifier and analyzed by atomic absorption (AA). Also included are INAA results that we obtained in the analysis of National Bureau of Standards (NBS) coal, ash, and orchard leaves standards and some of the results from an interlaboratory INAA comparison of NBS coal and fly ash.[10]

Experimental

Unknowns and standards

Our trace element analyses were performed on 100 mg samples of coal, ash, alumina, and dolomite, whereas 100-200 mg amounts were taken for the various NBS standard samples. Coal samples were air dried at 50 °C for 6 h; ash, alumina, and dolomite were air dried at 115 °C for a period of 4 h. Prior to irradiation, standards were maintained in accordance with the vendor's recommendation. Both samples and standards were prepared for irradiation by encapsulating them in 2.5 cm by 1 cm diameter snap-top polyethylene vials that had previously been cleaned in distilled water and ethanol.

Gold flux monitors weighing approximately 1 mg were also encapsulated in small polyethylene tubes to avoid sample contamination. These monitors were strategically placed with respect to the samples within the irradiation capsule in order to monitor reactor flux gradients.

Irradiation conditions

Samples, standards, capsule blanks, and flux monitors were irradiated in a thermal flux at the Argonne CP-5 Research Reactor. One-hour irradiations were made in the large pneumatic facility of CP-5, where the neutron flux is approximately $2 \cdot 10^{13}$ n · cm^{-2} · sec^{-1}. Longer irradiations were made in the isotope-tray position where the neutron flux is about $5 \cdot 10^{12}$ n · cm^{-2} · sec^{-1}.

Ge(Li) gamma-ray counting

The initial counting of the samples began about 3 h after the irradiation using an absolutely calibrated 4% efficient Ge(Li) detector capable of a 4 keV full-width-half-maximum (FWHM) resolution for the 1.33 MeV gamma-ray of ^{60}Co. This detector, because of its relatively poor resolution and low efficiency, was used to determine the shorter lived activities, such as ^{24}Na, ^{56}Mn, and ^{42}K. About 8 – 10 h after the irradiation, when the total activity level was reduced sufficiently, the samples were transferred to an automatic sample changer coupled to an 8% Ge(Li) detector whose resolution was 2.0 keV FWHM for the 1.33 MeV gamma-ray. Each of these detectors was a part of a 4096-channel multianalyzer system which was

equipped with a read-write magnetic tape data storage capability for off-line computer analysis of the Ge(Li) gamma-ray spectra.

Counting of each sample for the particular nuclide of interest was repeated at least three times within three half-life periods from the end of the irradiation. The principal gamma-ray of each nuclide was counted for a sufficient length of time to provide, in most cases, counting statistics ranging from 1 – 10%, and the precision for replicate counts was required to be within this same range. Counting geometries were adjusted to provide a maximum total count rate which did not exceed 1700 counts · sec^{-1} within the multichannel analyzers. For these sample counting rates, the error due to dead-time corrections was less than 1%.

Detector calibration

The accuracy limitation in absolute Ge(Li) counting is primarily in the determination of detector efficiency. Our detectors are calibrated by counting radioactive standards whose disintegration rates have been determined in an absolute manner, namely, by 4π beta or beta-gamma coincidence counting techniques. These standards, ranging in energy from 0.1 to 2.0 MeV, are supplied primarily by NBS and the Amersham Searle Corporation. In general, absolute accuracies of the standard nuclei are quoted to be ±0.3 to ±0.9%; however, our experience, based upon comparison of standards from different suppliers, has been that accuracies are more realistically ±1 – 2%. The absolute efficiency calibration of the detector is made for a fixed sample (standard) position, which is a distance of about 10 cm from the detector face. The values of efficiency (counts/photons) as a function of gamma-ray energy determined at the calibrated 10 cm position are mathematically fit to a fifth-order polynomial, the coefficients of which are used in a computer analysis program for determining the efficiency of any gamma-ray within the energy range of calibration. Counting versatility was provided by relating efficiencies at other counting geometries to this absolute calibration by means of a shelf factor. From the relative count rates of 32 gamma-ray energies, ranging from 0.122 to 1.84 MeV, shelf factors for eight different distances were established. A weighted least squares polynomial fit of these data indicates that for distances between 5 and 80 cm a constant shelf factor can be used with an accuracy within ±1.5%. Samples of coals, ashes, and comparative standards were counted initially at geometries of 40 – 20 cm on the low-efficiency (4%) detector and finally at the 10 cm geometry on the higher efficiency detector (8%).

Geometry corrections for sample size and sample thickness were made by employing a factor determined from a 0.411 MeV gamma-ray uniformly dispersed in 100 mg of sample matrix relative to the same gamma-ray

Table 1
Comparison of absolute INAA analysis with NBS coal, fly ash and orchard leaves standards

Element	Element concentration, ppm unless % indicated					
	NBS SRM 1632 (Coal)		NBS SRM 1633 (Fly ash)		NBS SRM 1571 (Orchard leaves)	
	Value	This work[a]	Value	This work	Value	This work[a]
Na	414 ± 20[b]	353 ± 21	3200 ± 400[b]	2603 ± 156	82 ± 6[c]	78 ± 5
K (%)	0.28 ± 0.03[b]	0.26 ± 0.02	1.72[d]	1.29 ± 0.09	1.47 ± 0.03	1.42 ± 0.09
Mn	40 ± 3	45 ± 3	493 ± 7	464 ± 46	91 ± 4[c]	90 ± 6
Cr	20.2 ± 0.3	24 ± 3	131 ± 2	131 ± 9	2.3[d]	2.5 ± 0.4
Co	6[d]	5.3 ± 0.4	38[d]	35 ± 2	0.2[d]	0.15 ± 0.03
Fe (%)	0.87 ± 0.03	0.83 ± 0.07	6.2 ± 0.3[b]	5.7 ± 0.3	0.03 ± 0.002[c]	0.03 ± 0.004
As	5.9 ± 0.6	5.1 ± 0.5	61 ± 6	49 ± 5	14 ± 2[c]	12 ± 1
Se	2.9 ± 0.3	-	9.4 ± 0.5	11 ± 3	0.08 ± 0.01[c]	-
Zn	-	-	-	-	25 ± 3[c]	26 ± 4
Br	19.3 ± 1.9[b]	18 ± 2	-	-	10[d]	10 ± 1
Rb	21 ± 2[b]	23 ± 7	-	-	12 ± 1[c]	12 ± 2
Sc	3.7 ± 0.3[b]	3.9 ± 0.2	-	-	-	0.063 ± 0.008

[a] Two detectors and replica samples.
[b] Ref. 10
[c] Provisional value.
[d] Uncertified, information value only.

Table 2
Lurgi gasifier coal and ash trace element concentrations determined by INAA and AA[a]

Element	Trace element concentration, ppm							
	Coal 1		Coal 2		Ash 1		Ash 2	
	INAA	AA	INAA	AA	INAA	AA	INAA	AA
As	2.3 ± 1	1.6	2.5 ± 1.2	1.0	ND[b]	0.3	ND	0.1
Co	3.8 ± 0.6	3.7	3.2 ± 0.5	4.3	38 ± 4	NR[c]	34 ± 3	40
Cr	15 ± 2	15	18 ± 3	22	592 ± 59	551	806 ± 81	705
Mn	23 ± 2	21	19 ± 2	20	305 ± 31	338	156 ± 16	243
Sb	0.1 ± 0.05	0.3	ID[d]	0.1	ND	0.3	ND	0.2
Zn	242 ± 121	182	ID	43	1600 ± 160	1580	ID	469

[a] AA – Analysis carried out by an independent laboratory.
[b] ND – Not detected.
[c] NR – Not reported.
[d] ID – Identified only.

unattenuated at the absolutely (10 cm) calibrated position. Also, corrections were made for sample self-absorption and capsule attenuation. The total correction for all these conditions was $<2\%$.

The total cumulative RMS error associated with the absolute Ge(Li) counting is estimated to be $\pm 6\%$. This assumes that counting statistics of a nuclide can be $\leq 1\%$, which, of course, is not always possible in multielement analysis. Included also in the RMS error is a 5% uncertainty associated with the nuclear data, namely, the activation cross-section, branching ratio, and half-life. However, to limit the uncertainty to 5%, a judicious selection of reliable data[11-13] is required.

Summarized in Table 1 are element concentrations common to different NBS standards, which have been determined by utilizing our absolute INAA method. In addition, INAA trace element analysis was performed on coal and ash samples generated from a coal gasification facility (Lurgi gasifier), and these results are compared in Table 2 with independent results[14] obtained by the atomic absorption technique. The uncertainty of the atomic absorption (AA) data is estimated to be $\pm 10\%$. For most elements, the agreement of our results with the NBS standards in Table 1 and the AA results in Table 2 is extremely encouraging. The results obtained for sodium and potassium in Table 1, although low with respect to the uncertified values, compare favourably with the results reported by RICCI.[15]

Data analysis

The computer code used in the analysis of our Ge(Li) spectra was originally written by GUNNINK et al.[16] for use at Lawrence Livermore Laboratory (LLL), Livermore, California. This code was the precursor to a more sophisticated LLL code,[17] but the more important features of the code, such as peak finding, nuclide identification, peak integration, and efficiency determination, are essentially unchanged and the earlier code is adequate for our application.

Descriptively, the code locates peaks within the spectrum by describing a tangent to the peak and noting where the tangent changes sign. Peak boundaries are determined by noting in both the forward and backward direction where the slope of the peak either levels off or changes sign. If an overlap of two or three peaks occurs, the boundaries are determined in the same manner but after the last peak in the cluster. Background is determined by subtracting the area under the defined boundaries from the gross counts under the peak. A statistical uncertainty is then assigned to the net count under the peak. Peak energies are determined by relating the peak position or channel number to a unique polynomial equation which describes the nonlinearity of the counting system. Required also is a relationship between energy and channel position, which is linearly proportional to this polynomial.

An auxiliary library program provides information on nuclide numbers, half-lives, parent-daughter relationships, accurate gamma-ray energies and branching ratios, efficiency calibrations, and geometry factors. In addition to the primary gamma-ray of a particular nuclide, up to two associative gamma-rays are also listed, and these are used for purposes of identification. The detector efficiency information is generated in the manner described previously, namely, from absolute gamma-ray standards and these efficiencies are used to convert counts per minute to photons per minute.

The library program is also used to establish peak identification. Six criteria must be met before a positive identification can be realized. The first of these is that the computer-determined energy of a given peak must fall within ±3 keV of the library energies. Since several nuclides may have energies within this criteria, other tests must be made to eliminate unlikely candidates. These are an evaluation of half-life vs. decay time and the search for associative gammas. Each associative gamma-ray must also meet energy test criteria and a relative-intensity test criteria. How well a nuclide scores on these tests is determined by multiplying each test score together to obtain a confidence index. The nuclide with the highest confidence index is then identified as being responsible for the peak or peaks in question. The success of this portion of the program depends primarily upon an accurate energy calibration of the detector and accurate nuclear data, namely, gamma-ray energies and intensities.

Results and discussion

A total of four fluidized-bed experiments were performed to assess the behaviour of trace elements during coal combustion. In Table 3 are the minor and trace element compositions (in ppm) of the materials introduced into the fluidized-bed combustor in these experiments. The coal used (Pittsburgh seam coal) appears to be within the quantitative trace element range of typical Midwest or Eastern United States coals,[1] with the notable exception of the chromium content. This aberrant concentration is about a factor of 5 higher than normal and is considered to be caused by the grinding and pulverizing of the coal in preparation for the fluidized-bed process. Two experiments, No. 1 and 2, involved the combustion of coal to which high-purity Type 38 Alundum grain alumina was added as the fluidized-bed material. Gallium was one of the prominent trace elements found in this material and was significantly retained in the combustor bed, as indicated in Table 4. The remaining two experiments, No. 3 and 4, initially utilized half-calcined and partially sulfated dolomite; and, for this reason, somewhat

Table 3
Trace element concentrations (ppm[a]) of input materials used in fluidized-bed coal experiments

Element	Starting bed materials				
	Alumina	Half-calcined and partially sulfated dolomite		Additives	
	Expt. No. 1 and 2	Expt. No. 3	Expt. No. 4	Coal	Dolomite
As	–	15.5(A)	–	6(B)	2.3(B)
Br	6(B)	7(B)	–	13(B)	–
Ce	–	–	5(C)	–	2(C)
Co	–	–	3.1(A)	1.8(B)	2(C)
Cr	–	57(B)	96(A)	104(A)	14(B)
Cs	–	–	–	–	0.9(C)
Dy	–	–	–	0.2(B)	–
Fe	240(A)	$1.1 \cdot 10^4$(A)	$1.2 \cdot 10^4$(A)	$1.0 \cdot 10^4$(A)	$5.6 \cdot 10^3$(A)
Ga	110(A)	–	–	–	–
Hf	1.7(A)	13(C)	–	–	–
K	–	$3.2 \cdot 10^3$(A)	$2.8 \cdot 10^3$(A)	580(C)	$4.6 \cdot 10^3$(B)
La	–	5.6(B)	6(B)	4.2(A)	3.4(A)
Mn	–	111(A)	106(B)	26(A)	55(A)
Na	$1.7 \cdot 10^3$(A)	533(A)	613(A)	687(A)	368(A)
Sb	–	5(C)	–	0.3(A)	–
Sc	0.03(A)	2.5(B)	2.5(A)	1.7(A)	1.5(A)
Zn	–	98(C)	–	–	–

[a]Parts per million followed by error rating.
A = ⩽10% ⩽C = 50%
B = ⩽15% ID = Identification only.

Table 4

Trace element experiments 1 and 2, using alumina additive: trace element concentrations in ppm[a] at site of depositions. Operating conditions: Expt. 1 – bed temperature 1550 °F, pressure 10 atm; Expt. 2 – bed temperature 1670 °F, pressure 8 atm

Element	Primary cyclone		Secondary cyclone		Primary filter	Final bed	
	Expt. 1	Expt. 2	Expt. 1	Expt. 2	(Expt. 2 only)	Expt. 1	Expt. 2
As	30(A)	–	–	ID	–	4.1(B)	–
Br	–	–	3(B)	–	–	–	ID
Co	11(B)	14(B)	19(A)	21(A)	29(A)	–	0.8(B)
Cr	183(A)	567(A)	297(A)	455(A)	499(A)	12(C)	11(B)
Fe	$5.9 \cdot 10^4$(A)	$9.8 \cdot 10^4$(A)	$3.6 \cdot 10^4$(A)	$6.0 \cdot 10^4$(A)	$6.5 \cdot 10^4$(A)	$5.5 \cdot 10^3$(A)	$3.3 \cdot 10^3$(A)
K	$3.7 \cdot 10^3$(C)	–	$5 \cdot 10^3$(C)	–	–	657(B)	–
La	31(A)	–	52(A)	29(C)	ID	3.7(A)	ID
Mn	109(B)	353(C)	142(B)	201(B)	258(C)	39(B)	16(A)
Na	$4.1 \cdot 10^3$(A)	$7.7 \cdot 10^3$(A)	$7.2 \cdot 10^3$(A)	$1.3 \cdot 10^4$(A)	$2.2 \cdot 10^4$(A)	$1.3 \cdot 10^3$(A)	$1.6 \cdot 10^3$(A)
Sc	9(A)	13(A)	19(A)	24(A)	32(A)	1.8(A)	0.8(B)
Elements determined, but not used in mass balance							
Ba	354(C)	601(B)	863(B)	940(C)	$1.6 \cdot 10^3$(C)	–	–
Ce	19(C)	33(C)	13(C)	21(C)	22(C)	8(C)	–
Cs	–	3(B)	–	–	6(C)	–	0.4(C)
Dy	1.8(C)	–	2.9(A)	3(C)	5(C)	–	–
Ga	–	–	–	–	–	–	116(B)
Hf	2.9(C)	3(C)	6(C)	6.1(B)	–	92(A)	2.4(B)
Sb	3(C)	–	6.2(B)	–	–	0.7(B)	–
Ta	–	1(C)	–	3(C)	4(A)	–	–
Tb	–	–	–	–	4(C)	–	–
Yb	4(C)	–	7.5(C)	–	5.5(C)	5.2(B)	–
Zn	–	–	–	–	–	–	46(C)

[a]Parts per million with error ratings.
A = ⩽10% C = ⩽50%
B = ⩽15% ID = Identification only.

Table 5

Trace element experiments 3 and 4, using dolomite additive: trace element concentrations in ppm[a] at site of deposition. Operating conditions:
Expt. 3 – bed temperature 1550 °F, pressure 10 atm; Expt. 4 – bed temperature 1660 °F, pressure 8 atm

Element	Overflow		Primary cyclone		Secondary cyclone		Primary filter		Final bed	
	Expt. 3	Expt. 4	Expt. 3	Expt. 4	Expt. 3	Expt. 4	Expt. 3	Expt. 4	Expt. 3	Expt. 4
As	11(A)	19(A)	17(A)	20(C)	39(B)	ID	–	88(A)	7(B)	–
Br	5(B)	ID	6(C)	ID	26(B)	ID	56(A)	–	9(A)	–
Co	–	2.9(A)	7(A)	8(A)	19(B)	18(B)	22(A)	32(A)	1.7(B)	4.1(A)
Cr	36(B)	120(A)	313(A)	679(A)	512(A)	430(B)	726(A)	605(A)	14(C)	106(A)
Fe	$8.7 \cdot 10^3$(A)	$1.2 \cdot 10^4$(A)	$4.2 \cdot 10^4$(A)	$5.0 \cdot 10^4$(A)	$3.7 \cdot 10^4$(A)	$4.9 \cdot 10^4$(A)	$3.1 \cdot 10^4$(A)	$6.2 \cdot 10^4$(A)	$5.4 \cdot 10^3$(A)	$1.6 \cdot 10^4$(A)
K	$2.2 \cdot 10^3$(A)	$1.6 \cdot 10^3$(C)	$5.6 \cdot 10^3$(C)	$4.9 \cdot 10^4$(C)	$1.9 \cdot 10^4$(B)	$1.5 \cdot 10^4$(C)	$2.6 \cdot 10^4$(A)	$2.0 \cdot 10^4$(B)	$1.5 \cdot 10^3$(B)	$1.6 \cdot 10^3$(C)
La	4(A)	5(C)	14(A)	ID	53(A)	ID	60(A)	80(B)	3.3(A)	6(A)
Mn	73(A)	ID	197(A)	ID	200(B)	ID	177(A)	380(B)	60(A)	137(A)
Na	453(A)	584(A)	$2.2 \cdot 10^3$(B)	$3.3 \cdot 10^3$(A)	$7.3 \cdot 10^3$(A)	$8 \cdot 10^3$(A)	$8.4 \cdot 10^3$(A)	$1.3 \cdot 10^4$(A)	288(A)	753(A)
Sc	1.9(A)	2.2(A)	5(A)	7(A)	21(A)	21(A)	25(A)	34(A)	1.3(A)	2.7(A)
Elements determined, but not used in mass balance										
Ba	–	–	–	399(C)	$1.1 \cdot 10^3$(C)	103(C)	918(C)	$1.7 \cdot 10^3$(B)	–	–
Ce	–	56(C)	–	21(C)	–	18(C)	12(C)	24(C)	–	3(C)
Cs	–	–	–	2.6(B)	8(C)	6(B)	9(B)	10(C)	–	–
Dy	–	–	–	ID	–	–	3(C)	–	–	–
Hf	–	ID	–	2(C)	6(C)	5(C)	6(B)	7(C)	–	0.5(C)
Sb	–	0.5(C)	1.4(C)	–	3.4(B)	–	–	–	ID	–
Ta	–	–	–	0.7(B)	–	0.7(B)	1(C)	3(C)	–	–
Tb	–	–	–	–	–	–	4(C)	–	–	–
Yb	–	ID	2(B)	ID	8.3(B)	ID	–	13(C)	–	–
Zn	86(C)	ID	194(C)	–	–	–	–	–	ID	–

[a] Parts per million followed by error rating.
A = ⩽10% C = ⩽50%
B = ⩽15% ID = Identification only.

Table 6

Mass balance - % recovery[a] for 10 trace elements in alumina and dolomite additives in coal combustion experiments (mass balance based on solid sample analysis only)

Element	Alumina combustion		Dolomite combustion		Average[b]
	Expt. 1	Expt. 2	Expt. 3	Expt. 4	
As	85	I[c]	85	>83	85
Br	0	I	36	I	18
Co	79	100	88	96	91
Cr	27	64	83	120	74
Fe	92	120	95	92	100
K	120	I	77	74	90
La	120	>74	89	I	104
Mn	110	170	110	I	130
Na	79	120	85	100	96
Sc	110	110	83	88	98

[a]Percent of element entering combustor accounted for in product streams.

[b]Average recovery for experiments in which a balance was determined.

[c]I - Indeterminate due to incomplete data.

higher trace element concentrations are expected in this material as compared to trace element concentrations found in the unreacted dolomite additive.

Summarized in Tables 4 and 5, respectively, are the trace element results obtained in the alumina-bed and dolomite-bed experiments for samples taken at various stages of the process. In these tables, the upper portion contains the ten trace elements for which mass balances were established (see Table 6). Mass balances were not determined for the remaining elements, which are shown in Table 4 and 5, for the purpose of illustrating the extent of the INAA analysis.

Table 6 represents material balances based on solid samples only. Inputs to the mass balances consisted of trace element concentrations from the initial bed materials, the coal, and the dolomite additive. Output from the system consisted of trace element concentrations from the final beds, overflow material (sulfated dolomite), and entrained solids recovered in the primary and secondary cyclones and filters. The high recoveries, particularly for arsenic,

indicates that the fluidized-bed combustor can be more efficient in the retention of trace elements than conventional combustors.[18] The low recovery of chromium is suspect because of the possible contamination problem that was previously mentioned.

These analytical results for multielement trace elements in coal, ashes, and related materials used in coal-combustion facilities indicate that INAA provides a reliable nondestructive method with the requisite accuracies. With the expected growth of energy-conversion systems and the application of necessary pollution controls, multielement INAA can contribute significantly to the elucidation of important environmental problems.

*

The authors wish to express their thanks to R. MALEWICKI for his able assistance in this work and to E. COBB of the CP–5 Reactor staff for his assistance in the irradiations.

References

1. R. R. RUCH, H. J. GLUSKOTER, N. F. SHIMP, Occurrence and distribution of potentially volatile trace elements in coal, A Final Report, Ill. State Geo. Surv., Environ. Geol. Notes, No. 72, 1974.
2. D. W. SHEIBLEY, Trace element analysis of coal by neutron activation, 166th National Meeting, Amer. Chem. Soc., Div. Fuel Chem. 18, 4 (1973) 59.
3. J. A. CARTER, R. L. WALKER, J. R. SITES, Trace impurities in fuels by isotopic dilution mass spectroscopy, 166th National Meeting, Amer. Chem. Soc., Div. Fuel Chem. 18, 4 (1973) 78.
4. N. SCHULTZ, E. A. HATTMAN, W. B. BOOKER, The fate of trace elements during coal pretreatment and combustion, 166th National Meeting, Amer. Chem. Soc., Div. Fuel Chem. 18, 4 (1973) 108.
5. J. W. KOAKINEN, R. M. JORDEN, M. H. LAWASANI, R. E. WEST, Environ. Sci. Tech., 9 (1975) 862.
6. N. E. BOLTAN, J. A. CARTER, J. F. EMERY, C. FELDMAN, W. FULKERSON, L. D. HULETT, W. S. LYON, Trace element mass balance around a coal-fired steam plant, 166th National Meeting, Amer. Chem. Soc., Div. Fuel Chem. 18, 4 (1973) 114.
7. A. ATTARI, Fate of trace constituents of coal during gasification, Environ. Prat. Technol. Ser., EPA–650/2–73–004, 1973.
8. G. J. VOGEL, W. M. SWIFT, J. F. LENC, P. T. CUNNINGHAM, W. I. WILSON, A. F. PANEK, F. G. TEATS, A. A. JONKE, Reduction of atmospheric pollution by the application of fluidized-bed combustion and regeneration of sulfur-containing additives, Annual Report No. ANL/ES/CEN–1007, Argonne National Laboratory, Argonne, Illinois, 1974.
9. W. M. SWIFT, G. J. VOGEL, A. F. PANEK, Potential of fluidized-bed combustion for reducing trace element emissions, Proc. Air Pollut. Control Assoc., 75–46. 3 (1975).
10. J. M. ONDOV, W. H. ZOLLER, ILHAN OLMEZ, NIK. ARAS, G. E. GORDON, L. A. RANCITELLI, K. H. ABEL, R. H. FILBY, K. R. SHAH, R. C. RAGAINI, Anal. Chem., 47 (1975) 1102.

11. W. W. BOWMAN, K. W. MacMURDO, Atomic Data and Nuclear Data Tables 13 (1974).
12 R. G. HELMER, R. C. GREENWOOD, Nucl. Technol., 25 (1975) 258.
13. S. F. MUGHABGHAB, D. I. GARBER, Neutron cross-sections, Vol. 1, Resonance parameters, Brookhaven National Laboratory Report BNL–325, 3rd Edition, Brookhaven, New York, 1973.
14. Peabody Coal Co., private communication.
15 E. RICCI, Trans. Amer. Nucl. Soc., 21 (1975) 99.
16. R. GUNNINK, H. B. LEVY, J. B. NIDAY, Identification and determination of gamma emitters by computer analysis of Ge(Li) spectra, Lawrence Livermore Laboratory Report UCID–15140, Livermore, California, 1967.
17. R. GUNNINK, J. B. NIDAY, Computerized quantitative analysis by gamma-ray spectrometry, Lawrence Livermore Laboratory Report UCRL–51061, Livermore, California, 1972.
18. W. M. SWIFT, private communication.

Journal of Radioanalytical Chemistry, Vol. 32 (1976) 151–171

ACTIVATION ANALYSIS AND DENDROCHRONOLOGY FOR ESTIMATING POLLUTION HISTORIES

K. K. S. PILLAY

Department of Nuclear Engineering, The Pennsylvania State University
University Park, Pennsylvania 16802 (USA)

Neutron activation analyses of wood shavings from tree rings have shown that plant tissues grown through periods of varying environmental conditions keep permanent records of the trace elements they received through nutrients from their immediate surroundings. Detailed examination of several species of trees, along with dendrochronological data, suggest the possibilities of utilizing this technique for pollution monitoring as well as for developing valuable information for environmental modelling.

Introduction

There is abundant evidence to indicate that the growth and well-being of plants and animals are influenced, among other things, by the amounts of various substances in their environment.[1,2] Environmental changes happen continually in space and time and have done so all through one's life. The present conditions of an animal are the product of its total environmental history as it has affected the actions of its inherited genetic code. Similarly, every plant has a unique and continually changing environment, and since plants are fixed in one spot, their environmental changes are principally in time. Thus, the knowledge of the changes in a plant over a period of time could be a unique indicator of the environmental changes that happen around the plant.

Dendrochronological measurements have long been used in the study of climate history and there is heavy reliance on this method in various archeological studies.[3,4] The tree rings, which are generally obvious on the cross-sections of most trees, can be more accurately described as successive layers of xylem growth – each layer having been formed by the tree in response to some environmental fluctuations which may include differences in the concentrations of heavy metals and other nonessential ions. Tree rings are normally of an annual nature in seasonal climates. This well known

principle[5] of tree ring dating in conjunction with activation analysis may be applied to study the chronological sequence of the environmental history of trace elements.

Background

The potentials of using plant specimens for examining both essential and toxic materials in the environment are obvious from several early investigations. In 1961, SCHRODER and BALASSA,[6] in their survey of the lead contents of various plant and animal tissues, reported that the center areas of an old elm tree had relatively little lead compared to the sections near its bark. In 1970, AULT et al.[7] and HOLTZMAN[8] examined several tree species for ^{210}Pb concentrations in tree rings. HOLTZMAN's data indicated that the ^{210}Pb concentrations decreased exponentially with the age of the tree ring, thus suggesting that the variations in lead content of tree rings have paralleled the environmental releases of lead. A recent report by SHEPPARD and FUNK[9] reports the use of trees as environmental sensors monitoring long-term heavy metal contamination of a river.

The concern over environmental pollution has initiated numerous studies during the last decade, some of which have adequately demonstrated that plants are reliable indicators of dissolved metal ion concentrations in the soils. PARVES and MACKENZIE[10] showed that there is considerable accumulation of certain elements such as boron, lead, zinc, and copper in herbages from soils known to have been contaminated as a result of air pollution. In studies examining lead and mercury burdens of urban woody plants, SMITH[11, 12] pointed out that lead accumulation in certain plant tissues far exceeds the levels in trees grown in areas with geological lead deposits. In a recent review article, HUISINGH[13] clearly implicates certain observed toxicites to agricultural crops to heavy metallic pollution of soils. In addition to plants, bryophytes[14] and lichens[15] also have demonstrated potentials to be monitors of environmental pollutants.

Numerous investigations conducted during the past decade have revealed the public health problems associated with the presence of several of the trace elements in the food supply, drinking water, and air. There is, however, a serious limitation on reliable information regarding long-term changes in the trace element concentrations in the environment. Much of the available historic information is generated from preserved museum specimens of plant and animal tissues. Ironically, these specimens have always been preserved using compounds of many of the elements such as lead, arsenic, mercury, etc. as components of preservatives.[16, 17] Yet, the analyses of some of these specimens have been considered as historical data. There are, however,

some reliable data collected through careful experimentation using Arctic ice layers and deep lake and ocean sediments as well as corings from undisturbed interiors of caves. While these techniques are superior to the analyses of museum specimens of unknown preservation history, these methods can be applied only on very limited areas of the earth's surface. Since trees are grown on most regions of the earth's surface, the method of employing tree ring analysis as an indicator of pollution histories seems very desirable.

Experimental

The various techniques used in tree sampling and analysis during this investigation are briefly described below. Because of the nature of the samples used, a new series of studies was performed to determine the best procedures for preparing, drying, preserving, irradiating, and counting the samples. The selection of the species of tree samples for this preliminary investigation was based on the availability of samples which, in turn, was dependent on the tree cutting plans at The Pennsylvania State University during the summer months of 1972 and 1973.

Preparation of samples

The tree sections used during this investigation were collected from the University Park campus of The Pennsylvania State University. The tree sections taken from about one meter above the ground level were approximately 15 cm thick and were transferred to the laboratory in large polyethylene bags. The tree rings were approximately dated by carefully counting the rings on one of the clean-cut surfaces. The samples for analyses were collected using a carbon steel drill tip (4 mm diameter). The wood shavings removed from preselected tree rings were collected in clean porous filter paper containers and were dried in a desiccator or freeze-dried until they attained a constant weight. While this method of sample collection is satisfactory for trees which have been cut, other methods of extracting corings and dating the samples can be used in collecting and analyzing samples from living trees.[3]

Preparation of analytical standards

Through a systematic examination, the trace elements present in tree rings as well as those that can be reliably quantitated were determined. A series of analytical standards were then carefully prepared and preserved for use during the analyses of tree rings. The following mixtures (Table 1) were prepared and used as analytical standards during this investigation.

Table 1
Analytical standards

Identification	Elemental standards	Form in which irradiated
Mixture 1	Na, Cl, I	Aqueous solution in polyethylene bags
Mixture 2	Cu, Mn, Ca	Aqueous solution in polyethylene bags
Mixture 3	Al, V, Ti, Mg	Aqueous solution in polyethylene bags
Mixture 4	K, Br, S	Aqueous solution in polyethylene bags
Mixture 5	Cr, Hg, Zn, Co	Freeze-dried aliquotes in quartz tubes
Mixture 6	Se, Sb, La, Sc	Freeze-dried aliquotes in quartz tubes
Mixture 7	Au, As, Ag, Rb	Freeze-dried aliquotes in quartz tubes
Flux monitors	Fe, Cu	wire

In addition, the NBS Orchard Leaves Standard (SRM-1571) was periodically analyzed along with the tree ring samples. Because the irradiation conditions chosen for the analyses of wood samples induced excessive amounts of radioactivity in the Orchard Leaves Standards, these analyses used only 10 to 15 mg quantities of orchard leaves in comparison to the suggested 250 mg or more as the minimum amount for homogeneity in samples. Generally, a quantity of 100-250 mg of tree ring sample was used for each analysis.

Neutron activation analysis

The multielemental analyses of tree ring samples were done using multiple neutron irradiation and gamma-ray spectrometry using a high resolution Ge(Li) detector and a soft-were oriented programmable multichannel analyzer. The neutron activation analysis consisted of two reactor irradiations and at least three countings at different decay periods. The irradiation and counting schedules used are shown in Table 2.

Short irradiation. The wood shavings were weighed and sealed in clean polyethylene bags. These bags were then placed in a 2 dram polyethylene vial, containing a copper flux monitor. Both the flux monitor and wood shaving samples were placed in the polyethylene rabbit. After reactor irradiation, the wood shavings were gathered and placed in a 2 dram vial containing a 1 cm thick polyurathane sponge. A suction device attached to the bottom of the polyvial enabled the quantitative collection of wood

Table 2
Activation* and counting schedule used in the determination of trace elements in tree rings

Irradiation period	Irradiation facility	Decay period	Counting period, sec	Elements determined
5 min	Pneumatic transfer system using polyethylene rabbits	2 min	50-200	Ti, I, Br, Mn, Cu, V, Cl, Na, Ca, Mg, K
25 h	Merry-go-round quartz encapsulated samples in aluminum holder	3-4 d	40-4000	As, Au, Br, La, K, Sm
		4-6 weeks	10,000 to 40,000	Se, Hg, Cr, Sb, Ag, Rb, Sc, Zn, Co, Fe, Eu, Hf

*The thermal neutron fluxes at both the irradiation facilities were about 10^{13} n · cm^{-2} · sec^{-1}.

shavings and a reproducible geometry for mounting and counting the samples. The whole procedure of opening the plastic bag and gathering and mounting the samples can be accomplished in less than 30 seconds. The flux monitors were separated and counted following the counting of the wood sample. The samples were counted with a 2-minute decay, while the flux monitors were counted with a 7-minute decay.

L o n g i r r a d i a t i o n . The samples used for long irradiations were placed in 10 mm I. D. (1 mm thick) quartz tubes and they were prefabricated for ease of heat sealing after placing the samples inside and during the opening of the capsule after irradiation. The samples, analytical standards, and the flux monitors were then irradiated at a thermal flux of about 10^{13} n · cm^{-2} · sec^{-1} for a 25 hour period using a rotatable irradiation facility called a "Merry-Go-Round". This device allows the irradiation of up to 24 samples to a uniform neutron flux for extended periods. These irradiations are generally performed within a 50 hour period. The irradiated samples are allowed to decay for about 3 days prior to first counting. The samples are

Table 3

Thermal neutron activation products and the gamma-radiations used in the analysis of trace elements in tree rings

Radioisotope	Half-life	Specific γ-ray used, E, keV	Other γ-radiations E, keV
^{51}Ti	5.8 m	320.0	608.4, 928.5
^{128}I	25.0 m	442.7	526.3, 743.5, 968.9
^{80}Br	18.0 m	617.0	640.0, 665.7
^{56}Mn	2.58 h	846.8	1811.0, 2113.2
^{27}Mg	9.5 m	1014.1	844, 170
^{66}Cu	5.1 m	1039.0	833.6
^{52}V	3.8 m	1434.4	-
^{42}K	12.5 h	1524.7	312
^{38}Cl	37.3 m	1642.0	2166.8
^{28}Al	2.3 m	1778.9	-
^{24}Na	15.0 h	2754.1	1368.5
^{49}Ca	8.5 m	3083.0	4071.0, 4680.0
^{37}S	5.1 m	3102.4	-
^{75}Se	120.4 d	264.6	121.1, 279,5, 400.6
^{153}Sm	47 h	103.2	69.7
^{203}Hg	46.57 d	279.2	-
^{51}Cr	27.8 d	320.1	-
^{198}Au	64.63 h	411.8	657.9, 1087.7
^{181}Hf	43 d	482.0	133.0, 345.9
^{76}As	26.5 h	559.1	657.0, 1216.3
^{110m}Ag	253.0 d	657.6	884.5, 937.3, 1384.3
^{46}Sc	84.0 d	889.3	1120.5
^{86}Rb	18.6 d	1076.6	-
^{65}Zn	243.8 d	1115.5	β^+, (511.1)
^{59}Fe	45.0 d	1291.6	1099.7
^{60}Co	5.25 y	1332.5	1173.2
^{152}Eu	12.4 y	1408.1	121.8, 244.5, 344.2, 779.1, 964.2, 1112.2
^{140}La	40.2 h	1596.2	328.7, 487.0, 815.8
^{124}Sb	60.3 d	1691.0	602.7, 722.7, 2091.1

removed and placed in counting vials using the procedures described earlier for extracting the wood shavings. the analytical standards are extracted with carrier solutions containing the combinations of elements in each of the mixtures. These rinsings are absorbed on a 1 cm thick polyurathane sponge

placed in counting vials. The analytical standards in the counting vials were then centrifuged to retain a uniform geometry during counting. These samples were then counted with a 3-day decay and with a decay period of about 40 to 50 days. The data from these countings are used to determine the concentrations of various trace elements listed in Table 2.

Gamma-ray spectrometry. The detector system used was a 56 cm^3 high resolution Ge(Li) detector (ORTEC) with a resolution of 2.0 keV at 1.33 MeV. This detector was used in combination with a multichannel analyzer (ND-4410) with a 12 K core size having a useable 4096 channels for data accumulations. The data were recorded on a 9-track magnetic tape using a PERTEC tape drive. Initial data processing was done using a Penn State version of a Lawrence Radiation Laboratory computer program for gamma-ray spectrometry called "Energy". An IBM system 370/Model 165 computer was used in the data reduction using the above mentioned program. The various radioisotopes and specific gamma emissions used for the quantitative analyses of the different elements are listed in Table 3.[18-20] It was recognized that some of these observed gamma peaks could have interference as well as possible contributions from other radioisotopes. These interferences were minimized by counting the samples at various decay times and by applying appropriate corrections using the gamma peaks of the analytical standards irradiated along with the samples.

Results

During this investigation, six different species of trees were used and the specimens ranged in age from 25 to 105 years. Several procedures for drying the wood shavings were examined. These include air drying, low temperature oven drying, desiccator drying and freeze-drying. While some of these procedures showed significant loss of several trace elements from the wood, desiccator drying and freeze-drying showed no recognizable loss of trace elements from most of the wood shavings. However, in samples containing large concentrations of mercury, the freeze-drying procedure often showed partial loss of mercury, while long-term desiccator drying using anhydrous calcium sulfate as desiccant did not result in similar losses of this or other trace elements.

Although the analytical techniques used here were capable of detecting and quantitating about 30 trace elements (see Table 2) in tree rings, only about 20 listed in Table 4 were found in measurable quantities in most of the specimens analyzed. The observed range of the concentrations of these elements are as shown in Table 4. The periodic comparison of the analyses

Table 4
Trace elements found in measurable quantities in tree ring samples

Elements	Concentration range*	Elements	Concentration range*
Calcium	200 - 14,000	Lanthanum	0.01 - 1
Potassium	300 - 4,000	Mercury	0.01 - 75
Chlorine	ND** - 150	Arsenic	0.05 - 5
Sodium	ND - 50	Chromium	0.02 - 0.5
Iron	ND - 50	Silver	ND - 1
Manganese	1 - 25	Cobalt	ND - 0.5
Aluminum	1 - 25	Antimony	ND - 0.2
Zinc	1 - 10	Gold	ND - 0.5
Copper	ND - 10	Scandium	ND - 0.01
Rubidium	0.1 - 2		

*All concentrations are in μg of element/g of dry wood.
**"ND" denotes trace element levels "not detectable" in this matrix using the analytical procedures described here.

of NBS Orchard Leaves (SRM-1571) gave good agreement (5 - 15%) with the certified values for Ca, K, Na, Mn, As, Fe, Rb, Zn, and Cu.

The precision of the analyses of wood samples is influenced by the natural variation of trace elements within the samples, although the methods described here have shown 5 - 10% precision for a single determination in the analyses of SRM-1571. In order to determine the variations in the trace element levels in samples from tree rings, a series of 16 samples was taken from different locations of the same tree ring of an oak tree approximately 1 meter in diameter.

Table 5 lists the means (μ), standard deviations (σ), and the coefficients of variance of these analyses. The quotient, σ/μ, known as the coefficient of variance, is the standard deviation with the mean expressed as unity. Replicate analyses of samples from a location over the same tree ring showed considerably less variation between samples. These results indicate that tree ring samples are not ideally homogeneous in their trace element composition. However, there are measurable variations between various tree rings and this is evident when these data are compared with the summary of results given in Table 6. Table 6 lists the μ, σ, and σ/μ values for the same oak tree, these samples were taken from 22 different tree rings in increments of 5 tree

Table 5

Analysis of multiple samples from various locations of a tree ring, in μg g of dry wood

Elements	Mean	Standard deviation	Coefficient of variance
Mn	7.64	3.00	0.39
Cu	1.53	0.06	0.04
K	1057	383	0.36
Cl	27.6	3.7	0.13
Al	3.0	0.6	0.20
Na	11.9	4.2	0.35
Ca	344	45	0.13
Hg	1.65	0.39	0.24
Cr	0.11	0.02	0.18
Au	0.095	0.019	0.20
As	0.50	0.004	0.01
Sb	0.017	0.005	0.29
Ag	0.04	0.01	0.25
Sc	0.002	0.0003	0.15
Rb	0.70	0.11	0.16
Zn	0.79	0.09	0.11
Fe	15.2	2.3	0.15
Co	0.16	0.05	0.31
La	0.40	0.06	0.15

Note: All the samples used were from the 75th year tree ring of an oak tree (Quercus ruboa).

rings going from pith toward cambium. These results indicate that there are considerable variations in the level of trace elements within the tree rings of a particular tree, and that these variations are different for the various elements examined during this investigation. A close examination of the detailed results given in Tables 7, 8, and 9 would bring out the significant variations in some of the elements such as mercury, silver, zinc, iron, arsenic, gold and antimony among others. Tables 7 and 8 include the analyses of tree ring samples from five different species ranging in age from 25 to 40 years, while Table 9 lists the results of detailed analyses of the cross-section of a large oak tree, which was 105 years old at the time of cutting.

Table 6
Summary of the results of the analyses of trace elements in various tree rings of an oak tree, in μg/g of dry wood

Elements	Mean	Standard deviation	Coefficient of variance
Mn	13.06	6.50	0.50
Cu	2.18	1.57	0.72
K	1098	754	0.67
Cl	35.7	61.4	1.72
Al	2.09	2.39	1.14
Na	8.24	5.78	0.70
Ca	263	421	1.60
Hg	7.02	18.94	2.70
Cr	0.17	0.13	0.76
Au	0.025	0.029	1.16
As	0.099	0.114	1.15
Sb	0.038	0.046	1.21
Ag	0.050	0.023	0.46
Sc	0.0012	0.0006	0.50
Rb	0.91	0.67	0.74
Zn	1.32	1.07	0.81
Fe	184.3	354.0	1.92
Co	0.17	0.15	0.88
La	0.14	0.097	0.69

Note: All the samples were from 22 different tree rings of a 105 year old oak tree (Quercus ruboa).

Figs 1 through 4 illustrate the variations of some of the trace elements in two of the species analyzed. These illustrations are generally representative of the very large variations of some of the elements within the various tree rings of the specimens. Elements such as Zn, Ag, and Hg have generally shown large variations in the tree rings ascribable to growth periods from 1930 to 1970, although the extent of these variations seems to differ with different plant species.

A futher comparison of the results is presented in Table 10. Here the coefficients of variance of several of the elements determined in all the six species of trees are listed. Among the six species studied, the oak tree

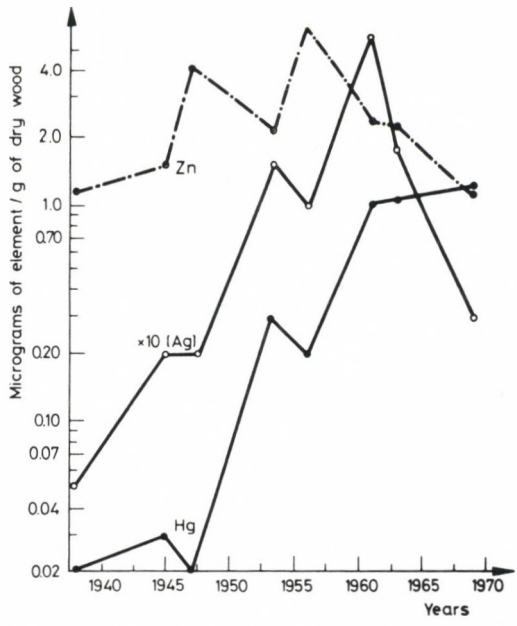

Fig. 1. Tree ring growth period (calender years) in the case of a flowering cherry

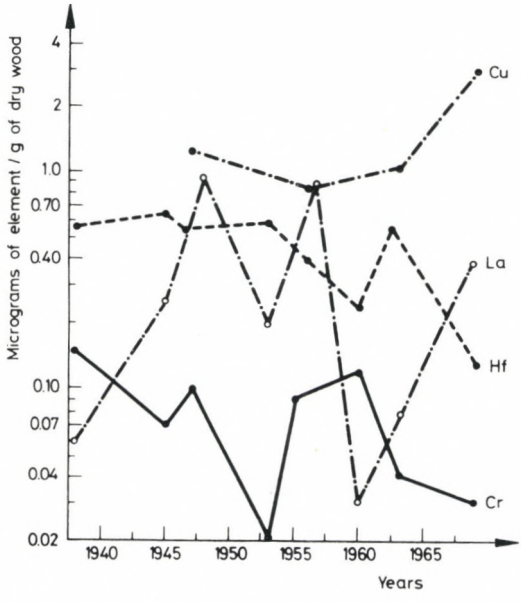

Fig. 2. Tree ring growth period (calender year) in the case of a flowering cherry

Table 7
Trace element concentrations of tree ring

Year*	Mn	Cu	K	Cl	Al	Na	Ca
1. Flowering cherry (Prunus Serrulata)							
1938	2.82	-	1834	33.0	23.5	15.5	528
1945	2.39	-	651	25.8	5.70	30.5	494
1947	1.21	1.23	700	71.5	2.16	24.6	558
1953	2.48	-	690	28.1	11.0	17.9	543
1956	1.44	0.82	1030	20.0	20.5	21.8	586
1961	5.94	-	1847	33.6	16.2	31.9	528
1963	1.10	1.04	517	5.6	2.21	13.9	658
1969	2.23	2.86	1795	ND**	20.2	18.7	566
2. Honey locust (Gleditsia Triacanthos. L)							
1947	1.77	0.49	3593	30.4	11.9	5.0	478
1954	1.40	-	2688	54.8	5.8	5.0	308
1959	1.31	0.86	3059	62.8	5.3	2.9	300
1964	3.81	2.50	1518	40.4	8.0	11.5	422
1969	3.43	1.07	2992	145.5	5.7	7.1	512

*Approximate year of growth of the tree ring as estimated by counting the distinctly visible rings in the tree section.

**"Not Detectable" by the analytical procedures used.

samples, in $\mu g/g$ of dry wood

Hg	Au	As	Ag	Rb	Zn	Fe	Co	La
0.02	-	-	0.005	-	1.2	35.4	0.02	0.06
0.03	-	-	0.020	-	1.5	21.1	0.01	0.25
0.02	0.011	0.027	0.020	0.34	4.1	13.7	0.05	0.96
0.30	-	-	0.210	-	2.3	10.9	0.02	0.10
0.20	0.022	0.025	0.100	0.26	6.4	48.2	0.02	0.89
1.07	-	-	0.595	-	2.7	30.8	0.02	0.03
1.05	0.014	0.080	0.180	0.19	2.5	23.2	0.02	0.08
1.24	0.014	0.140	0.030	0.56	1.2	48.3	0.02	0.40
0.01	0.011	0.13	0.020	1.47	0.6	13.5	0.03	0.07
0.01	-	-	0.020	-	0.4	8.7	0.02	0.01
0.35	0.011	0.17	0.020	1.82	0.9	11.3	0.02	0.06
0.14	-	-	0.235	-	1.4	3.7	0.05	0.01
0.93	0.004	0.14	0.020	1.68	1.6	10.1	0.05	0.04

Table 8
Trace element concentrations of tree ring

Year*	Mn	Cu	K	Cl	Al	Na	Ca
3. Hemlock (Tsuga Canadensis)							
1943	21.9	0.48	1668	15.8	5.7	51.0	909
1955	12.8	1.21	1027	11.2	2.5	44.6	719
1967	5.9	6.31	632	100.5	3.4	23.7	745
4. Lilac (Syringa Vulgaris)							
1947	24.5	0.25	430	ND**	3.4	ND	1380
1960	8.6	5.47	368	6.5	1.3	ND	1157
1969	6.7	4.22	570	10.1	1.3	ND	13742
5. Arborvitae (Thuja Occidentalis)							
1947	2.8	1.38	1803	41.5	25.8	8.7	1419
1958	2.1	1.27	387	60.9	6.5	15.2	1161
1966	4.0	1.98	1172	70.7	10.5	25.2	974

*Approximate year of growth of the tree ring as estimated by counting the distinctly visible rings in the tree section.

**"Not Detectable" by the analytical procedures used.

samples, in μg/g of dry wood

Hg	Au	As	Ag	Rb	Zn	Fe	Co	La
0.55	0.009	0.09	0.06	0.43	4.7	13.5	0.010	0.06
0.65	0.005	0.07	0.02	0.25	2.1	9.1	0.005	0.01
0.95	0.003	0.03	0.06	0.10	1.1	7.9	0.006	0.01
0.28	0.007	0.17	0.05	0.21	7.7	42.8	0.24	0.15
0.22	0.004	0.23	0.06	0.19	4.3	8.2	0.21	0.07
0.18	0.006	0.12	0.03	0.20	4.5	11.8	0.23	0.04
20.3	0.047	3.46	0.06	ND	4.0	20.6	0.020	1.00
0.82	0.012	0.30	0.02	0.08	2.0	12.0	0.005	0.18
1.62	0.020	0.37	0.03	0.16	5.9	23.4	0.014	0.26

Table 9

Trace element concentrations of tree ring

6. Northern Red Oak (Quercus ruboa)

Year*	Mn	Cu	K	Cl	Al	Na	Ca
(Pith)	18.1	ND**	665	15.6	3.24	ND	374
1873	20.9	ND	644	ND	1.83	ND	698
1878	18.5	1.80	805	11.1	1.20	ND	511
1883	14.9	ND	697	8.9	1.07	25.2	752
1888	13.5	1.55	815	15.2	1.24	ND	764
1893	14.7	ND	1070	17.0	2.35	ND	818
1898	12.8	2.29	938	14.8	1.09	7.5	646
1903	22.4	4.57	1171	13.4	4.08	ND	2270
1908	7.6	1.10	1044	11.8	1.09	5.2	396
1913	6.4	1.37	866	9.0	1.05	4.1	345
1918	9.3	1.37	1037	10.6	0.96	7.0	269
1923	12.5	ND	853	9.3	1.50	3.9	322
1928	18.9	7.10	1802	25.2	12.1	ND	683
1933	9.9	ND	844	15.0	0.93	5.0	353
1938	7.5	1.34	921	20.1	0.46	4.6	386
1943	6.5	1.37	945	26.7	2.45	10.4	300
1948	3.7	1.20	710	23.6	0.90	4.1	315
1953	6.6	0.85	560	23.5	0.40	3.9	460
1958	9.6	1.82	529	37.2	1.41	7.8	247
1963	5.6	1.28	657	32.2	0.76	5.3	502
1968	17.2	3.03	2780	290.3	2.76	13.2	791
1971	30.3	2.95	3786	120.0	3.10	16.5	1416

*Approximate year of growth of the tree ring as estimated by counting the distinctly visible rings in the tree section.

**"Not Detectable" by the analytical procedures used.

samples, in μg/g of dry wood

Hg	Au	As	Ag	Rb	Zn	Fe	Co	La
0.078	0.136	0.34	0.058	ND	1.8	1578	0.13	0.04
0.032	0.018	0.13	0.038	0.52	0.8	492	0.06	ND
0.011	0.028	0.14	0.070	0.41	0.7	588	0.04	0.02
0.013	0.070	0.11	0.041	0.51	0.8	524	0.05	0.16
0.018	0.040	0.13	0.112	0.64	1.1	492	0.04	0.08
0.017	0.028	0.08	0.055	0.76	0.9	231	0.04	0.01
0.027	0.007	0.10	0.104	0.72	1.2	84	0.08	ND
0.065	0.021	0.15	0.078	1.00	3.9	73.3	0.33	0.10
0.045	0.061	0.10	0.059	0.97	1.0	26.1	0.05	0.01
0.018	0.043	0.05	0.036	0.67	0.5	11.6	0.05	ND
0.038	0.041	0.10	0.040	0.56	0.4	38.3	0.06	0.01
0.080	0.034	0.12	0.086	0.66	1.9	32.3	0.14	ND
1.76	0.010	0.04	0.075	1.49	2.0	ND	0.35	0.11
10.42	0.006	0.01	0.029	0.79	1.7	5.9	0.33	0.18
70.8	0.005	0.01	0.027	0.83	0.7	3.8	0.25	0.15
1.59	0.010	0.50	0.040	0.73	0.8	14.4	0.14	0.40
1.11	0.006	0.08	0.030	0.69	0.5	4.2	0.09	0.10
0.61	0.005	0.02	0.038	0.51	0.5	6.9	0.09	0.10
1.05	0.004	0.01	0.034	0.38	0.6	5.3	0.12	0.08
1.34	0.003	0.23	0.033	0.38	0.9	3.2	0.10	0.10
2.75	0.016	0.01	0.048	2.07	3.4	8.0	0.35	0.11
1.95	0.012	ND	0.045	3.59	4.5	6.9	0.71	0.09

Table 10

A comparison of the coefficients of variance of trace element analyses in the rings of six different species

Elements	σ/μ Values					
	1	2	3	4	5	6
Mn	0.59	0.45	0.48	0.60	0.26	0.50
Cu	0.54	0.62	0.97	0.71	0.20	0.72
K	0.49	0.25	0.39	0.19	0.52	0.67
Cl	0.60	0.61	0.97	0.22	0.21	1.72
Al	0.63	0.34	0.35	0.50	0.58	1.14
Na	0.28	0.46	0.29	1.08	0.48	0.70
Ca	0.50	0.22	0.11	1.78	0.15	1.60
Hg	1.02	1.17	0.24	0.50	1.19	2.70
Au	0.27	0.33	0.33	0.33	0.58	1.16
As	0.67	0.13	0.50	0.29	1.07	1.15
Ag	1.28	1.37	0.40	0.20	0.50	0.46
Rb	0.41	0.87	0.50	0.05	0.33	0.74
Zn	0.59	0.50	0.57	0.29	0.39	0.81
Fe	0.46	0.35	0.24	0.74	0.26	1.92
Co	0.50	0.33	1.71	0.06	0.46	0.88
La	1.00	0.50	0.67	0.56	0.77	0.69

1 Prunus Serrulata,
2 Gleditsia Triacanthos L.,
3 Tsuga Canadensis,
4 Syringa Vulgaris,
5 Thuja Occidentalis,
6 Quercus ruboa.

specimen was very extensively examined. The variations in the concentrations of the trace elements in one of the rings, about 80 cm in diameter, was investigated using 16 different samples, and this may represent the maximum variations in the levels of trace elements within a tree ring. The average value of the coefficients of variance (Table 5) is 0.2 with a range from 0.01 to 0.4. This, when compared with the "within-the-tree" variations (Table 10), indicates that there are indeed considerable differences in the levels of many of the trace elements among the tree rings in all the speci-

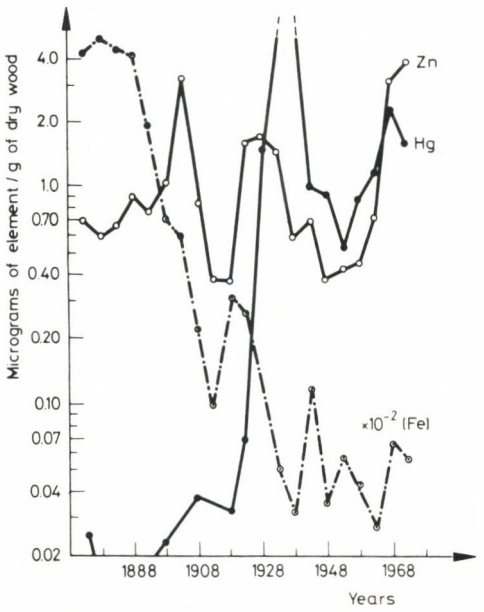

Fig. 3. Tree ring growth period (calender year) in the case of a Northern Red Oak

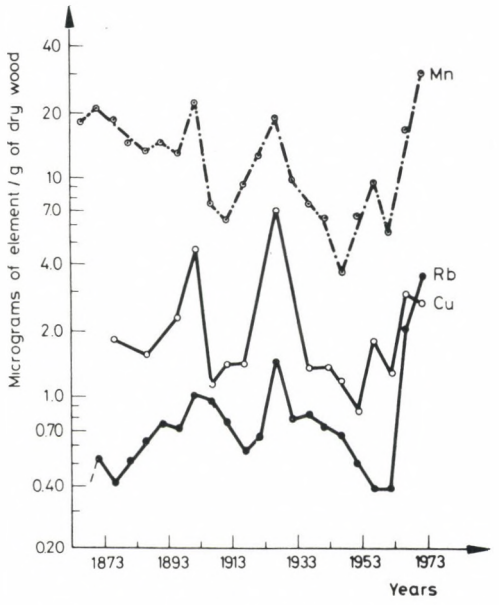

Fig. 4. Tree ring growth period (calender year) in the case of a Northern Red Oak

mens examined. Since the primary source of these trace elements is from the nutrients flowing through the xylem and phloem, the major source of these materials are from the immediate environment of the plant. The variations in the trace elemental compositions in different growth layers therefore are attributable to variations in the available elements to the plant during that period.

Discussion

Activation analyses of various plant tissues and wood samples have been previously reported by several investigators.[9, 21-23] More recent studies reported by MEYER et al.[22] and SHEPPARD et al.[9] generally contribute to the possibilities suggested in the title of this paper.

Some of the limitations imposed on this work because of the nature of this investigation and the continuously revealing complexity of the subject make it difficult to draw general conclusions. However, these and similar investigations would be very promising in learning the many facets of the accumulation, migration, and retention of trace elements in plant tissues.

The recognized limitations of this study include the following: (1) There are no records of the environmental history of the plant specimens used and the possible changes that may have resulted from the supply of artificial nutrients to these species. (2) The specimens used in this investigation were selected at random based primarily on the availability at the time of sample collection. (3) There are no analyses of several specimens of one species to determine the possible specificity of a particular species to accumulate specific elements. (4) This investigation, at this point, does not have detailed information about the horizontal as well as the vertical migration patterns of these trace elements within a living tree.

In spite of the above mentioned limitations, there is adequate evidence here to believe that plants do accumulate and preserve materials from their immediate environment and a detailed investigation of this phenomenon can be a rewarding experience intellectually as well as for generating some unique applications for environmental modelling and pollution studies.

*

The author wishes to acknowledge the assistance of Dr. R. J. HUTNIK, Professor of Forest Ecology at The Pennsylvania State University for many valuable discussions during this investigation.

References

1. A. ANDERSSON, K. O. NILSSON, Ambio, 1 (1972) 176.
2. D. B. LOURIA, M. M. JESELOW, A. A. BROWDER, Ann. Intern. Med.,76 (1972) 307.
3. M. A. STOKES, T. L. SMILEY, An Introduction to Tree-Ring Dating, University of Chicago Press, Chicago, 1968.
4. B. BANNISTER, Dendrochronology in Science in Archeology, THAMES and HUDSON (Eds), Basic Books, Inc., New York, 163, p. 161.
5. H. C. FRITTS, Science, 154 (1966) 973.
6. H. R. SCHRODER, J. J. BALASSA, J. Chronic Deseases, 14 (1961) 408.
7. W. V. AULT, R. G. SENECHAL, W. E. ERLEBACH, Environ. Sci. Technol., 4 (1970) 305.
8. R. B. HOLTZMAN, Environ. Sci. Technol., 4 (1970) 314.
9. J. C. SHEPPARD, W. H. FUNK, Environ. Sci. Technol., 9 (1975) 638.
10. D. PURVES, E. J. MACKENZIE, J. Soil Sci., 20 (1969) 288.
11. W. H. SMITH, Science, 175 (1971) 195.
12. W. H. SMITH, Science, 176 (1972) 1237.
13. D. HUISINGH, Heavy Metals: Implications for Agriculture, Journal Series Paper No. 4210 of North Carolina State University Agricultural Experimental Station, Raleigh, North Carolina, 1974, p. 375.
14. G. TYLER, Ambio, 1 (1972) 52.
15. K. K. S. PILLAY, V. HUNT, (unpublished data).
16. K. K. S. PILLAY, Mercury Pollution, letter to the editor of C and E News, American Chemical Society, (Jan. 10, 1972) 46.
17. D. W. JENKINS, The Toxic Metals in Your Future – and Your Past, Smithsonian, 1972, p. 62.
18. I. M. H. PAGDEN, G. J. PEARSON, J. W. BEWERS, J. Radioanal. Chem., 8 (1971) 127.
19. I. M. H. PAGDEN, G. J. PEARSON, J. W. BEWERS, J. Radioanal. Chem., 8 (1971) 373.
20. I. M. H. PAGDEN, G. J. PEARSON, J. W. BEWERS, J. Radioanal. Chem., 9 (1971) 101.
21. W. A. HALLER, L. A. RANCITELLI, J. A. COPPER, J. Agr. Food Chem., 16 (1968) 1036.
22. J. A. MEYER, J. E. LANGWIG, Wood Sci., 5 (1973) 270.
23. J. E. LANGWIG, J. A. MEYER, Wood Sci., 6 (1973) 39.

Journal of Radioanalytical Chemistry, Vol. 32 (1976) 173–178

MERCURY AND CADMIUM CONCENTRATIONS IN MILK IN PUERTO RICO

S. CHELLAPAN, K. B. PEDERSEN, H. PLAZA

University of Puerto Rico and Puerto Rico Nuclear Center (Puerto Rico)

Milk was collected over a four-month period from three representative sectors of Puerto Rico. Instrumental neutron activation analysis (INAA) performed on the samples showed that the mercury concentration was slightly higher than the safe upper limit set by the World Health Organisation on food products. INAA for cadmium yielded high values when compared with atomic absorption.

Introduction

It has been reported that neutron activation analysis can be used in instrumental, non-destructive form to measure mercury levels in many kinds of important matrices down to levels as low as 0.01 ppm.[1]

A previous study[2] done in Puerto Rico used instrumental neutron activation analysis (INAA) on various foods to determine metal contaminations. That study found that a high daily intake of mercury and cadmium by the average Puerto Rican is primarily due to the consumption of fresh milk. In the present work only milk samples were analyzed in order to determine mercury and cadmium concentrations statistically, using INAA.

Experimental

Sample collection

Milk samples for the analysis were collected from three areas of the island, divided according to milk production and processing. These three areas, shown in Fig. 1, represent the whole island.[3] Information received from the "Oficina de la Reglamentación de la industria Lechera" notes that the milk collected from different dairy farms is mixed together in the pasteurization process and then homogeneized. Because the milk collected areawide is a mixture of milk from all sources, it was decided that any portion of the bulk quantity will represent the whole milk production area.

Other investigations done on determination of trace elements in milk have used milk samples collected from the market.[4]

The number of samples that should be analyzed can be determined from the desired confidence level if the maximum standard deviation of individual measurements is known. The standard deviation for an individual sample calculated from counting statistics was high due to the high background measurements, and the corresponding number of samples required was found to be large. The number of samples finally used per determination was fixed by the capacity of the sample container as 7.

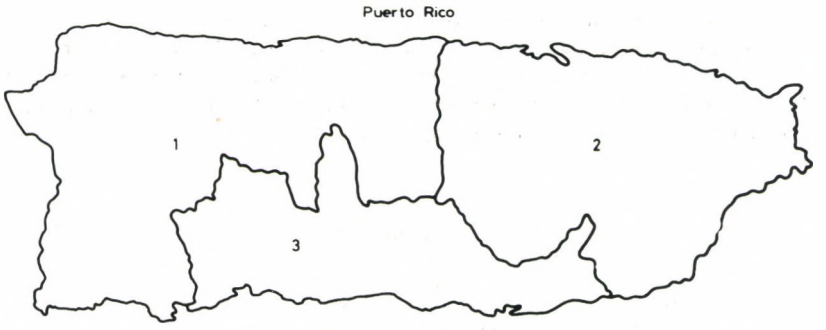

Fig. 1. Sample collection areas. Area No. 1: Mayagüez and Arecibo Region; Area No. 2: San Juan and Caguas Region; Area No. 3: Ponce Region

Sample and standard preparation

A standard solution was prepared by dissolving known amounts of mercuric oxide and cadmium metal in a small amount of concentrated nitric acid and then diluting to a known volume, using triply-distilled, deionized water, to yield a solution of known concentration of metals. One ml of the standard containing 10 μg each of mercury and cadmium metal was used for the analysis. Many reports have shown that losses of mercury ions occur by adsorption to container walls. ROSAIN and WAI[5] studied losses of mercury in solution during storage, and they found large losses at pH 2 and 7. Because of these possible losses, a freshly prepared standard was used for each irradiation.

JERVIS[6] reported the losses of mercury during freeze drying of the samples. For this reason the samples used in this investigation were not freeze dried.

It has been found that treatment of polyethylene vials with concentrated nitric acid at 80 °C for an hour will diminish the losses of mercury from the vials during irradiation.[7] However, it was found difficult to prevent the opening of some vials due to pressure buildup and so, in order to eliminate any problem associated with polyethylene vials, it was decided to use a high-purity synthetic quartz ampoule for all of the irradiations.

The ampoules were cleaned with aqua regia and then washed thoroughly about ten times with doubly-distilled, deionized water. Equal volumes of standard and sample were used in order to avoid errors due to geometry during counting. After filling with the desired amount of standard or sample the ampoules were heat sealed while being kept in liquid nitrogen to avoid heating of the sample. After sealing the ampoules were again cleaned in order to remove any surface contamination.

Irradiation and counting

A cylindrical plastic vessel, 50 mm I.D. x 70 mm long, fitted with a 22 mm diameter polyethylene vial at the center, to form an annulus 14 mm wide, was used as an irradiation container. For each irradiation seven samples, one standard, and one empty vial were placed in the annular space.

During irradiation the container was rotated at 30 rpm in order to expose all of the ampoules to the same integrated flux. The thermal-neutron flux was approximately $5 \cdot 10^{12}$ n $\cdot$ cm^{-2} $\cdot$ sec^{-1}, and the irradiation time varied from 6 to 12 hours. Samples were subsequently cooled in the reactor pool for periods of 3 to 4 days. After cooling they were again thoroughly cleaned with aqua regia.

The samples and the standard were counted in their ampoules in a fixed geometry for two hours, using a Princeton Gamma Tech 25 cm^3 coaxial Ge(Li) detector and a Nuclear Data 4096 channel pulse-height analyzer. For identification of the peaks the ND 4410 peak extraction overlay program was used; this contains routines for peak search, energy calibration and data smoothing.

The concentrations of the metals were computed using a computer routine written in FORTRAN IV, employing WASSON's method of photopeak integration.[8] The program included the decay correction for all of the samples back to the time when the standard was counted. For mercury and cadmium the 77.3 keV peak of ^{197}Hg and the 336 keV peak of ^{115m}In were used, respectively.

Results and discussion

Table 1 shows the mean values of the mercury concentrations and their standard deviations.

A high average of 0.080 ppm was noted for the month of October for Area No. 3; otherwise, the differences in mercury concentration were insignificant from one sampling period to another as well as between areas.

The values reported here for mercury concentrations are very similar to those found for dairy products in the Toronto area of Canada in 1970, but considerably higher than some reported from the United States in 1964.[9] The present investigation of mercury concentration in fresh milk indicates that Puerto Rico has a concentration slightly higher than the safe upper limit set by the World Health Organisation on food products in 1971.

Generally, a considerable difference between recent and earlier studies has been reported, and the concentration in recent years in other countries may be in the same range as in Puerto Rico. The increase in concentration with respect to time may indicate that the methods of analysis used are becoming more accurate, or that the mercury concentration has actually increased (or a combination of both). Either of the two possibilities appears reasonable because not only has instrumentation improved, so has also industrialization, and probably the use of mercury-containing fungicides in agriculture, increased.

Table 1

Mean values of mercury concentration in fresh milk (values are in ppm based on wet weight)

Sampling time	Area No. 1*	Area No. 2*	Area No. 3*
September	0.056±0.013	0.051±0.008	0.057±0.011
October	0.048±0.004	0.040±0.010	0.080±0.008
November	0.059±0.006	0.056±0.008	0.056±0.008
December	0.042±0.009	0.050±0.008	0.046±0.008

*Area No. 1: Western and part of the northern section of Puerto Rico, including the cities of Mayagüez and Arecibo.

Area No. 2: Northern and eastern part of the island, including the cities of San Juan and Caguas.

Area No. 3: Middle and southern part of the island, including the city of Ponce.

Table 2
Mean values of cadmium concentration in fresh milk (values in ppm based on wet weight)

Sampling time	Area No. 1	Area No. 2	Area No. 3
September	0.189±0.030	0.344±0.079	0.136±0.024
October	0.143±0.030	0.153±0.035	0.118±0.044
November	0.161±0.042	0.183±0.018	0.137±0.028
December	0.126±0.041	0.133±0.022	0.138±0.025

Mean cadmium concentrations and their standard deviations are shown in Table 2. These were found to be higher than the values reported in the literature.[10] Some variations in cadmium concentrations were observed areawide as well as a function of time. MURTHY et al.[11] reported the cadmium concentration in milk to be 0.018 to 0.03 ppm in the United States in the year 1967; this is about one sixth of the concentrations found in this study for Puerto Rico.

In addition to INAA atomic absorption photospectrometry was used on a smaller number of samples to verify the concentration levels of cadmium. For this determination nine milk samples and two blanks were analyzed. The concentrations were found to vary between 0.01 and 0.06 ppm. These values are in better agreement with the values reported for the United States than are the ones obtained from using INAA; however, their spread is much greater.

It is possible that the large difference in the results between the two methods is caused by the sample matrix in INAA and may indicate that it is not a satisfactory method for the determination of cadmium in milk. Suitable radiochemical separation of the cadmium before counting should improve the precision of the result.

For determination of mercury concentration purely instrumental neutron activation analysis is probably the most sensitive method since it precludes the loss of mercury.

References

1. V. P. GUINN, Determination of Mercury by Instrumental Neutron Activation Analysis. Technical Reports Series No. 137, IAEA, Vienna, 1972, p. 87.
2. K. LINGAPPAN, H. PLAZA, K. B. PEDERSEN, Mercury, Arsenic, Cadmium and Cobalt Determination in the Average Puerto Rican diet Using Instrumental Neutron Activation Analysis. Proc. of American Nuclear Society Topical Meeting on Nuclear Methods in

Environmental Research, University of Missouri, Columbia, July 29–31, 1974. (M. S. Thesis, University of Puerto Rico).
3. Relación de Vaquería de Primera clase que Entregan su Producción a las Plantas Elaboradoras por Región y Municipio. Departamento de Agricultura, San Juan, Puerto Rico, 1974.
4. G. K. MURTHY, U. RHEA, J. Dairy Science, 51 (1968).
5. R. M. ROSAIN, C. M. WAI, Anal. Chim. Acta, 65 (1973) 279.
6. R. E. JERVIS, B. TIEFENBACH, Trace Mercury Determinations in a Variety of Foods. Proc. of American Nuclear Society Topical Meeting on Nuclear Methods in Environmental Research, University of Missouri, Columbia, Aug. 23–24, 1971.
7. H. V. WEISS, Naval Undersea Center, San Diego, California, USA Private communication.
8. P. A. BAEDECKER, Anal. Chem., 43 (1971) 405.
9. F. M. D'ITRI, The Environmental Mercury Problem, The Chemical Rubber Co., 1972.
10. L. FRIBERG, M. PISCATOR, G. NORDBERG, Cadmium in the Environment. The Chemical Rubber Co., 1971.
11. G. K. MURTHY, V. RHEA, J. T. PEELER, Environ. Sci. Technol., 5 (1971) 436.

Journal of Radioanalytical Chemistry, Vol. 32 (1976) 179–188

Special Developments and Applications of Neutron Activation Analysis

PRECISION HIGH-SPEED NEUTRON ACTIVATION ANALYSIS VIA VERY SHORT-LIVED ACTIVITIES

D. A. MILLER,* V. P. GUINN

Department of Chemistry, University of California, Irvine
Irvine, California 92664 (USA)

An automated, highly reproducible fast-transfer system (0.36 ± 0.01 sec) has been developed, an oscillator/multichannel-scaling system has been developed to follow rapidly-changing spectrometer dead-times, the mathematics has been developed, and the data processing steps have been computerized. Three induced activities have been studied in some detail: ^{207m}Pb (0.80 sec), ^{38m}Cl (0.70 sec) and ^{20}F (11.03 sec). Both steady-state and high-intensity pulsed reactor irradiations, with and without a Cd liner, have been used. The dead-time correction method has been carefully checked, and the overall method has been tested by the analysis of two NBS Standard Reference Materials: orchard leaves (for Cl and Pb) and bovine liver (for Cl).

Introduction

While there exist over a hundred neutron-induced radionuclides with half-lives in the range of tenths of a second to one minute, only a small number of these have been routinely applied in neutron activation analysis (NAA). One explanation for this may be the relative insensitivities associated with many of these short-lived activities, since traditionally, and most frequently, neutron activation analysis has been employed because of its excellent sensitivity of detection for many elements. However, additional barriers are due to the difficulties inherent in the production and counting of such short-lived species. Such problems as rapid and reproducible methods of sample transfer from irradiator to counter, and the need for corrections due to dead-time in the multichannel analyzer (MCA) and pulse pile-up in the preamplifier associated with high and rapidly decreasing counting rates, have

*This paper represents a portion of the Ph. D. thesis of D. A. MILLER.

precluded the routine utilization of short-lived radionuclides in the field of NAA.

Previous research in these areas has circumvented many of these difficulties. This work was designed to attack existing problems, and to explore the use of short-lived radionuclides for routine instrumental neutron activation analysis (INAA). Use of these short-lived activities offers the possibilities of new or possibly more sensitive means for the determination of many elements via INAA, as well as a very rapid technique for serial analyses. A system for performing such analyses is described herein.

MCA dead-time corrections

In order to achieve adequate counting statistics, the counting of short-lived radionuclides usually involves the measurement of considerable activity in a very short period of time. This results in a rather high and rapidly decreasing dead-time in the MCA. Pulses received by the MCA during the time the analyzer is busy will not be counted. For longer-lived activities, analyzer dead-time is compensated for by the live-timer, which extends the counting interval for a period of time equal to the total time the analyzer was busy. For short-lived activities, the counting interval may equal one or more half-lives, hence this method of dead-time compensation is not applicable. Cyclic activation and measurement at lower counting rates could partially eliminate this problem, but the buildup of long-lived activities can severely interfere with this method. An alternative would be the use of single-channel analyzers (SCA) and scalers which could tolerate much higher counting rates with negligible associated dead-time losses. The major disadvantages of this approach include SCA drift, proper background compensation, and the need for several SCA/scaler combinations for the measurement of any one activity.

Several methods of dead-time compensation have been proposed. They have been mathematical in nature,[1-3] or have suggested the use of additional electronics to correct for MCA dead-time.[4-11] A comparison of several of these methods has been made by WIERNIK,[12] and more recently by HUYSMAS, GIJBELS, and HOSTE.[13] However, earlier work by the authors[14] indicated the need for a suitable method of correction for the general case of a mixture of several short-lived and long-lived radionuclides. The method developed and employed in this study proposes to allow for this general case, as well as for more selected conditions.

The basic equation for dead-time correction for the general case, as derived by SCHONFELD,[15] is given by:

$$C = \int_0^{t_c} A_0 \, e^{-\lambda t} \, [1-DT(t)] \, dt \qquad (1)$$

where C – actual acquired net counts in photopeak of interest;
A_0 – true photopeak count rate of radionuclide of interest at the start of the counting period, i.e., for zero dead-time;
t_c – length of counting period (clock-time);
λ – decay constant of radionuclide of interest;
$DT(t)$ – fractional MCA dead-time at time t.

Solution of Eq. (1) requires a knowledge of the instantaneous fractional dead-time of the MCA during the counting period. Fig. 1 outlines the

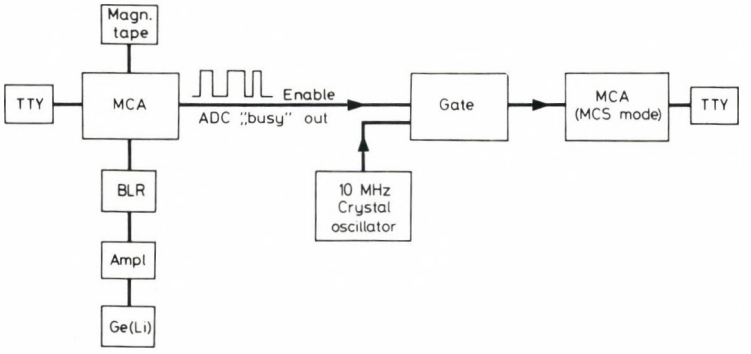

Fig. 1. Block diagram of the dead-time measurement system

circuitry assembled in the authors' laboratory to measure DT(t). During those periods of analyzer dead-time, the analog-to-digital converter (ADC) outputs a "busy" signal. This output can be used to trigger a gate that allows passage of clock pulses to a storage device. A 1024-channel MCA (Nuclear Data 100), operating in the multichannel-scaling (MCS) mode, is used to record the clock pulses as a function of time.

A comparison of those clock pulses recorded per unit time with the clock frequency yields the fractional dead-time during this period. The MCS sampling time should be small compared to the counting interval being used. For a counting time of 3 sec, a MCS sampling interval of 100 millisec was found to be adequate. For longer counting times, the sampling interval may be increased with a corresponding decrease in the clock frequency (see below).

The clock pulses recorded by the multichannel scaler yield a decaying dead-time function, as illustrated in Fig. 2. The exact shape of the curve, of course, is dependent upon the half-lives and amounts of the activities producing the dead-time in the MCA. The function DT(t) may be approximated by fitting these points with a polynomial expression. Experiments have shown that a third or fourth-order least-squares polynomial fit is sufficient. Such an expression for DT(t) is also shown in Fig. 2. Computer programs allow for the rapid fitting of the dead-time data and the solution of Eq. (1) for A_0 or the net photopeak counts corrected for analyzer dead-time.

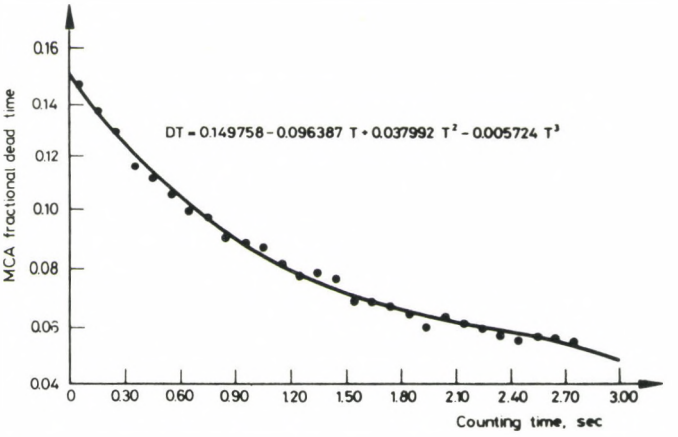

Fig. 2. Fractional dead-time vs. counting time. NBS Bovine Liver sample, chlorine analysis using ^{38m}Cl

This method was initially applied[16] to the determination of lead using the ^{207m}Pb activity (T = 0.80 sec), and has subsequently been used for the determination of several other short-lived radionuclides. The results presented below suggest the feasibility of this technique and the advantages of such analyses. A method similar to the one described here has been used successfully by WISPELAERE et al.[11] for dead-time corrections in the analyses of iron and iron ores, for induced activities with half-lives of the order of 2 - 3 min.

Experimental

Irradiations were carried out using the fast-transfer system (FTS) in the Nuclear Reactor Facility at the University of California, Irvine (UCI). Details of the UCI FTS have been presented elsewhere.[17] This system uses the

UCI 250 kW TRIGA reactor, and offers either Cd-lined (E-ring) or unlined (F-ring) irradiation positions. The thermal-neutron flux in these positions is $1.89 \cdot 10^{11}$ n · cm^{-2} · sec^{-1} and $6.57 \cdot 10^{12}$ n · cm^{-2} · sec^{-1}, respectively.

The activated samples are directly transferred in polyethylene "rabbits" to a lead cave housing a 38 cm^3 Ge(Li) detector (Nuclear Diodes) for counting. Normally operated at 90 psig of nitrogen pressure, the FTS has a transfer time from reactor to counter of 0.36 ± 0.01 sec for irradiation times greater than three seconds.

The counting equipment includes a 4096-channel Nuclear Data 50/50 MCA coupled to a Tennelec TC 611 Baseline Restorer and a Tennelec TC 202 Linear Amplifier. The FTS is controlled by a precision timer that enables exact (± 0.01 sec) and reproducible timing of irradiation and decay times for activation in either the steady-state or pulsing mode of the reactor. The timer, in its automatic mode, can initiate a cycle of:

(1) Load sample;
(2) Irradiate for preset time;
(3) Return sample and delay for preset time;
(4) Start analyzer acquiring;

with just the press of a single button. Difficulties due to bouncing associated with the reproducible positioning of the "rabbit" by the detector are eliminated by restricting the delay time to a minimum of 0.50 sec.

The polyethylene "rabbits" can accommodate either liquid or solid samples. However, sample size is restricted to approximately 0.7 cm^3. Liquid samples are more conveniently absorbed into cotton fiber, acting as a "rabbit" filler.

Results

A series of liquid standards of lead, chlorine, and fluorine were run as a check of the system, and to determine the interference-free sensitivities for these elements. Table 1 lists some pertinent nuclear data for the radionuclides measured, and also the optimum irradiation and counting conditions employed.

The counting was carried out in the clock-time mode in all cases. The lead samples were activated in the Cd-FTS, while the chlorine and fluorine samples were activated in the unlined system. A 100-millisec MCS interval was used for the ^{207m}Pb and ^{38m}Cl measurements, while 1 sec was found suitable for the ^{20}F counting (in this latter case, the gated oscillator frequency was decreased from 10 MHz to 625 kHz).

Table 1
Data concerning short-lived species studied

Radionuclide	Possible mode(s) of production	Half-life*	Principal γ-energy,* keV	Irradiation time, sec	Delay time, sec	Count time, sec
^{207m}Pb	$^{206}Pb(n, \gamma)$ $^{207}Pb(n, n')$ $^{208}Pb(n, 2n)$	0.80 s	570	4.00	0.50	3.0
^{38m}Cl	$^{37}Cl(n, \gamma)$	0.70 s	671	4.00	0.50	3.0
^{20}F	$^{19}F(n, \gamma)$	11.03 s	1633	30.00	2.00	30.0

*Values taken from Ref. [18]

The effects of the dead-time correction on the initial count rate (or net photopeak counts) can be seen in Figure 3. In this case, lead standard solutions were used which ranged in concentration from 100 μg Pb to 5000 μg Pb, causing the initial dead-time reading to range from 12% to 34%. As can be seen from the curves, substantial losses (up to 23% in the worst case illustrated) can occur without proper dead-time compensation. Even correcting the data for a single contribution (0.80 sec ^{207m}Pb) to the MCA dead-time fails to properly compensate for all losses. In the case of these single-element

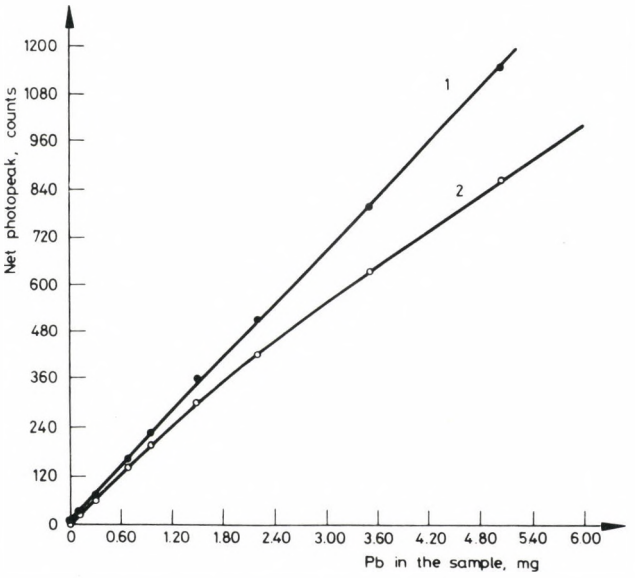

Fig. 3. Calibration curve for lead standards. Irradiation time 4.00 sec, delay time 0.50 sec, count time 3.00 sec. Each data point is the average of 10 runs. Curve 1 - corrected for dead time; curve 2 - uncorrected for dead time

standards, the additional contributions to the MCA dead-time are primarily N-16 from the oxygen in the aqueous solution and Al-28 from aluminum in the polyethylene "rabbits". Similar linearity was observed for the other elements, in which the standards concentration varied by at least a factor of 10 and the inital MCA dead-time ranged from 7% to 20%.

These results suggest a suitable method of analyzer dead-time correction. However, at analyzer dead-times exceeding approximately 30 - 35% (equivalent to about 10^4 total CPS with an average gamma-ray energy of

0.5 MeV), and for instances where a large (>10%) background dead-time due to long-lived species exists, appreciable losses (>10%) in the corrected net photopeak count rate (for a given sample) were observed, presumably due to coincidence events in the detector. A simultaneous broadening of the photopeak also occurs. This is in agreement with results obtained by WYTTENBACH.[19] Unless suitable corrections for this pile-up problem are made, this places an upper limit on this correction method.

Table 2
Sensitivities achieved for three elements in steady-state and pulsed irradiations

Radionuclide	Irradiation facility	Corrected net photopeak, counts/unit weight of element	
		Steady state (250 kW)	Pulse (1000 MW)
^{207m}Pb	Cd-FTS	496±14 cts/mg	18±2 cts/μg
^{38m}Cl	Unlined FTS	1089±40 cts/mg	(54 cts/μg)*
^{20}F	Unlined FTS	14± 1 cts/μg	58±2 cts/μg

*Calculated value, based on theoretical pulse enhancement factor.

Experiments with the standards yielded the interference-free sensitivities listed in Table 2. For activations using 1000 MW reactor pulses, an irradiation time of 400 millisec from the firing of the pulse was employed. Otherwise, the delay and counting conditions are identical to those given in Table 1 for steady-state irradiations at 250 kW.

The values reported for the steady-state conditions represent the mean of 3 or more samples, each activated and counted 5 times. The pulse-mode results represent 3 or more samples, each activated and counted twice. In this cyclic procedure both the photopeak data and the MCS dead-time data are summed. This summing and averaging technique has been shown empirically to be mathematically valid,[20] and tends to yield better statistics. All ± values represent uncertamties of the distribution, and tend not to exceed values calculated from the counting statistics by more than 1 - 2%.

Only in the determination of chlorine is a blank correction necessary. In this case, the blank typically contributes 75 - 80 counts for the steady-state irradiation and counting conditions. This somewhat restricts the practical limit of detection for chlorine, at least until a cleaner polyethylene rabbit material is found.

Table 3
Results obtained with two NBS Standard Reference Materials

Standard	Cl, ppm (dry wt. basis)		Pb, ppm (dry wt. basis)	
	Uncertified value	This study	Certified value	This study
Orchard Leaves	700	732±29	45±3	42±4
Bovine Liver	2600	2632±67	-	-

It may be of interest to note that the ^{207m}Pb activity observed in the Cd-lined position is approximately 2 times greater than in the unlined position. In view of the relative thermal, epithermal, and fast neutron fluxes in each position, this suggests a rather small contribution to the ^{207m}Pb activity from the (n, γ) reaction.

This dead-time correction method has also been checked by the analysis of two NBS Standard Reference Materials (Orchard Leaves and Bovine Liver). Table 3 lists the results of the analyses of these materials for chlorine and lead. The chlorine data were obtained from steady-state irradiations and the single value for lead resulted from irradiation in the pulse mode.

At present, several other short-lived radionuclides are being studied for their limits of detection by this method, and in selected cases for their application to routine analysis in specific sample matrices. As an example, the determination of lead by this method has been applied to the analyses of cartridge primer residues in an ongoing forensic chemistry program at U. C. Irvine.[21]

Conclusions

The advantages of employing short-lived radionuclides for INAA include: a very short sample analysis time (typically a few minutes per sample or less); the reduction of matrix interferences by using short irradiation and counting times; and reasonable sensitivities, due to the ability to tolerate high and rapidly changing counting rates. Hopefully, the results of this study demonstrate the availability of short-lived radionuclides for INAA, and that this and further work will lead to their routine application in work in which precise, rapid, and in many cases sensitive, analyses are desired.

References

1. M. WIERNIK, S. AMIEL, J. Radioanal. Chem., 3 (1969) 245.
2. H. A. DAS, J. ZONDERHUIS, Nucl. Technol., 10 (1971) 328.
3. E. JUNOD, J. Radioanal. Chem., 20 (1974) 113.
4. J. HARMS, Nucl. Instr. Methods, 53 (1967) 192.
5. H. H. BOLOTIN, M. G. STRAUSS, D. A. MCCLURE, Nucl. Instr. Methods, 83 (1970) 1.
6. W. GÖRNER, G. HÖHNER, Nucl. Instr. Methods, 88 (1970) 193.
7. F. ADAMS, J. HOSTE, J. BARTOŠEK, J. MAŠEK, J. Radioanal. Chem., 15 (1973) 479.
8. J. BARTOŠEK, G. WINDERS, J. HOSTE, Nucl. Instr. Methods, 103 (1972) 43.
9. J. BARTOŠEK, F. ADAMS, J. HOSTE, Nucl. Instr. Methods, 103 (1972) 45.
10. D. N. RAO, J. L. GLEN, D. TAYLOR, Nucl. Instr. Methods, 103 (1972) 175.
11. S. DE WISPELAERE, J. OP DE BEECK, J. HOSTE, Anal. Chem., 45 (1974) 547.
12. W. WIERNIK, Nucl. Instr. Methods, 95 (1971) 13.
13. K. HUYSMANS, R. GIJBELS, J. HOSTE, J. Radioanal. Chem., 20 (1974) 51.
14. D. A. MILLER, V. P. GUINN, High-speed determination of lead by neutron activation analysis, a paper presented at the Pacific Conference on Chemistry and Spectroscopy (ACS and SAS), San Diego, 1973.
15. E. SCHONFELD, Nucl. Instr. Methods, 42 (1966) 213.
16. V. P. GUINN, Dead-time corrections in the counting of one or more short-lived radionuclides, a paper presented at the American Chemical Society Nuclear Chemistry Division Meeting, Newport Beach, Calif., 1973.
17. V. P. GUINN, D. A. MILLER, G. E. MILLER, in Irradiation Facilities for Research Reactors, IAEA, Vienna, 1973, p. 441.
18. P. BODE, M. DE BRUIN, P. S. M. KORTHOVEN, J. Radioanal. Chem., 26 (1975) 209.
19. A. WYTTENBACH, J. Radioanal. Chem., 8 (1971) 335.
20. D. A. MILLER, unpublished data.
21. G. R. JOHNSON, M. A. PURCELL, V. P. GUINN, (to be published).

Journal of Radioanalytical Chemistry, Vol. 32 (1976) 189–193

MEASUREMENTS OF ARGON LEAKS THROUGH SEALS OF LIQUID SODIUM PUMPS BY NEUTRON ACTIVATION ANALYSIS

A. VAN DALEN, J. W. H. VAN DEN BERGH

Reactor Centrum Nederland, Petten (The Netherlands)

The leak-rate of Ar through seals of liquid sodium pumps for sodium-cooled fast reactors is measured by thermal neutron activation analysis of oil and air samples taken from the cooling and lubrication systems of the seals. A method to calculate the leak-rate through a triple seal from the increase of the Ar concentrations is given.

Introduction

Gas-leak-rates are most frequently measured with helium, a practical method because the background level of helium in air is low, the diffusion speed through leaks is high and the sensitivity is very high. So this technique was used to measure the leak-rate of gases through a mechanical triple seal of a sodium pump. No helium leak was detected, however, even after running the mechanical seal for a long period in a mock-up stand. The cause of this failure proved to be: the low solubility of helium in oil. So the helium enters very slowly through the oil film in the seal into the cooling and lubrication systems. Because these systems contain large volumes of oil and air (each about 0.1 m^3 of oil and 0.15 m^3 of air), it takes too much time before the increase in helium concentration can be measured. Argon, normally used as the covergas in sodium pumps, has a higher solubility in oil, so it is much more attractive in this case. In contrast to helium, argon can be determined directly in oil samples by instrumental activation analysis.

By using argon for leak detection, the leakage indicator is identical with the gas to be used in practice and no conversion factor has to be evaluated for helium to argon leak. The presence of argon in normal air to about 1 vol.% means, however, that the accuracy of the measurements should be high.

Procedure

The triple mechanical seal contains two oil systems to cool and lubricate the seals. Both systems contain a volume of air (omitted in the schematic drawing in Fig. 1) to pressurize the systems in case of a power outage to prevent damage to the seals by loss of lubrication and cooling. Samples of oil and air for analysis are taken from special by-pass systems in polythene tubing with constrictions. When sufficient oil or air has passed through the tubing to have representative aliquots, the tubing is sealed off at the constrictions. The resulting samples contain about 2 - 3 cm^3 oil or air.

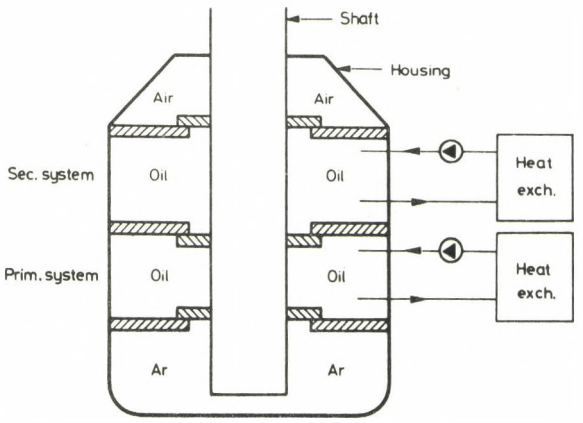

Fig. 1. Schematic drawing of a triple seal

They are analysed for argon by thermal neutron activation. After irradiation of the sealed tubes for one minute in a thermal flux of $5 \cdot 10^{13}$ $n \cdot cm^{-2} \cdot sec^{-1}$ the aliquots are counted for ^{41}Ar on a Ge(Li) detector. Although the capsules were airtight some diffusion of argon took place during the time of transport to the reactor (about 4 hrs). These losses were corrected for by redetermination of the Ar content the next day and applying Fick's diffusion law.

The amount of oil in each capsule was determined by weighing, the volume of air by releasing the air from the capsule under water and collecting in a calibrated tube. Standards were capsules with normal air.

Air and gas samples from a system with pressure less than atmospheric can be taken in quartz ampoules. This has two advantages. No diffusion of Ar takes place and the capsule itself acts as flux monitor by the reaction of

$^{29}Si(n, p)^{29}Al$ T = 6.56 m; E_γ = 1273.3 keV
$^{30}Si(n, \gamma)^{31}Si$ T = 2.62 h; E_γ = 1266 keV.

The corresponding data for argon are: ^{41}Ar: T = 110 m; E_γ = 1293.6 keV.

Interpretation of the measured argon concentrations

The argon pressure in the pump under the seal is kept constant so the leak-rate of argon into the oil system is proportional to the difference between the ultimate and the actual argon concentration in the oil system.

The increase of the argon concentration in the oil system is

$$dC/dt = K_1 (C_\infty - C) \tag{1}$$

The constant K_1 depends on the characteristics of the first seal and can be seen as the reciprocal of a resistance. C_∞ is the concentration at equilibrium. From the oil system the argon leaks into the air, the rate depending on the concentration in the oil system. The outflow or decrease in argon concentration in the oil system is

$$-dC/dt = K_2 C \tag{2}$$

The combination of the in- and outflow of argon results in the equation of the total increase of argon in the oil system:

$$dC/dt = K_1 (C_\infty - C) - K_2 C,$$

and after integration:

$$C = \frac{K_1 C_\infty}{K_1 + K_2} \left[1 - e^{-(K_1+K_2)t} \right] + C_0 \tag{3}$$

C_0 being the natural initial argon concentration in the system and air.

Combination of (3) at $t = \infty$ and (2) results in the expression for the rate of argon leak at steady state through the seal.

$$\frac{dC}{dt} = \frac{K_1 K_2 C_\infty}{K_1 + K_2} \tag{4}$$

In practice the initial amount of argon in the oil system (t=0) is subtracted, and instead of concentrations in an oil system, the sum of the amounts of Ar in oil and air is used because the system is closed.

In the case of a triple seal with two separate oil systems the complex problem was solved step by step. In the first step Eq. (3) is applied to the sequence first seal, primary oil system, and as the last seal the remainder (second seal, secondary oil system, third seal).

The second step is similar: the complex first seal (first seal, primary oil system, second seal), the secondary oil system, and the third seal. For both steps expression (3) is applied to the experimental points. This results in the determination of C_∞, and combinations of K values. The K values are reciprocal resistances, so for the combination in series they have to be added via the reciprocal form e. g. the primary system consisting of the first seal, the primary oil system, and the second seal:

$$1/K_1 + 1/K_2 = 1/K_p.$$

The resistance of the oil system is negligible compared with that of the seal because the pumping velocity is high. The individual values of K_1, K_2, and K_3 can be solved by using the fact that at stationary state ($t = \infty$) the leak-rate through both systems is equal. In practice the straight forward calculation is not used but an approximation method is applied, because the summation of the small K values in the reciprocal form leads to large errors.

For this triple seal the following results were obtained: $K_1 = 0.0027$, $K_2 = 0.0027$ and $K_3 = 0.00165\ h^{-1}$. The leak-rate at stationary state was $0.29\ cm^3$ STP Ar h^{-1} or $0.6 \cdot 10^{-4}$ torr $\cdot$ l $\cdot$ sec^{-1}. After 500 hrs running the primary system attained 82% of the stationary state, and the secondary system 78%.

Remarks and conclusions

When the seal starts running, the temperature increases due to friction in the seals, and consequently the solubility of argon in the oil changes. Fig. 2 shows the ratio of argon concentrations in air and oil samples from both systems as a function of the running time. The origin of the large excursion from the equilibrium state of the secondary system is unknown. Together with the long time needed to reach the new thermal equilibrium the homogeneity of the samples was noted to be not better then about 4 - 5% despite the high pumping velocity, about one quarter of the oil volume passed the pump per minute.

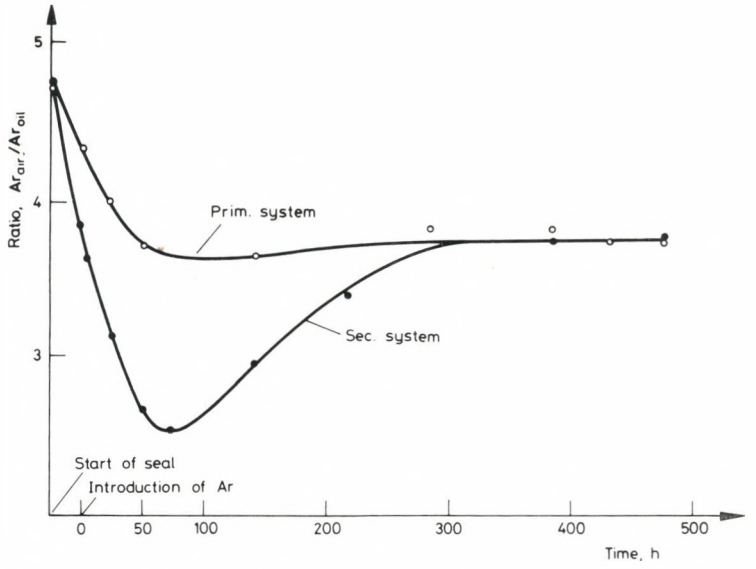

Fig. 2. Ratio of argon concentrations in air and oil samples

The errors in the determination of argon concentrations are 1% for oil, and 2% for air samples.

The equal values of K_1 and K_2 are in good agreement with the identical construction of both seals. Seal 3 was of another type.

Smaller volumes of oil in the systems will allow lower detection limits for the leak-rates and shorter respons times. For another seal type for which in principle only air samples had to be analysed, the complete leak measurement was performed within one week.

Journal of Radioanalytical Chemistry, Vol. 32 (1976) 195–205

OXYGEN AND NITROGEN IN COAL BY INSTRUMENTAL NEUTRON ACTIVATION ANALYSIS

IMPLICATIONS FOR CONVERSION

W. D. JAMES, W. D. EHMANN, C. E. HAMRIN,* L. L. CHYI**

Department of Chemistry, University of Kentucky, Lexington, Kentucky 40506 (USA)
**Department of Chemical Engineering, University of Kentucky, Lexington, Kentucky 40506 (USA)*
***Institute of Mining and Minerals Research, University of Kentucky, Lexington, Kentucky 40506 (USA)*

The feasibility of using fast neutron (14 MeV) activation analysis techniques for the determination of oxygen and nitrogen in coal has been investigated. Conditions that favor instrumental neutron activation analysis (INAA) include the absence of problems associated with sample dissolution and the capability of extremely rapid analyses as compared to older techniques such as the Kjeldahl method for nitrogen. Most previous oxygen determinations have been by difference after major component analyses. In the present study, oxygen was determined in sized coal and its low temperature ash (LTA) with the difference representing the organic oxygen content. Both the oxygen and nitrogen analyses employ a multiscaling technique with the former based on the $^{16}O(n, p)\,^{16}N$ reaction, while the latter utilizes the annihilation radiation produced by the product of the $^{14}N(n, 2n)\,^{13}N$ reaction. The high-energy gamma-radiation associated with the decay of ^{16}N was essentially free of spectral interferences for coal analysis, although fluorine could cause a primary interference if the F/O ratio exceeds 0.02. In the nitrogen work, experiments were performed to determine correction factors to account for the effects of the $^{12}C(p, \gamma)\,^{13}N$ and $^{13}C(p, n)\,^{13}N$ "knock-on" reactions and the $^{39}K(n, 2n)\,^{38}K$ reaction which produce interfering β^+ emitting radionuclides. Data are presented for oxygen in Western Kentucky No. 9 and No. 11 coal and coal ash and for nitrogen in eleven different coals.

Introduction

The importance of the organic oxygen content for process calculations, conversion studies, and classification of coal has been well documented.[1-8] Several methods have been developed for oxygen determinations.[9] However, these procedures are relatively laborious and have not generally been applied to coal analysis. For example, the analysis of coal by ASTM methods

specify the oxygen content (%) as the difference between 100 and the sum of all other major component concentrations.[10] The propagation of the errors involved in all of these major element determinations presents obvious problems in obtaining accurate oxygen measurements by this method.

We earlier presented a procedure for determining the organic oxygen content in coal by instrumental neutron activation analysis (INAA).[11] In this method the total oxygen content of the whole coal (O_{total}) and in its low temperature ash[12] (O_{inorg}) are measured and the organic oxygen is then calculated as the difference:

$$O_{org} = O_{total} - O_{inorg} \qquad (g\ LTA/g\ coal)$$

Although the full effects of nitrogen content on the conversion processes are unknown at this time, knowledge of nitrogen concentrations is desirable due to atmospheric pollution considerations. Nitrogen has been determined routinely by the well known Kjeldahl method. Although generally accurate, this procedure is relatively time-consuming and requires sample dissolution. INAA has already been proven a valuable tool in the determination of nitrogen in various matrices.[13-17] In the present investigation, a scheme has been developed for the routine determination of nitrogen in coal samples by fast neutron activation analysis. The method utilizes the $^{14}N(n, 2n)^{13}N$ reaction (T = 10 m) which produces a positron emitting nuclide. The resulting annihilation radiation is counted in coincidence as a measure of nitrogen content. Several positron emitters are produced and corrections are performed to account for those whose effects were significant.

Experimental

Oxygen determination

The oxygen contents were determined by an instrumental 14 MeV neutron activation technique similar to that described by MORGAN and EHMANN.[18] The technique is based on the $^{16}O(n, p)^{16}N$ reaction induced by 14 MeV neutrons produced by a Cockcroft-Walton neutron generator and subsequent multiscaler counting of the spectral region encompassing the 6.13 and 7.12 MeV, 7.1 sec half-life, ^{16}N photopeaks with a 10.2 cm x 10.2 cm NaI(Tl) well type detector and a Nuclear Data (ND 2200) 4096 channel analyzer. High levels of fluorine or boron could cause serious interferences in the oxygen determination only if the fluorine-to-oxygen ratio approaches 0.02, or the boron-to-oxygen ratio exceeds 100.[19] Since fluorine and boron

contents in coal are far below these levels,[20] these potential interferences are negligible. Since our oxygen procedure has been well documented, additional details will not be given here.

Nitrogen determination

The pertinent reaction in the nitrogen work is the (n, 2n) reaction which produces ^{13}N which decays via positron emission with a 10 min half-life. The 0.511 MeV annihilation radiation is counted in coincidence, using two 7.6 cm x 7.6 cm NaI(Tl) detectors positioned at 180° with respect to the sample counting position. Two single channel analyzers are each gated on the 0.511 MeV radiation triggering a fast coincidence unit and the output of this unit is fed to the ND 2200 multichannel analyzer operating in the multiscaler mode. Activation of the samples was achieved by the 14 MeV neutron generator connected with the counting station by a pneumatic transfer system. A typical multiscaler output is shown in Fig. 1.

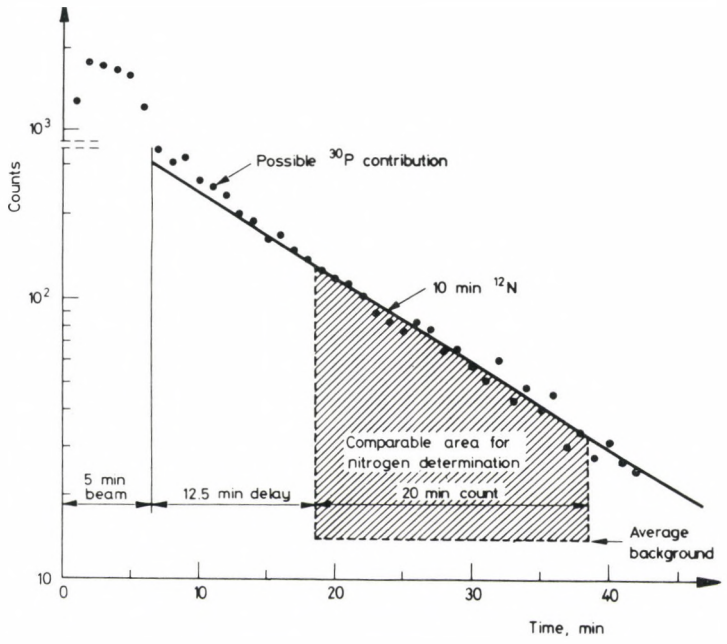

Fig. 1. Multichannel scaling spectrum shows the beam monitor BF_3 counts during irradiation and the subsequent sample decay. The shaded area is used for the nitrogen calculations

Table 1

Nuclear data for pertinent reactions in nitrogen analysis

Element	Approximate concentration in bituminous coal	Reaction	Half-life	Cross-section (14 MeV), mb	Possible error, %
N	1.5%	$^{14}N(n, 2n)^{13}N$	10 m	19	
Potential interferences:					
P	50 ppm	$^{31}P(n, 2n)^{30}P$	2.5 m	11	0.3
K	0.16%	$^{39}K(n, 2n)^{38}K$	7.7 m	27	1.1*
C	45%	$^{12}C(p, \gamma)^{13}N$	10 m		} 1.5*
		$^{13}C(p, n)^{13}N$	10 m		
Mo	9 ppm	$^{92}Mo(n, 2n)^{91}Mo$	15.5 m	119	<0.1
F	167 ppm	$^{19}F(n, 2n)^{18}F$	110 m	51	<0.1
Cl	0.36%	$^{35}Cl(n, 2n)^{34}Cl$	32 m	3.5	<0.1
Na	0.07%	$^{23}Na(n, 2n)^{22}Na$	2.6 y	13.8	<0.1

*Determined experimentally.

Although recent experiments[21] show the amount of nitrogen adsorbed on the surface of the coal is probably negligible, all samples used in this study were packaged under an inert (helium) atmosphere. Since coals absorb moisture to a great and varied extent, the samples were dried at 105 °C overnight in a vacuum oven, prior to packaging. A mass of about 1.5 - 2.0 g was obtained for each sample by carefully riffling the powdered samples. Because great care was taken in doing this, the splits of each sample can be considered replicate analyses of the same sample.

Since all positron emitters produced will be counted, a survey of potential interferences is included in Table 1. The most significant interference in coal samples is that caused by the $^{31}P(n, 2n)^{30}P$ (T = 2.5 m) reaction. The interference is minimized by use of a long delay which descriminates against the short-lived ^{30}P. After a 5 min irradiation and a 12.5 min delay, calculations show a 20 min count of the ^{13}N results in a maximum phosphorus contribution to the activity of 0.3% relative, for phosphorus concentrations common in bituminous coals.

The other significant interferences to the nitrogen determination occurred as a result of the $^{12}C(p, \gamma)^{13}N$ and $^{13}C(n, p)^{13}N$ "knock-on" reactions, which produce the same product as the desired reaction, and the $^{39}K(n, 2n)^{38}K$ reaction whose product decays by β^+ emission with a 7.7 min half-life. These interferences were evaluated experimentally by irradiating and counting carbon and potassium standards under the nitrogen determination conditions. Emperical correction factors were calculated and are employed in nitrogen calculations, although they were very small and account for no more than approximately 2% of the total accumulated counts.

Nitrogen content is calculated by comparison of the sample activity with nitrogen standards. Several standards have been used for nitrogen analysis by INAA.[17] In this work n-1-naphthylacetamide (7.56% N)[15] and NBS Standard Reference Material 1571, Orchard Leaves (2.76% N), were used as primary standards.

Results and discussion

In the case of the oxygen analysis, the multichannel scaling data were reduced by computer analysis and reported as oxygen content. Table 2 shows the results of five replicate determinations on each of two splits of Kentucky No. 11 coal and one sample of Kentucky No. 11 LTA. The previously published data from our group for Kentucky No. 9 coal and LTA are also summarized in this table. Both the Kentucky No. 9 and No. 11 coals analyzed in this study were from Western Kentucky. Error limits are based on the standard deviation of the mean and are ±0.2% O and ±0.3% O for the coal and the LTA, respectively.

Table 2
Oxygen analysis of coals, wt.%

Determination, No.	Western Ky. No. 11 Coal (Split) 1	Western Ky. No. 11 Coal (Split) 2	Western Ky. No. 11 LTA	Western Ky. No. 9 Coal*	Western Ky. No. 9 LTA**
1	22.1	22.6	47.8		
2	22.5	22.6	48.3		
3	22.4	22.1	48.5		
4	22.2	22.7	48.0		
5	22.8	22.2	48.2		
Mean	22.4	22.4	48.2	19.7	42.9
Std. dev. of mean	±0.2	±0.2	±0.3	±0.4	±0.4

*Mean of replicate analyses of seven splits.[11]
**Mean of replicate analyses of six splits.[11]

The organic oxygen was then calculated as follows:

$$O_{organic} = 0.224 \text{ g O/g dry coal} - 0.482 \text{ g O/g LTA } (0.297 \text{ g LTA/ g dry coal})$$

or

$$O_{organic} = 0.081 \text{ g O/g dry coal}$$

An organic oxygen content of 0.077 g O/g dry coal has been determined in our earlier work for Kentucky No. 9 coal. These values compare to ASTM values of 0.064 (Kentucky No. 11) and 0.065 g O/g dry coal (Kentucky No. 9), respectively. The reasons for the discrepancies in our experimental values and the ASTM values are not completely understood at this time, but may be related to corrections to the ASTM values required for CO_2 released from carbonates, H_2O released from clay minerals and the appropriate amount of S in the organic matter. The potential for error in calculating oxygen by difference, as in the ASTM method has been noted previously.

The calculation of nitrogen content is done according to the following equations:

$$\text{Specific activity} = \frac{\text{Area}_R - \left[\text{Area}_B \cdot \frac{\text{Beam}_R}{\text{Beam}_B}\right] - \text{Beam}_R[\text{CCF} \cdot \text{wt. C} + \text{KCF} \cdot \text{wt. K}]}{\text{Beam}_R \cdot \text{Weight}}$$

$$\text{N content} = \frac{\text{Specific Activity of Sample}}{\text{Mean Specific Activity of Standards}} \cdot 100\%$$

where Area_R, Area_B – integrated counts accumulated in the counting period for the run and blank, respectively;

Beam_R, Beam_B – relative beam monitor BF_3 counts accumulated during the irradiation period for the run and blank, respectively, corrected for the dead time of the BF_3 neutron detector;

CCF, KCF – empirical correction factors to account for the interferences of carbon and potassium, respectively, in the sample (based on typical literature values in coal);

Weight – total weight of a sample or weight of nitrogen in a standard.

The response of the determination to varying nitrogen concentration was studied by use of the standard addition method. Several splits of a coal sample were "doped" with different quantities of urea (urea content of splits = 0 – 23.2%). The results shown in Fig. 2 confirm the linearity of the experi-

mentally observed nitrogen contents with respect to amount of added nitrogen standard.

The nitrogen content has been calculated by comparison with the standard n-1-naphthylacetamide. NBS standard reference material 1571 (Orchard Leaves) was also used as a standard for the earlier analyses, but was found to be undesirable due to corrections required for its high phosphorus content. The n-1-naphthylacetamide standard was determined to be a satisfactory nitrogen standard by comparative analyses with NBS standard reference materials

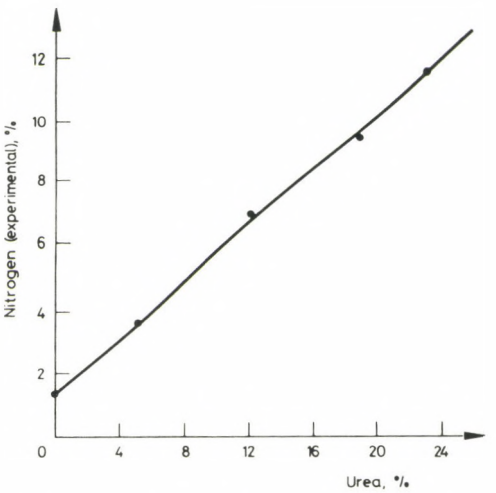

Fig. 2. Coal-urea standard addition plot shows the linear relationship of the experimentally determined nitrogen content to added nitrogen standard in a coal sample

148 (nicotinic acid – 11.38% N) and 912 (urea, which we diluted with spectroscopically pure silica to approximately 5% N).

Table 3 presents the nitrogen data we have obtained on various coal samples by the fast neutron activation technique described. The error limits are based on the standard deviation of the mean. The average standard deviation is 0.07% absolute. In every case, the determined nitrogen content has been compared to the value obtained by ASTM methods, with the mean deviation of our data being +6.8% (absolute $\simeq$ +0.1% N) relative to data obtained by the ASTM method. The Kjeldahl method which is the basis of the ASTM method is often described in the literature as being subject to

Table 3

Nitrogen analysis of coal, wt. %

Determination, No.	Beulah mine	Kentucky Homestead	Ireland W. Va.	Illinois No. 6	Clearfield, Pa.	Bruceton mine
1	0.80	1.60	1.47	1.39	1.29	1.81
2	0.98	1.55	1.22	1.30	1.44	1.69
3	0.85	1.42	1.43	1.30	1.58	1.61
4	0.78	1.35	1.39	1.23	1.58	1.54
Mean	0.85	1.48	1.38	1.31	1.47	1.66
Std. dev. of mean	±.05	±.06	±.08	±.04	±.07	±.06

Determination, No.	Lower Banner Camp Branch No. 1*	Ohio No. 12*	Navaho No. 7*	Wadge Seam Edna Mine*	Fish Creek Seam Energy Mine No. 2*
1	1.71	1.85	1.71	2.12	2.21
2	1.82	2.01	1.73	1.93	2.47
3	2.23		1.91	2.20	2.09
4	2.01		1.63	1.91	2.45
Mean	1.94	1.93	1.75	2.04	2.31
Std. dev. of mean	±.11	±.08	±.06	±.07	±.10

* These samples are demineralized coals.

loss of elemental nitrogen or nitrogen oxides, especially when nitrogen is in the form of nitro, azo and azoxy groups and certain resistant heterocyclic nitrogen compounds. The fate of the nitrogen in the sulfuric acid digestion step of the Kjeldahl procedure is highly dependent upon its chemical form in the sample, inorganic compounds added to catalyze the hydrolysis, and amounts and types of salts used to raise the boiling point of the digestion mixture. Inadequacies of the Kjeldahl method may lead to low results for samples as complex as coal.

In each case where we have compared our nitrogen data with data by the ASTM method, the ASTM (Kjeldahl) values are lower. We suggest the INAA determination as described here should lead to superior nitrogen determinations, since the method is independent of the chemical form of the nitrogen in the sample.

Nitrogen in coal is deleterious in either combustion processes or conversion processes such as gasification or liquefaction. In recent fluid-bed combustion studies at Argonne National Laboratory it was demonstrated that nitrogen in the coal gives rise to the NO_x in the flue gas.[22] This was accomplished by substituting a mixture of oxygen and an inert gas for air. Outlet concentrations of NO_x were the same for the mixture and air. In pulverized-coal combustion, FINE, SLATER, SAROFIM, and WILLIAMS[23] concluded that fuel nitrogen does not contribute significantly to nitric oxide formation, but that further studies of nitrogen in coal are needed before a definitive statement can be made.

In gasification processes coal nitrogen comes off as molecular nitrogen, ammonia, hydrogen cyanide, pyridine bases, and nitric oxide.[24] Other than nitrogen itself these gases must be removed before catalytic methanation takes place. In some liquefaction processes little if any nitrogen removal takes place. Processing conditions for good sulfur removal are not stringent enough to attack the more stable nitrogen compounds. These compounds, however, must be removed for refinery feedstocks because of their catalyst poisoning effect.

The organic oxygen content of coal is important in process calculations for combustion and conversion processes such as gasification and liquefaction. In the former case allowance is made for the organic oxygen content in determining the theoretical amount of air required for complete combustion. For conversion processes the amount of steam or hydrogen consumed is related to the organic oxygen content. The oxygen atom is postulated as an active site for both coal conversion processes; it thus plays an important role in controlling their reaction rates.[4, 5]

Determining process flow-rates, sizing of equipment, and closing of material balances are all dependent on the accurate determination of coal oxygen and nitrogen compositions. The techniques described in this paper should prove to be of value in these determinations.

*

The authors wish to express their appreciation to Dr. H. R. APPELL (U. S. Bureau of Mines) and Prof. P. H. GIVEN (Pennsylvania State University) for supplying some of the analyzed coals used in this work. The Pennsylvania State samples were collected by W. SPACKMAN under contract 14–01–0001–390 from the Office of Coal Research. The LTA samples used in this work were prepared by A. J. JOHANNES. Financial assistance by the Institute for Mining and Minerals Research, University of Kentucky, is gratefully acknowledged.

References

1. D. W. VAN KREVELEN, Coal, Elsevier, Amsterdam, 1961, p. 113.
2. P. H. GIVEN, Coal Science, Advances in Chemistry Series, No. 55, Am. Chem. Soc., Washington, D. C., 1966, p. 192.
3. R. H. ESSENHIGH, J. B. HOWARD, Combustion Phenomena in Coal Dusts and the Two-Component Hypothesis of Coal Constitution, Penn. State Univ. Studies No. 31, 1971, p. 17.
4. J. D. BLACKWOOD, D. J. McCARTY, Aust. J. Chem., 19 (1966) 797.
5. T. J. BIRCH, J. D. BLACKWOOD, Nature, 20 (1964) 797.
6. C. A. SEYLER, Proc. S. Wales Inst., Engrs, 63 (1948) 213.
7. W. FRANCIS, Coal, Arnold, London, 1954.
8. K. KINSON, C. B. BELCHER, Fuel, 54 (1975) 205.
9. H. H. LOWRY (Ed.), Chemistry of Coal Utilization, Supplementary Volume, Wiley, New York, 1963, p. 219.
10. ASTM, Pt. 19 D2492–68, 1969.
11. C. E. HAMRIN Jr., P. S. MAA, L. L. CHYI, W. D. EHMANN, Fuel, 54 (1975) 70.
12. H. J. GLUSKOTER, Fuel, 44 (1965) 285.
13. D. E. WOOD, P. L. JESSEN, R. E. JONES, 52nd Annual Meeting of the American Association of Cereal Chemists, Los Angeles, Calif., April, 1967.
14. H. SEVINLI, H. OZYOL, E. BARUTCUGIL, S. DINCER, Turk. A. E. C., Tech. J., 1 (1974) 15.
15. C. L. SYA, M. S. Thesis, University of Kentucky, 1973.
16. S. SEMEL, S. HELF, J. Radioanal. Chem., 11 (1972) 91.
17. D. M. BIBBY, H. M. CHAMPION, Radiochem. Radioanal. Letters, 18 (1974) 177.
18. J. W. MORGAN, W. D. EHMANN, Anal. Chim. Acta, 49 (1970) 287.
19. J. R. VOGT, W. D. EHMANN, Proc. 1965 Intern. Conf. Modern Trends in Activation Analysis, Texas A and M Press, 1966, p. 82.
20. R. R. RUCH, H. J. GLUSKOTER, N. F. SHIMP, Illinois Geol. Survey, Environmental Geology Note, 1974, p. 18.
21. C. E. MELTON, A. A. GIARDINI, Fuel, 54 (1975) 162.
22. A. A. JONKE, private communication, 1975.
23. D. H. FINE, S. M. SLATER, A. F. SAROFIM, G. C. WILLIAMS, Fuel, 53 (1974) 120.
24. A. V. SLACK, Sulfur Dioxide Removal from Waste Gases, Pollution Control Review, 1971.

Journal of Radioanalytical Chemistry, Vol. 32 (1976) 207–217

X-Ray Fluorescence Techniques

ANALYTICAL USE OF PROTON-INDUCED X-RAY EMISSION

T. B. JOHANSSON,* M. AHLBERG,* R. AKSELSSON,** G. JOHANSSON,* K. MALMQVIST*

**Department of Nuclear Physics, Lund Institute of Technology, Sölvegatan 14, S–223 62 Lund (Sweden)*
***Department of Environmental Health, University of Lund, Sölvegatan 21 S–223 62 Lund (Sweden)*

Proton-induced X-ray emission, PIXE, is capable of simultaneous quantitative determination of 10–15 elements. An introduction to the physical properties of the method is given and detection limits are shown for a routine analysis of a thin aerosol sample. Examples of applications to both thick and thin samples are presented. Human tooth dentine is analysed for lead, with simple sample preparation, indicating lead values of a few ppm for Swedish children. Quantitative analyses of several other elements are obtained simultaneously. Cascade impactors are used for sampling aerosols in work environment during welding operations giving information of size distribution and concentrations of the elements present. The aerosol is dominated by particle sizes between 0.5 and 2 μm as measured by the impactor, but the size distributions are different for different elements and welding techniques and depend on the distance from the welding source. The relative abundance of the elements found in the aerosol indicates the presence of fractionation mechanisms.

Introduction

Over the past several years, proton-induced X-ray emission analysis, PIXE, has been developed into a reliable analytical tool for routine determination of many elements present in very small amounts in small samples. [1]

A recent review of the field has been done by JOHANSSON and JOHANSSON. [2] In this paper we will briefly discuss some properties of the analytical method and present results from its application to both thin and thick samples.

Principles of PIXE analysis

In a typical analysis, a sample is irradiated for 1 – 10 minutes by protons of a few MeV energy from a Van de Graaff accelerator using beam currents of 1 – 500 nA. The spectrum recorded by a Si(Li) detector is stored for subsequent computer evaluation.

The low detection limits of the method depends on a favourable signal-to-background ratio from the relative X-ray production efficiency for characteristic and continuum radiation, and the availability of intense fluxes of exciting radiation, e. g. focussed low energy proton beams from Van de Graaff accelerators.

Fig. 1 shows a spectrum obtained during the bombardment of a thick sample of human tooth dentine. The shape of the continuum illustrates the background generating mechanisms in PIXE analysis, i. e. bremsstrahlung from the deceleration of secondary electrons and secondary processes induced by high energy γ-rays. The latter is dominant in the high energy part and in this spectrum also in the low energy end ($\leqslant$channel 50) due to the thick external absorber used, which absorbs the low energy X-rays. The electron bremsstrahlung is the hump between 3 and 10 keV. The characteristic X-rays

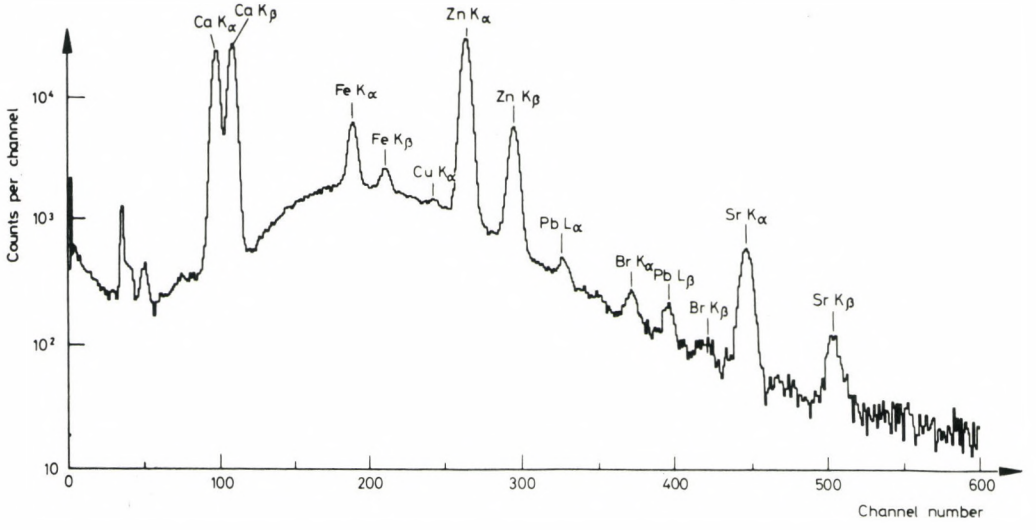

Fig. 1. Spectrum from a 13 minutes analysis of a tooth dentine sample with 2.5 MeV protons. The beam current was 50 nA. The low energy X-rays are absorbed by a 25 μm Al and a 720 μm mylar absorber. The lead concentration in this sample was found to be 7 ppm

are found imposed on this background and the spectrum clearly shows the multi-element capability of PIXE.

The physical processes in the background generation have been thoroughly discussed by FOLKMANN et al.[3] AKSELSSON and JOHANSSON together with many others (see Ref.[2]) have measured X-ray production cross-sections and they also present a useful semi-empirical formula for K X-ray production cross-sections.

The weight in grams, G, of a detected element is calculated from

$$G = \frac{NW}{n\sigma \frac{\Omega}{4\pi} \varepsilon \, tA} \qquad (1)$$

where N – the number of counts in a corresponding peak;
W – the atomic weight of the element;
n – the number of protons per cm^2;
σ – the X-ray production cross-section in cm^2;
Ω – the solid angle subtended by the detector;
ε – the detector efficiency including absorption losses in windows between the target and the detector;
t – the fraction of the produced X-rays that escapes absorption in the target in the direction of the detector;
A – Avogadro's number.

Fig. 2 presents detection limits for routine analysis of thin samples. The curves relate to both normal beam and micro beam[4, 5] analysis, where the curves for the micro beam have been extrapolated from the normal beam data, in which the beam was much wider than the sample spot. Due to the assumption that all the continuum is produced by the sample and not by the backing foil (50 $\mu g/cm^2$ polystyrene) the micro beam detection limits given in the figure may be far too high in the bremsstrahlung area and they should be regarded as upper limits. The data are for the same count rate and the same time. Thus the micro beam current is low compared to the macro beam. The micro beam current/cm^2 is high and polystyrene may be exchanged to carbon foils. The detection criteria have been set to $N \geqslant \max(3\sqrt{B}, 10)$, where B is the number of counts in the 2 × FWHM background.

The accuracy of PIXE is usually 10%. The precision depends on e.g. the amount of the element in the proton current and the time of analysis. For elements well above their detection limits one can easily obtain a precision of $\lesssim 10\%$.[1]

PIXE is advantageous if only a minute amount of the sample is available or large samples are very expensive to obtain. There are many situations in which this is the case.

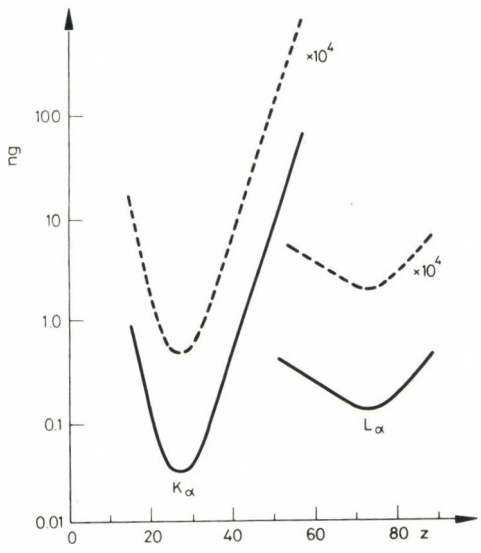

Fig. 2. Detection limits for a thin sample target with a 2 MeV proton beam, 80 counts per second counting rate and 250 seconds analysing time. An aluminum absorber of 6.5 mg · cm^{-2} with a hole covered with a 2.3 mg · cm^{-2} Be foil, is used for absorbing low energy X-rays. The cross-section area of the hole subtends 3% of the detector solid angle. The solid curves show the detection limits for a proton beam with an area of 5 x 5 mm^2 and a 80 nA beam current. The dashed curves show the estimated detection limits, multiplied by 10^4, for a micro beam with a diameter of 25 μm and a beam current of 1 nA. These detection limits were calculated by a transformation of the results from broad beam excitation

Experimental

Thick target analysis - lead in children's teeth

Although most PIXE applications to date have focussed on thin targets, the analysis of thick targets is an interesting field. The small penetration depth of the projectile and the absorption of X-rays limit the analysis to a surface volume with a depth in the order of 10 μm. In a simple irradiation, detection limits for many elements are in the 1 - 100 ppm range. For

elements in this range, PIXE is often a fast, inexpensive and convenient method to use. Steel samples[6] and archeological samples[7] have been investigated in this laboratory. We have applied PIXE to the analysis of Pb in children's teeth as part of a program to estimate the Pb exposure of children.

Lead is known to cause biochemical and neurological changes even at low levels. Damage may occur to specific organelles and enzyme systems with a variety of symptoms. Children are more susceptible than adults to this type of poisoning, partly due to their higher metabolic rate. Lead levels in blood have been reported, but they offer no information on earlier exposure to lead. However, tooth storage of lead is permanent[8] and dose-related. To correct the tooth distribution of certain individuals in the lower teen-ages, a permanent tooth (premolar) is sometimes extracted and these teeth constitute a suitable material for investigation since they were grown at the age of 1 – 3 years, at which period the individual is considered to be the most susceptible to lead damage.

Tooth analysis by PIXE has been studied in detail by AHLBERG and AKSELSSON,[9] who also present curves to estimate the contribution to the observed signal from various layers of the tooth. An important finding is that the observed roughness of the broken tooth surface introduces an error of less than 5% for Pb in these analyses. A technical problem of importance when analysing thick, insulating targets is charge build-up on the sample. This build-up results in keV electrons, which produce bremsstrahlung and increase the continuum considerably. This problem can most easily be handled by allowing the chamber pressure to rise somewhat or by spraying electrons from a low-energy electron source over the sample. Both these approaches work well and have been reported separately.[10]

Before analysis the extracted tooth is divided by applying pressure on it with two sharp edges applied to opposite sides of the tooth. The uncontaminated surfaces thus obtained are bombarded by 2.5 MeV protons to an accumulated charge of 20 μC. The detection limit for Pb in our arrangement is then 2.5 ppm. In addition to Pb, the elements Ca, Fe, Cu, Zn, Br and Sr are detected. Fig. 1 shows a typical spectrum from a tooth analysis.

Table 1 summarizes our measurements of Pb in 83 teeth from various locations in Sweden. Also, values reported in the literature[11,12] are included for comparison. These values refer to other teeth, grown under other periods of the individual's life and may thus be difficult to compare, if we wish to establish exposure of lead to different age groups in different parts of the world.

A distinct advantage of using PIXE in this application is the uncomplicated sample handling procedure that minimizes the risks of contamination. Also,

Table 1

The lead content in human tooth dentine

Location	Tooth type	Analytical method	Number of determinations	Average Pb-concentration, ppm	Reference
Malmö, Sweden	permanent (premolar)	PIXE	26	4.5 ± 3.5^{a} 3.6 ± 1.5^{b}	This work This work
Stockholm, Sweden	permanent (premolar)	PIXE	38	3.4 ± 1.4^{a} 3.2 ± 1.0^{b}	This work This work
Jönköping, Sweden	permanent (premolar)	PIXE	23	3.2 ± 1.3^{a} 2.8 ± 0.6^{b}	This work This work
Cities in the USA[c]	deciduous[d]	Anodic Stripping Voltammetry, ASV	9	54.8 ± 10.8^{a}	11
Boston, USA[e]	deciduous	ASV	20	16.9 ± 2.7^{a}	11
Cities on Iceland[f]	deciduous	ASV	17	5.4 ± 0.6^{a}	11
Helsinki, Finland	deciduous	Atomic Absorption Spectroscopy, AAS	[g]	0.71 ± 0.82^{a}	12
Tervola, Finland	deciduous	AAS	[g]	0.46 ± 0.25^{a}	12

[a] Arithmetic mean ± standard deviation.

[b] Arithmetic mean ± standard deviation calculated after exclusion of the two highest results in the series. This number is reported in order to demonstrate the skewness of the distribution.

[c] Philadelphia and Boston.

[d] Teeth are collected from children who have suffered from unequivocal lead poisoning.

[e] From suburban areas.

[f] Reykjavik and Akranes.

[g] The number of determinations from Helsinki and Tervola together was 136.

in this case the Pb content varies between different parts of a tooth and we are able to minimize this source of data variation by bombarding only the dentine part of the tooth.

Thin target analysis - welding aerosols

PIXE has been applied to many types of thin samples. The analysis of aerosols represents a most active field and work on biological specimen[13] and geological samples[14] have also been reported. In addition to measurements of ambient aerosols, we have investigated aerosols produced in work environments, predominantly by welding operations. Cascade impactors have previously been used extensively in the investigation of ambient aerosols.[15] In this study, samples are also collected using single orifice cascade impactors operating for several minutes at a flow rate of 1 l · min^{-1}. The air stream is drawn through jets of decreasing diameters, thus increasing the speed of the air. Particles following the air mass with too high a momentum to make the bend when the air deflects at a perpendicular plate will impact on

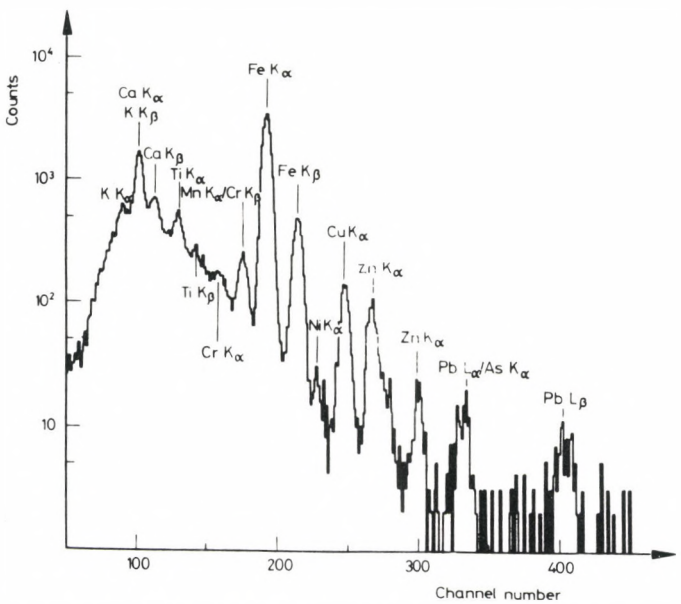

Fig. 3. Spectrum from an analysis of a sample from stage number one in a cascade impactor. The sample was collected in the breathing zone of a welder using a low hydrogen coated electrode. In the analysis 2 MeV protons were used with a beam current of 90 nA for 120 seconds. Foils of 25 μm Al + 25 μm Be were used as absorbers

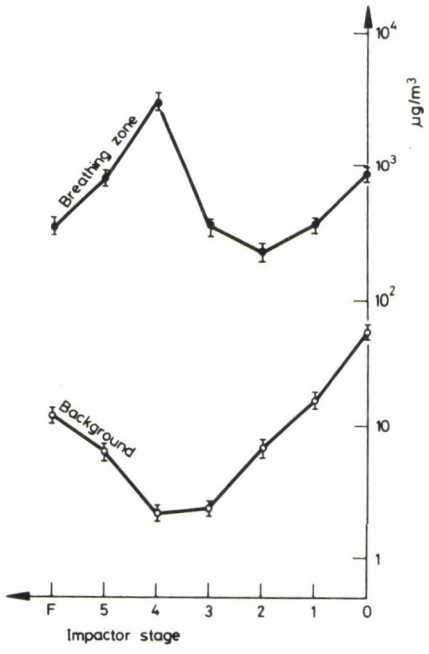

Fig. 4. Size distribution of Fe in a welding hall in a Swedish shipyard obtained by cascade impactors. The upper curve shows the distribution in the breathing zone of a welder using a low hydrogen coated electrode. Sampling time was 15 seconds at an air flow of 1 l · min^{-1}. The lower curve shows the size distribution for Fe in the background aerosol far from welding sources. Sampling time was 8 minutes. The impactor cut-off diameters imply a logarithmic particle size scale along the horizontal axis. (F indicates the back-up filter.)

the latter and stick to it. The plate is covered with a thin film coated with paraffin to make it sticky. The film is subsequently removed and transferred to the accelerator for bombardment.

The Battelle designed impactor provides particle size fractionation from 0.25 μm particle diameter and upwards: Stage 5: 0.25 – 0.5 μm; stage 4: 0.5 – 1 μm; stage 3: 1 – 2 μm, stage 2: 2 – 4 μm; stage 1: 4 – 8 μm and stage 0: >8 μm. The particles less than 0.25 μm will end up on the back-up filter – thus covering the size range of welding aerosols as well as the most interesting size range from the point of interest for deposition

in the respiratory system. A number of welding techniques have been investigated.[16,17] Fig. 3 shows a typical spectrum obtained during the bombardment of a welding aerosol sample collected on stage 1 of the cascade impactor.

In Fig. 4 we compare the Fe-content of the aerosol in the breathing zone of a welder with that of the background aerosol in the welding hall of a shipyard in Sweden. Clearly, the concentration increases dramatically in the breathing zone, especially for particles with diameters between 0.25 and 1 μm. These are generated during the welding. In the background the larger particles dominate. These may be dust stirred up from the floor by the continuous movement of people and material through the hall. There is a rather low contribution from particles between 0.5 and 2 μm, which have been found to be the dominating particle sizes produced by normal welding operations. The increase in the abundance of very small particles (<0.5 μm) may be due to the smallest welding-generated particles that have not coagulated or sedimented.

Fig. 5 shows the relative elemental abundance for some elements in the welding aerosol. Ti/Fe ratios show very little variations for the different

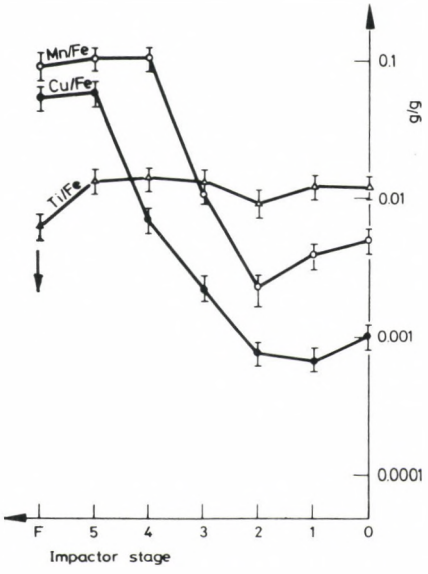

Fig. 5. Mass ratios Ti/Fe, Mn/Fe and Cu/Fe in the welding aerosol on the different impactor stages. (F indicates the back-up filter and ↓ indicates a value less than the given detection limit.) Sampling time was 8 minutes at an air flow of 1 l · min^{-1}

particle sizes. Mn/Fe and Cu/Fe ratios, however, increase with decreasing particle size. Ti in contrast to Mn and Cu has almost the same boiling and melting temperature and vapour pressure of the same order of magnitude as Fe, which, together with properties of oxidated metals, may contribute to the size distributions.

Generally, the elements declared by the manufacturers to be present in the welding piece and the electrodes were found in the aerosol. However, in addition to these elements several others were also detected suggesting incomplete declarations and contributions from contamination of the pieces, as e. g. surface coatings. The relative abundances of the elements found in the aerosol were different from those in the material and the electrode pointing to the operation of fractionation mechanisms. The size distributions were different for different elements, as pointed out above, and they were also influenced by welding techniques.

The exposure of the welders leads to deposition of metals in the lungs in a complicated way. An approach to studying this problem, measuring inhaled and exhaled air aerosol content, has been reported.[18]

Conclusions

PIXE is very suitable for simultaneous determination of 10 – 15 elements present in amounts between 10^{-8} and 10^{-11} g in small samples which can be applied to supporting foils on an area of the order of the cross-section of a uniform accelerator beam ($\lesssim 1$ cm^2). Thick samples are conveniently prepared and bombarded giving analysis in the ppm range. The extension of the method to use of very narrow beams is especially interesting. PIXE is not a universally applicable analytical method but very powerful in areas suitable to its properties. The examples given in this paper point to some areas of this type.

*

We want to acknowledge the cooperation with Prof. M. BERLIN, Department of Environmental Health and Dr. B. MÖLLER, Department of Oral Histopathology, both University of Lund, in the lead experiment.

References

1. T. B. JOHANSSON, R. E. VAN GRIEKEN, J. W. NELSON, J. W. WINCHESTER, Anal. Chem., 47 (1975) 855.
2. S. A. E. JOHANSSON, T. B. JOHANSSON, Submitted to Nucl. Instr. Methods.
3. F. FOLKMANN, C. GAARDE, T. HUUS, K. KEMP, Nucl. Instr. Methods, 116 (1974) 487.
4. P. HOROWITZ, L. GRODZINS, Science, 189 (1975) 795.
5. J. A. COOKSON, A. T. G. FERGUSON, F. D. PILLING, J. Radioanal. Chem., 12 (1972) 39.
6. M. AHLBERG, R. AKSELSSON, D. BRUNE, J. LORENZEN, Nucl. Instr. Methods, 123 (1975) 385.
7. M. AHLBERG, R. AKSELSSON, B. FORKMAN, G. RAUSING, Archaeometry, 18 (1975) 39.
8. C. H. STREHLOW, Doctorial dissertation, New York University, 1972.
9. M. AHLBERG, R. AKSELSSON, Intern. J. Appl. Radiation Isotopes (in the press).
10. M. AHLBERG, G. JOHANSSON, K. MALMQVIST, Nucl. Instr. Methods, 131 (1975) 377.
11. I. M. SHAPIRO, B. DOBKIN, O. C. TUNCAY, H. L. NEEDLEMAN, Clin. Chim. Acta, 46 (1973) 119.
12. I. RYTÖMAA, H. TUOMPO, Naturwiss., 61 (1974) 8.
13. J. L. CAMPBELL, B. H. ORR, A. W. HERMAN, L. A. MCNELLES, J. A. THOMSON, W. B. COOK, Anal. Chem., 47 (1975) 1542.
14. R. E. VAN GRIEKEN, T. B. JOHANSSON, J. W. WINCHESTER, L. A. ODOM, Z. Anal. Chem., 275 (1975) 343.
15. R. AKSELSSON, C. ORSINI, D. L. MEINERT, T. B. JOHANSSON, R. E. VAN GRIEKEN, H. C. KAUFMANN, K. R. CHAPMAN, J. W. NELSON, J. W. WINCHESTER, Adv. X-ray Anal., 18 (1975) 588.
16. R. AKSELSSON, G. JOHANSSON, K. MALMQVIST, J. FRISMARK, T. B. JOHANSSON, Proc. 2nd Intern. Conf. on Nuclear Methods in Environmental Research, 1974, p. 395.
17. K. MALMQVIST, G. JOHANSSON, R. AKSELSSON, T. B. JOHANSSON, Status Report, 1975, LUNP 7508.
18. R. AKSELSSON, G. DESAEDLEER, T. B. JOHANSSON, J. W. WINCHESTER, Presented at the 4th Intern. Symp. on Inhaled Particles and Vapours, 1975.

Journal of Radioanalytical Chemistry, Vol. 32 (1976) 219–228

DETERMINATION OF PPB CONCENTRATIONS OF TRANSITION METALS BY RADIOISOTOPE-EXCITED ENERGY-DISPERSIVE X-RAY SPECTROMETRY

A. H. PRADZYNSKI,* R. E. HENRY, J. S. STEWART

The University of Texas at Austin (USA)

Using ammonium pyrrolidine dithiocarbamate as precipitant and iron as a carrier, ppb concentrations of the following elements were coprecipitated from fresh water: vanadium, chromium, manganese, nickel, copper, zinc, selenium, mercury, and lead. Precipitates were collected on membrane filters then element concentrations were determined using energy dispersive X-ray fluorescence spectrometry. Calibration curves indicate sensitivities ranging from 0.4 ppb for V, Zn, As and Hg to 1.2 ppb for Pb. It is likely that this method of preconcentration can be directly incorporated into field sampling procedures, thus eliminating the problems of sample contamination or trace element losses by absorption on container walls.

Introduction

Water pollution monitoring for trace elements requires quantitative multielement analyses of large numbers of samples. The maximum permissible levels for heavy metals in public water supplies are mostly in the ppb region. The mean concentrations of trace elements found in waters of the United States as published by KRONER,[1] range from 0.19 ppb for berylium to 217 ppb for strontium, with most of the transition metals lying in the area below 100 ppb.

In order to develop a rapid and inexpensive multielement analytical method, capable of analyzing natural waters for transition metals, we focussed our study on the lower region of ppb concentrations, from the detection limit up to 200 ppb. The same method can eventually be used for higher concentrations, by expanding the calibration curves and/or diluting the sample.

*Correspondence should be directed to A. H. PRADZYNSKI, Nuclear Reactor Laboratory Dept. of Mechanical Engineering, University of Texas at Austin, Austin, Texas 78712 (USA).

Problems in water analysis

There is general agreement among most analytical chemists that natural water cannot be reliably and accurately analyzed for trace elements on the lower ppb level without a preconcentration step. Even though some methods display adequate sensitivity for several elements in direct analysis, e.g. special techniques of atomic absorption, neutron activation analysis, spark source mass spectrometry or proton induced X-ray emission spectrometry, they are either sequential and time-consuming or involve complicated equipment and sample preparation. In addition, these methods are relatively expensive.

The question of what to remove from the sample, water or the trace elements, has been repeatedly discussed in literature on water preconcentration. The evaporation method, as recommended by the ASTM Standard D-1888[2] is very time-consuming. In addition, the sample can very easily be contaminated. The lyophilization method, as recently discussed by HARRISON, LA FLEUR, and ZOLLER,[3] though eliminating the contamination problem, is rather complex, time-consuming and expensive.

Still another problem of great importance in water analysis not yet satisfactorily solved is the preservation of the sample to prevent losses of trace elements by adsorption on the walls of the container during the time between sampling and analysis.

In the authors' opinion, the problems of preconcentration, contamination and preservation of water samples can be minimized if not eliminated by performing the trace element separation on the spot of sampling. The trace elements preconcentrated on a membrane filter or bound in an ion-exchange resin loaded filter paper can easily be delivered to the analytical laboratory without contamination. Applying adequate precautions and blank subtraction, the problem of reagent and filter contamination can be minimized. A method of on-site preconcentration has been recently developed in Holland by VAN DALEN et al.[4] in conjunction with instrumental neutron activation analysis, as reported at this conference.

In this work, it was desired to apply preconcentration in conjunction with a rapid and inexpensive multielement detection method, such as energy dispersive X-ray fluorescence (EDXRF) spectrometry. Since the thin specimen method of EDXRF spectrometry is known to minimize matrix effects,[5] the capability of producing a uniform, thin specimen was added to the criteria for the preconcentration technique.

Experimental

Materials and methods

The use of ion-exchange resin loaded filter paper as a collector of trace elements was rejected because of the relatively high backscattered background produced by the substrate. This method has been used by some authors[6] in conjunction with wave-length dispersive XRF spectrometry, where the highly colimated system registers much less backscattered background than the EDXRF spectrometer.

The method of coprecipitation of trace elements with a carrier using ammonium pyrrolidine dithiocarbamate (APDC) as the precipitant was chosen instead. This technique assured the necessary sensitivity and reproducibility, as outlined in our paper on determination of selenium in water,[7] and fulfilled all other criteria. An extensive discussion of APDC precipitation as a preconcentration method for EDXRF was given by ELDER et al.[8] The idea of increasing sensitivity of trace element separation for XRF determinations by coprecipitation with a carrier was described by LUKE.[9]

Procedure

Water samples were prepared by addition of single elements (V, Cr, Mn, Cu, Zn, As, Se, Hg and Pb) in concentrations ranging from zero to two hundred ppb to 500 ml volumes of deionized water. The trace elements were coprecipitated using APDC, a strong chelating agent, as the precipitant and Fe^{3+} (200 μg) as the carrier. Iron was selected as a carrier because it is usually present in natural waters in higher concentrations than the trace metals and thus serves as a natural carrier in many cases. The iron concentration can be determined in a 100 ml sample before the carrier is added to the main sample.

The optimum concentration of the iron carrier was determined experimentally by precipitating 5 μg quantities of Se with various quantities of carrier ranging from 0 to 500 μg. From Fig. 1 can be concluded that precipitation efficiency of Se depends on the amounts of carrier up to approximately 200 μg. Excess carrier was avoided in order to comply with the thin specimen criterion.[5] Solutions were filtered onto 25 mm diameter millipore HAWP membranes, having a pore size of 0.45 microns. The membranes were then dried gently in air while lying flat upon a filter paper in a contamination-free closed cabinet. Precipitations were carried out at pH 4.0.

Samples were measured on an X-ray fluorescence spectrometry system composed of a lithium-drifted silicon detector with a resolution of 250 eV and a 2048-channel analyzer. Spectra were collected in 1024-channel memory

groups. The spectrometer was linked directly with a monitoring and data processing unit consisting of a NOVA-800 minicomputer, fixed head magnetic disc and a teletype or plotter. An annular radioisotope source, ^{238}Pu, having an activity of 100 mCi was used for excitation of the fluorescent X-rays in the specimens.

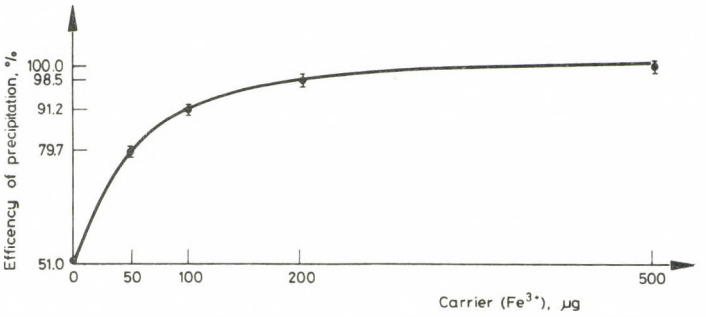

Fig. 1. Precipitation efficiency of Se in relation to Fe concentration

Results

Calibration curves were obtained by plotting the measured intensities of characteristic X-ray peaks of single trace elements versus the amounts of each element added to the solutions. In Figs 2 - 4 calibration curves are shown for single elements V, Cu and Se. In Fig. 5 calibration curves are shown for Se, Hg and Pb simultaneously coprecipitated, using Fe as a carrier, from solutions containing all three elements. Fig. 6 shows calibration curves obtained by using the iron carrier as an internal standard. In Fig. 7 a typical spectrum is shown of 50 μg selenium in the presence of copper, mercury and the iron carrier. Figs 8 and 9 show spectra of trace elements in natural water samples from unpolluted sources precipitated with and without carrier. The water samples were filtered before precipitation of trace elements in order to remove suspended matter.

The minimum determination limits (3σ of the backgrounds) shown in Table 1 were calculated for all the studied elements from a blank sample containing the carrier only.

Coprecipitation efficiency was determined by measurements of standards prepared by the deposition of calibrated solutions on HAWP membrane filters. Solutions were deposited dropwise in a geometric pattern to assure uniform

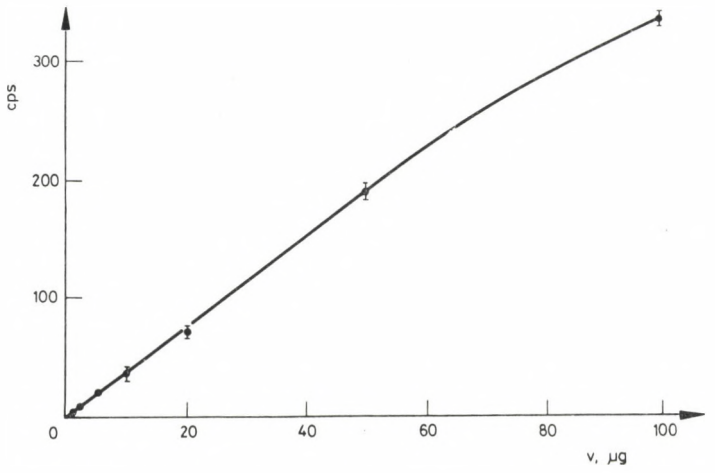

Fig. 2. Calibration curve for V. Carrier: 200 µg Fe^{3+}; pH = 4.0

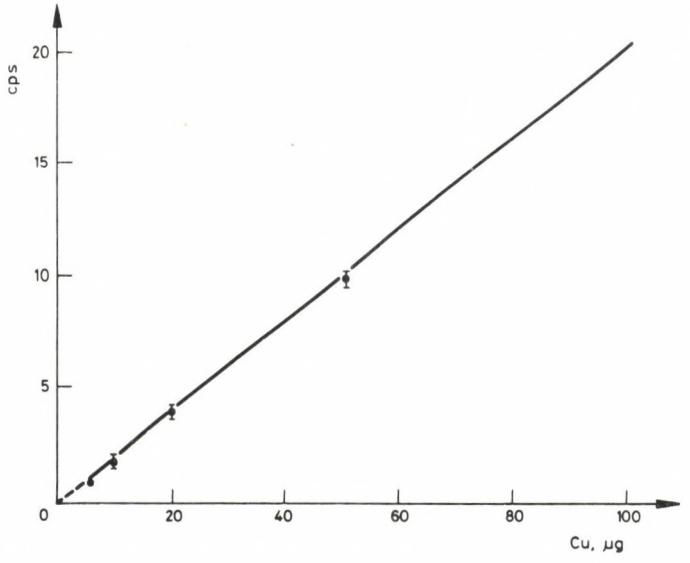

Fig. 3. Calibration curve for Cu. Carrier: Fe^{3+}; pH = 4.0

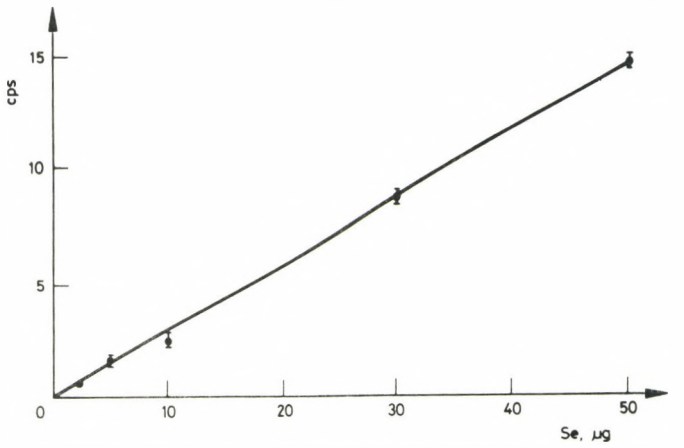

Fig. 4. Calibration curve for Se. Carrier: 200 μg Fe^{3+}; pH = 4.0

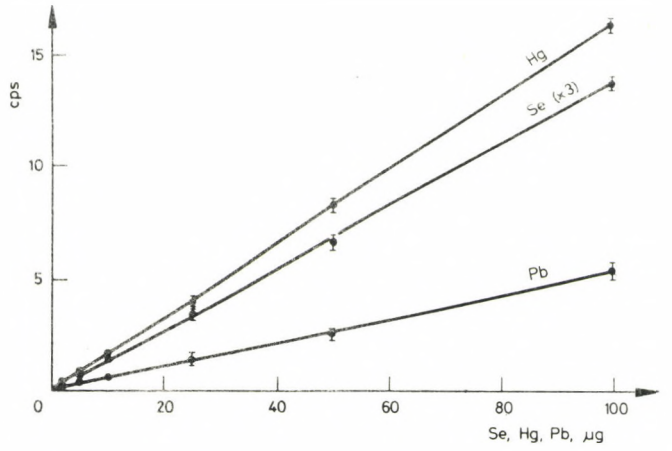

Fig. 5. Calibration curves for Se, Hg, Pb precipitated simultaneously. Carrier: 200 μg Fe^{3+}; pH = 4.0

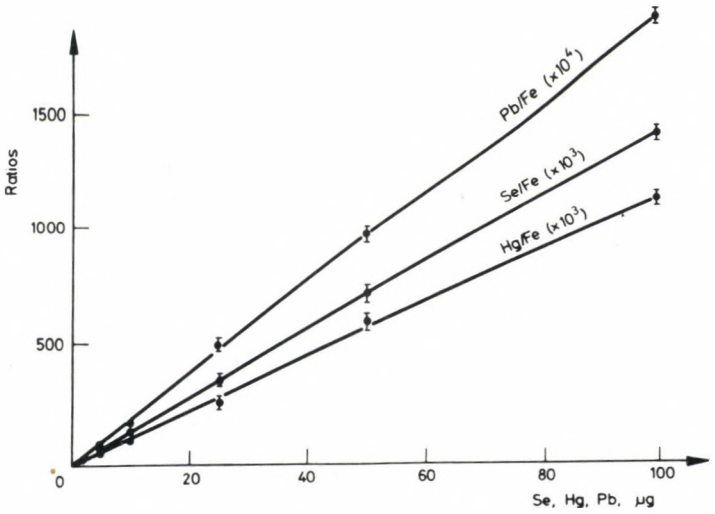

Fig. 6. Calibration curves for Se, Hg, Pb using Fe-carrier as an internal standard

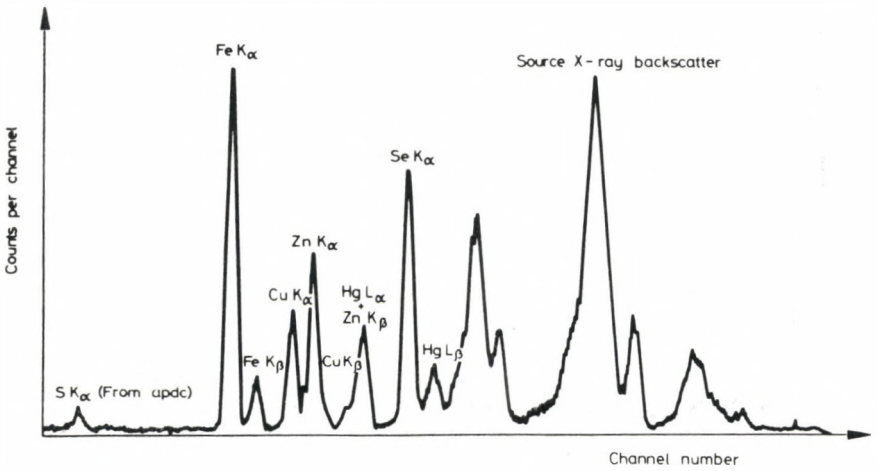

Fig. 7. Spectrum of 100 ppb selenium in the presence of other metals

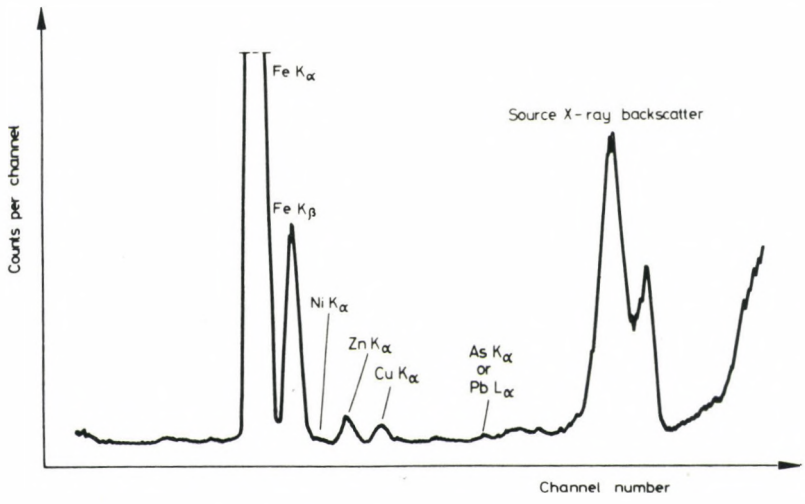

Fig. 8. Spectrum of natural water with Fe added as carrier

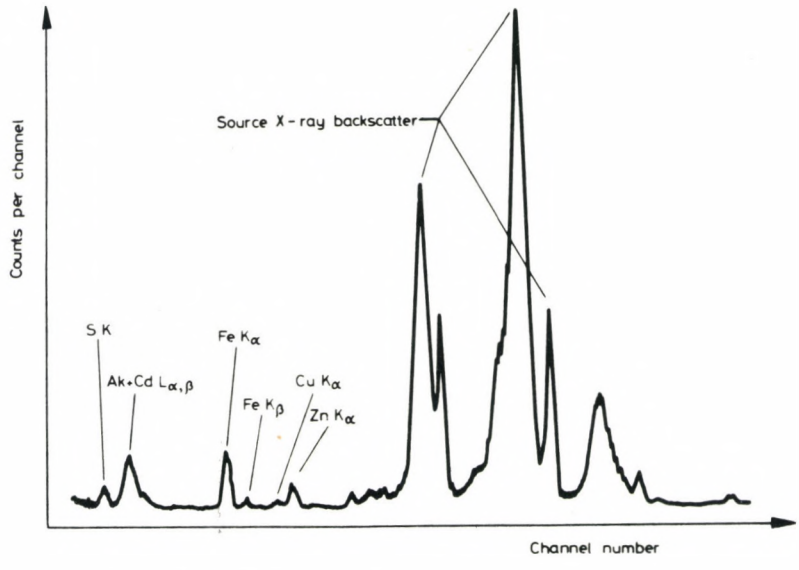

Fig. 9. Spectrum of natural water with no carrier

distribution then dried. Description of the standard preparation method has been published by PRADZYNSKI and RHODES.[10] The efficiencies of precipitation at pH = 4.0 were found between 92 and 95% for the investigated elements except for Cr and Mn, which were much lower. Different precipitation conditions for these two elements are presently being investigated. Further experimentation determined that, on the ppb level, the trace elements do not interfere with each other during the coprecipitation process.

A problem that has to be solved before the method can be used in field is excessive filtration time. It has been observed that precipitates from spiked samples of deionized water filter much quicker than those from natural waters. A study of the filtration process and design of a field sampling and trace element separation device are underway.

Table 1
Minimum determination limits (MLD)
(3σ of the background under the single peaks)

Element	MDL, ppb
Vanadium	0.4
Chromium	1.1
Copper	0.5
Zinc	0.4
Arsenic	0.4
Selenium	0.6
Lead	1.2
Mercury	0.4

Conclusion

Using APDC coprecipitation in conjunction with energy dispersive X-ray fluorescence spectrometry and the thin film technique, the concentration of V, Cr, Cu, Zn, As, Se, Hg and Pb in natural water can be determined with minimum detection limits ranging from 1.2 ppb for Pb to 0.4 ppb for V, Zn, As and Hg. In the case of water containing iron in concentrations of 400 ppb or greater, no carrier needs to be added.

References

1. R. C. KRONER, Proc. Conf. Traces of Heavy Metals in Water Removal Processes and Monitoring, EPA–902/9–74–001, 1974, p. 311.
2. ASTM, Standard D–1888.
3. S. H. HARRISON, P. D. LA FLEUR, W. H. ZOLLER, Anal. Chem., 47 (1975) 1685.
4. A. VAN DALEN, H. A. DAS, J. LUTEN, H. A. V. D. SLOOT, Trans. Am. Nucl. Soc., 21 (1975) 20.
5. J. R. RHODES, A. H. PRADZYNSKI, et al., Application of Low Energy X- and Gamma-Rays, C. A. ZIEGLER (Ed.) Gordon and Breach, N. Y., 1971, p. 317.
6. W. J. CAMPBELL, E. F. SPANO, T. E. GREEN, Anal. Chem., 38 (1966) 987.
7. A. H. PRADZYNSKI, R. E. HENRY, J. L. S. STEWART, Radiochem. Radioanal. Letters, 21 (1975) 277.
8. F. J. ELDER, S. K. PERRY, F. P. BRADY, CH. R. GOLDMAN, Trace Metal Analysis of Natural Samples by Dithiocarbamate Precipitation Coupled with X-Ray Fluorescence, Preprint, 1973.
9. C. L. LUKE, Anal. Chim. Acta, 41 (1968) 237.
10. A. H. PRADZYNSKI, J. R. RHODES, Development of Synthetic Standard Samples for Trace Analysis of Air Particulates, Symp. on Air Pollution Instruments Calibration – Problems and Techniques, ASTM, Committee D–22, Boulder, Colorado, August 5–7, 1975 (in the press).

Journal of Radioanalytical Chemistry, Vol. 32 (1976) 229–239

A MECHANISTIC MODEL FOR THE METABOLISM OF CORROSION PRODUCTS AND OF BIOLOGICAL TRACE ELEMENTS IN METALLOSIS TISSUE BASED ON RESULTS OBTAINED BY ACTIVATION ANALYSIS*

F. LUX**, J. SCHUSTER***, R. ZEISLER**

***Institut für Radiochemie der Technischen Universität München, D–8046 Garching (F. R. Germany)*
****Chirurgische Klinik und Poliklinik rechts der Isar der Technischen Universität München, Ismaninger Str. 22, D–8000 München 80 (F. R. Germany)*

Instrumental neutron activation analyses have been carried out on tissues adjacent and distant from metal implants. From the time-dependence of the concentrations of the corrosion products some conclusions have been drawr on the routes of metal transport from the implant. Additionally, the behaviour of haematoma iron has been shown as well as the dependence of the zinc concentrations on different biochemical processes, during implantation and then at the following stages of the development of the metallosis tissue.

Introduction

Instrumental activation analysis is a useful tool for the investigation of metallosis, which is an inflammatory tissue reaction in the vicinity of metal implants, e. g. stainless steel (V4A-steel) used for restoring fractured bones. The results of previous analytical investigations and our analytical work on clinical cases have been discussed elsewhere.[1-5] However, some interesting questions could not be solved with clinical investigations: The time-dependence of the process, the behaviour of implants of different metals, and the investigation of the muscle tissue adjacent to the metallosis tissue. In order to widen the picture of the development of metallosis more thorough experiments were performed using animals.

Based on the results of these animal experiments and of the foregoing clinical investigations a summarized discussion is given in this paper on the present state of knowledge of the processes associated with metallosis.

*This work was supported by the Bundesministerium für Forschung und Technologie, the Deutsche Forschungsgemeinschaft, and the Fonds der Chemischen Industrie.

Analytical procedure

The treatment of the problems in question requires multi-element analyses of tissues. The tissue samples were lyophilized in the quartz irradiation tubes and were measured by γ-ray spectroscopy directly in these containers after neutron activation. The concentrations of the elements found refer to the wet weight of the respective sample since the lyophilization did not yield reproducible degrees of desiccation.

The elements shown in Table 1 are determined in this way with the exception of manganese which requires a chemical separation of ^{24}Na.[1,3] It is of practical importance that all of the nine elements accessible instru-

Table 1
Instrumental activation analysis of biological material

			detect. limit exp. in $\mu g/g$[a]	$\mu g/g$ simulated by quartz container of 1 g for 100 mg sample	
				suprapure	normal
V4A-steel	pure metal implants	Cr[b]	0.1	0.03	0.03
		Mn[b)c)]	0.01	–	–
		Fe[b]	5	5	1
		Ni[b]	0.3	0.002	0.042
		Mo[b]	0.07	0.012	0.063
		Ag	0.1	0.00015	0.0015
		Ta	0.005	–	–
biolog. trace elem.	essential	Zn	0.5	0.003	0.024
		Co	0.001	0.0014	0.0012
	non-essential	Sb	0.01	0.0006	0.63

$\phi = 2 \cdot 10^{13}$ n · cm^{-2} · s^{-1},
$t_{irrad.} = 200$ h, $t_{couling} = 5 - 7$ d, $t_{counting} = 800$ min.

a) 100 mg wet weight, counting after removal from the irradiation container
b) also essential trace element
c) separation of ^{24}Na required

mentally can be determined in one sample despite their different concentration ranges. The concentrations of the implant components were in the range of 1 to 1000 μg/g, the concentrations of the biological trace elements were between 10^{-2} and 50 μg/g. The detection limits shown are the real experimental values, but for counting the sample in a non-radioactive tube after the removal from the irradiation container. For the actual conditions of counting in the irradiation tube, the detection limit is determined by the background caused by the respective element present as impurity in the irradiation vial. This background is expressed as "concentration of the element in the sample simulated by the quartz container (simulated μg/g)". As shown in Table 1, in containers of suprapure quartz the simulated μg/g are mostly far below the detection limits, and in the unfavorable cases of iron and cobalt they only reach the detection limit. Therefore they do not affect the quantitative results. Further details of the analytical procedure are described elsewhere.[1, 6]

Types of tissue investigated

In the clinical investigations, tissue sampling was undertaken when an implant had to be removed for medical reasons. The samples were always taken from the capsule of connective tissue formed around the implant (Fig. 1). The tissue directly at the implant is called contact tissue CT.

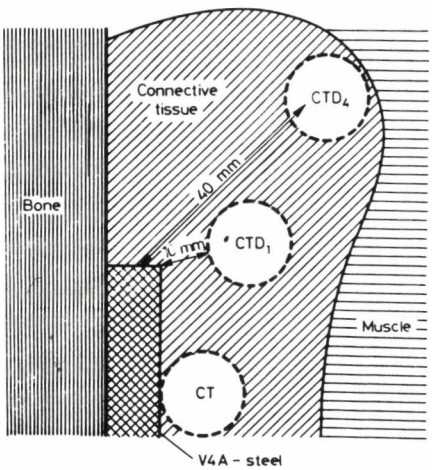

Fig. 1. Sampling of clinical material. 48 clinical cases. Samples taken 12 to 18 month after implantation. CT: Contact tissue, CTD: Capsule tissue at distance, CTD_2: 20 mm distance, CTD_3: 30 mm distance, sample weight: 100 - 200 mg (wet weight)

Additional samples were taken at distances of 1 to 4 cm from the implant, designated as CTD, the abbrevation for "capsule tissue at distance". For comparison, so-called unaffected tissue was taken from freshly injured patients before the insertion of the implant.

In the animal experiments the connective tissue capsules, designated as CT (Fig. 2), were too small for a differentiated sampling as with the clinical material. In most cases the entire capsule has been used as one sample. On the other hand, in the animal experiments samples could also be taken from

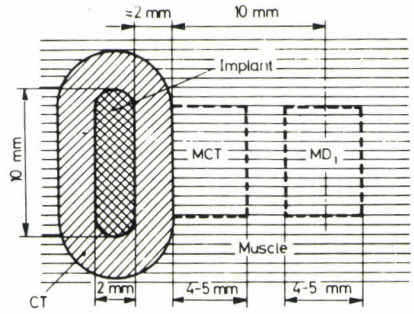

Fig. 2. Sampling in animal experiments, 23 rabbits, 87 implantations (in different extremities). Implants: V4A-steel, vitallium, alloy components as pure metals and Ag, TA. CT: connective tissue capsule. Entire capsule used as one sample. MCT: Muscle contact tissue. $MD_1 \ldots MD_6$: Muscle tissue at distances of 1 to 6 cm from the implant. Sample weight: 100 - 200 mg (wet weight).

the muscle tissue adjacent to the capsule. Of this muscle tissue only the muscle contact tissue MCT, which is directly adjacent to the connective tissue capsule, is considered in this paper.

Mechanistic model of the implant corrosion and of the metabolism of the corrosion products in the metallosis time

For the interaction between the implant and the surrounding tissue a mechanistic model can be derived which may be best illustrated by the time dependence of the changes of the chromium and nickel concentrations in the tissue near to the implant, shown in Fig. 3. Only the results for stainless steel implants are given since no remarkable differences are found for the implantation of pure metals.

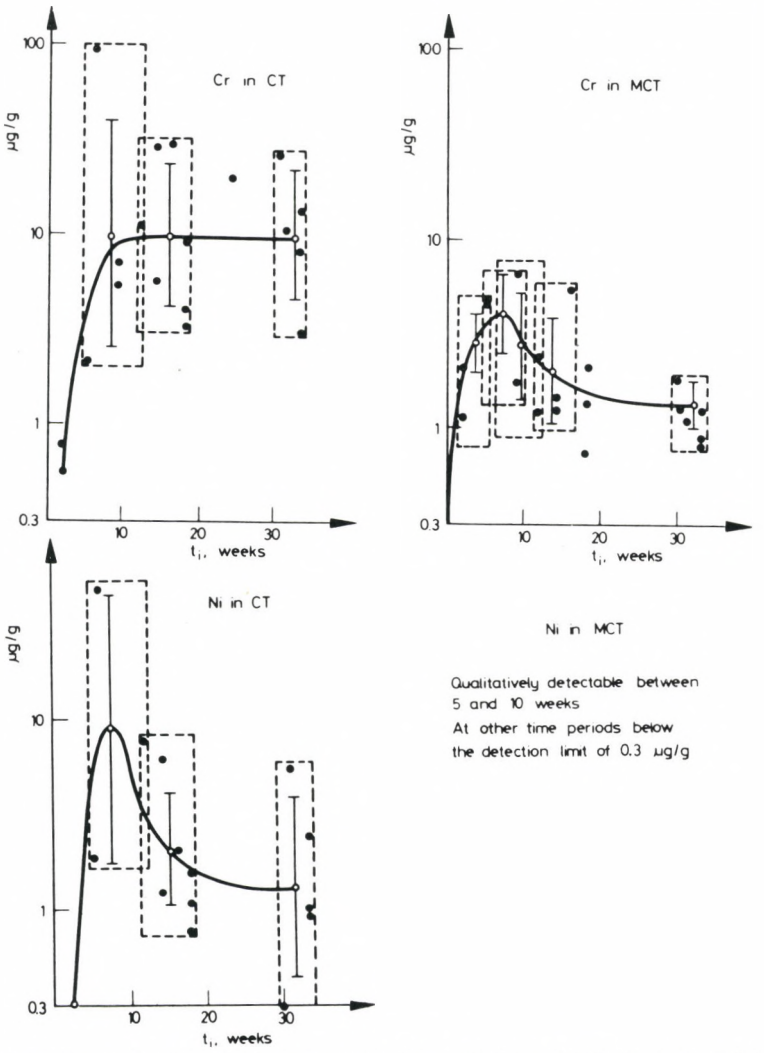

Fig. 3. Time dependence of the concentrations of Cr and Ni in CT and MCT. Implants of V4A-steel. Animal experiments. ●: Experimental values. o: Mean logarithmic values[7] based on the selected experimental values falling within the fields indicated by the dashed rectangles. t_i: Interval between implantation and sampling.

Curve	Analogous results
Cr in CT	Implants of Cr, Mo from V4A, implants of Mo
Cr in MCT	Implants of Cr, Ag, Ta
Ni in CT	Implants of Ni, Ag, Ta

During the first 6 to 12 weeks after implantation the implant corrodes strongly. It has been shown in the clinical cases[1-3, 5] that this corrosion occurs by a splitting off of the individual crystallites (size 10 to 50 μm) of the alloy. In the tissue, these crystallites are further degraded via microcrystallites (size 20 to 200 nm). This degradation process needs time, and therefore in the first impregnation phase the concentrations of the different implant components increase strongly and with an approximate ratio as in steel[1] in the tissue adjacent to the implant, the crystallites are essentially only subdivided.

After 6 to 12 weeks a capsule of connective tissue has been formed around the implant increasing in size very slowly during the following period. On the other hand, the increase in concentration of each implant component comes to an end. Therefore, one can assume that the cessation of the increases of the concentrations is caused by a strong decrease in corrosion due to a shielding of the implant by the capsule that has been formed. The corrosive interstitial fluid from the muscle tissue is prevented from penetrating through to the implant.

For an explanation of the occurrences in the following period it must first be repeated that in the animal experiments the whole capsule was taken for the CT-analyses. The concentrations found for CT are therefore the mean concentrations of the entire connective tissue capsule.

The microcrystallites of the implant material already mentioned are, of course, further degraded and the individual components are removed. A non-specific decrease in all transport processes in the CT due to the fibrous concentrating process of the connective tissue would cause, to the same extent, a decrease in the corrosion rate and in the metal removal rate. This would explain the fact that after 12 weeks the chromium concentrations remain more or less constant in CT, but decrease in MCT. However, the nickel concentrations in CT should also remain constant. But this is obviously not the case.

The model is therefore probably too simple and to obtain agreement with the experimental results we introduce a modification by taking into account the non-uniformity of the capsule tissue as well as an individual biochemical behaviour of the different corrosion products.

One can assume a histological structure of the connective tissue capsule as follows (Fig. 4). Directly at the implant a layer is formed which is rich in fibrous tissue. Only minute amounts of corrosive interstitial fluid can penetrate to the implant through this layer. Similarly, only minute amounts of corrosion products can migrate out of this layer. This means that the already mentioned barrier function of the capsule, leading to the cessation of the increases in the concentration of the corrosion products, is to a large

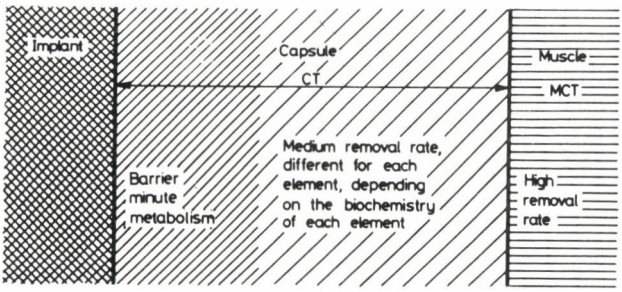

Fig. 4: Schematic presentation of the structure of the connective tissue capsule.

extent caused by the dense layer near the implant. In the direction of the MCT the connective tissue is less compact. Thus, from this larger part of the CT a noticeable removal of the corrosion products is still possible via the bloodvessels and the lymphatic vessels. This removal changes the mean concentrations of the metals in the entire capsule despite the almost complete lack of metabolism in the barrier at the implant.

However, the time-dependent changes of the mean concentrations are obviously different for the individual corrosion products. This fact can be taken into account in the mechanistic model by additional biochemical considerations.

In the clinical cases it has been shown that iron is bound in the cells after degradation of the microcrystallites. This intermediary storage may occur in a form similar to the well known iron storage compounds ferritin and haemosiderin.[8] One can assume that after the degradation of the microcrystallites the other elements are also initially bound in the cells or weakly bound at the fibers and embedding ground substance. In each case these intermediary storage points are gradually degraded again. In addition, for metals having little tendency to form biochemical compounds one can assume a frequent loosening of bonds, resulting in the metal atoms becoming mobile again. Toxic metals can lead to necroses, the frequency of occurence depending on the degree of the toxicity of the metals. In the progress of these necroses the damaged cells are degraded. Consequently, the elements concerned become often mobile again, in this way too.

The sum of these different processes results in different removal rates. In the animal experiments this is shown by the different decreases of the mean concentrations of the individual implant components in the entire capsule with increasing time (Fig. 3). In the clinical cases this is indicated by the different decreases in concentrations of the individual implant components in the connective tissue capsule with increasing distance from the implant.[1-3, 5]

Table 2
Removal rates of metals in connective tissue capsules
(Tissue impregnation by corrosion)

Metal	Removal rate
iron	low
chromium, molybdenum	medium
nickel, silver, tantalum	high

Taking into account all results of both clinical cases[1, 6] and animal experiments,[6] which are not fully described here, the implant metals, which come into the tissue by corrosion, can be classified into three groups with respect to their removal rates (Table 2).

The different removal rates may be regarded as indicators of the specific metabolism of the individual elements. However, the metabolism not only varies for different elements, but is also different for the same element.

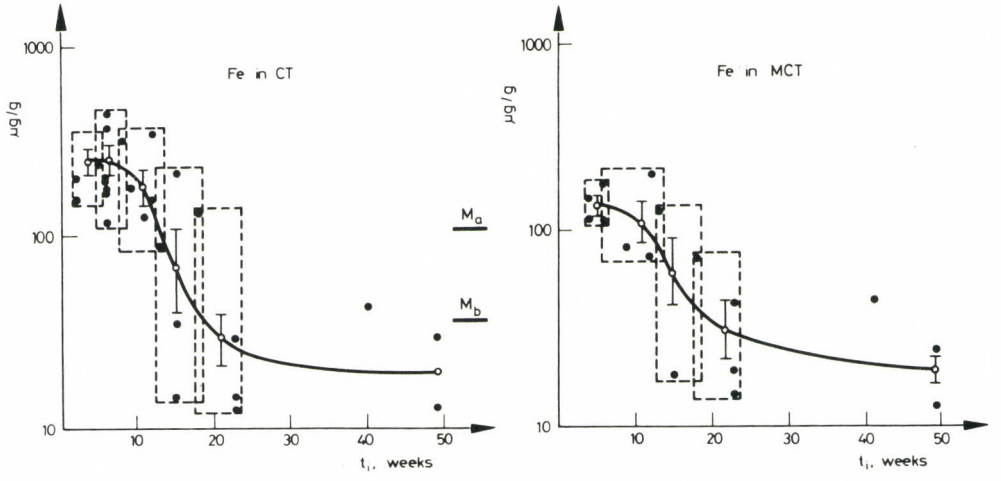

Fig. 5. Time dependence of the concentrations of iron in haematoma. Pure metal implants (not including iron). Animal experiments. ●, ○: See Fig. 3, M_b: Muscle tissue before implantation, mean logarithmic value[7] of 32 analyses. M_a: Muscle tissue after implantation, mean logarithmic value[7] of 25 analyses. Sampling 20 – 30 min after removal of M_b. t_i: See text.

The behaviour of iron in heametoma

The results on this effect are summarized in Fig. 5. With respect to the discussion below, it must be mentioned that for Fig. 5 only results were used of samples that fulfil one of the following conditions

i) no surgery was performed between implantation and sampling, or

ii) a minimum of 15 weeks lapsed after the last surgery.

In the tissue near to the implant the iron concentration is raised immediately after implantation even in the case of iron-free implants. This can be attributed to the wound haematoma, to be exact, to the haemosiderin residues resulting from the latter. The removal of the haemosiderin iron is completed after 15 to 20 weeks, i.e. relatively quickly, whereas the corrosion iron is removed slowly as shown above. Therefore, the reaction rate is obviously much larger for the degradation of the haemosiderin iron than it is for the iron storage compound formed with the corrosion iron. In other words, the removal process of an element can depend on the nature of the enrichment.

Increase and decrease of the zinc level in the tissue adjacent to the implant

The essential biological trace element zinc also exhibits two different types of behaviour in metallosis tissue. Fig. 6 shows the first effect. 20 to 30 minutes after an operative treatment the zinc concentration increases to about two and a half times the normal level in the tissue treated. This increase of the zinc level is predominately not due to the blood enrichment in the wound area, i.e. the wound haematoma. According to Fig. 5 the difference between the iron concentrations in M_a and M_b is 76 μg/g. The Fe/Zn ratio in the blood of rabbits is 500/5.[9] Therefore, a zinc enrichment caused by the haematoma would only be 0.8 μg/g. However, the difference between the zinc concentrations in M_a and M_b is 13.2 μg/g.

A zinc migration in the direction of a wound has also been observed by other authors.[10] Apparently, zinc is required in the healing process of the wound. In this connection it has been shown in clinical cases as well as in animal experiments that wound healing proceeds markedly slower in the case of a zinc deficit.[10, 11]

This surplus of zinc cannot be detected anymore in MCT after two weeks and is degraded in CT after 10 to 15 weeks.

Then another effect occurs which, however, is not detectable in the comparatively short overall period of the animal experiments. But it is clearly seen in the clinical samples, which were removed over a year after

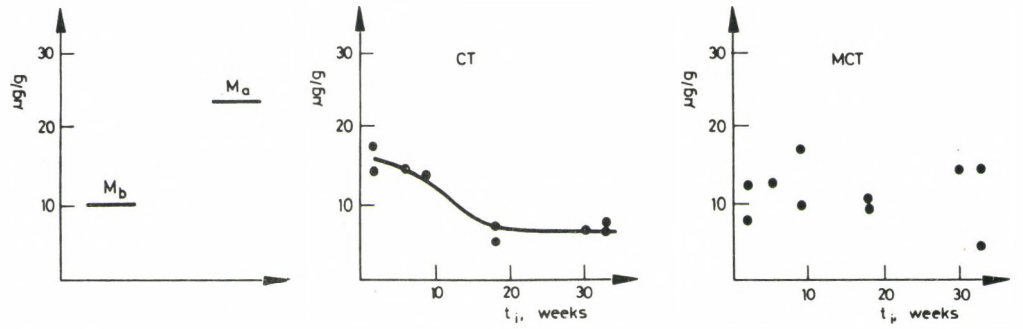

Fig. 6. Concentrations of zinc in different tissues. Implants of V4A-steel. Animal experiments. ●: Experimental values. M_b: See Fig. 5, based on 20 analyses. M_a: See Fig. 5, based on 8 analyses. Sampling 20 – 30 min after removal of M_b. t_i: Interval between implantation and sampling, no surgery in between.

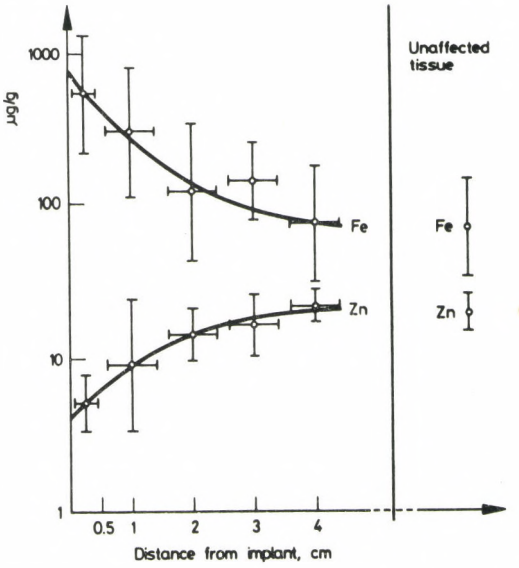

Fig. 7. Concentrations of iron and zinc in metallosis tissue at different distances from the implant. Implants of V4A-steel. Clinical material
o: Mean logarithmic values[7] of experimental data in Tab. 7 and 8 of Ref. 1.

implantation. After degradation of the zinc enrichment the zinc concentration becomes lower than that in the normal tissue, falling as the concentration of corrosion products rises (Fig. 7).

One can show in a more detailed evaluation described in our foregoing publications[1-3] that the extent of the decrease in the zinc concentration in fact depends only on the portion of iron biochemically bound, not on the total iron concentration. It is therefore a reasonable assumption that zinc is displaced from its biochemical compounds by the components of the implant. This can lead to changes in the enzymatic processes which perhaps could be governing factors in the development of metallosis.

It is expected that further investigations may usefully contribute to the problem of the metabolism of metals as well as to the question of the role of biological trace elements in wound healing.

References

1. F. LUX, R. ZEISLER, Z. Anal. Chem., 261 (1972) 314.
2. J. SCHUSTER, F. LUX, R. ZEISLER, Mschr. Unfallheilk., 76 (1973) 537.
3. F. LUX, R. ZEISLER, J. Radioanal. Chem., 19 (1974) 289.
4. F. LUX, R. ZEISLER, J. SCHUSTER, Langenbecks Arch. Chir., 337 (1974) 615.
5. J. SCHUSTER, Die Metallose, Ferdinand Enke Verlag, Stuttgart, 1975.
6. R. ZEISLER, Thesis, Technische Universität München, 1974.
7. K. DOERFFEL, Z. Anal. Chem., 185 (1962) 1.
8. R. R. CRICHTON, Structure and Bonding, Vol. 17, p. 67, Springer, Berlin–Heidelbert–New York, 1973.
9. D. BOŽANIĆ, Unpublished results,
10. E. L. LICHTI, J. A. SCHILLING, H. M. SHYRLEY, Am. J. Surg., 123 (1972) 253.
11. A. RAHMAT, J. N. NORMAN, G. SMITH, Br. J. Surg., 61 (1974) 271.

AUTHOR INDEX

ISBN 963 05 1014 6